Spectroscopic and chemical characterization of Co, Rh and Co-Rh on Al2O3, SiO2 and TiO2 catalysts

SPECTROSCOPIC AND CHEMICAL CHARACTERIZATION OF Co, Rh AND Co-Rh ON Al_2O_3, SiO_2 AND TiO_2 CATALYSTS

H.F.J. VAN 'T BLIK

SPECTROSCOPIC AND CHEMICAL CHARACTERIZATION OF Co, Rh AND Co-Rh ON Al$_2$O$_3$, SiO$_2$ AND TiO$_2$ CATALYSTS

PROEFSCHRIFT

TER VERKRIJGING VAN DE GRAAD VAN DOCTOR IN DE TECHNISCHE WETENSCHAPPEN AAN DE TECHNISCHE HOGESCHOOL EINDHOVEN, OP GEZAG VAN DE RECTOR MAGNIFICUS, PROF. DR. S.T.M. ACKERMANS, VOOR EEN COMMISSIE AANGEWEZEN DOOR HET COLLEGE VAN DEKANEN IN HET OPENBAAR TE VERDEDIGEN OP VRIJDAG 24 FEBRUARI 1984 TE 16.00 UUR

DOOR

HENRI FREDERIK JOZEF VAN 'T BLIK

GEBOREN TE GELEEN

In dankbare herinnering aan mijn vader
Aan mijn moeder

Aan Ine en Hester

CONTENTS

chapter 1

GENERAL INTRODUCTION

       Catalytic processes and reactions have been applied for a
long time before any knowledge on catalysis was available. The
first indications that gases are adsorbed on metals and may
react with each other resulted from investigations done by
H. Davy. In 1815 he was asked to investigate the disastrous
explosions in coal mines which at that time occurred too
frequently. Davy found that a flame could be safely exposed in
an explosive mixture on inflammable gas and air, provided that
it was surrounded by a wire gauze of a particular mesh. He
wrote: "It was obvious that the oxygen and coal gas in contact
with the wire combined without flame, and yet produced heat
enough to preserve the wire ignited, and to keep up their own
combustion" (1). In 1836 J.J. Berzelius reviewed a number of
observations on homogeneous and heterogeneous reactions (2) by
H. Davy, M. Faraday, J.W. Döbereiner, J. Liebig, W. Henry and
P. Phillips. In this review Berzelius introduced the term
'catalysis', which has literally the same meaning as 'analysis'.
For an interesting historical review about heterogeneous
catalysis we refer to Robertson (3).
       Catalysis by metals has become very important in the
chemical and petroleum industries and finds its applications
particularly in reactions involving hydrogen, such as hydrogena-
tion, hydrogenolysis, dehydrogenation and isomerisation. Now-
adays alloy catalysts and TiO_2 as a support are of considerable

interest because of their promising catalytic behaviour for
several reactions.

In this introduction the geometric structure of small
metallic particles is discussed first, because a knowledge of
the structure of metallic particles is necessary to understand
the catalytic properties (activity, selectivity and stability)
of metal catalysts. Secondly, a brief consideration about
alloys will be given, followed by a discussion about some im-
portant aspects of the use of TiO_2 as a support. In this thesis
attention will also be paid to the catalytic behaviour of the
catalysts under investigation for CO hydrogenation. Therefore,
the mechanism of this reaction will be given in the last but one
section, followed by scope and outline of this investigation.

1.1 STRUCTURE OF SMALL METAL PARTICLES

Heterogeneous catalysis by metals takes place at the metal
surface. From the economical point of view it is obvious that
as many metal atoms as possible have to be exposed. However,
even for a very finely divided unsupported metal catalyst the
fraction exposed is too low. For a metal particle 1 μm in size
the fraction exposed is about 0.001. When metals are deposited
on supports as Al_2O_3 and SiO_2 with high surface areas (100 –
200 m^2/g) very small metallic particles may be formed and the
fraction of metal exposed increases two or three orders of
magnitude and in some cases it even approaches unity.
The catalytic behaviour of a supported metal catalyst may depend
on the structure of the crystallites. When there is a strong
metal-support interaction, the metal may be spread out in the
form of two-dimensional rafts. However, it is generally accepted
that metal aggregates have a three-dimensional shape. One would
expect that the packing structure of a small particle of a face-
centered-cubic (fcc) metal such as Rh is fcc. However, this is
probably incorrect (4, 5). When a very small particle is grown
atom by atom in vacuum a 13-atom icosahedron will always be
formed. This structure is different from that of a 13-atom

fcc particle, because it exhibits five fold rotational axes (see figure 1).
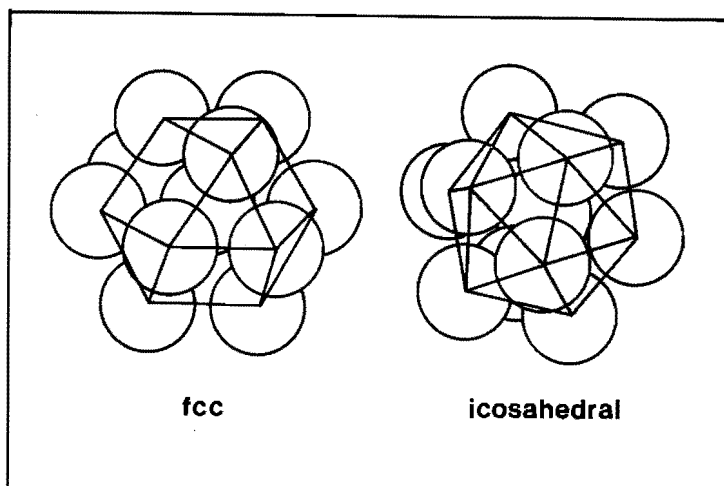
Figure 1 A 13-atom particle in an fcc and an icosahedral packing structure.

Note that the icosahedral 13-atom particle has 42 nearest neighbour contacts whereas the corresponding fcc particle has only 36 nearest neighbour contacts. Prestridge and Yates (6) have published a paper showing a high-resolution micrograph of a 10 Å rhodium particle with five fold rotational axes (pentagonal structure). A striking feature is that even 100 Å pentagonal particles have been observed (7-9). The conversion from icosahedral to fcc packing should occur when the bulk strain energy introduced into the icosahedral particle overcomes its surface energy advantage. Calculations by Ogawa and Ino (9) suggest that this conversion to fcc structure might occur for particles around 100 Å for typical fcc metals.

1.2 ALLOYS

In the 1950's studies of alloys concentrated the attention on the investigation of the so-called 'electronic factor' in catalysis (10-13), but then fell into disfavour for several reasons. More recently, the study of bimetallic systems has been revived, stimulated by the industrial use of bimetallic catalytic reforming catalysts and by a more sophisticated fundamental understanding of the structure of alloys and of the factors affecting the structure.

In terms of thermodynamics the bulk-phase properties of alloys can be roughly divided into three classes:

Mildly exothermic alloys are those for which the enthalpy of formation from the elements $\Delta H_f^0 < 0$ and of which $|\Delta H_f^0|$ is small. In terms of pairwise bond energies involving atom A and B, $(E_{AA} + E_{BB})/2 \approx E_{AB}$. The metals form a solid solution for all temperatures. There is no tendency for cluster formation in alloys and both metal atoms are randomly distributed. Examples are Co-Rh and Pd-Ag, the phase diagrams of which have no miscibility gaps (see for Co-Rh chapter 4, figure 1).

However, the surface layer with a thickness of not more than several atoms, is enriched in the component with the lowest surface Gibb's free-energy. This statement is valid when the differences in surface entropy and in the atomic size of components are low, which often is the case. The gas environment may influence the surface composition of bimetallic particles to a great extent. If gas phase molecules are selectively chemisorbed by atoms of element A, this will provide a driving force for the enrichment of the surface with the element A. This phenomenon has been called by Sachtler *c.s.* (14) 'chemisorption-induced surface segregation'. These authors have reported a study performed on Pd-Ag alloy films. The results suggest that the alloy surfaces were enriched in silver which was to be expected because the sublimation energy for silver is lower than that for palladium. However, CO chemisorption induced a segregation of palladium atoms to the surface - CO molecules are selectively chemisorbed on Pd atoms.

A similar effect can be anticipated for supported bimetallic

catalysts, where one component may segregate to the particle-support interface due to its greater affinity with the support. *Endothermic alloys* are characterized by values of $\Delta H_f^0 > 0$ and $(E_{AA} + E_{BB})/2 > E_{AB}$. For temperatures $T > \Delta H_f^0/\Delta S_f^0$, the equilibrium alloy forms clusters of A atoms and clusters of B atoms within the bulk because of the greater strength of A-A and B-B bonds relative to A-B bonds. An example of this type is Cu-Ni, the phase diagram of which shows a miscibility gap (15). If the relative concentrations of the components of a binary system are within the miscibility gap in equilibrium a two-phase system will exist. The concentrations of these two phases and their composition can be derived from the phase diagram using the lever rule. The binary system of small particles may be built up according to the 'cherry' model, proposed by Sachtler (16). This model described the bimetallic particles in terms of a kernel - the alloy phase with higher surface energy -, flesh - the alloy phase with lower surface energy - and skin - surface layers enriched with respect to 'flesh', because of the same arguments as mentioned for a mildly exothermic alloy.

Note that when bimetallic particles are small (< 100 Å, for instance in supported bimetallic catalysts), it may very well be that phase segregation does not occur, even when there is a miscibility gap for the bulk system (17, 18).

Highly exothermic alloys are characterized by values of $\Delta H_f^0 < 0$ and $(E_{AA} + E_{BB})/2 < E_{AB}$. In these alloys, ordering and formation of intermetallic compounds usually occur. An example is PtSn and Pt_3Sn in Pt-Sn alloys (19). The surface composition of the alloy depends also in this case on the crystal face.

1.3 TiO₂ AS SUPPORT

For a detailed review on this subject we refer to Huizinga (20). In this section we will discuss only the most important aspects of TiO_2 as a support in the context of the present thesis. Tauster *et al.* (21) were the first who reported a

remarkable metal-support interaction in titania-supported metal
catalysts. After reduction of the catalysts at 473 K normal
behaviour of hydrogen and carbon monoxide adsorption was found.
Reduction at 773 K, however, decreases the sorption capacity
to near zero, which was not due to sintering phenomena as
checked by electron microscopy. They assigned the suppression
of chemisorption capacity to interactions between the metal
and support and introduced the term 'Strong Metal Support
Interaction' (SMSI), although knowledge about the nature of
this interaction was lacking. In subsequent publications
(22, 23) this group reported the same phenomenon for Ir sup-
ported on V_2O_3 and Nb_2O_5 and emphasized that SMSI was most
easily evoked with reducible transition-metal oxide supports.
They also showed that after a mild oxidation at 448 K the SMSI-
state was nullified. A subsequent reduction at low temperature
restored the normal adsorption behaviour.

Although many explanations of SMSI have been put forward
no definitive evidence has been found yet for any of them. A
definitive elucidation of SMSI requires more experimental and
theoretical work. However, two models deserve to be mentioned.
The first model, the most popular one, is based on charge
transfer from the support to the metal, through which the
electron properties of the metal change. This possibility was
discussed by Horsley (24). The metal in M/TiO_2 is negatively
charged by SMSI which means for platinum that the electronic
configuration approaches that of gold. The explanation of
SMSI is then obvious, because H_2 and CO chemisorption does
not take place on gold. But it is difficult to see how SMSI
can be explained by the same reasoning in the case of Rh/TiO_2,
because the electronic configuration of rhodium in SMSI
approaches that of palladium, which should be active in H_2
and CO chemisorption.
Another explanation of SMSI is encapsulation of the metal by
suboxides of TiO_2 (schematically shown in figure 2).
Recently, Powell and Whittington (25) proposed such encapsula-
tion to be the mechanism of deactivation in catalytic
reactions. Using Auger and scanning electron microscopy they

found platinum to be immersed in the SiO_2 surface with con-
current formation of an SiO_2 ridge around the base of the Pt
particles for Pt/SiO_2, when annealed at 1200 and 1375 K.
By the technique of Nuclear Backscattering Spectrometry Cairns
et al. (26) observed an interdiffusion between the metal and
its support for planar specimens of Pt/Al_2O_3, Rh/Al_2O_3,
Pt/TiO_2 and Rh/TiO_2.
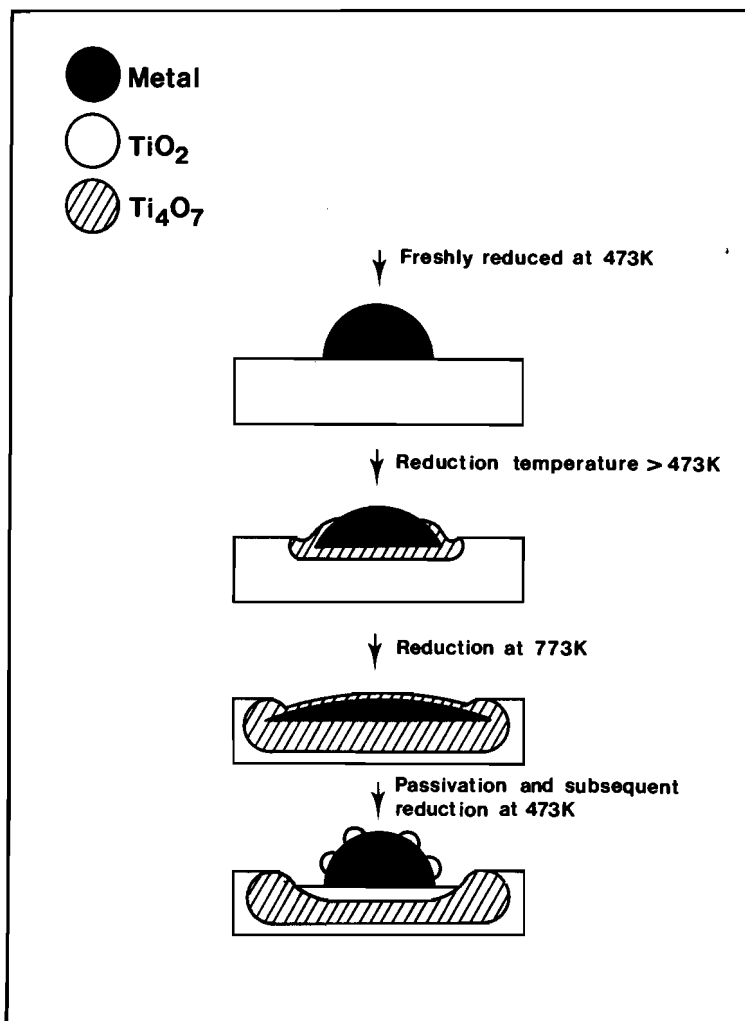
Figure 2 Covering model for SMSI.

As reported by several groups (27-31) a metal-assisted re-
duction of the support takes place during a high temperature
reduction of M/TiO_2. Baker and co-workers (23, 28) have found
that the support is partly reduced to Ti_4O_7. They also propose
that the metal 'wets' the Ti_4O_7 formed, because of an enhanced
interfacial interaction. However, this must be a symmetrical
effect, the oxide 'wets' the metal too. Due to the strong
interaction it may be energetically favourable that the metal
particles are embedded in Ti_4O_7, thus decreasing the surface
tension of the particles to a great extent. During reduction
the particles sink into the support - the specific volume of
Ti_4O_7 is smaller than that of TiO_2 - ultimately leading to
covering of the particles with a (mono)layer of Ti_4O_7. This
means that the chemisorption capacity of the metal is suppressed
by blocking. During a mild oxidation of M/TiO_2, Ti_4O_7 is still
present, as shown by Baker *et al.* (29). At higher temperatures,
however, Ti_4O_7 in direct contact with the metallic particle may
be oxidized by O_2 or H_2O to TiO_2. Consequently, the monolayer
is destroyed and metal atoms are exposed again.

From the point of view of catalytic reactions the be-
haviour of metals in the SMSI-state poses fascinating questions.
The reactions appear to fall into two distinct classes; one in
which the activity in the SMSI-state is much lower than that in
the non-SMSI-state, and a second class for which the opposite
is true. Furthermore, the extent of these differences is greatly
dependent on the metal in question. Generally, hydrogenolysis
and hydrogenation reactions belong to the first class. For
example, the activity for hydrogenation of benzene or de-
hydrogenation of cyclohexane decreased with Pt or Rh supported
on TiO_2 after reduction of these catalysts at high temperatures
(32, 33). The specific activity for ethane hydrogenolysis over
titania-supported group VIII metals, except ruthenium, de-
creased several orders of magnitude compared to the silica-
supported counterparts (34).
These reactions are strongly related to hydrogen chemisorption
capacities and therefore a suppression of their activities in
SMSI is not surprising.

For CO methanation and Fischer-Tropsch synthesis, however, the situation is apparently different. Although the metals in SMSI-state have been found to reveal a strongly inhibited chemisorption of H_2 and CO, some metals have been found to have their highest activities for CO hydrogenation when dispersed on TiO_2 (35-40). Titania-supported nickel catalysts show specific activities one to two orders of magnitude higher than other catalysts. The increase in activity is accompanied by an increase in selectivity to higher-molecular-weight paraffins (35). Burch and Flambard (38) inferred that for their Ni/TiO_2 catalysts the observed increase in activity compared to Ni/SiO_2 catalysts could not be interpreted in terms of strong metal-support interaction because the metallic particles were too large (100 Å) to obtain SMSI. The enhancement in activity was assigned to the role of titania in creating new unique sites for the H_2 + CO reaction which are situated at the interface between the metal particle and the support surface. As TiO_2 is partly reduced anion vacancies are present at the interface. The oxygen atoms of chemisorbed CO may interact with these vacancies (*cf.* figure 3) and consequently the CO dissociation, which is an important step in Fischer-Tropsch synthesis, may be facilitated.
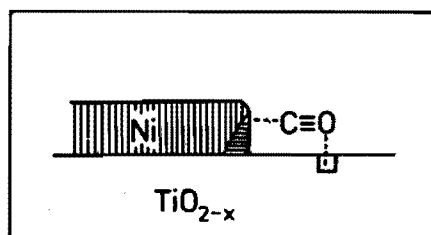
Figure 3 Model of the active site in H_2 + CO reaction at the interface between a nickel particle and the titania surface (38).
▥ Bulk Ni, ▤ Ni atoms at the interface, ☐ anion vacancy.

However, Vannice and Vasco-Jara (37) have rejected this model. They studied physical mixtures of Ni/TiO_2 and Pt/TiO_2. They assumed a catalyzed reduction of the titania in Ni/TiO_2 particles by hydrogen spill-over via Pt/TiO_2 particles to Ni/TiO_2. On the basis of the model proposed by Burch and Flambard one would expect an increase in the specific activity for Ni/TiO_2 with increasing Pt/Ni ratio in the physical mixtures, because the (Pt-reduced TiO_2 surface/Ni surface) ratio is increasing too. However, the specific activity for Ni did not change. Vannice and Vasco-Jara proposed that the intrinsic catalytic properties of Ni crystallites are altered by SMSI behaviour.

It may be clear that the interpretation of the anomalous catalytic behaviour of titania-supported metals in H_2 + CO reaction is still uncertain. Obviously, more research is needed to obtain information on this intriguing subject.

1.4 CATALYTIC HYDROGENATION OF CARBON MONOXIDE

Up to now, oil is still the major source of energy. However, the growing awareness that oil resources are not inexhaustible have led to a considerable interest in coal as an alternative energy source. The coal supply is beyond any doubt superior to the oil supply, being respectively 76% and 14% of the proven fossil fuel reserves. Coal, however, is a solid fuel and compared to liquids this is a disadvantage with respect to transport, handling and removal of pollutants. Hence, there is a clear incentive to convert coal into liquid hydrocarbons. This can be achieved by coal liquefaction and by coal gasification to synthesis gas – a mixture of carbon monoxide and hydrogen – which in it's turn is converted to hydrocarbons, either directly via Fischer-Tropsch synthesis or indirectly via the Methanol/ZSM-5 route. The Fischer-Tropsch type reactions form one of the subjects of this dissertation. Therefore, we will give brief descriptions of the history and mechanism of this process.

The history of the catalytic hydrogenation of CO - which has been adequately described in (among others) two review papers by Storch (41) and Pichler (42) - starts in 1902 when Sabatier and Senderens (43) reported the production of CH_4 from CO and H_2 over Ni. As early as 1913, Badische Anilin und Soda Fabrik (BASF) patented the production of longer-chain and oxygenated hydrocarbons at pressures over 10^4 kPa and at about 623 K over alkali-metal-activated transition-metal catalysts of cobalt and osmium oxides. In 1926, Fischer and Tropsch (44) published their classical work reporting on the synthesis, near atmospheric pressures and at 473 K, of various higher-molecular-weight hydrocarbons from CO and H_2. The original catalysts were both iron and cobalt with K_2CO_3 and copper as promoters. The reaction carried out in this manner is called the Fischer-Tropsch synthesis. The catalysts underwent many im-provements in the years that followed. At the height of World War II the production of synthetic fuel via the Fischer-Tropsch synthesis amounted to 100,000 barrels a day in Germany. The standard catalyst contained cobalt, thoria, magnesium oxide and kieselguhr (42, 45).
The advent of cheap oil in the 1950's caused a decrease in the interest in the Fischer-Tropsch syntheses, except in South Africa where with the use of promoted iron catalysts large-scale production of liquid and gaseous hydrocarbons from CO and H_2 was established. The oil crisis of 1973 and the awakening of consciousness of the limited supply of oil reserves have renewed the interest in coal as a feedstock. However, the out-look of the Fischer-Tropsch synthesis is not too bright be-cause the production of the reactants CO and H_2 from coal is very expensive. Therefore, the effort of present research on the hydrogenation of carbon monoxide is mainly directed to improve the selectivity to desirable products by using, *e.g.*, promoted and/or bimetallic catalysts.

We will discuss now the on all sides accepted mechanism for the Fischer-Tropsch synthesis. For detailed reviews on this subject we refer to Bell (46) and to Biloen and Sachtler (47). The hydrogenation of carbon monoxide is catalyzed by all group

VIII metals. Of course each metal has a different activity
and has its own characteristic product selectivity. The
mechanism of the Fischer-Tropsch reaction can be divided
into three steps: initiation, propagation (chain growth)
and termination. The initiation includes the adsorption of
reactants and the formation of surface intermediates containing
one carbon atom. Hydrogen is readily adsorbed and dissociated
on group VIII metals (48). Also CO adsorption occurs on
all these metals. However, CO dissociation at reaction
temperature, between 473 and 573 K, only occurs on Fe, Co,
Ni, Ru, Rh and Os, whereas CO is to a great extent molecularly
adsorbed on Pd, Ir and Pt. As shown by Araki and Ponec (49)
and later by Biloen (50) CO dissociation precedes C-H
bond formation in Fischer-Tropsch synthesis. We, therefore,
pay some closer attention to CO adsorption on metals. On all
group VIII metals CO is adsorbed perpendicularly to the
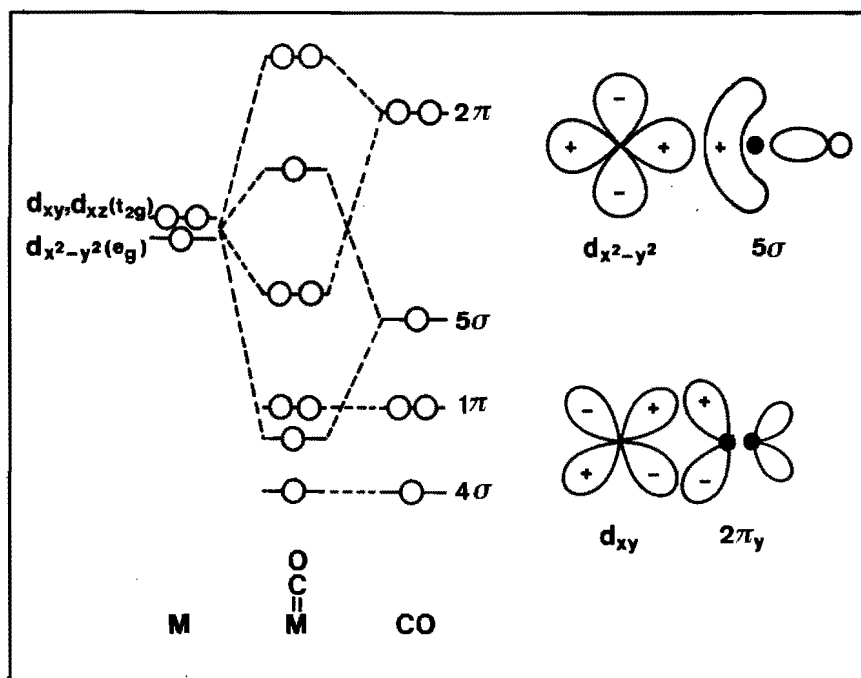
Figure 4 *Molecular orbital diagram of the interaction between*
CO and a transition-metal atom.

surface and with the C atom bonded to the metal. The bond
between CO and the metal is schematically presented in a
one-electron level scheme in figure 4. The 10 valence electrons
in CO are situated in the following orbitals (in order of
increasing energy): 3σ, 4σ, $1\pi_y$ and $1\pi_z$, and 5σ. The
lowest unoccupied molecular orbital is the antibonding 2π
orbital. There is a rather strong interaction between the
CO 5σ orbital and the metal e_g orbitals. The so-called σ bonding
interaction between metal e_g and CO 5σ orbitals leads to a
ligand-to-metal electron transfer. This interaction is further
strengthened by a backflow of electrons via an interaction
of metal t_{2g} and CO 2π orbitals. It is this 'backdonation'
which weakens the C-O bond and possibly promotes dis-
sociation of the CO molecule. When under Fischer-Tropsch
conditions CO is dissociated, the C* formed (* indicates
adsorbed species) is hydrogenated into CH_x*. Brady and
Pettit (51, 52) claim that before a polymerization of one
carbon species takes place, a methyl group (CH_3*) has to be
formed. They have found that diazomethane CH_2N_2 (which
decomposes into CH_2* and N_2) diluted with He or N_2 over some
group VIII metals rapidly and quantitatively led to
ethylene, whereas a gas mixture of H_2 and CH_2N_2 led to
unbranched hydrocarbons with a product distribution typical
for the Fischer-Tropsch reaction.
Discussion brings us now to the propagation step - the
formation of surface intermediates with more than one carbon
atom from the building blocks of one carbon atom. Brady and
Pettit postulate that CH_2* groups do polymerize on metal
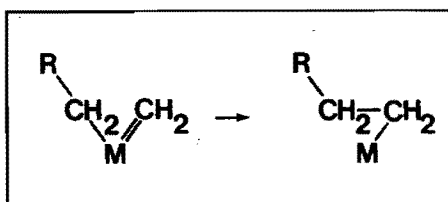
Figure 5 Chain growth by means of CH_2 insertion in alkyl groups
($R-CH_2-$) on the group VIII metal M.

surfaces but the polymerization is initiated by metal hydride bonds. Reduction of CH_2* to CH_3* followed by sequential insertion of CH_2* species into metal-alkyl bonds is the polymerization mechanism. The chain growth by means of CH_2 insertion in alkyl groups during Fischer-Tropsch is presented in figure 5. The termination reaction consists of either a β-hydride elimination of the metal-alkyl to produce an α-olefin or reduction of the metal-alkyl to give an alkane.

The mechanism of the Fischer-Tropsch reaction may be represented by the following reactions (M represents an active site):

$$
\begin{array}{lcl}
CO + M & \rightleftharpoons & CO* \\
CO* + M & \rightleftharpoons & C* + O* \\
H_2 + 2M & \rightleftharpoons & 2H* \\
O* + 2H* & \rightleftharpoons & H_2O + 3M \\
O* + CO* & \rightleftharpoons & CO_2 + 2M \\
C* + 2H* & \rightleftharpoons & CH_2* + 2M \\
CH_2* + H* & \rightleftharpoons & CH_3* + M \\
CH_3* + H* & \rightleftharpoons & CH_4 + 2M \quad \text{methane} \\
CH_3* + CH_2* & \rightleftharpoons & CH_3CH_2* + M \\
CH_3CH_2* & \rightleftharpoons & CH_2CH_2 + H* \text{ ethylene} \\
CH_3 CH_2* + H* & \rightleftharpoons & CH_3CH_3 + 2M \text{ ethane} \\
etc.
\end{array}
$$
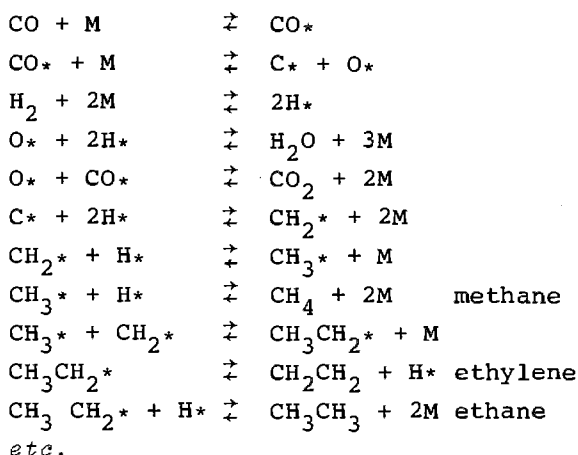
1.5 SCOPE AND OUTLINE OF THE PRESENT INVESTIGATION

This thesis deals with the characterization of supported monometallic cobalt and rhodium and bimetallic cobalt-rhodium catalysts. The choice for these two metals is based upon the following three arguments:
a) In our laboratory we are interested in the hydrogenation of carbon monoxide, for reasons mentioned in the previous section. Besides iron, cobalt is also a classical Fischer-Tropsch synthesis catalyst (44) and therefore an interesting metal to investigate. Over the past years rhodium has

attracted interest in the conversion of synthesis gas, since
its product range can include oxygenated products (alcohols,
aldehydes, acids) besides hydrocarbons (53-55). The bi-
metallic cobalt-rhodium system may be of interest because
it has been shown that alloying of metals, both of which are
active catalysts, may improve the catalytic properties com-
pared to the properties of the constituent metals (56).

b) It is known from literature that cobalt and rhodium form a
solid solution (57). Therefore, the thermodynamics favour
the formation of bimetallic particles.

c) Various cobalt-rhodium metal carbonyl clusters such as
$Rh_4(CO)_{12}$, $Rh_6(CO)_{16}$, $Co_4(CO)_{12}$, $Co_2Rh_2(CO)_{12}$ and $RhCo_3(CO)_{12}$
can be synthesized and isolated (58). Molecular metal cluster
compounds have already been used as precursor to produce
dispersed metallic catalysts. In some cases much higher
dispersions were obtained than by using the conventional
impregnation technique (59). Moreover, the bimetallic
particles formed are expected to have a uniform Co/Rh
stoechiometry.

We decided to study the metal systems on alumina as well as on
titania. Al_2O_3 was chosen because it is known to be a support
which gives good dispersions and stable catalysts, and TiO_2
because it is known to exhibit SMSI. In one case there was
some advantage in using SiO_2 as support, as will be explained
in chapter 5.

The main aim in this thesis is to contribute to the
solution of the following intriguing problems in the field of
catalysis by metals:

a) Formation and structure of bimetallic particles on supports.
In the literature not much information is available about the
rules governing the preparation of bimetallic catalysts.
It would be nice if one could predict the choice of pre-
cursor and treatment, in such a way that alloying of the
metals would be achieved. Once the bimetallic particles are
formed a question of interest is what the structure of the
crystallites will be. Will the two metals be homogeneously
mixed or will the surfaces of the crystallites be enriched
in one of the metals?

b) Influence of alloying on the catalytic properties of bi-
   metallic catalysts. An interesting question is if alloying
   of cobalt and rhodium induces a synergistic effect in the
   hydrogenation of carbon monoxide.
c) Influence of SMSI on the catalytic properties of the
   titania-supported catalysts. In the literature anomalous
   catalytic behaviour of titania-supported catalysts has been
   reported (32-40) and has often been assigned exclusively
   to SMSI. However, with many reported studies one may doubt
   if the SMSI effect was really important. Therefore, titania-
   supported catalysts in 'non-SMSI-state' and 'SMSI-state' have
   been studied in this thesis.
d) Structure of rhodium in highly dispersed rhodium catalysts.
   The preparation of a rhodium on alumina catalyst in which
   all rhodium atoms are exposed is relatively simple. Although
   many detailed characterization studies of highly dispersed
   catalysts have been reported, the state of the metal is not
   yet known exactly. There even exists a controversy about
   the structure and oxidation state of the rhodium in these
   ultra dispersed systems after reduction with hydrogen.
The main techniques used in this thesis are Temperature
Programmed Reduction-Oxidation (TPR, TPO) and Extended X-ray
Absorption Fine Structure (EXAFS). TPR and TPO can provide
useful information on the reducibility and oxidizability of
metal catalysts, while alloying of the two metals during
reduction can be followed by TPR. EXAFS is, in contradistinction
to diffraction techniques, sensitive to short-range order
and can provide unique structural information on highly dis-
persed catalysts. An additional advantage is that the metal
crystallites can be studied under reaction conditions.
For the benefit of the reader the backgrounds of TPR, TPO and
EXAFS will briefly be presented in chapter 2.
Chapter 3 is devoted to the application of TPR and TPO to
alumina- and titania-supported rhodium catalysts. It will be
shown that two different kinds of rhodium are present after
reduction and two kinds of rhodium oxide after oxidation: one
kind which is easily oxidized/reduced and the other kind which

is harder to oxidize/reduce. Transmission Electron Microscopy
has shown that the first kind of Rh_2O_3 consists of flat, raft-
like particles, the second kind of spherical particles.
The reduction and oxidation behaviour of the alumina- and
titania-supported bimetallic cobalt-rhodium catalysts are
discussed in chapter 4. A model is presented which explains
the formation of the supported bimetallic particles and the
change in strucutre of the particles after oxidation at room
temperature and oxidation at elevated temperatures.
Chapter 5 deals with the structure of bimetallic cobalt-rhodium
particles on silica after reduction as studied by means of TPR,
TPO and EXAFS. From the results it is concluded that the
particles formed after reduction consists of a core which is
rich in rhodium and an outer layer which contains mainly cobalt.
In order to justify a generalization of the results of the
formation and the structure of co-clustered Co-Rh particles to
other comparable bimetallic systems, we have characterized
bimetallic $FeRh/SiO_2$ catalysts, the results of which are dis-
cussed in chapter 6. Besides TPR and TPO, in situ Mössbauer
spectroscopy has been applied to obtain information about the
chemical state of iron after different treatments.
Chapter 7 is devoted to the structure of rhodium in highly
dispersed Rh/Al_2O_3 catalysts as studied by a suitable choice
of a number of techniques: EXAFS, TPR, IR, ESR and XPS.
It will be shown that after reduction of the catalyst three-
dimensional metallic rhodium crystallites are formed. This
study reveals a substantial morphological change of the rhodium
crystallites to $Rh^{1+}(CO)_2$ species during CO admission at room
temperature. The cause of this oxidative CO adsorption will be
discussed.
Chapter 8 describes an extensive in situ EXAFS study of the
structural change of rhodium crystallites in Rh/Al_2O_3 after
reduction with H_2, evacuation at elevated temperatures, CO
admission at room temperature, CO desorption, after the
Boudouard reaction ($2CO \rightarrow C + CO_2$) and after the Fischer-Tropsch
reaction. As chapter 8 will be published separately (Journal of
Molecular Catalysis, 1984) there is a considerable overlap

between this chapter and chapter 7.
The study of the catalytic behaviour in Fischer-Tropsch
reaction of alumina- and titania-supported cobalt-rhodium
catalysts is dealt with in chapter 9. Attention will be paid
to the influence of alloying, SMSI and dispersion on the
catalytic properties. In chapter 10 the main conclusions
arrived at in this thesis are summarized.

1.6 REFERENCES

1. H. Davy, Phil. Trans. R. Soc., 107, 77 (1817).
2. J.J. Berzelius, Annls. Chim. Phys., 61, 146 (1836).
3. A.J.B. Robertson, in "Catalysis of Gas Reactions by Metals",
   Logos Press Limited, London (1970).
4. J.J. Burton, Catal. Rev.-Sci. Eng., 9, 209 (1974).
5. J.J. Burton, in "Sintering and Catalysis", edited by G.C.
   Kuczynski, Plenum, New York (1975), p. 17.
6. E.B. Prestridge and D.J.C. Yates, Nature, 234, 345 (1971).
7. K. Kimoto and I. Nishida, J. Phys. Soc. Japan, 22, 940
   (1967).
8. J.G. Allpress and J.V. Sanders, Surf. Sci., 7, 1 (1967).
9. S. Ogawa and S. Ino, J. Cryst. Growth, 13/14, 48 (1972).
10. G.M. Schwab, Discuss. Faraday Soc., 8, 166 (1950).
11. D.A. Dowden and P. Reynolds, Discuss. Faraday Soc., 8, 184
    (1950).
12. W.K. Hall and P.H. Emmett, J. Phys. Chem., 63, 1102 (1959).
13. R.J. Best and W.W. Russell, J. Am. Chem. Soc., 76, 838
    (1954).
14. R. Bouwman, G.J.M. Lippits and W.M.H. Sachtler, J. Catal.,
    25, 300 (1972).
15. P. van der Plank and W.M.H. Sachtler, J. Catal., 12, 35
    (1968).
16. W.M.H. Sachtler, Le Vide, 164, 67 (1973).
17. D.F. Ollis, J. Catal., 23, 131 (1971).
18. J.H. Sinfelt, J. Catal., 29, 308 (1973).
19. H. Verbeek and W.M.H. Sachtler, J. Catal., 42, 257 (1976).

20. T. Huizinga, thesis, University of Technology, Eindhoven.

21. S.J. Tauster, S.C. Fung and R.L. Garten, J. Am. Chem. Soc., 100, 170 (1978).

22. S.J. Tauster and S.C. Fung, J. Catal., 55, 29 (1978).

23. S.J. Tauster, S.C. Fung, R.T.K. Baker and J.A. Horsley, Science, 211, 1121 (1981).

24. J.A. Horsley, J. Am. Chem. Soc., 101, 2870 (1979).

25. B.R. Powell and S.E. Whittington, J. Catal., 81, 382 (1983).

26. J.A. Cairns, J.E.E. Baglin, G.J. Clark and J.F. Ziegler, J. Catal., 83, 301 (1983).

27. R.T.K. Baker, J. Catal., 56, 390 (1979).

28. R.T.K. Baker, J. Catal., 63, 523 (1980).

29. R.T.K. Baker, E.B. Prestridge and R.L. Garten, J. Catal., 59, 293 (1979).

30. P.G. Menon and G.F. Froment, Appl. Catal., 1, 31 (1981).

31. T. Huizinga and R. Prins, J. Phys. Chem., 85, 2156 (1981).

32. P. Meriaudeau, O.H. Ellestad and C. Naccache, in "Proceedings of the 7th International Congress on Catalysis", edited by T. Seiyama and K. Tanabe, Elsevier, Amsterdam (1981), Part B, p. 1464.

33. P. Meriaudeau, P. Pommier and S.J. Teichner, C.R. Acad. Sci. Paris, 289C, 395 (1979).

34. E.I. Ko and R.L. Garten, J. Catal., 68, 233 (1981).

35. M.A. Vannice and R.L. Garten, J. Catal., 56, 236 (1979).

36. M.A. Vannice and R.L. Garten, J. Catal., 66, 242 (1980).

37. M.A. Vannice and J. Vasco-Jara, in "Stud. Surf. Sci. and Catal.", vol. 11, edited by B. Imelik *et al.*, Elsevier, Amsterdam (1982), p. 185.

38. R. Burch and A.R. Flambard, in "Stud. Surf. Sci. and Catal.", vol. 11, edited by B. Imelik *et al.*, Elsevier, Amsterdam (1982), p. 193.

39. M.A. Vannice and R.L. Garten, J. Catal., 63, 255 (1980).

40. M.A. Vannice, J. Catal., 74, 199 (1982).

41. H.H. Storch, Adv. Catal., 1, 115 (1948).

42. H. Pichler, Adv. Catal., 4, 271 (1952).

43. P. Sabatier and J.B. Senderens, C.R. Hebd. Seances Acad. Sci., 514 (1902).

44. F. Fischer and H. Tropsch, Brennst.-Chim., 7, 97 (1926).

45. H. Kölbel, Chem.-Ing.-Techn., 29, 505 (1957).

46. A.T. Bell, Catal. Rev.-Sci. Eng., 23, 203 (1981).

47. P. Biloen and W.M.H. Sachtler, Adv. Catal., 30, 165 (1981).

48. C.K. Rofer-De Poorter, Chem. Rev., 81, 447 (1981).

49. M. Araki and V. Ponec, J. Catal., 44, 439 (1976).

50. P. Biloen, J.N. Helle and W.M.H. Sachtler, J. Catal., 58, 95 (1979).

51. R.C. Brady III and R. Pettit, J. Am. Chem. Soc., 102, 6181 (1980).

52. R.C. Brady III and R. Pettit, J. Am. Chem. Soc., 103, 1287 (1981).

53. M. Ichikawa, Bull. Chem. Soc. Jap., 51, 2273 (1978).

54. D.G. Castner, R.L. Blackadar and G.A. Somorjai, J. Catal., 66, 257 (1980).

55. P.R. Watson and G.A. Somorjai, J. Catal., 74, 282 (1982).

56. V. Ponec, Catal. Rev.-Sci. Eng., 11, 41 (1975).

57. W. Köster and E. Horn, Z. Metallkunde, 43, 444 (1952).

58. S. Martinengo, P. Chini, V.G. Albano, F. Cariati and T. Salvatori, J. Organometal. Chem., 59, 379 (1973).

59. J.R. Anderson and D.E. Mainwaring, J. Catal., 35, 162 (1974).

chapter 2

THEORETICAL INTRODUCTION OF THE APPLIED TECHNIQUES:

TPR, TPO AND EXAFS SPECTROSCOPY

Temperature Programmed Reduction and Oxidation (TPR, TPO) and Extended X-ray Absorption Fine Structure (EXAFS) are the principal techniques which have been used to characterize the supported catalysts. For the benefit of the reader the most important aspects of reduction of metal oxides and of oxidation of metals will be discussed in this chapter. Also the influence of alloying on the reduction and oxidation behaviour will be considered. TPR and TPO results are presented in chapter 3, 4, 5, 6 and 7. A theoretical consideration of the EXAFS technique will be given too. It is certainly not the intention to review the subject, but only a simplified description will be given in order to facilitate the understanding of the EXAFS results presented in chapter 5, 7 and 8 of this dissertation.

2.1 TEMPERATURE PROGRAMMED REDUCTION AND OXIDATION

TPR and TPO are relatively new techniques which are highly sensitive and which do not depend on any specific property of the catalyst other than that species under study to be in, respectively, a reducible and oxidizable condition. Over the last few years TPR has been applied to the study of many supported and unsupported catalyst systems as becomes obvious from a recent review by Hurst *et al.* (1). However, up to now

little attention has been paid to TPO.

The techniques allow one to obtain (semi)quantitative in-
formation about the rate and ease of reduction (during TPR)
or of oxidation (during TPO) of all kinds of systems, and once
the apparatus has been built the analyses are fast and
relatively cheap.

The apparatus we used is schematically presented in figure 1.
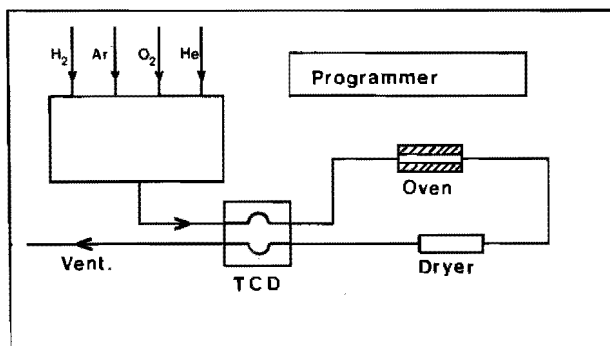
Figure 1 Schematic representation of TPR-TPO apparatus.

A weighed amount of a catalyst is placed in the reactor. Before
the actual TPR (TPO) measurement starts the catalyst may be
subjected to a variety of pretreatment using the gas-handling
system and oven. At the beginning of a TPR (TPO) experiment a
gas mixture which consists of 5% H_2/Ar (5% O_2/He) flows over
the catalyst at a temperature low enough to prevent reaction.
The temperature of the oven is then increased at a linear
programmed rate. The uptake of hydrogen (oxygen) is measured
by the difference in the thermal conductivity of the gas be-
fore and after reduction (oxidation). Since during reduction
of supported oxides by hydrogen water is formed, the reducing
gas leaving the reactor is dried over magnesium perchlorate
before entering the Thermal Conductivity Detector (TCD).
The change in hydrogen (oxygen) concentration with time is
displayed on a recorder. Since the gas flow is kept constant
the change in hydrogen (oxygen) concentration is proportional
to the rate of reduction (oxidation). Distinct reduction (oxida-

tion) processes in a, *e.g.*, supported metal catalyst, show up
as peaks in the TPR (TPO) profile.

We will continue with a brief exposition of some important
aspects of reduction and oxidation of, respectively, metal oxides
and metals.

2.1.1 REDUCTION OF METAL OXIDES

2.1.1.1 Thermodynamics

The reaction between metal oxide MO and hydrogen to form
metal M and water vapour can be represented by the general
equation:

$$MO(s) + H_2(g) \rightarrow M(s) + H_2O(g).$$

The standard Gibb's free-energy change for the reduction ΔG^0
is negative for a number of oxides and thus for these oxides
the reduction is thermodynamical feasible.

However, since the ΔG accompanying the reduction is given by:

$$\Delta G = \Delta G^0 + RT \ln\left(\frac{P_{H_2O}}{P_{H_2}}\right)$$

$$(\text{where } \Delta G^0 = -RT \ln\left(\frac{P_{H_2O}}{P_{H_2}}\right)_{equilibrium}),$$

it may still be possible for the reduction to proceed even
when ΔG^0 is positive. The TPR experiment is performed such
that the water vapour is constantly swept from the reaction
zone as it is formed. Thus, if P_{H_2O} is lowered sufficiently
at elevated temperatures it is possible that the term
$RT \ln(P_{H_2O}/P_{H_2})$ could be sufficiently negative to nullify a
positive ΔG^0.

2.1.1.2 Kinetics and Mechanism

The overall process of reduction is complex and comprises
transport phenomena to and from the reaction interface as well

as chemical steps such as adsorption and reaction. In general, the following steps can be distinguished : the external transport of hydrogen from the gas phase to the surface layer; the internal transport of hydrogen in the pores of the solid; chemisorption of hydrogen on the surface of the solid; the chemical transformation at the reaction interface with the participation of lattice oxygen, resulting in the reconstruction of the lattice, the desorption of water and the 'internal' and 'external' transport of water.

A very important step is the formation of nuclei when the oxide and hydrogen come into contact. When the reaction starts it usually shows an induction period during which the first nuclei of the solid product are formed. Oxygen ions are successively removed from the lattice by reduction and water desorption, and when the concentration of vacancies reaches a certain critical value they are annihilated by rearrangement of the lattice with a possible formation of metal nuclei (2). The number of nuclei formed per unit area of surface depends to a significant extent on factors like scratches (in general, defects) on the surface, the presence of impurities, *etc*.

In general, the formation of nuclei is greatly favoured at sites where the lattice structure has been distorted by impurities, line defects or mechanical deformation. Consequently, nuclei tend to be formed more readily on the grain boundaries, edges and corners of the specimen than on the ordered regions of the crystals.

Since the metallic product M does not have the same crystal structure as the parent phase MO, formation of an 'embryo' or a 'germ nucleus' is accompanied by a certain amount of local deformation of the oxide lattice. The fact that the molecular volumes of MO and M differ considerably only adds to the severity of the local deformation.

2.1.1.3 Bulk Oxides

Here we consider the process by which a sphere of metal oxide is reduced, directly to the metal, in a stream of flowing hydrogen. It is common to observe the degree of reduction, α,

as a function of time, t, for various temperatures and pres-
sures of hydrogen. The observed data can be interpreted in
terms of the nucleation model or the contracting sphere model.
For the mathematical treatments of these models we refer to
Hurst *et al.* (1).

Nucleation Model

After the first nuclei have been formed the reaction in-
terface between the nuclei of the metal and the metal oxide
begins to increase more and more rapidly by two processes:
the growth of the nuclei already formed and the appearence of
new ones. Oxygen ions may be removed by inward diffusion of
hydrogen to the metal/metal oxide interface or outward diffusion
of oxygen ions from the metal oxide to the metal/gas interface.
At a certain stage of the reduction the metal nuclei have
grown at the surface of the oxide grains to such an extent
that they begin to make contact with each other. From this
moment a decrease of the reaction interface begins because of
the overlapping of the metal nuclei and the steady consumption
of the oxide grains. These processes continue until the oxide
is completely reduced to the metal. In many cases, *e.g.*, nickel
oxide, the metal nuclei formed are thought to dissociate and
activate the hydrogen so that the reduction is autocatalytic.
Figure 2 illustrates this nucleation mechanism which results
in the S-shaped curve of conversion α against t. Also the
maximum in the dα/dt against α is shown. The quotient dα/dt,
which is the mass rate of reduction, is essentially a product
of two terms – one which is related to the rate of nucleation
and the other to the rate of growth of nuclei.
It should also be noted that a similar α against t curve is
obtained for autocatalytic reductions.

Contracting Sphere Model

A very rapid nucleation results in the total coverage of
the oxide grain with a thin layer of the product in the first
instant of the reaction. The reaction interface then decreases
continuously from the beginning of the reaction when it has its
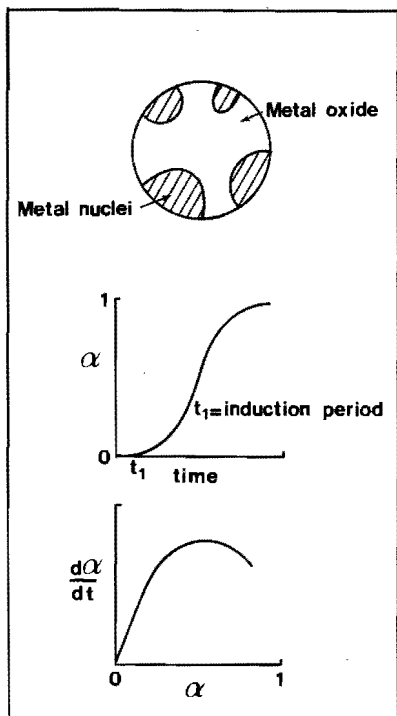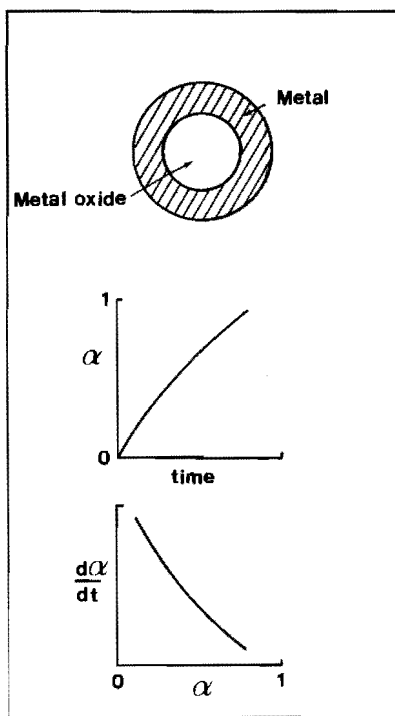
Figure 2   Figure 3

Figure 2 Metal oxide reduction by a nucleation mechanism.
α is the degree of reduction.
Figure 3 Metal oxide reduction by a contracting sphere
mechanism. α is the degree of reduction.

maximum value. The distinction between the nucleation and the
contracting sphere model is somewhat artificial in that the
contracting sphere model starts with very rapid nucleation
while the nucleation mechanism finishes by an essentially con-
tracting sphere model. However, the distinction is between a
reaction interface (and hence rate) which is increasing in
the early stages of the reduction process and a reaction inter-
face (and hence rate) which is contracting throughout the
reduction.

Figure 3 shows the contracting sphere model with its continuous-
ly decreasing metal/metal oxide interface area. This results in
the curve of α against t as shown, and to a continuous decrease
throughout the reaction of the rate $d\alpha/dt$ with time.

2.1.1.4 Supported Oxides

Supported metal oxides may be homogeneously distributed
along the surface of the support or may exist as islands of
oxide separated by uncovered regions of the support. The re-
duction of a homogeneously spread metal oxide may be hindered
or promoted, depending on the nature of the oxide/support
interaction, whereas reduction of islands of metal oxides may
be similar to unsupported oxide, in which case the support acts
purely as a dispersing agent.
Metal atoms and small metal crystallites are mobile on the
surface of oxidic supports (3) so that under appropriate con-
ditions the reduction of a homogeneously dispersed metal oxide
may proceed via the reduction of individual metal ions, or
groups of metal ions followed by surface diffusion to form
small metal crystallites which in their turn may migrate and
combine to form particles of the reduced phase. Such a reduced
phase may have an autocatalytic effect on the reduction.
The nucleation processes may, however, be hindered by metal/
support interactions reducing the mobility of metal atoms.
Furthermore, any autocatalytic effect of the reduced phase may
be hindered if activated hydrogen species are not mobile across
the support surface at the reduction temperature.

2.1.1.5 Bimetallics

First we will consider a metal oxide which has been doped
with a foreign metal. Nucleation can occur then at four dif-
ferent sites (4):
a) Undisturbed portions of the surface. This is natural or
   spontaneous nucleation and corresponds to a similar mechanism
   as on undoped samples.
b) Disordered regions of the surface, *i.e.*, regions that have
   been perturbed by the incorporating process, but where no

dopant is present.

c) Regions where the parent metal ion has,been replaced by the dopant ion.

d) Regions where the dopant, representing a distinct new phase, is in contact with the metal oxide.

For c) and d), nucleation occurs in contact with the dopant ion, and the ease of reducibility of the dopant ion, compared to the parent ion, is of major importance. If the dopant ion reduces first, it may produce a high concentration of active hydrogen on the surface which may promote the reduction. Reduction is autocatalytic when reduced metal formed in the early stages of reduction catalyzes the reduction by H_2 activation.

First row transition metals (Cr, Mn, Fe, Co, Ni) have been found to promote the reduction of CuO (5). In such cases the dopant ion is not thought to reduce before the parent ion, and the promoting effect is thought to arise due to increased nucleation at sites such as b) and c) above.

Now, we will consider supported bimetallic catalysts which are of increasing importance due to the promoting action that second components can have on the activity of a particular catalytic metal, usually by virtue of alloy formation. It is therefore vital to characterize the state of metallic components in such catalysts to dete_mine the role of the second metallic component. However, in such catalysts the metal species are often present in such small amounts and are so finely dispersed that identification of alloying is not straightforward. TPR has proven to be useful in characterization of supported bimetallic catalysts, provided that a significant difference in reduction behaviour of the constituent metal oxides exists. A number of investigations of bimetallic catalyst systems have been reported which are summarized in the review by Hurst *et al.* (1).

When a TPR profile for an oxidized bimetallic catalyst resembles the sum of the profiles of the two individual metal oxides, there is most likely little or no interaction between the

metallic species. However, when the TPR profile is characterized
by a single peak and the maximum of which is shifted towards
lower temperature compared to the reduction maximum of the less
noble metal, the influence of each component on the others
reducibility is obvious. This indicates that the two metal
oxides are close together and that the noble metal serves as
catalyst for the reduction of the less noble metal. The
catalytic effect can be explained by assuming that the noble
metal atoms, reduced by hydrogen, act as nucleation centres.
At these sites H_2 is dissociated to yield H atoms which are
sufficiently reactive to reduce the oxide of the less noble
metal. This mechanism is sometimes called 'intra particle
hydrogen spill-over' (6). It is not a necessary prerequisite
that the metal oxides are in intimate contact. The hydrogen
atoms formed on the noble metal may spill over to the support
and when these species are mobile across the support surface
at the reduction temperature they can reach the oxide of the
less noble metal which is reduced then.
Using TPR in order to obtain information about formation of
alloys in impregnated bimetallic catalysts the situation is
complicated by the nature of salts used in the preparation (*e.g.*,
nitrate and nitrite). During TPR a simultaneous reduction
of the salts (*i.e.* metal ions) can occur. Despite this problem
one can obtain useful information about the reduction of im-
pregnated catalysts as demonstrated in chapter 4, 5 and 6.

2.1.2 TEMPERATURE PROGRAMMED OXIDATION

In contrast with TPR, TPO is a technique which has not
frequently been used in the investigation of reduced supported
catalysts. This may be caused by the fact that TPO profiles
are normally characterized by broad peaks which are difficult
to interpret. In this dissertation, however, the strength of
the TPO technique will be demonstrated.

2.1.2.1 <u>Thermodynamics</u>

The overall driving force of metal-oxygen reactions is
the Gibb's free-energy change associated with the formation
of the oxide from the reactants:

$$M(s) + \tfrac{1}{2}O_2(g) \rightarrow MO(s).$$
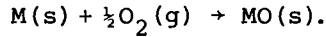
Thermodynamically the oxide will be formed only if the ambient
oxygen pressure is larger than the dissociation pressure of
the oxide in equilibrium with its metal.
In this context it should be noted that oxides formed are
defective and they exhibit deviations from stoechiometry and
that the partial pressure of oxygen above an oxide is a function
of the non-stoechiometry and the defect structure. Most of the
Gibb's free-energy data reported in the literature have been
determined only for stoechiometric oxides, and such data may
not be used for an accurate evaluation of the dissociation
pressure of a non-stoechiometric oxide.
Although the Gibb's free-energy change is the driving force,
it may bear little or no relation to the rates of reaction.
This is a kinetic problem. Rates of reaction are dependent on
the reaction mechanism and the rate-determining reaction or
process.

2.1.2.2 <u>Kinetics and Mechanism</u>

The initial step in the metal-oxygen reaction involves
the adsorption of gas on the metal surface. As the reaction
proceeds, oxygen may dissolve in the metal; then oxide is
formed on the surface either as a film or as separate oxide
nuclei. Both the adsorption and the initial oxide formation
are functions of surface orientation, crystal defects at the
surface, surface preparation, and impurities in both the metal
and the gas.
An important feature of this initial oxide formation is that
isolated oxide nuclei nucleate at what appear to be random
positions on the surface.

Low Temperature Oxidation

It is characteristic for the oxidation of a large number
of metals at low temperatures (generally below 573-673 K) that
the reaction is initially quite rapid and then the ratio drops
off to lower negligibly small values. This behaviour can often
be described by a logarithmic equation (see figure 4).
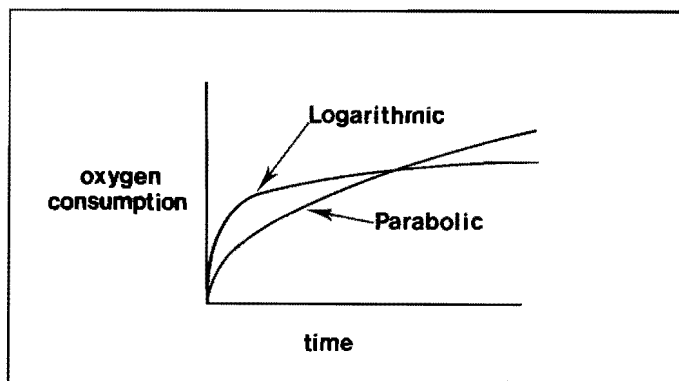
Figure 4 Examples of logarithmic and parabolic oxidation,
characteristic for, respectively, low and high
oxidation temperatures.

In the theory developed by Mott and Caberra (7, 8) it is
assumed that oxygen atoms are adsorbed on the oxide surface
and that electrons can pass rapidly through the oxide by
tunneling to establish an equilibrium between the metal and
adsorbed oxygen. This process creates an electric field which
facilitates the transport of ions across the oxide film.
Mott and Cabrera's model for this oxide growth may be expected
to be valid only for oxide thicknesses smaller than 20 Å,
which is the largest thickness for which sufficient electrons
can tunnel through the oxide (8).
However, Hauffe (9) has shown that the same rate equation may
be derived on the assumption of a rate-determining transport
of ions through the film.

High Temperature Oxidation

Most frequently, high temperature oxidation of metals re-
sults in the formation of an oxide film or scale on the metal
surface. The mechanism of oxidation depends on the nature of
the scale. If solid scales are formed, the oxidation behaviour
depends on whether the scales are compact or porous.
A compact scale acts as a barrier which separates the metal and
the oxygen gas. If sufficient oxygen is available at the oxide
surface, the rate of oxidation at high temperatures will be
limited by solid-state diffusion, for example by lattice grain
boundary, or short-circuit diffusion through the compact scale.
As the oxides grows in thickness, the diffusion distance in-
creases, the rate of reaction will decrease with time and can be
described by the parabolic rate equation (see figure 4). A
widely applied theory of high temperature parabolic oxidation
has been formulated by Wagner (10). It is assumed that a volume
diffusion of the reacting ions (or corresponding point defects)
or a transport of electrons across the growing scale is the
rate-determining process of the total reaction. Electrons and
ions are considered to migrate independently of each other.
As diffusion through the scale is rate-determining, reactions
at phase boundaries are considered rapid, and it is assumed
that thermodynamic equilibrium is established between the
oxide and oxygen gas at the oxide/oxygen interface and between
the metal and the oxide at the metal/oxide phase boundary.
A schematic representation of diffusion processes which may
take place in a compact scale, is presented in figure 5.
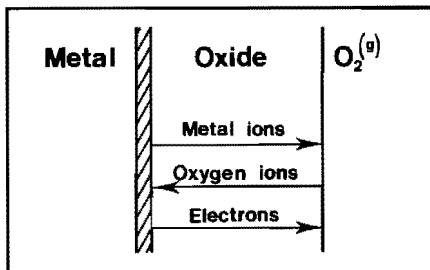
Figure 5 Schematic representation of diffusion processes which
may take place in a compact scale during high tempera-
ture parabolic oxidation of metals.

A commonly observed feature is that a compact scale is formed during initial stages of reaction but ruptures in and fragmentation of the oxide scale will occur after it has reached a certain critical thickness.

2.1.2.3 Oxidation of Alloys

Oxidation of alloys involves the same general phenomena as for unalloyed metals. But as alloys in general contain two or more oxidizable constituents, a number of additional factors and parameters must be taken into account if a comprehensive description of the oxidation behaviour of alloys is to be given. As a result oxidation mechanisms are more complex for alloys than for pure metals.

The components of alloys have different affinities for oxygen, and the reacting atoms do not diffuse at the same rates either in the oxide or the alloy phases. As a result, oxide scales on alloys will not contain the same molar fractions of the alloy constituents as the alloy phase does. Furthermore, the composition and structure of oxide scales on alloys will often change when the oxidation proceeds, and the oxidation kinetics, in their turn, often markedly deviate from ideal and simple rate equations. Other complicating factors arise in that low-melting oxide eutectics may sometimes be formed and cause accelerated oxidation.

In general, during alloy oxidation more than one oxide may be formed. Alloy oxidation can be classified in terms of different types of behaviour:

a) Selective oxidation in which the least noble metal of the alloy is preferentially oxidized.

b) Formation of composite scales consisting of oxides which may be considered to be mutually insoluble and which do not react with each other.

c) Formation of scales with mixed oxides.

The oxidation behaviour of an alloy A-B, in which B is the less noble metal, which oxides AO and BO are practically insoluble in each other, can in most cases be divided into three main regions: 1) at high A concentrations the oxide scale consists

solely of AO, 2) at high B concentrations the scale consists
of BO, 3) in an intermediate concentration range a composite
scale consisting of AO and BO is formed. A theoretical analysis
of the diffusion processes in both the alloy and the oxide
phase during oxidation of alloys leading to composite scales
has been given by Wagner (11). A schematic representation of
the diffusion processes during oxidation of A-B alloys is
presented in figure 6.
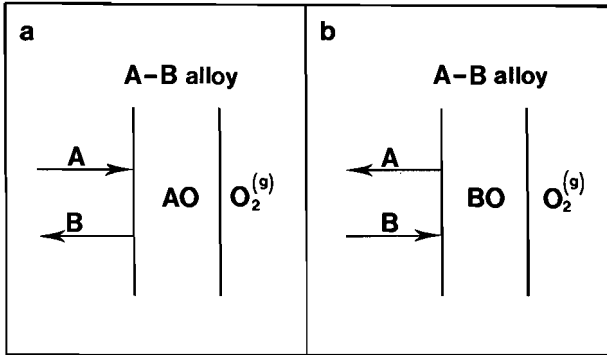
Figure 6 Diffusion processes during oxidation of A-B alloys.
a) Exclusive formation of A oxide at low concentration
of metal B.
b) Selective formation of B oxide at low concentration
of metal A.

When the oxides of the alloying components may react with each
other and form a more stable complex oxide (double oxides,
spinels, *etc.*) at least part of the oxide scale will also con-
sist of the mixed oxide. Diffusion rates in double oxides and
spinels are often appreciably smaller than in the single
oxides, and protective scales on high-temperature oxidation-
resistant alloys often consist of complex oxides.

2.2 EXTENDED X-RAY ABSORPTION FINE STRUCTURE

2.2.1 WHAT IS EXAFS?

EXAFS refers to the fine structure of the X-ray absorption coefficient that appears for photon energies in the range of approximately 0-1500 eV above an absorption edge as illustrated in figure 7b for rhodium foil. Although the extended fine structure has been known for over 50 years, the structural information it offers was not fully recognized until the work of Stern, Lytle and Sayers (12, 13). In addition, the recent availability of synchrotron radiation has resulted in the establishment of EXAFS as a practical structural tool. EXAFS is a final state interference effect involving scattering of the outgoing photoelectron from the neighbouring atoms as is shown schematically in figure 7 (for details see text below).
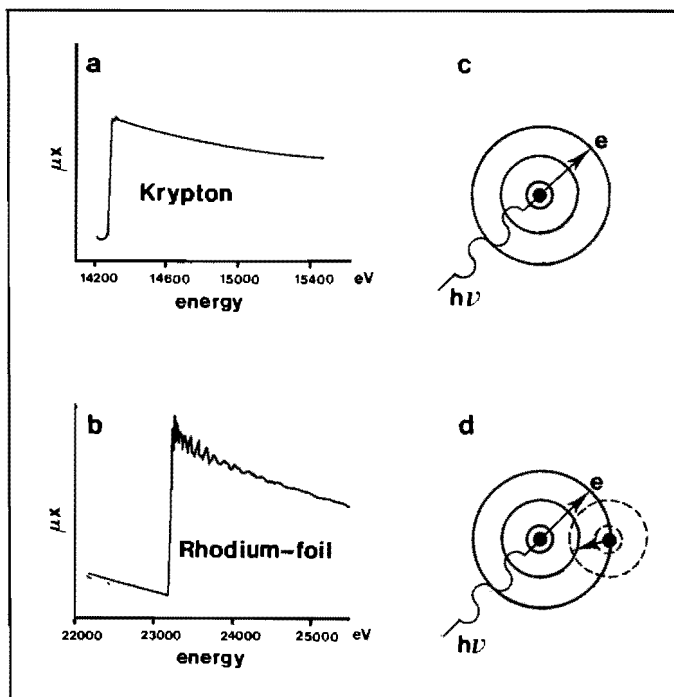
Figure 7 Qualitative rationalization of the absence and presence, respectively, of EXAFS in a monatomic gas such as Kr (a and c) and rhodium foil (b and d).

EXAFS is sensitive to short-range order and can provide unique
structural information on chemical or biological systems also
in those cases where conventional diffraction methods are not
applicable. For instance, this technique is well suited for
determining coordinations of very finely dispersed metal atoms
in catalysts.

For a monatomic gas such as Kr (figure 7a and 7c) with no
neighbouring atoms, the ejection of a photoelectron by ab-
sorption of an X-ray photon results in a spherical wave with
a wavelength $\lambda = 2\pi/k$, where

$$k = \sqrt{\frac{2m}{\hbar^2}(E - E_0)} \; . \tag{1}$$

Here E (= $h\nu$) is the incident photon energy and E_0 is the
threshold energy of that particular absorption edge. The
μ vs. E curve follows the usual smooth λ^3 decay (cf. figure
7a). In the presence of neighbouring atoms (e.g., in Rh-foil,
figure 7b and 7d), this outgoing photoelectron can be back-
scattered from the neighbouring atoms thereby producing an
incoming wave which can interfere either constructively or
destructively with the outgoing wave near the origin, re-
sulting in the oscillatory behaviour of the absorption
(cf. figure 7b). The amplitude and frequency of this sinusoidal
modulation of μ vs. E depend on the type (and bonding) of the
neighbouring atoms and their distances away from the absorber,
respectively.
This simple picture of EXAFS has been formulated into the
generally accepted short-range single-electron single-scattering
theory (12-16). For reasonably high energies above the edge
(> 40 eV) and moderate thermal or static disorders, the modula-
tion of the absorption, normalized to the 'background' ab-
sorptions (μ_0) is given by

$$\chi(E) = \frac{\mu(E) - \mu_0(E)}{\mu_0(E)} \; . \tag{2}$$

In order to relate $\chi(E)$ to structural parameters, it is necessary to convert the energy E into the photoelectron wave-vector k via equation (1). This is illustrated in figure 8a, which shows the EXAFS function $\chi(k)$ of the Rh K-edge of Rh-foil as a function of wavenumber k.

2.2.2 EQUATIONS DESCRIBING THE EXAFS

For K-edges, the derivations of Sayers *et al.* (17) as well as those of Ashley and Doniach (14) have led to a semi-empirical equation for the EXAFS function $\chi(k)$ in terms of the atoms coordinating the specific species whose edge is being studied The $\chi(k)$ is given by:

$$\chi(k) = -\sum_{j} A_j(k) \sin[2kR_j + \delta_j(k)]. \qquad (3)$$

The summation extends over all neighbour shells j separated from the absorbing atom by a distance R_j. $\delta_j(k)$ is twice the phase shift of the outgoing electron wave relative to the 1s core state together with the phase shift on backscattering. $A_j(k)$ is the total amplitude and assuming that the neighbour shell consists of identical atoms the amplitude is given in the single scattering approximation by:

$$A_j(k) = (N_j/kR_j^2) f_j(k) e^{-2\sigma_j^2 k^2} e^{-2R_j/\lambda(k)} \qquad (4)$$

N_j is the coordination number of the absorbing atom for the jth shell, $f_j(k)$ is the backscattering amplitude of the scatterer atom, σ_j^2 is the Debye-Waller factor and the second exponential term is a damping term due to inelastic scattering (mean free path $\lambda(k)$ of the photoelectrons). Realizing that we have presented only a simplified version of the equations of the EXAFS function we refer the reader to reference (18) for a more detailed discussion of this function.
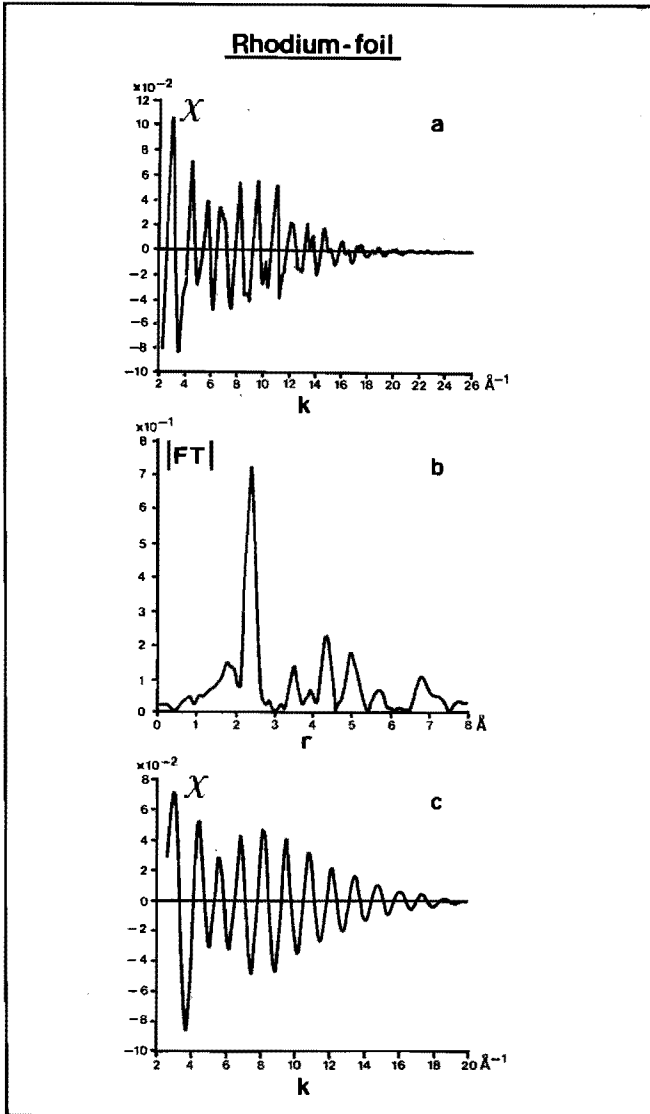
Figure 8 a) *Normalized EXAFS data of the K absorption edge of Rh-foil recorded at liquid nitrogen temperature.*

b) *The associated k^1-weighed Fourier transform taken over the range of wavevector $2.7 \leqslant k \leqslant 20\ \overset{\circ}{A}{}^{-1}$.*

c) *The inverse transform of the latter over an r-range of $0.5 - 3.0\ \overset{\circ}{A}$.*

2.2.3 EXAFS ANALYSIS

The contributions of various neighbour shells to the $\chi(k)$ can be sorted out by Fourier transformation of the EXAFS signal yielding the radial structure function,

$$FT(r) = -\frac{1}{\sqrt{2\pi}} \int_{k_{min}}^{k_{max}} \chi(k) k^n W(k) e^{-2ikr} dk. \qquad (5)$$

n is usually chosen $1 \leqslant n \leqslant 3$ depending on whether the low ($n = 1$) or high ($n = 3$) EXAFS range is to be emphasized. $W(k)$ is a window function and as we choose k_{min} and k_{max} in nodes of $\chi(k)$ a suitable function for $W(k)$ is given by:

$$W(k) \begin{cases} 1 & k_{min} \leqslant k \leqslant k_{max} \\ 0 & \text{otherwise.} \end{cases}$$

The peaks in the magnitude function $|FT(r)|$ occur at distances which are related to the real neighbour shell distance via a phase shift $\delta_j(k)$ (see equation (3)). An illustration of the Fourier transform of the EXAFS function of Rh-foil is presented in figure 8b. The various neighbour shells in the radial structure function can clearly be seen. The sidelobe at the left side of the main peak around 2.4 Å will be discussed later. The EXAFS data discussed in this dissertation are analysed by using reference samples with known crystal structures (the theory-independent analysis) and the Fourier filtering approach has been used. A neighbour shell to be analysed (which corresponds to a specific peak in $|FT(r)|$) is isolated by using a suitable window function in r space. A $W(r)$ has been used as given by:

$$W(r) \begin{cases} 1 & r_{min} \leqslant r \leqslant r_{max} \\ 0 & \text{otherwise.} \end{cases}$$

The inverse transform of the complex function FT(r),

$$\chi'(k) = \frac{2}{k^n \sqrt{2\pi}} \int_{r_{min}}^{r_{max}} FT(r) W(r) e^{2ikr} dr, \qquad (6)$$

produces a real and imaginary part,

$$\chi'(k) = A(k) e^{i\phi(k)} = X(k) + iY(k), \qquad (7)$$

with amplitude $A(k) = [X^2(k) + Y^2(k)]^{\frac{1}{2}}$ and phase $\phi(k) = 2kR + \delta(k) = \arctan[X(k)/Y(k)]$.

An illustration of the inverse transformation from the Rh-foil Fourier transform is given in figure 8c. This transformation taken over a limited r-range of 0.5 - 3 Å yields the EXAFS part limited to contributions from the nearest neighbour rhodium atoms.

By comparing the phase $\phi(k)$ and amplitude $A(k)$ of a sample which structure is not known and a properly chosen reference sample with the same absorbing atom and backscatterer atom one obtains the structural parameters: the average coordination number $\bar{N}$, the interatomic distance R and the Debye-Waller factor $\Delta\sigma^2$ of the unknown system, relative to the reference compound.

2.2.3.1 Phase analysis

Let $\phi_s(k) = 2kR_s + \delta(k)$ be the experimentally determined phase for the 'standard' with known distance R_s between a given atom-pair. For the unknown system consisting of the same atom-pair we denote the determined phase $\phi_x(k) = 2kR_x + \delta(k)$. In both cases the scattering phase shift $\delta(k)$ is the same except for a small difference due to possible changes in bonding. This concept of 'phase shift transferability' (19) has its physical origin in the fact that the core-electron potential dominates the scattering process for $k > 4$ Å^{-1}. We allow for differences in bonding by introducing an 'inner potential' ΔE. The momentum

of the photoelectron is then redefined as (compare equation (1))

$$k' = \sqrt{(2m/\hbar^2) \times (E - E_0 - \Delta E)},$$ (8)

or

$$k' = (k^2 - 0.2625\ \Delta E)^{\frac{1}{2}}.$$ (9)

Comparison of the two phases yields the unknown bond length R_x:

$$R_x = R_s + (\phi_x - \phi_s)/2(k^2 - 0.2625\ \Delta E)^{\frac{1}{2}}.$$ (10)

R_x can be plotted as a function of k for various values of ΔE. For the proper choice of ΔE (-10 eV < ΔE < 10 eV) R_x should be a constant for all k-values. This procedure determines the distance R_x and ΔE in a self-consistent fashion.

2.2.3.2 Amplitude Analysis

       Determination of the coordination number requires comparison with a model system, a procedure which relies on amplitude transferability. According to Stern c.s. (18) this concept, however, does not work as well as that for the phase because both the Debye-Waller and inelastic loss terms in equation (4) are inherently determined by the chemically sensitive valence electrons, even at larger k ($> 4\ \text{Å}^{-1}$) values. That is why even in favourable cases coordination numbers can only be determined to an accuracy of about 10%.
Comparison of amplitudes is usually done by plotting $\ln[A_s(k)/A_x(k)]$ as a function of k^2. Here $A_s(k)$ is the amplitude function corresponding to a given neighbour shell of a standard and $A_x(k)$ is that of the system under investigation. From equation (4) it follows that:

$$\ln[A_s(k)/A_x(k)] = \ln(N_s R_x^2/N_x R_s^2) + 2k^2(\sigma_x^2 - \sigma_s^2) + 2(R_x/\lambda_x - R_s/\lambda_s).$$ (11)

For an isotropic electron the mean free paths are about $\lambda_x \sim \lambda_s \sim \lambda$, and therefore the last term can be neglected because $2|R_x - R_s| \approx 0.1\ \text{Å} \ll \lambda \approx 5\text{Å}.$

Equation (11) also assumes that the backscattering amplitude
$f_x(k) = f_s(k)$. A linear plot of $\ln[A_s(k)/A_x(k)]$ versus k^2
yields the unknown coordination number N_x from the ordinate
intercept at $k = 0$ and $\Delta\sigma^2 (= \sigma_x^2 + \sigma_s^2)$ from the slope.

2.2.3.3 Phase Shift and Amplitude Correction

A phase shift correction on the Fourier transform is
applied in order to obtain real interatomic distances R in
r-space.

In general, the complex Fourier transform of one shell which
is corrected for an arbitrary phase is given by:

$$FT^{\delta^*}(r) \approx \int_{k_{min}}^{k_{max}} A(k)k^n W(k)\sin(2kR + \delta)e^{-2ikr - i\delta^*}dk, \qquad (12)$$

with the imaginary part given by:

$$ImFT^{\delta^*}(r) \approx \int_{k_{min}}^{k_{max}} A(k)k^n W(k)\sin(2kR + \delta)\sin(2kr + \delta^*)dk. \qquad (13)$$

If the phase used for correction originates from the same
scatterer pair as the analysed one ($\delta^* = \delta$) it has been shown
by Lee and Beni (16) that $ImFT^{\delta}(r)$ is a symmetric function
which peaks positively at $r = R$ and the maximum coincides with
the maximum of the absolute value of the Fourier transform
$|FT^{\delta}(r)|$.

From equation (13) it can be clearly seen that the imaginary
part peaks negatively when the phase used for phase shift
correction differs π radians with the one to be analysed.
$(ImFT^{\delta+\pi}(r) = -ImFT^{\delta}(r))$.

The radial structure function of a nearest neighbour Rh-Rh
distance is characterized by a main peak and a sidelobe, as
can be clearly seen for Rh-foil in figure 8b. The sidelobe
is caused by the non-linear k-dependences of the backscattering
amplitude and the phase of rhodium. When the Fourier transform
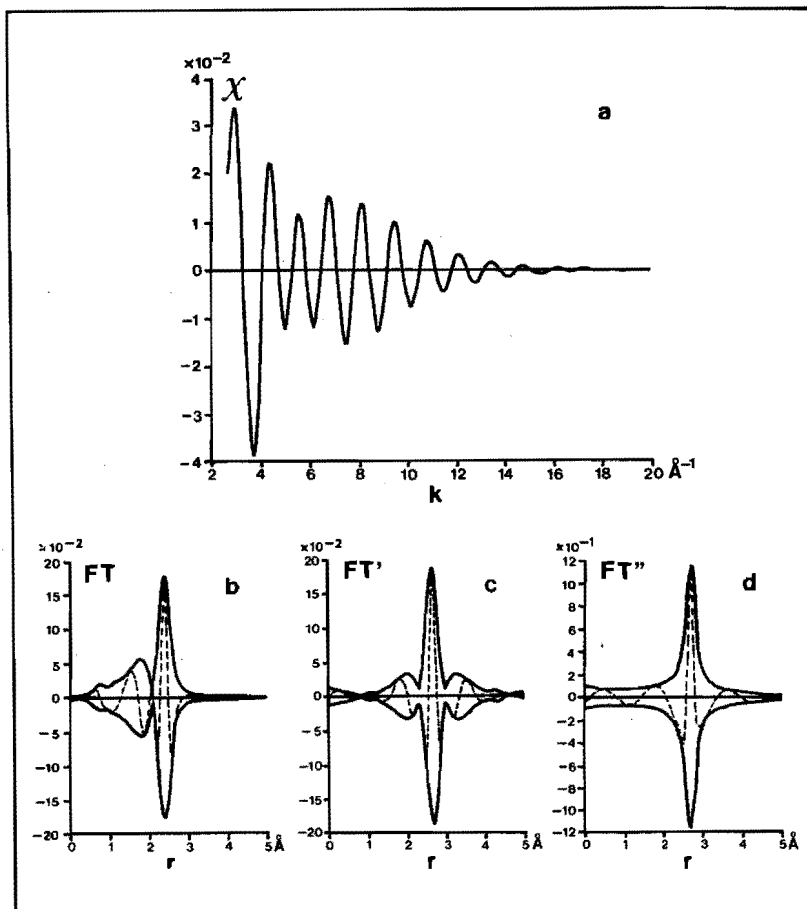
Figure 9 *Influence of phase shift and amplitude correction on the radial*
structure function of a calculated rhodium-rhodium nearest
neighbour EXAFS using parameter values characteristic for highly
dispersed rhodium catalysts (N(Rh-Rh) = 6, R = 2.68 Å, $\Delta\sigma^2$ =
0.005 $Å^2$). For the calculation the phase and amplitude have been
used which have been obtained from measurements on Rh-foil.
a) The calculated EXAFS function.
b) The k^1-weighed Fourier transform (FT) of the EXAFS signal
presented in a) taken over a k-range of 2.7 - 15 $Å^{-1}$. The solid
line and dotted line represent respectively the absolute value
and imaginary part of FT.
c) The Fourier transform corrected for rhodium phase shift (FT').
d) The Fourier transform corrected for rhodium phase shift and
backscattering amplitude (FT'').

44

is corrected for phase shift and divided by the amplitude the
sidelobe is eliminated. The mathematical description of the
Fourier transform of one shell corrected for backscattering
amplitude and phase shift is given by:

$$FT^{\delta_s, A_s}(r) \approx \int_{k_{min}}^{k_{max}} \frac{A(k)}{(kR_s^2/N_s) \cdot A_s(k)} \cdot k^n W(k) \sin(2kR + \delta) e^{-2ikr - i\delta_s} dk. \tag{14}$$

The subscript stands for 'standard'.
When the normal procedure for analysing EXAFS is modified by
using phase shift and backscattering amplitude corrections
small contributions of shells in the EXAFS can be determined
in a reliable way. This has been illustrated in chapter 7 and
8 for the EXAFS of the Rh K-edge of highly dispersed Rh/Al_2O_3
catalysts where a small contribution of Rh-carrier O may be
hidden by a main Rh-Rh peak.

Figure 9 attempts to convey, pictorially, the influence
of phase shift and amplitude correction on the radial
structure function of a calculated rhodium-rhodium nearest
neighbour EXAFS using parameter values characteristic for
highly dispersed Rh catalysts (N(Rh-Rh) = 6, R = 2.68 Å,
$\Delta\sigma^2$ = 0.005 Å^2). For the calculation the phase (δ_s) and the
amplitude ((kR_s^2/N_s) x $A_s(k)$) of Rh-foil have been used.

2.3 REFERENCES

1. N.W. Hurst, S.J. Gentry and A. Jones, Catal. Rev.,-Sci.
   Eng., 24, 233 (1982).
2. J. Haber, J. Less-Common Met., 54, 243 (1977).
3. E. Ruchenstein and B. Pulvermacher, J. Catal., 29, 224
   (1973).
4. H. Charcosset and B. Delmon, Ind. Chim. Belg., 38, 481
   (1973).

5. S.J. Gentry, N.W. Hurst and A. Jones, J. Chem. Soc., Faraday I, 77, 603 (1981).

6. J.R. Anderson, "Structure of Metallic Catalysts", Academic Press, New York, (1975).

7. N.F. Mott, Trans. Faraday Soc., 43, 429 (1947).

8. N. Cabrera, in "Semiconductor Surface Physics", edited by R.H. Kingston, University of Pennsylvania Press, Philadelphia, (1957).

9. K. Hauffe, in "The Surface Chemistry of Metals and Semiconductors", edited by H.C. Gatos, J. Wiley & Sons, New York, (1960).

10. C. Wagner, Z. Physik. Chem., B21, 25 (1933).

11. C. Wagner, Z. Electrochem., 63, 773 (1956).

12. E.A. Stern, Phys. Rev. B, 10, 3027 (1974).

13. E.A. Stern, D.E. Sayers and F.W. Lytle, Phys. Rev. B, 11, 4836 (1975).

14. C.A. Ashley and S. Doniach, Phys. Rev. B, 11, 1279 (1975).

15. P.A. Lee and J.B. Pendry, Phys. Rev. B, 11, 2795 (1975).

16. P.A. Lee and G. Beni, Phys. Rev. B, 15, 2862 (1977).

17. D.E. Sayers, E.A. Stern and F.W. Lytle, Phys. Rev. Lett., 27, 1204 (1971).

18. E.A. Stern, B.A.Bunker and S.M. Heald, Phys. Rev. B, 21, 5521 (1980).

19. P.H. Citrin, P. Eisenberger and B.M. Kincaid, Phys. Rev. Lett., 36, 1346 (1976).

chapter 3

THE MORPHOLOGY OF RHODIUM SUPPORTED ON TiO$_2$ AND Al$_2$O$_3$ AS STUDIED WITH TPR, TPO AND TEM

3.1 ABSTRACT

Supported Rh/Al$_2$O$_3$ and Rh/TiO$_2$ catalysts with varying metal loadings have been investigated with chemisorption and temperature programmed reduction and oxidation. Hydrogen chemisorption shows that all the rhodium on Al$_2$O$_3$ is well dispersed (H/Rh > 1 for loadings < 5 wt% and H/Rh > 0.5 up to 20 wt%), dispersion on TiO$_2$ is much lower. TPR/TPO shows this is due to the growth of two different kinds of Rh$_2$O$_3$/Rh on TiO$_2$; one kind is easily reduced/oxidized, showing high dispersion, the other kind is harder to reduce/oxidize, showing lower dispersion. TEM has shown that the first kind of Rh$_2$O$_3$ consists of flat, raft-like particles, the second kind of spherical particles.

3.2 INTRODUCTION

Over the past years rhodium has been gaining importance in catalytic chemistry. Not only is rhodium widely recognized as the best catalyst to promote the reduction of NO in three way catalysts (1-3), it also takes a special place in the conversion of synthesis gas, since its product range can include oxygenated products (alcohols, aldehydes, acids) besides hydrocarbons (4-11). Various workers have tried to influence the

selectivity and activity of the supported rhodium catalysts in syngas conversion via a special preparation (4, 5), via additives (6-8) and via control over the oxidation state of the rhodium in the catalysts (9-11).

Ichikawa deposited rhodium-carbonyl clusters on various supports (4, 5) and after pyrolysis of the clusters, he found a large range of selectivities towards oxygenates in the hydrogenation of CO. He explained this by the acid-base properties of the supports (12).

Somorjai c.s. tried to hydrogenate CO over unsupported rhodium and rhodium foil, and found only hydrocarbons, unless they pre-oxidized the metal (9). $H_2 + CO$ atmosphere led to the reduction to rhodium metal and the production of hydrocarbons, whereas $Rh_2O_3 \cdot 5H_2O$ was better resistant towards reduction and produced oxygenates for a long time (10).

Where the influence of additives or mixed oxides worked out into the right direction of enhanced oxygenate production, some workers traced this to the presence of rhodium ions in the surface (11, 13). The supposed presence of rhodium ions has been a point of discussion for quite some time. Several authors claimed it to be present in monometallic rhodium catalysts. Worley et al. investigated among others a 0.5 wt% Rh/Al_2O_3 catalyst via infrared spectroscopy of adsorbed CO (14-16), and ascribed several infrared bands to CO molecules bound to isolated Rh^{1+} sites. This is in contrast with earlier findings by D.J.C. Yates et al. (18). They investigated some Rh/Al_2O_3 catalysts with electron microscopy and found rhodium to be present as metallic rafts. They did not mention any isolated Rh^{1+} sites, but, as Worley and co-workers stipulated themselves, the two groups used very different methods of preparation of the samples.

In all cases it seems obvious that the support plays an important role in either bringing or keeping the metal in a certain state of (un)reactivity. A special example of such an interaction between metal and support has been described by Tauster et al. (19, 20) and is now known as Strong Metal Support Interaction (SMSI). Supported noble and transition

metals such as Pt, Rh, Ru etc. are normally capable of chemisorbing among others H_2 and CO. But if they are supported on oxides as TiO_2, V_2O_3 and Nb_2O_5, and if they have been reduced at high temperatures (e.g., 773 K), this chemisorption capability is greatly diminished. This SMSI phenomenon has been related to the occurrence of lower oxides of the supports (21), although these are known to be formed at lower temperatures than necessary to cause SMSI (22) and the exact nature of the interaction still remains unclear. The SMSI state can be destroyed according to Tauster c.s. by oxidation at elevated temperatures, followed by low temperature reduction (473 K): this procedure restores normal chemisorption behaviour (19).

All of the above mentioned phenomena have to do with one common property: the oxidation and reduction behaviour of supported rhodium catalysts. We therefore decided to study a number of Rh/Al_2O_3 and Rh/TiO_2 catalysts with varying metal loadings (see Experimental). Al_2O_3 was chosen because it is known as a support giving good dispersions and stable catalysts, and TiO_2 because it is known to exhibit SMSI. We varied the metal loading to create a variation in particle size, to see if and how oxidation, reduction and SMSI behaviour are influenced by particle size.

Before we come to the experimental techniques we used, we want to introduce another item: passivation. It is obvious that reduced catalyst systems cannot simply be removed from the reduction reactor and then be stored in air for later use; we stabilize the metal surface by applying a layer of oxygen upon the metal particles in a controlled way (see Experimental): we passivate the catalysts. Although a simple low temperature reduction is sufficient to remove the passivation oxygen again (as will be shown), some authors have given attention to the state the catalysts are in after storage in air. One can see this as a prolonged passivation, but without the precautions we take to prevent uncontrollable effects upon the first contact between air and the reduced metal catalyst. So Burwell Jr. et al. used Wide Angle X-ray Scattering, Extended X-ray Absorption Fine Structure, hydrogen chemisorption and hydrogen-

oxygen titration to characterize their supported Pt and Pd catalysts (23-26), and they found their catalysts to be oxidized to a great extent after prolonged storage in air.

We will show that a good insight into all these matters can be gained with the aid of Temperature Programmed Reduction and of Temperature Programmed Oxidation (TPR and TPO), supported by chemisorption measurements. TPR as a characterization technique was presented by Jenkins, Robertson and McNicoll in 1975 (27, 18) and has been used extensively in the past few years. The development has been reviewed by Hurst *et al.* (29). The technique allows one to get (semi)quantitative information about the rate and ease of reduction of all kinds of systems, and once the apparatus has been built the analyses are fast and relatively cheap. We used an apparatus as described by Boer *et al.* (30), which enabled us to extend the analyses to Temperature Programmed Oxidation, and to gather information about the rate and ease of oxidation as well.

3.3 EXPERIMENTAL SECTION

TiO_2 (anatase, Tioxide Ltd., CLDD 1367, surface area 20 m^2/g, pore volume 0.5 cm^3/g) and $\gamma-Al_2O_3$ (Ketjen, 000-1.5 E, surface area 200 m^2/g, pore volume 0.6 cm^3/g) were impregnated with aqueous solutions of $RhCl_3 \cdot xH_2O$ via the incipient wetness technique to prepare the catalysts. Their characteristics are presented in table 1 and table 2.

Table 1 Hydrogen chemisorption of the Rh/Al_2O_3 (RA) catalysts.

wt% Rh	H/Rh
2.3	1.53
4.6	0.96
8.5	0.81
11.6	0.67
20.0	0.54

Table 2 Hydrogen chemisorption of the Rh/TiO$_2$ (RT) catalysts.

wt% Rh	H/Rh	
	LT[1]	HT[2]
0.3	1.10	0.00
0.7	0.61	0.01
1.0	0.41	0.01
2.0	0.35	0.01
3.2	0.22	0.02
8.1	0.12	0.04

[1] reduced in situ at 523 K

[2] reduced in situ at 773 K

The catalysts will be denoted from now on as RT (Rh/TiO$_2$) and RA (Rh/Al$_2$O$_3$) catalysts, followed by the metal loading. After impregnation the catalysts were dried in air at 355, 375 and 395 K for 2 hours successively, followed by direct pre-reduction in flowing H$_2$ at 773 K for one hour. Prior to removing the catalysts from the reduction reactor they were passivated at room temperature by replacing the H$_2$ flow by N$_2$ and subsequently slowly adding O$_2$ up to 20%. Then the catalysts were taken out of the reactor and stored for further use.

In the TPR-TPO apparatus used, a 5% H$_2$ in Ar or a 5% O$_2$ in He flow can be directed through a microreactor, which is connected to a temperature programmer. H$_2$ or O$_2$ consumption is being monitored continuously by means of a Thermal Conductivity Detector (TCD). A typical sequence of experiments is as follows:
- the passivated or oxidized sample is flushed under Ar at 223 K,
- Ar is replaced by the Ar/H$_2$ mixture, causing at least an apparent H$_2$ consumption (first switch peak),
- the sample is heated under Ar/H$_2$ flow with 5 K/min to 873 K,
- after 15 min at 873 K, the sample is cooled down with 10 K/min to 223 K,
- the reduced sample is flushed with Ar,

- Ar flow is replaced by the Ar/H_2 mixture once more, now
  causing only an apparent H_2 consumption (second switch peak).

An identical sequence is followed during TPO, so the final
oxidation temperature in TPO is also 873 K, unless stated
otherwise.

The switch peak procedure deserves some closer attention.
The strong signal we call the first switch peak is due mainly
to the displacement of Ar by Ar/H_2 in the reactor, but in some
cases real hydrogen consumption might take place, even at 223 K.
Therefore, we repeat the whole procedure after the TPR has
been performed: in that case the catalyst has been reduced
and cooled down to 223 K, and as a consequence it is covered
by hydrogen. Then we replace the Ar/H_2 by pure Ar. Subsequently,
we switch back to Ar/H_2. Since we cannot expect any hydrogen
consumption from the reduced, hydrogen covered sample at this
time, the resulting second switch peak will be due solely to
the displacement of Ar by Ar/H_2. So the difference between the
first and second switch peak reveals the real hydrogen con-
sumption at 223 K, if there is any.

The reactions that might take place during TPO and TPR are:

$$4Rh + 3O_2 \rightleftarrows 2Rh_2O_3 \qquad (O_2/Rh = 0.75)$$
$$Rh_2O_3 + 3H_2 \rightleftarrows 2Rh + 3H_2O \quad (H_2/Rh = 1.50).$$
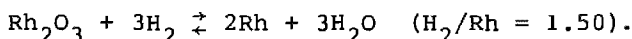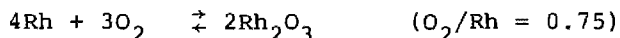
The quantities between brackets are the hydrogen or oxygen
consumptions in TPR or TPO expected for reduction of bulk
Rh_2O_3 or formation of this very material (apart from chemisorp-
tion of any kind). In a standard experiment a TPR is done on
a passivated catalyst, followed by TPO (on the now reduced
catalyst), followed by TPR (on the now oxidized catalyst).

Chemisorption measurements were carried out in a con-
ventional glass apparatus after reduction of the passivated
catalysts at 773 K in flowing H_2 for one hour, followed by
evacuation at 473 K for another hour. After hydrogen
admission at 473 K desorption isotherms were measured at
room temperature. For the RT series 773 K (High Temperature)
reduction will induce SMSI, and so the RT catalysts were also
reduced at 523 K (Low Temperature) to study their normal

chemisorption behaviour. In measuring the desorption isotherms desorption became only noticeable at pressures below 200 torr (1 torr = 133.3 N/m^2) so we believe that the chemisorption value above that pressure is representative of monolayer coverage (*cf*. Frennet *c.s.* (31)).

Transmission Electron Microscopy was carried out on a Jeol 200 CX top entry stage microscope. Photographs were taken at a magnification of 430,000 times, and then enlarged further photographically to `a final magnification of 1,290,000 times. TEM measurements were done on samples pre-oxidized at 900 K. This temperature was chosen because, as TPO measurements will show, for some samples this temperature is necessary to cause total oxidation. Samples were prepared by applying a slurry of the catalyst in alcohol onto a coal coated copper grid, and evaporating the alcohol.

Metal loadings were established for the passivated samples colourimetrically.

3.4 RESULTS

3.4.1 HYDROGEN CHEMISORPTION
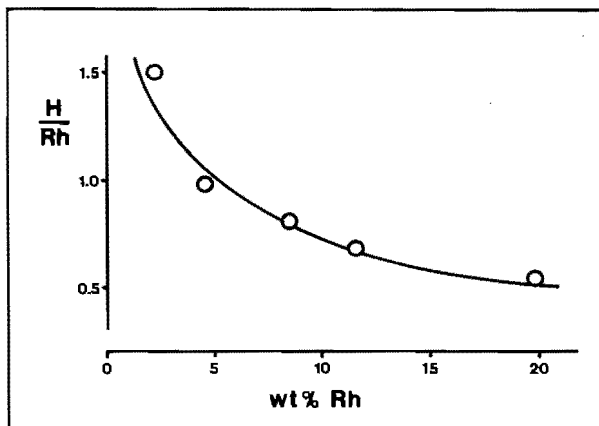
Figure 1 Hydrogen chemisorption of Rh/γ-Al$_2$O$_3$ catalysts as a function of metal loading. Reduction temperature was 773 K.

The hydrogen chemisorption data as given in table 1 for the RA series (Rh/Al_2O_3) are represented graphically in figure 1. In a similar way the data from table 2, for the RT series (Rh/TiO_2), are presented in figure 2.
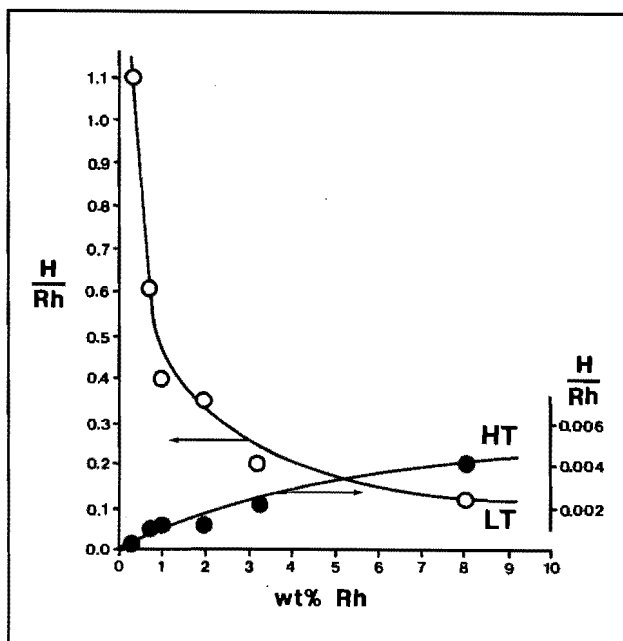
Figure 2 Hydrogen chemisorption of Rh/TiO_2 catalysts as a function of metal loading. Reduction temperature was 473 K (LT) or 773 K (HT).

For Rh/Al_2O_3, the H/Rh value drops below 1.0 somewhere around 5 wt% loading but H/Rh is still above 0.5 at 20 wt% (which catalyst had to be prepared via two successive impregnation and drying steps). For Rh/TiO_2 reduced at 523 K H/Rh decreases much faster with increasing metal loading, and drops below 1.0 before the metal loading reaches 0.5 wt%. Of course we must keep in mind the 10 times larger surface area of the alumina, but it is obvious that anatase is less capable of stabilizing small rhodium particles than alumina. For Rh/TiO_2 reduced at

773 K, some hydrogen chemisorption is still measurable at high metal loadings, but the measured values are of the order of magnitude of experimental error.

The attentive reader will have noticed by now that the catalysts must have been already in the SMSI-state after the pre-reduction at 773 K. The fact that they do show normal chemisorption behaviour after 523 K reduction implies that the passivation treatment they received has nullified SMSI.

The reduction and oxidation behaviour of a selected number of these catalysts, RA 2.3, 4.6 and 20.0 and RT 0.3, 1.0, 3.2 and 8.1 will be presented below.

3.4.2 TPR/TPO OF THE RA SERIES

The Temperature Programmed Reduction profiles of the passivated RA catalysts are similar. The one for RA 2.3 is shown in figure 3.

H$_2$-uptake

223   273   573   873 K
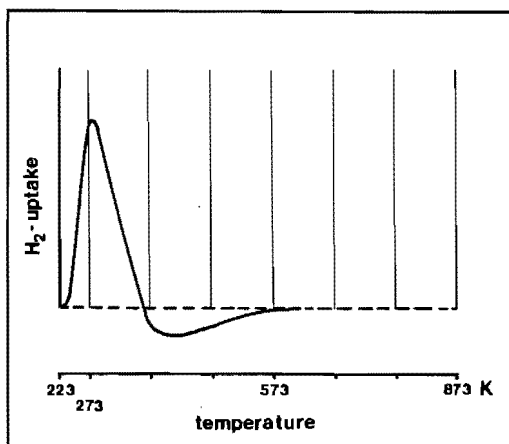
temperature

Figure 3 Temperature Programmed Reduction of passivated 2.3 wt% Rh/γ-Al$_2$O$_3$.

The horizontal axis shows the temperature, the vertical axis hydrogen consumption in arbitrary units.

All three catalysts show a hydrogen consumption maximum

below 300 K, followed by a slight desorption. Hydrogen con-
sumption decreases from 1.33 H_2/Rh for RA 2.3 (which is almost
enough to account for the reduction of stoichiometric Rh_2O_3),
to 0.49 H_2/Rh for RA 20.0 (average oxidation state of the rhodium
in this case was +1).

The subsequent TPO profiles show more difference. For all
three catalysts (see figure 4a, b, c), oxygen consumption
starts at 223 K, that is in the switch peak.
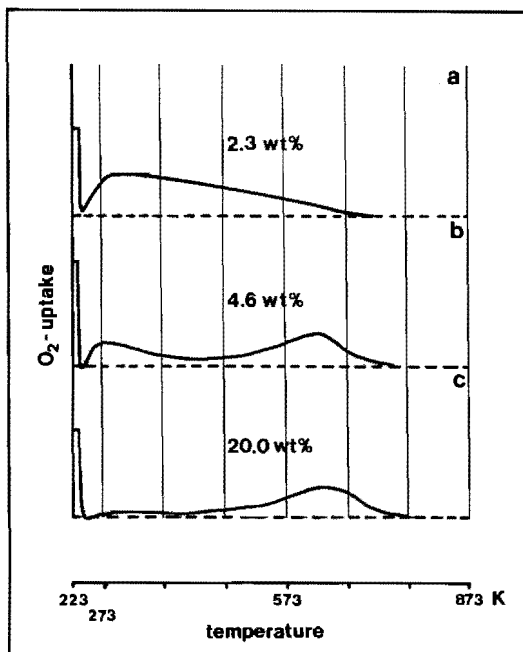
Figure 4 Temperature Programmed Oxidation of reduced
        $Rh/\gamma-Al_2O_3$: 2.3 wt% (a), 4.6 wt% (b) and 20.0 wt% (c).

For RA 2.3 the oxygen consumption rises at the beginning of
the temperature ramp, to reach a maximum at 300 K, and to fall
down slowly towards higher temperatures. Total oxygen con-
sumption mounts up to 0.65 O_2/Rh. The behaviour of RA 20.0
(figure 4c) is quite different. After some oxygen consumption
in the switch peak, oxygen consumption keeps a low level for

several hundreds degrees of temperature raise, to reach a maximum at 628 K. O_2/Rh is 0.70. The behaviour of RA 4.6 was an intermediate one (figure 4b). Integration of the oxygen consumption signal proved difficult, because of the small thermal conductivity of O_2, and due to the small sample sizes (typically 50-75 micromole of metal).

The TPR profile of the oxidized catalysts is shown in figure 5, and is alike for all three of them.
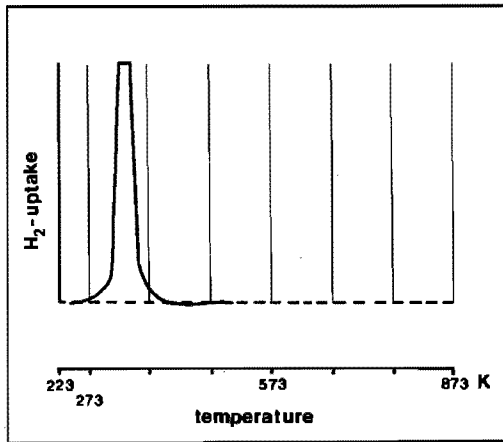
Figure 5 TPR of oxidized 20.0 wt% Rh/γ-Al$_2$O$_3$.

One sharp and well-defined peak at about 340 K, with an H_2/Rh value ranging from 1.3 (RA 20.0) to 1.6 (RA 2.3). In all three cases we assume we have to do with the reduction of supported Rh_2O_3. Unsupported Rh_2O_3 in our apparatus showed a reduction peak at 400 K, while bulk rhodium metal only started to become bulk-oxidized above 870 K.

3.4.3 TPR/TPO OF THE RT SERIES

Figure 6 shows the TPR profiles of the passivated catalysts RT 0.3, RT 1.0, RT 3.2 and RT 8.1. With increasing metal loading, in other words decreasing H/Rh values, we see the reduction peak disappear into the switch peak at 223 K. For RT 0.3 the
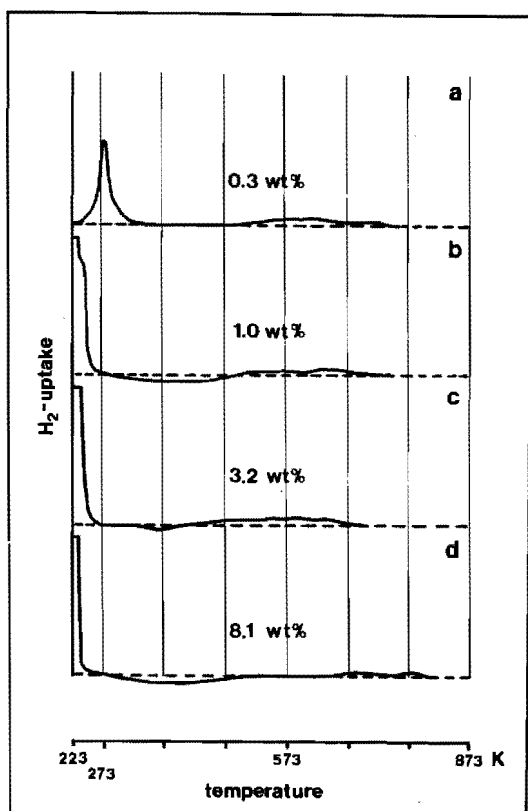
Figure 6 TPR of passivated Rh/TiO$_2$; 0.3 wt% (a), 1.0 wt% (b), 3.2 wt% (c) and 8.1 wt% (d).

reduction peak is still completely separated from the switch peak, with a maximum at 273 K and an H$_2$/Rh of 0.56, for RT 8.1 the reduction peak has merged with the switch peak and the hydrogen consumption has dropped to H$_2$/Rh = 0.25. We believe the explanation for this lies in the fact that with decreasing H/Rh (and for RT 1.0 the H/Rh ratio is not more than 0.41, still lower than for RA 20.0) the metal particles keep a metallic core upon passivation. Hydrogen molecules can diffuse through the outer passivated layer of the particle, reach the metallic core and dissociate there to provide atomic hydrogen

for an easy reduction of the oxide layer at low temperature.

   We find a support for this idea in figure 7 showing the
TPO profiles of the respective catalysts.
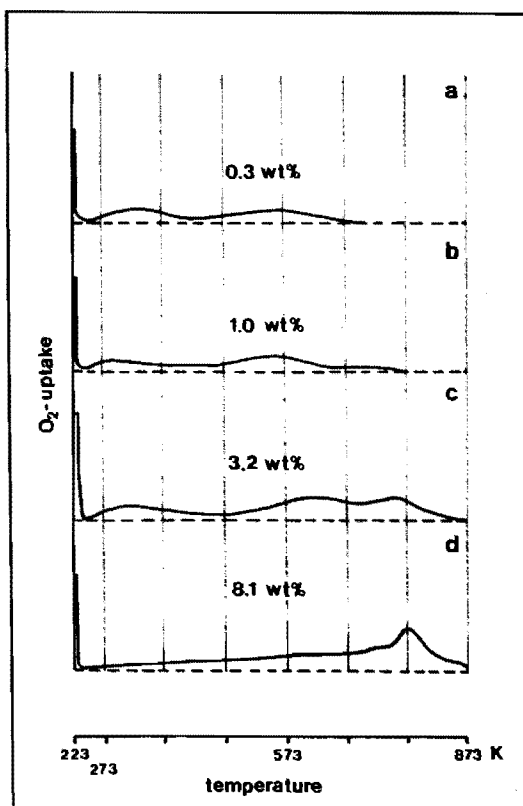
*Figure 7 TPO of reduced Rh/TiO$_2$; 0.3 wt% (a), 1.0 wt% (b),
3.2 wt% (c) and 8.1 wt% (d).*

All catalysts show some oxygen consumption as soon as the
temperature ramp has been started. The two low-loaded catalysts,
RT 0.3 and RT 1.0 (7a and 7b) have an early consumption
maximum around 300 K, like RA 2.3, but also show distinct con-
sumption around 600 K, while RA 20.0 had a maximum around 620 K.
In figure 7c, RT 3.2, we can distinguish three areas of
oxygen consumption apart from the switch peak: around 350 K,

600 K and a new maximum at 770 K. This consumption at 770 K is dominant in figure 7d, the TPO of the reduced RT 8.1 catalyst. At first glance we can attribute the low temperature oxygen consumption to chemisorption and the high temperature oxygen consumption to thorough oxidation, but we will come back to this in the Discussion. Anyway, it is this last observation, the high temperature needed for thorough oxidation, that con-firms the presence of a metallic core in larger particles after passivation. O_2/Rh is about 0.7 for all RT catalysts.

In figure 8 we see the TPR profiles of the oxidized catalysts, and a very interesting phenomenon shows up here.
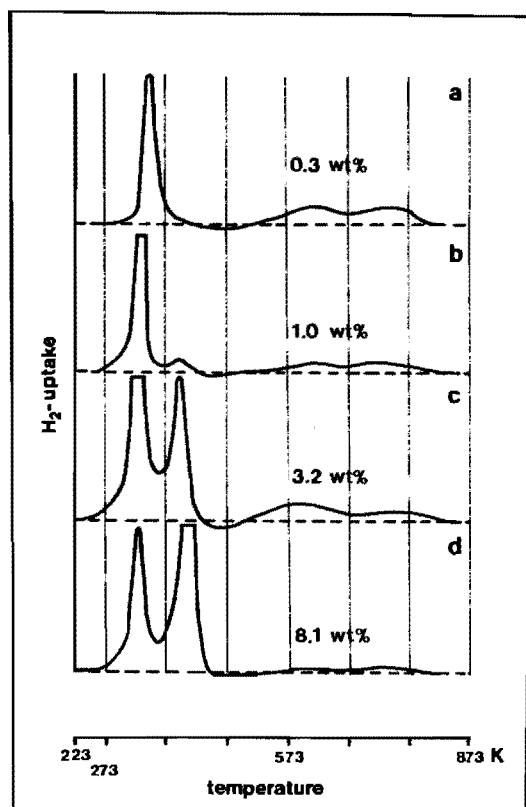
Figure 8 TPR of oxidized Rh/TiO$_2$; 0.3 wt% (a), 1.0 wt% (b), 3.2 wt% (c) and 8.1 wt% (d).

RT 0.3 and RT 1.0 show only one clear consumption maximum, 330-340 K, H_2/Rh = 1.20, like the RA catalysts (figure 5). But RT 3.2 and RT 8.1 have a second consumption maximum at 385-400 K, about the temperature where unsupported bulk Rh_2O_3 reduces. Taken both peaks together, H_2/Rh is about 1.70 for RT 3.2 and 1.41 for RT 8.1, so both peaks can without any doubt be ascribed to the reduction of Rh_2O_3. To be more specific, the low temperature TPR peak must belong to well-dispersed, ill-defined Rh_2O_3, which is also easily formed, while the high temperature TPR peak belongs to the reduction of bulk-like, crystalline Rh_2O_3, which can only be formed by the high temperature oxidation. This was proven earlier (32) by halting a TPO experiment at a temperature intermediate between the two maxima at 600 and 770 K. A subsequent TPR proved to miss the second reduction peak, so the 770 K TPO peak is connected to the 400 K TPR peak, and the low temperature TPR and TPO peaks must, as a consequence, be connected too.

In all cases, after a slight desorption of H_2, H_2 consumption rises again above baseline, showing two maxima around 600 and 740 K. We think this must be attributed to reduction of the support in the neighbourhood of the metal; the bare support does not reduce below 800 K.

3.4.4 TEM MEASUREMENTS

To make the difference between the Rh_2O_3 reducible at 330 K and the Rh_2O_3 reducible at 400 K more clear, we reduced part of the impregnated RT 1.0 batch at 773 K without drying, a method already used by Burwell $c.s.$ (24) to prepare catalysts with low dispersions. After oxidation at 900 K for 1 hour we performed a TPR, shown in figure 9a. One single reduction peak for Rh_2O_3, at 410 K was observed. The subsequent TPO, shown in figure 9b, run this time up to 973 K, shows that oxidation proceeds readily only at about 900 K. The H/Rh value of the catalyst, after the 900 K oxidation and a 523 K reduction in situ, was 0.20.
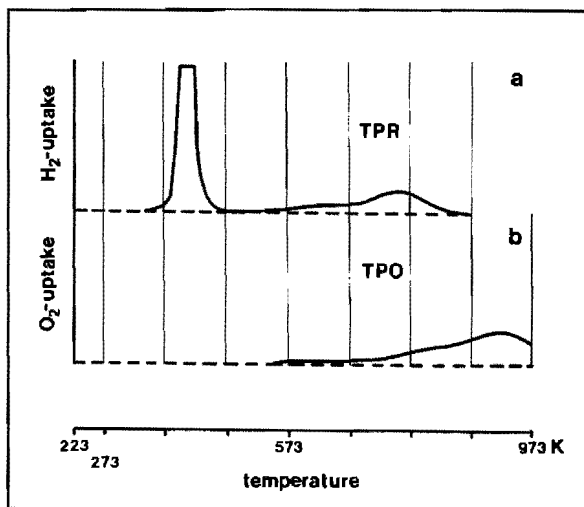
*Figure 9 1.0 wt% Rh/TiO$_2$, wet reduced; TPR of oxidized system
(a) and TPO of reduced system (b).
Note the temperature axis in TPO.*

We examined this catalyst, RT 1.0 (wet), and the comparable
RT 1.0 (figure 8b, 7b) catalyst with Transmission Electron
Microscopy (TEM). Samples were prepared by applying a slurry of
the at 900 K oxidized catalysts in absolute alcohol on a coal
coated grid, and evaporating the alcohol. TEM micrographs are
shown in figure 10. Figure 10a shows the bare support, anatase,
as received from the manufacturer. Clearly visible is that the
TiO$_2$ particles (in the order of magnitude of 50 nm in diameter)
are covered with very tiny seed-crystals of TiO$_2$, which
apparently, due to the poor sintering capacities of these kinds
of oxides, did not get the chance to grow into larger particles.
In figure 10b (RT 1.0) we find them back as conglometares
(clustered together in the impregnation and drying steps of the
preparation) like the one indicated by arrow A. The other
particles on the TiO$_2$ surface show the uniform density and smooth
outline characteristic for heavy metal oxide particles, diameter
ranging from 1-6 nm. The uniform colour of the particles is
an indication that they are actually flat (raft-like). In

62
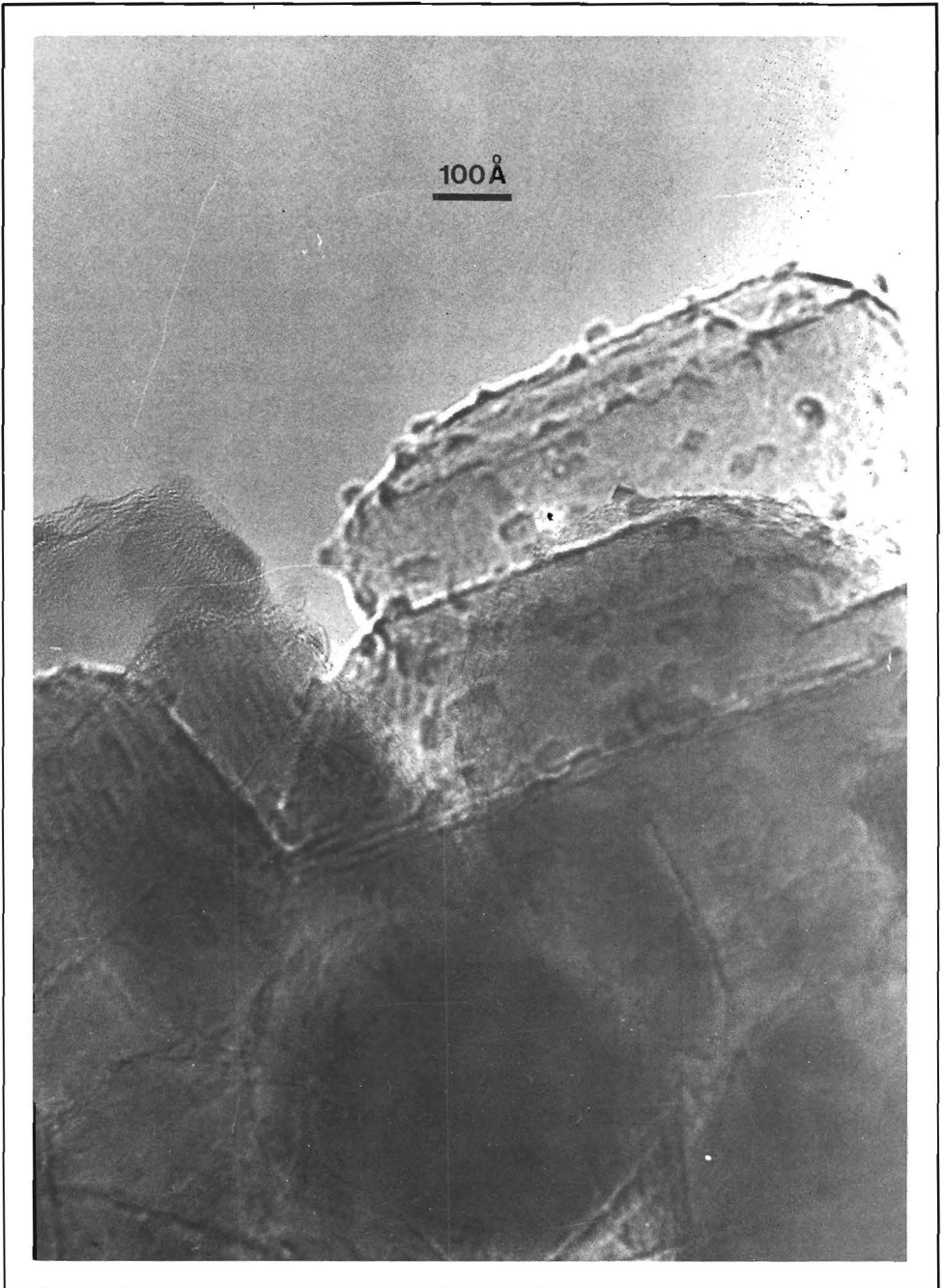
Figure 10a Transmission electron micrograph of anatase TiO_2.
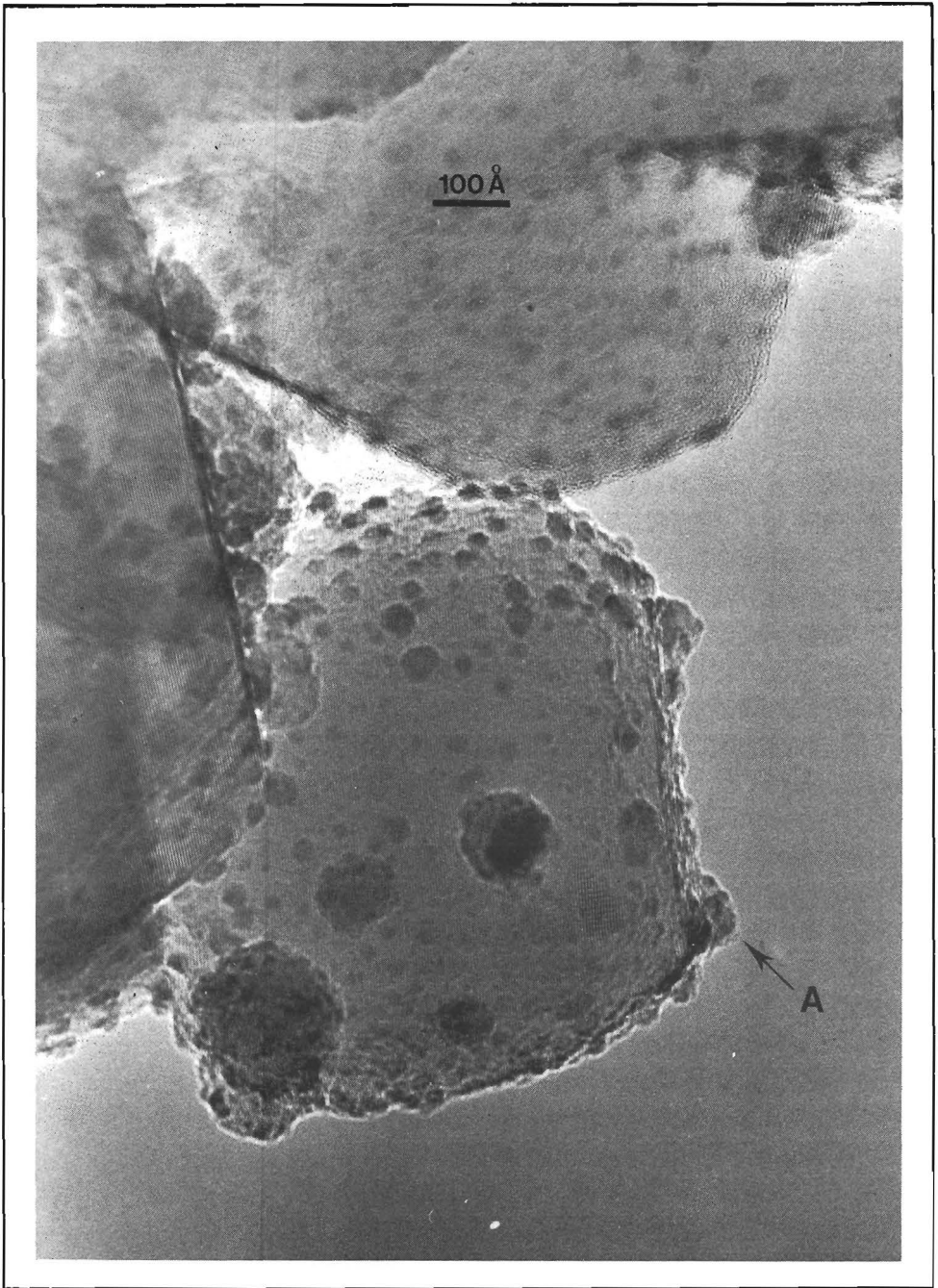
Figure 10b Transmission electron micrograph of 1.0 wt%
Rh_2O_3/TiO_2 (H/Rh = 0.4).
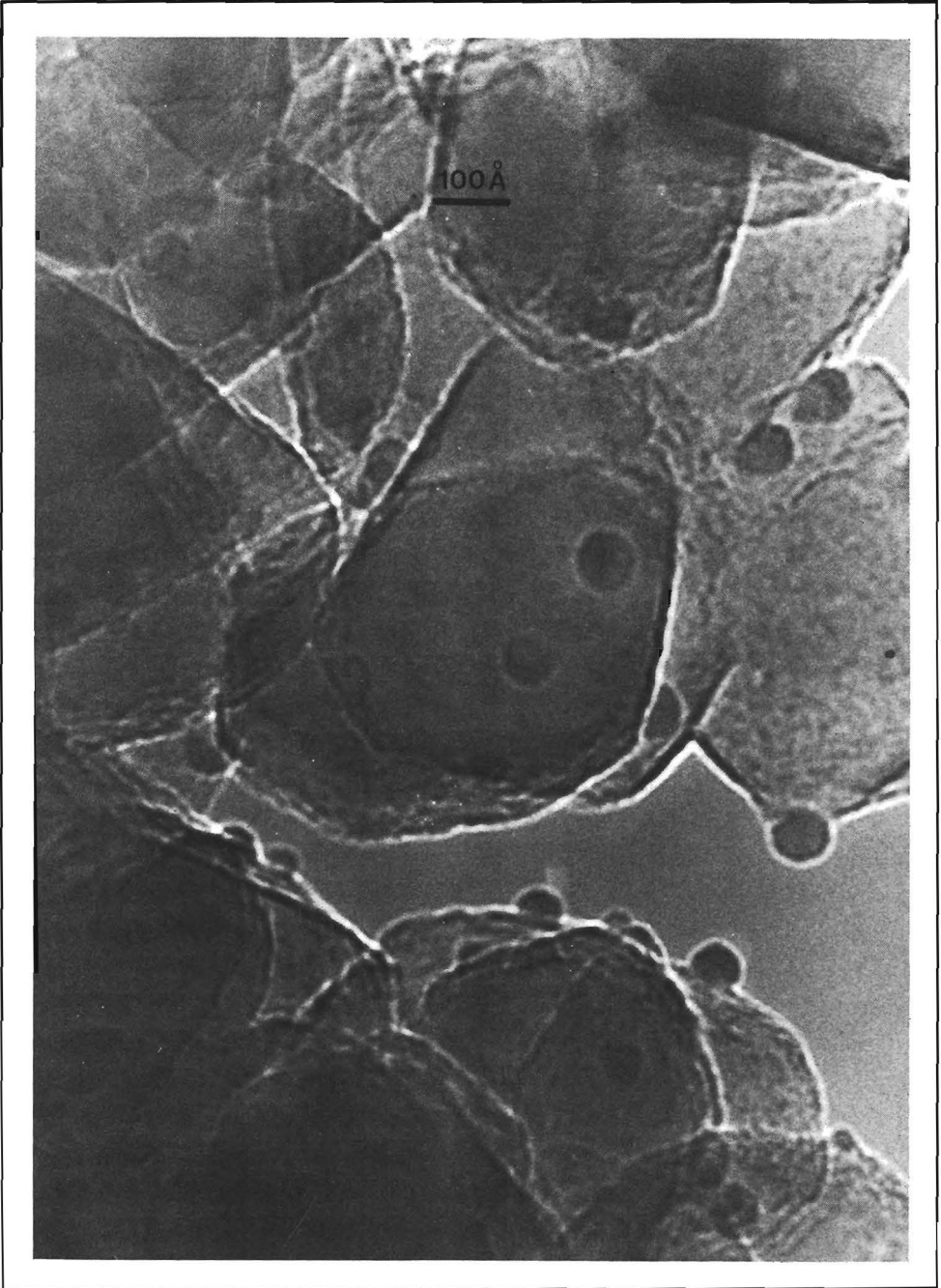
Figure 10c Transmission electron micrograph of 1.0 wt%
Rh_2O_3/TiO_2 (H/Rh = 0.2).

figure 10 c (RT 1.0 (wet)) the TiO_2 conglomerates are no longer
visible. Apparently they got the chance during the high
temperature reduction in the presence of water to spread over
the surface of the large TiO_2 particles. The particles we do
see, are Rh_2O_3 particles. The lighter contours of the particles
indicate that they are spherical. Their diameter is about 7 nm.

3.5 DISCUSSION

Hydrogen chemisorption has been used through the years
by many workers to characterize metal surfaces (10, 12, 13,
17, 19, 23-26, 33, 34) and when attempts were made to calculate
metal surface areas from hydrogen chemisorption data, a
hydrogen-metal stoechiometry of one was always used. On the
other hand, if CO was involved, some authors (35) chose a
stoechiometry of one, while others (18) preferred higher
stoechiometries. From figures 1 and 2 it becomes clear though,
that also H/Rh values can exceed unity. For Rh/TiO_2 this
occurs for metal loadings below 0.5%, and for Rh/Al_2O_3 even
for metal loadings up to 5%. Although in this study only two
catalysts occur with an H/Rh value above unity, we have reported
about other ultra dispersed systems elsewhere (32, 36). And in
our opinion, if one accepts a metal atom, such as rhodium, to
adsorb two or more CO molecules, one should not reject the
idea of that same atom adsorbing more than one hydrogen atom.
So we think that also in those cases where H/Rh exceeds unity,
the hydrogen chemisorbed does not exceed a monolayer
(*cf.* Frennet (31)) and is all bound to the metal. A consequence
of this is the impossibility to calculate a particle size from
chemisorption data for highly dispersed systems, since there
is no way of calculating the number of rhodium surface atoms.
For larger, well defined particles as we found in RT 1.0 (wet),
with an H/Rh of 0.2, the calculated particle size is 6 nm
which is in good accordance with our TEM measurements (figure
10 c).

The H/Rh values measured for Rh/TiO_2 after reduction at

773 K (figure 2), that is with rhodium in the SMSI-state, seem to show a tendency to increase, but the values measured are still that small that we do not want to draw any con-clusions from that without further study.

From all TPR/TPO measurements presented here the following picture comes up. Rhodium on a support can occur in either a dispersed form, or in a bulk-like form. The dispersed form is easy to reduce to the metal, giving a reduction peak in TPR around 340 K. It is also easily oxidized, which manifests itself in TPO's such as figures 4a, 7a and 7b, and from the fact that upon passivation the oxidation state of the Rh can almost reach 3+ (*cf.* figure 3, H_2/Rh = 1.33). That reaction with oxygen is vehement, even at room temperature, shows also in the fact that prolonged passivation breaks SMSI (if not, one would not have seen any hydrogen consumption at all after the low temperature reduction, since the RT catalysts would still be in the SMSI-state induced by the 773 K pre-reduction). The exact assignment of the three TPO peaks is difficult since the literature does not provide much material about the mechanism of oxidation of supported metal catalysts. But the metal oxidation theory, dealing with bulk materials, does provide three separated phenomena as stages in the oxidation process. Rapid chemisorption is known to occur at clean surfaces (37) at low temperatures. Formation of an oxide film occurs at temperatures typically up to 573-673 K, following logarithmic rate equations, and leading to an oxide film with a thickness from 2 nm (38) to 100 nm (39, 40). Finally, Wagners oxidation theory (41) describes how the oxidation process goes on, rate-controlled by volume diffusion of the reacting ions and/or of electrons through the growing oxide scale, leading to parabolic rate equations. We can imagine that analogous models can describe the oxidation processes in supported metal particles as well, dependent on their sizes.

It is very clear that no matter how the rhodium is present on the support, dispersed or not, oxidized or passivated, reduction to metallic rhodium is complete at 400 K, that is, above that temperature no hydrogen consumption can be ascribed anymore to the reduction of rhodium oxide. We cannot conclude

from this evidence only that bimetallic systems such as the Rh/Fe system discussed above (11, 13) will be metallic at that temperature too. But in the case of a bimetallic system reduction tends to take place completely at the temperature where the easier reducible compound would have been reduced in a monometallic system (42).

We can conclude from our measurements that the systems which Worley et $al.$ have studied (14-16) must have been fully reduced prior to admission of carbon monoxide. They found four major infrared absorption peaks: 2100 and 2030 cm^{-1}, called the twin absorption and attributed to an $Rh^{1+}(CO)_2$ compound; 2050-2080 cm^{-1}, attributed to an Rh^0CO compound; 1850-1900 cm^{-1}, attributed to bridged carbonyl species. Of interest is also that the twin absorption peaks are attributed to isolated rhodium sites, since the wavenumbers of these two peaks are independent of CO coverage, unlike the others. For 2.2 wt% rhodium catalysts they found that Al_2O_3 as a support led to more twin absorption than TiO_2, and $RhCl_3$ as a precursor gave more twin than $Rh(NO_3)_3$. They concluded that $Rh(NO_3)_3$ is more easily reduced than $RhCl_3$, and better still on TiO_2 than on Al_2O_3, thus leaving most unreduced rhodium in the case of $RhCl_3/Al_2O_3$, the catalyst with the most intense twin absorption. We prefer another explanation, since we know that reduction must have been complete in all cases. Rh/Al_2O_3 gives the most twin absorption because it is the best dispersed system after reduction. Upon CO adsorption the very small rhodium particles are broken up by CO dissociation, what leads to graphitic carbon on the support and Rh^{1+}, ready to adsorb two CO molecules to give the twin IR absorption. EXAFS proof for this explanation has been published elsewhere (36).

Our findings are in good accordance with the results published by Burwell Jr. $c.s.$ for Pd and Pt on SiO_2 and Al_2O_3 (23-26). Upon exposure to air larger metal particles form an oxide skin which slows down further oxidation. Logarithmic law type oxidation is a separate step (figure 4c $e.g.$), and thorough (parabolic) oxidation occurs first at 700 K. Apparently diffusion through the oxide layer is strongly hindered.

The finding of two distinguishable phases of rhodium on a support has been reported earlier by Yao and Shelef (43), although they used Al_2O_3 as a support. We did not succeed in creating bulk-like rhodium on Al_2O_3 by increasing the metal loading the way we did in the case of TiO_2, but by wet reduction of the impregnated catalyst it proved possible to make a catalyst which is oxidized above 700 K and reduced at 390 K.

3.6 CONCLUSIONS

Hydrogen chemisorption clearly showed the difference between Al_2O_3 and TiO_2 as a support for rhodium. On Al_2O_3 H/Rh was above 1.0 up to 5 wt% and still was above 0.5 for 20.0 wt%, whilst in the case of TiO_2 H/Rh dropped below 1.0 before 0.5 wt% was reached. The meaning of this difference for the behaviour of rhodium in oxidation-reduction showed in TPR/TPO.

On Al_2O_3 Rh_2O_3 reduces around 340 K, and rhodium oxidizes via chemisorption, starting at 223 K, followed by formation of an oxide skin around 630 K.

On TiO_2 part of the rhodium behaves in the same way. The other part is harder to reduce (around 390 K) and to oxidize (around 800 K).

When we make a catalyst by wet reduction (supposed to be sintered), all of the reduction takes place at 400 K, and all of the oxidation even above 850 K. In TEM we see these Rh_2O_3 particles as spherical, about 7 nm diameter, while in an equally loaded, properly reduced catalyst Rh_2O_3 particles ranged from 1 to 6 nm and showed no sign of a spherical form.

Hydrogen chemisorption does show a tendency at higher metal loadings to survive high temperature reduction, that is part of the rhodium seems to be unaffected by SMSI, but the chemisorption measured is actually too small to draw conclusions from it at this very moment.

It has been shown in this paper that with a suitable choice of a limited number of techniques one can obtain a very

good insight into the state a catalyst can be brought in by impregnation and oxidation-reduction. Needless to say this is of major importance for further use of the catalyst.

3.7 REFERENCES

1. K.C. Taylor, in "The Catalytic Chemistry of Nitric Oxides", edited by R.L. Klinisch and J.G. Larson, Plenum Press, New York (1975).
2. T.P. Kobylinski and B.W. Taylor, J. Catal., 33, 376 (1974).
3. H.C. Yao, Y.-F. Yao and K. Otto, J. Catal., 56, 21 (1979).
4. M. Ichikawa, Bull. Chem. Soc. Jap., 51, 2268 (1978).
5. M. Ichikawa, Bull. Chem. Soc. Jap., 51, 2273 (1978).
6. E.I. Leupold, H.-J. Schmidt, F. Wunder, H.-J. Arpe and H. Hachenberg, E.P. 0 010 295 A1.
7. F.A. Wunder, H.-J. Arpe, E.I. Leupold and H.-J. Schmidt, Ger. Offen. 28 14 427.
8. W.J. Bartley and T.P. Wilson, Eur. Pat. Appl. 0 021 443.
9. D.G. Castner, R.L. Blackadar and G.A. Somorjai, J. Catal., 66, 257 (1980).
10. P.R. Watson and G.A. Somorjai, J. Catal., 72, 347 (1981).
11. P.R. Watson and G.A. Somorjai, J. Catal., 74, 282 (1982).
12. M. Ichikawa and K. Shikakura, in "Proceedings of the 7th International Congress on Catalysis", edited by T. Seyana and K. Tanabe, Elsevier, Amsterdam, (1981), Part A, p.925.
13. T.P. Wilson, P.H. Kasai and P.C. Ellgen, J. Catal., 69, 193 (1981).
14. C.A. Rice, S.D. Worley, C.W. Curtis, J.A. Guin and A.R. Tarrer, J. Chem. Phys., 74, 6487 (1981).
15. S.D. Worley, C.A. Rice, G.A. Mattson, C.W. Curtis, J.A. Guin and A.R. Tarrer, J. Chem. Phys., 76, 20 (1982).
16. S.D. Worley, C.A. Rice, G.A. Mattson, C.W. Curtis, J.A. Guin and A.R. Tarrer, J. Phys. Chem., 86, 2714 (1982).
17. M. Primet, J.C.S. Farad. Trans. II, 74, 2570 (1978).
18. D.J.C. Yates, L.L. Murrell and E.B. Prestridge, J. Catal., 57, 42 (1979).

19. S.J. Tauster, S.C. Fung and R.L. Garten, J. Am. Chem. Soc., 100, 170 (1978).

20. S.J. Tauster, S.C. Fung, R.T.K. Baker and J.A. Horsley, Science, 211, 1121 (1981).

21. R.T.K. Baker, E.B. Prestridge and R.L. Garten, J. Catal., 50, 464 (1979).

22. T. Huizinga and R. Prins, J. Phys. Chem., 85, 2156 (1981).

23. T. Uchijima, J.M. Herrmann, Y. Inoue, R.L. Burwell Jr., J.B. Butt and J.B. Cohen, J. Catal., 50, 464 (1977).

24. M. Kobayashi, Y. Inoue, N. Takahashi, R.L. Burwell Jr., J.B. Butt and J.B. Cohen, J. Catal. 64, 74 (1980).

25. R.K. Nandi, P. Georgopoulos, J.B. Cohen, J.B. Butt and R.L. Burwell Jr., J. Catal., 77, 421 (1982).

26. R.K. Nandi, F. Molinaro, C. Tang, J.B. Cohen, J.B. Butt and R.L. Burwell Jr., J. Catal. 78, 289 (1983).

27. S.D. Robertson, B.D. McNicol, J.H. de Baas, S.C. Kloet and J.W. Jenkins, J. Catal., 37 424 (1975).

28. J.W. Jenkins, B.D. McNicol and S.D. Robertson, Chem. Tech., 7, 316 (1977).

29. N.W. Hurst, S.J. Gentry, A. Jones and B.D. McNicol, Catal. Rev.-Sci. Eng., 24, 233 (1982).

30. H. Boer, N.F. Boersma and N. Wagstaff, Rev. Sci. Instr., 53, 349 (1982).

31. A. Crucq, L. Degols, G. Lienard and A. Frennet, Acta Chim. Acad. Sci. Hung., 1982, 111.

32. J.C. Vis, H.F.J. van 't Blik, T. Huizinga, J. van Grondelle and R. Prins, J. Mol. Catal., in press.

33. J.H. Sinfelt and D.J.C. Yates, J. Catal., 10, 362 (1968).

34. S.E. Wanke and N.A. Dougharty, J. Catal., 24, 367 (1972).

35. M.M. Bhasin, W.J. Bartley, P.C. Ellgen and T.P. Wilson, J. Catal., 54, 120 (1978).

36. H.F.J. van 't Blik, J.B.A.D. van Zon, T. Huizinga, J.C. Vis, D.C. Koningsberger and R. Prins, J. Phys. Chem., 87, 2264 (1983).

37. G. Ehrlich, in "Conference on Clear Surfaces", Ann. N.Y. Acad. Sci., 101 (1963), Art. 3.

38. N. Cabrera, in "Semiconductor Surface Physics", edited by
    R.H. Kingston, University of Pennsylvania Press,
    Philadelphia (1957).

39. N. Birks and H.G. Meier, in "Introduction to High Tempera-
    ture Oxidation of Metals", Edward Arnold (Publishers) Ltd.,
    London (1983).

40. P. Kofstad, in "High-temperature Oxidation of Metals",
    Wiley & Sons, New York (1966).

41. C. Wagner, in "Atom Movements", Amer. Soc. Metals,
    Cleveland, (1951), p. 153.

42. N. Wagstaff and R. Prins, J. Catal., 59, 434 (1979).

43. H.C. Yao, S. Japar and M. Shelef, J. Catal., 50, 407
    (1977).

chapter 4

CHARACTERIZATION OF BIMETALLIC Co-Rh/Al$_2$O$_3$ AND Co-Rh/TiO$_2$ CATALYSTS WITH TPR AND TPO

4.1 ABSTRACT

Temperature programmed reduction and oxidation has been used to characterize the metal compounds in a series of Co-Rh/γ-Al$_2$O$_3$ and Co-Rh/TiO$_2$ catalysts. The results show that the presence of rhodium improves the reducibility of cobalt based catalysts. However, in the case of cobalt-rhodium/alumina addition of rhodium does not prevent the formation of cobalt aluminate which compound proves to be irreducible below 773 K. Strong evidence has been obtained that the different metal ions are in intimate contact with each other after co-impregnation of the supports leading to the formation of bimetallic particles after catalyst reduction. The bimetallic Co-Rh/TiO$_2$ catalyst as well as the corresponding monometallic catalysts show strongly reduced chemisorption properties after reduction above 773 K (SMSI). Passivation of the reduced bimetallic catalysts leaves the bimetallic particles largely intact but cobalt is oxidized to a great extent whereas rhodium is hardly affected by oxygen. This suggests a covering of rhodium by cobalt oxide. A thorough oxidation of the bimetallic catalysts leads to a remodelling of the particles by which both metal oxides are in intimate contact. High temperatures are needed for complete oxidation of Co-Rh/TiO$_2$ through which formation of CoRh$_2$O$_4$ is possible. The TPR results obtained for the monometallic Co/TiO$_2$ catalyst clearly demonstrate that reduction

of Co_3O_4 is a two-stage process: Co_3O_4 is reduced to metallic cobalt via CoO.

4.2 INTRODUCTION

Bimetallic catalysts are of interest for several industrial processes. The attractiveness of these catalysts lies in their superior stability and selectivity for many reactions (1-3). With respect to the Fischer-Tropsch reaction it has been shown that alloying of two metals, both of which are active catalysts, may improve the catalytic properties compared to the properties of the constituent monometallic catalysts (4-7). Wise and co-workers have reported a maximum in selectivity for C_2 plus C_3 hydrocarbons for unsupported precipitated (1:1) FeCo catalysts (8). Using an FeRh/SiO$_2$ catalyst, Bhasin *et al.* observed an increase in selectivity for methanol and ethanol compared to either supported iron or supported rhodium catalysts (9).

In our laboratory we are interested in Co-Rh catalysts supported on γ-Al_2O_3 and titania. γ-Al_2O_3 is a support which shows little or no effect on activity or selectivity in the Fischer-Tropsch reaction, whereas some metals exhibit their highest activities for CO hydrogenation when dispersed on titania (10, 11). Little information has been published concerning Fischer-Tropsch synthesis using the Co-Rh catalytic system. Recently, however, Villeger *et al.* (12) have shown that addition of Rh to Co results in an increase of the selectivity to ethene and propene. In chapter 9 we will discuss the catalytic behaviour of the bimetallic Co-Rh system with respect to the Fischer-Tropsch reaction.
But before doing so we will in this chapter pay attention to the preparation of Co-Rh catalysts and the formation of small bimetallic clusters dispersed on the surface of γ-Al_2O_3 and TiO_2. The monometallic Rh/Al_2O_3 and Rh/TiO_2 systems have been extensively discussed in chapter 3. A comprehensive characterization study of Co supported on titania has not been published

up to now, whereas substantial information is available about monometallic Co on alumina (13-21). It is known that cobalt strongly interacts with γ-Al_2O_3 to produce a Co-aluminate-spinel which is difficult to reduce (22). Chin and Hercules (13) used X-ray photoelectron spectroscopy and secondary ion mass spectrometry to study the surface properties of a series of impregnated Co/Al_2O_3 catalysts. They observed changes of the surface characteristics of the catalysts and attributed these to metal-support interactions which arise from the diffusion of Co ions into lattice sites of the γ-Al_2O_3 support during calcination. The fraction of Co ions interacting with the support increased as the metal loading was decreased and/or the calcination temperature was increased. Moreover, the reducibility of the catalysts was shown to be directly related to the degree of metal-support interaction. Characterization studies performed on Co-Rh systems have not been published yet.

Before using a bimetallic catalyst for catalytic studies a question of interest is: will the very small metal particles, formed during preparation, be monometallic or will there be mixing of atoms of the different metals to form bimetallic particles? On purely statistical grounds one might expect that the individual particles would contain atoms of both metals. Direct experimental verification of the presence of bimetallic particles is complicated by limitations in the ability of physical methods. The Temperature Programmed Reduction and Oxidation technique (TPR, TPO) can, however, serve as a sensitive tool to obtain evidence for the interaction between the atoms of the two metallic components.

One of the first studies in which TPR was used as a characterization technique was performed by Robertson *et al.* (23, 24). They studied the reduction of Cu-Ni/SiO_2 catalysts and from the results they affirmed complete reduction of the metals and they were able to identify alloying. TPR has proven useful also in the characterization of Pt-Re/Al_2O_3 and Pt-Ir/Al_2O_3 reforming catalysts (25-27). For Pt-Re/Al_2O_3 evidence was found for an intimate contact between the two metals after reduction.

Calcination in air of the reduced samples above 473 K caused
segregation of platinum oxide and rhenium oxide.
Paryjczak *et al.* (28) demonstrated the power of TPO in the
characterization of bimetallic Rh-Ag/SiO$_2$ catalysts. The
TPO profiles for these systems showed features intermediate to
the characteristics of the pure components. Furthermore, it
was found that the shape of the TPO profiles and the relative
contributions of individual peaks depend on the degree of metal
dispersion.

In this chapter we present the results of a characteriza-
tion study of the Co-Rh system supported on alumina and titania
with the aid of TPR and TPO. Hydrogen chemisorption and ferro-
magnetic resonance (FMR) spectroscopy have been used for further
characterization. The formation of the bimetallic particles
during reduction of the impregnated catalysts and their stability
during oxidation will be discussed.

4.3 EXPERIMENTAL SECTION

The bulk metals Co and Rh and the bulk Co-Rh alloy with
a Co/Rh atomic ratio of 1 were prepared by evaporating the
corresponding aqueous solutions of the metal salts Co(NO$_3$)$_2$.6H$_2$O
(Merck P.A.) and RhCl$_3$.xH$_2$O (39 wt%, Drijfhout) at 393 K,
followed by a direct reduction by heating at 5 K/min to 1073 K
and staying at that temperature for 5 hours. The monometallic
bulk oxides Co$_3$O$_4$ and Rh$_2$O$_3$ were prepared by oxidizing the
reduced metals at 1073 K for 72 hours. CoO was obtained from
Merck. The mixed oxide CoRhO$_x$ was prepared by evaporating an
aqueous solution of the metal salts followed by a direct
oxidation at 1073 K (heating rate 5 K/min) for 48 hours.
TiO$_2$ (anatase, Tioxide Ltd., CLDD 1367, surface area 20 m^2/g,
pore volume 0.5 cm^3/g) and γ-Al$_2$O$_3$ (Ketjen, 000-1.5 E, surface
area 200 m^2/g, pore volume 0.6 cm^3/g) were (co-)impregnated
with aqueous solutions of the metal salts via the incipient
wetness technique to prepare monometallic Co and Rh and
bimetallic Co-Rh catalysts. The catalysts were dried in air at
393 K for 24 hours after which a part of each batch was stored

for further use and the other part was directly reduced in flowing H_2 by heating at 5 K/min to 773 K staying at that temperature for one hour, and subsequently cooled in H_2 to room temperature. Prior to their removing from the reduction reactor the catalysts were passivated at room temperature by replacing the H_2 flow by N_2 and by subsequently slowly adding O_2 up to 20%. The Co and Rh contents of the dried catalysts were determined by using respectively atomic absorption spectroscopy and colourimetry. The catalysts which have been prepared are summarized in table 1.

Table 1

Catalyst	wt% Co	wt% Rh	H/M 473[1]	H/M 773[2]
Co/Al_2O_3	4.44			0.09
Co_4Rh/Al_2O_3	3.18	1.39		0.13
$CoRh/Al_2O_3$	1.97	3.43		0.39
Rh/Al_2O_3		2.30		1.53
Rh/Al_2O_3		4.70		0.96
Rh/Al_2O_3		8.53		0.81
Co/TiO_2	2.01		0.14	0.06
Co/TiO_2	1.00		0.13	0.04
$Co_{1.2}Rh/TiO_2$	1.19	1.72	0.19	0.09
Rh/TiO_2		3.20	0.22	0.02

[1] Based on H_2 adsorption at room temperature after re-reduction at 473 K.

[2] Based on H_2 adsorption at room temperature after re-reduction at 773 K.

Hydrogen chemisorption measurements were carried out in a conventional volumetric glass apparatus after reduction of the passivated γ-Al_2O_3 catalysts at 773 K in flowing hydrogen for one hour, followed by evacuation at 573 K for another hour, or after reduction of the passivated TiO_2 catalysts at 473 K

or 773 K for one hour, followed by evacuation at 473 K for
another hour. After H_2 admission at 473 K and cooling down
adsorption isotherms were measured at room temperature. The
H/M value was obtained by extrapolating the linear higher
pressure region (P > 30 kPa, above which monolayer coverage
has been reached) of the isotherm to zero pressure and by sub-
traction of the contribution of the bare support. The H/Rh
values thus obtained for the various catalysts are presented
in table 1.

In order to measure FMR spectra a reactor designed by
Konings *et al.* (29) has been used. X-band FMR spectra were
recorded with a Varian E-15 spectrometer at room temperature.
Signal intensity, position of the signal and quality factor
of the FMR cavity were calibrated with the aid of a Varian
strong pitch sample (g = 2.0028, 3×10^{15} spins/cm).

TPR, TPO and TPD experiments were carried out with 5%
H_2 in Ar, 5% O_2 in He and 100% Ar respectively, with about
200 mg catalyst in an apparatus similar to that described by
Boer *et al.* (30). The flow rate of gases through the reactor
was 5 cm^3/min and the temperature was raised at 5 K/min during
TPR and TPO and at 15 K/min during TPD within the temperature
range of 223 K to 773 K.
The following typical sequence of treatments in the TPR
apparatus has been used:
- the impregnated, passivated or oxidized sample was flushed
  under Ar flow at 223 K,
- Ar was replaced by the Ar/H_2 mixture, causing at least an
  apparent H_2 consumption (first switch peak),
- the sample was heated under Ar/H_2 flow with 5 K/min to 773 K,
- after 1 hour at 773 K the sample was cooled down with
  10 K/min to 223 K,
- the reduced sample was flushed with Ar,
- Ar flow was replaced by the Ar/H_2 mixture once again, now
  causing only an apparent H_2 consumption (second switch peak).
  The reason for this switch peak procedure has been discussed
  in chapter 3.
A similar sequence has been followed during TPO, albeit that
the final temperature was varied. When the TPR of an Al_2O_3

supported catalyst was followed by a TPO the sequence was
extended by heating the catalyst at 573 K for half an hour,
in order to desorb hydrogen, after which the catalyst was
cooled down to 223 K again. Note that for a TiO_2 supported
catalyst this extension is not necessary, because after
reduction at 773 K hydrogen chemisorption is suppressed. The
latter phenomenon is known as Strong Metal Support Interaction
(SMSI) (31).

4.4 RESULTS AND DISCUSSION

4.4.1 UNSUPPORTED BULK Co, Rh AND Co-Rh

It is known from literature that Co and Rh are completely
miscible (32). The phase diagram of the two metals is presented
in figure 1.
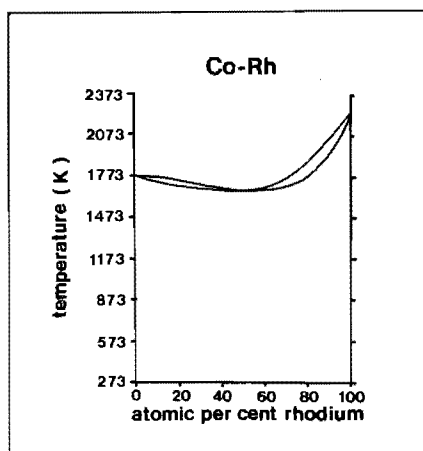
Figure 1 Co-Rh phase diagram.

In figure 2 the X-ray diffraction (XRD) patterns (Cu Kα radiation)
are shown for a physical mixture of cobalt and rhodium and for
the Co-Rh alloy. About the crystallographic structure of the
alloy, however, not much information is available. The
diffraction pattern in figure 2a is formed by two peaks, the

larger one being the (111) diffraction peak of rhodium with fcc structure and the smaller one the (111) diffraction peak of cobalt with fcc structure.
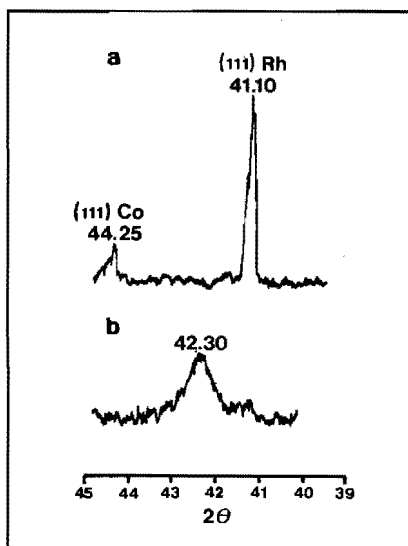
Figure 2. X-ray diffraction patterns (Cu Kα radiation).
        a) Physical mixture of metallic Co and Rh.
        b) Co-Rh alloy (molar ratio is 1).

From the 2θ values the Rh-Rh and Co-Co interatomic distances are calculated to be 2.688 Å and 2.505 Å, respectively. The XRD pattern for the alloy (see figure 2b) shows a main peak at $2\theta = 42.30°$ which is in between the peaks of the constituent alloy components. On the assumption that the structure of the alloy is fcc and that the peak can be attributed to the (111) diffraction the shortest metal-metal distance is on the average 2.615 Å. This value is slightly higher (0.017 Å) than predicted by Vegard's rule (which rule assumes a linear relation between the interatomic distance in an alloy and the atomic ratio of the metals).

    In figure 3 the XRD patterns (Cu Kα radiation) are presented for a physical mixture of Co_3O_4 and Rh_2O_3 and the mixed $CoRhO_x$ oxide. Between $\Delta 2\theta = 32° - 38°$ four diffraction peaks can be distinghuished for the physical mixture. The peaks at
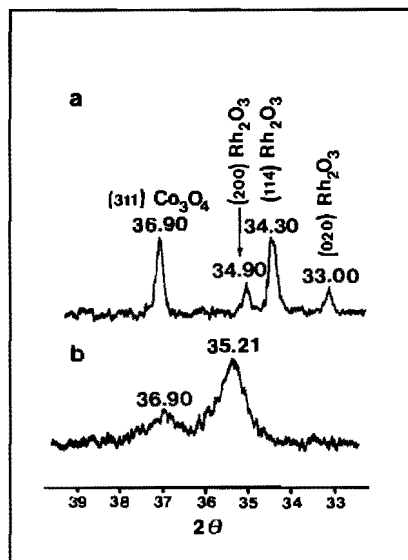
Figure 3 X-ray diffraction patterns (Cu Kα radiation).
a) Physical mixture of Co_3O_4 and Rh_2O_3.
b) $CoRhO_x$ mixed oxide.

$2\theta = 33.00°$, $34.30°$ and $34.90°$ are assigned to, respectively, the (020), (114) and (200) diffractions of Rh_2O_3 (corundum structure) and the peak at $2\theta = 36.90°$ to the (311) diffraction of Co_3O_4 (spinel structure). The XRD pattern of the mixed oxide is characterized by two peaks. We assign the larger peak to a diffraction of $CoRh_2O_4$ which can be formed at 1073 K and higher temperatures (33). $CoRh_2O_4$ is a normal spinel with Co^{2+} ions at tetrahedral positions and Rh^{3+} at octahedral positions. As we used an oxide with a Co/Rh stoechiometry of 1 a residue of cobalt is present after the formation of $CoRh_2O_4$. The position of the weaker diffraction peak is equal to the one in Co_3O_4. Therefore, we conclude that the residual cobalt was oxidized to Co_3O_4.

In order to obtain more insight into the reducibility of the bulk oxides we recorded TPR profiles of the different oxides mixed with Al_2O_3. The results are presented in figure 4.
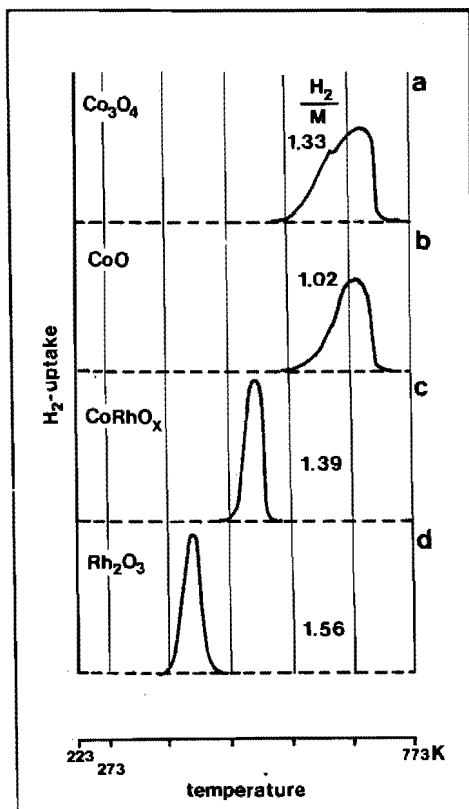
Figure 4 TPR profiles for bulk oxides.
a) Co_3O_4, b) CoO, c) $CoRhO_x$ and d) Rh_2O_3.

The numbers next to the TPR profiles correspond to the ratio
between hydrogen consumed and the total amount of metal in
moles. The reduction process of bulk Co_3O_4 and CoO starts
not until 523 K (cf. respectively, figure 4a and 4b). It is
seen that the profiles for the two bulk oxide samples are very
similar, with peak maxima of 685 K for CoO and 703 K for Co_3O_4.
However, for Co_3O_4 a second maximum at 648 K is observed. The
two maxima for Co_3O_4 suggest a two-stage reduction process.
This result is in a satisfactory agreement with the investiga-
tions carried out by Brown et al. (22) and Paryjczak et al. (34).

However, the latter group observed a maximum of the main peak in the Co_3O_4 TPR profile at 673 K, which is 12 K lower than in our case, even though they used a higher heating rate as well as a higher gas flow, which factors induce in general a shift of the peak maximum to higher temperatures (35).

The observed H_2/M value of 1.02 for CoO is consistent with the theoretically expected value of 1.00. Note that the H_2 consumption in the TPR has been calibrated by means of Co_3O_4 (i.e. $CoO_{1.33}$). The TPR profile of bulk Rh_2O_3 is characterized by a sharp single peak at 408 K (figure 4d). The observed H_2/M value of 1.56 is equal to the theoretical value within experimental error.

The reduction of the oxidized Co-Rh alloy with an atomic Co/Rh ratio of 1 takes place within the temperature range of 453-523 K (figure 4c). According to the XRD results the mixed oxide consists of $CoRh_2O_4$ and Co_3O_4. The theoretical H_2/M value is therefore 1.33. Within the expected experimental error, the observed H_2/M value of 1.39 is in accordance with this. A striking feature is that the reduction profile is characterized by a sharp single peak. This indicates that the phase separated Co_3O_4 is nevertheless in intimate contact with $CoRh_2O_4$ and that the latter serves as a catalyst for the reduction of Co_3O_4, because the Co_3O_4 is already reduced at a temperature at which it would start to reduce without the presence of cobalt rhodate.

4.4.2 Co, Rh and Co-Rh supported on $\gamma-Al_2O_3$

The hydrogen chemisorption results for Co, Rh and Co-Rh on $\gamma-Al_2O_3$ are summarized in table 1. The H/M values of a 4.70 and a 8.53 wt% Rh/$\gamma-Al_2O_3$ are given too. By a linear interpolation between these two values one obtains a value of H/M = 0.84 for a 7.75 wt% Rh catalyst. This loading corresponds to the same ratio between the amount of metal and the surface area of the support as for the monometallic cobalt catalyst, and dramatically demonstrates the high difference in dispersion of cobalt and rhodium on Al_2O_3. It can be clearly seen that the dispersion of the bimetallic catalysts increases with rhodium

content. As described in the Experimental Section we admitted
hydrogen at 473 K. Although, in contradistinction to rhodium,
adsorption of hydrogen on cobalt is an activated process (36),
we did not observe an effect of temperature on the ultimate
amount of adsorption. Adsorption was accelerated though, and
equilibrium was reached much faster.

TPR, TPO and TPD profiles of the alumina-supported Co,
Co_4Rh and Rh catalysts are shown in figure 5. The numbers next
to the profiles correspond to the ratio between the amount of
gas consumed and the total amount of metal.
Reduction of the 4.44 wt% $Co/\gamma-Al_2O_3$ catalyst after impregnation
and drying occurs within the temperature range 443-653 K and
is characterized by a single broad peak with its maximum at
543 K (figure 5a). The theoretical H_2/M value for the reduction
of Co^{2+} to metallic Co is 1.00. The observed H_2/M value of 1.75
exceeds the theoretical value because of the simultaneous
reduction of residual nitrate groups. The reduction of the
impregnated and dried 2.30 wt% $Rh/\gamma-Al_2O_3$ catalyst already
starts at 273 K (figure 5a). The TPR profile peaks at 363 K
and has a weak tail up to 773 K. In anticipation of the TPR
results of the impregnated Rh/TiO_2 we assign the peak to the
reduction of well dispersed $RhCl_3$, probably bound to the support
in the form of $-(OH)_3-RhCl_3$ complexes, the hydroxyl molecules
of which belong to the support. The reduction behaviour of
these species might be similar to the one of passivated or
oxidized highly dispersed rhodium. No crystalline $RhCl_3$ is
present because in that case the peak maximum would have been
at about 413 K (37). As hydrogen consumption is only caused by
the reduction of rhodium ions to metallic rhodium the observed
H_2/M value of 1.50 indicates that, indeed, the starting
material was in the 3+ oxidation state.
A striking feature of the TPR profiles for the bimetallic
catalysts is that the impregnated and dried Co_4Rh and CoRh
supported catalysts are already reduced to a great extent before
the reduction of the monometallic cobalt catalyst even starts.
This indicates that the initiation of the reduction of the
cobalt salt is aided by the presence of rhodium. The catalytic
effect of rhodium can be explained by assuming that the very

84
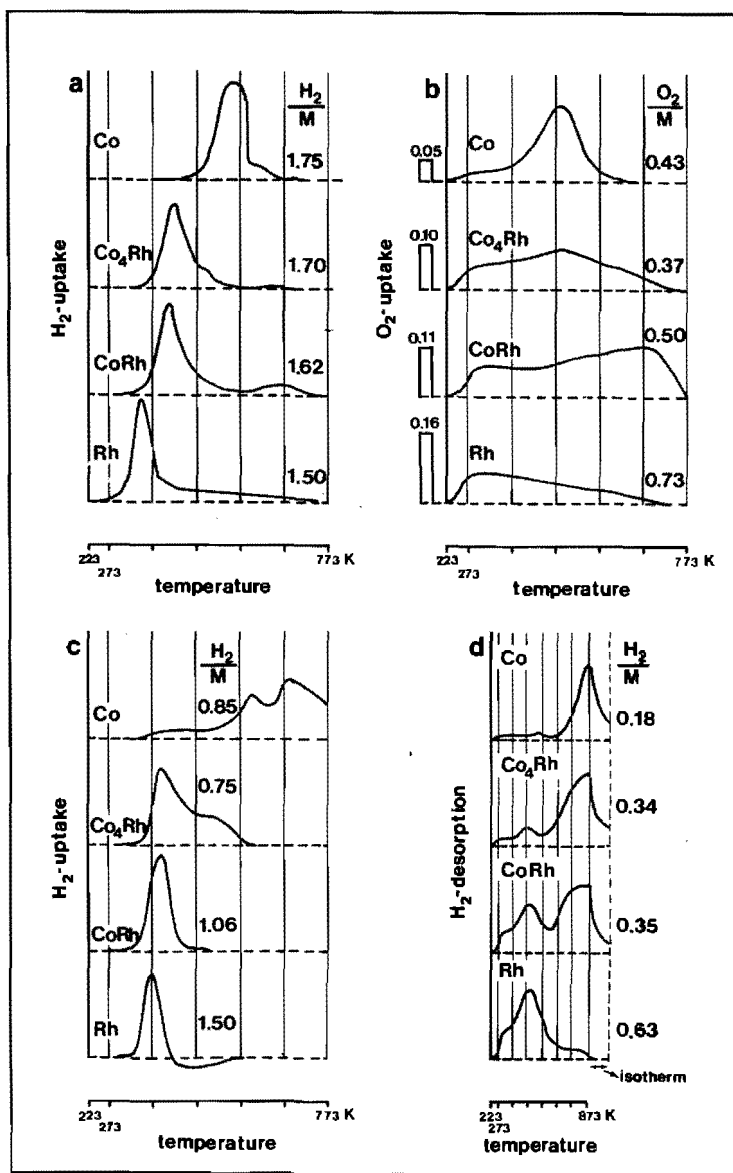
Figure 5 TPR, TPO and TPD profiles for alumina-supported Co
(4.44 wt%), Co₄Rh (4.57 wt%) CoRh (5.40 wt% and
Rh (2.30 wt%) catalysts.
a) TPR of the impregnated and dried catalysts.
b) TPO of the reduced catalysts.
c) TPR of the oxidized catalysts.
d) TPD of the reduced catalysts, the metal particles
of which are covered with hydrogen.

first formed metallic rhodium acts as a nucleation centre.
(Note that supported rhodium chloride is reduced before the
reduction of cobalt nitrate starts.) At these sites hydrogen
molecules are dissociated to yield hydrogen atoms which are
more reactive for reduction than the molecules and consequently
reduce the cobalt nitrate earlier. The maxima of the TPR profiles
corresponding to the bimetallic systems are shifted to higher
temperatures compared to the one of the impregnated monometallic
rhodium catalysts. The shift is more pronounced with increasing
cobalt content. The positions of the maxima are at about 413 K,
the same temperature at which crystalline $RhCl_3$ is reduced. For
the same reason as mentioned for the reduction of supported
$Co(NO_3)_2$ the observed H_2/M values for both supported bimetallic
catalysts cannot be used to determine the degree of reduction
of the catalysts.
These TPR results of the impregnated catalysts give strong
evidence for the formation of bimetallic Co-Rh particles after
reduction. We exclude the possibility that the two metals are
segregated, because in bulk these metals are completely miscible.

The hydrogen chemisorption results show that the dis-
persion of the bimetallic catalysts and the monometallic cobalt
catalyst is significantly lower than that of the monometallic
rhodium catalyst (*cf*. table 1). This raises the intriguing
question by what factors the dispersions of these catalysts are
determined. We will first focus our attention to the mono-
metallic systems. Beyond all doubts the interaction between
cobalt and alumina is stronger than the interaction between
rhodium and the support. It appears that in Co/Al_2O_3 cobalt always
forms a cobalt spinel, possibly as an epitaxial layer between
the $\gamma-Al_2O_3$ and the cobalt metal (14). Interactions based on
interdiffusion of metal oxides with the oxidic support are
strong. However, from the hydrogen chemisorption results it is
clear that rhodium is much better dispersed on alumina than
cobalt. Although we must make a correction for the loss of
cobalt metal caused by cobalt aluminate formation (see later),
which when taken into account leads to an increase of the
cobalt H/M value, the real H/M value for the monometallic

cobalt catalyst will not exceed 0.20. The low dispersion can only be understood when it was assumed that before reduction the cobalt was poorly dispersed on alumina. This might be explained by sintering of CoO which is formed by decomposition of $Co(NO_3)_2$ during drying of the impregnated catalyst. The change in colour of the impregnated catalyst from violet to black proves the decomposition of $Co(NO_3)_2$. Another explanation might be that no sites for the adsorption of cobalt ions are present. The pH of the aqueous solution of cobalt nitrate used for the impregnation is about 3, which means that the hydroxyl groups of the support are protonated to $\overset{H^+}{-}$ OH. Therefore, the adsorption of cobalt ions which are present as $Co(H_2O)_6^{2+}$ in solution might be hindered by repulsion.

$RhCl_3$ does not suffer from adsorption problems because it is present as a neutral molecule $(RhCl_3(H_2O)_3)$ in an acidic aqueous solution, or even as an anionic chloride complex. An explanation for the relative low H/M values observed for the bimetallic catalysts might be that during co-impregnation and drying the metal salts have not been homogeneously spread over the support. This vision is supported by the TPR results. The TPR profiles obtained for the impregnated bimetallic catalysts peak at about the same temperature (413 K) as crystalline $RhCl_3$, whereas well dispersed $RhCl_3$ gives rise to a TPR profile with a maximum at 363 K. Apparently, the presence of cobalt nitrate hinders the formation of a well dispersed $RhCl_3$-phase on the alumina surface. During the impregnation a cobalt surface spinel $(CoAl_2O_4)$ might be formed, through which a modification of the alumina surface occurs. Adsorption of $RhCl_3$ might then be hampered.

It is obvious that the upper level of dispersion for a metal catalyst is already determined in an early stage of preparation: the choice of metal precursor. In order to improve the dispersions for the cobalt containing catalysts we propose to use in future an aqueous solution of $CoCl_2$.

The TPO profiles (figure 5b) of the four systems supported on alumina show already oxygen consumption at 223 K due to chemisorption. From the observed O_2/M values one can determine

the degree of reduction of the catalyst after the first TPR by
assuming that after oxidation Co_3O_4 and Rh_2O_3 are formed.
Oxidation of the reduced monometallic cobalt catalyst already
starts at 223 K and is complete after 593 K. Maximum oxygen
consumption takes place at 483 K. The observed O_2/M value of
0.43 indicates that the average oxidation state of cobalt after
the first TPR, and before the TPO measurement, was 0.95+. TPO
profiles of a reduced 1.00 and a 2.02 wt% $Co/\gamma-Al_2O_3$ catalyst
(not shown) displayed hardly any O_2 consumption. The average
oxidation states of cobalt in these catalysts after reduction
were calculated to be respectively 2+ and 1.9+. The formation
of $CoAl_2O_4$ in the three cobalt catalysts, mentioned above,
after the first TPR and a subsequent passivation has been
determined using UV reflectance spectroscopy. The $CoAl_2O_4$
signal hardly differed in intensity for these catalysts.
Therefore, we conclude that after reduction of the 4.44 wt%
$Co/\gamma-Al_2O_3$ catalyst $CoAl_2O_4$ as well as metallic cobalt were
formed and that during the subsequent TPO only the metallic
cobalt was oxidized to Co_3O_4. It is known that after calcination
of a Co/Al_2O_3 catalyst three cobalt species exist on the
catalyst surface: 1) a species resulting from diffusion of Co
ions into tetrahedral lattice sites of $\gamma-Al_2O_3$ (often referred
to as a 'surface spinel' (38)), 2) Co ions in octahedral sites
of the support and/or 3) 'bulk-like' Co_3O_4. The presented results
demonstrate that even after a direct reduction of the impregna-
ted and dried cobalt catalyst a significant amount of the so-
called 'surface spinel' is still present. From the observed
O_2/M value it is calculated that the amount of cobalt which
had been converted to $CoAl_2O_4$ was 1.55 wt%.
The TPO profile recorded for the reduced 2.3 wt% $Rh/\gamma-Al_2O_3$
catalyst (figure 5b) is characteristic for an ultra dispersed
system. This has been discussed in detail in chapter 3. The
observed O_2/M value of 0.73 indicates that after the TPR run
all rhodium was completely reduced and that all rhodium was
oxidized to Rh_2O_3 during the TPO run.
The TPO profiles for the two reduced bimetallic catalysts
demonstrate that oxidation of the catalyst is more difficult

with increasing rhodium content. In order to discuss this phenomenon we refer to chapter 3 where a TPO profile for a less well dispersed 11.64 wt% $Rh/\gamma-Al_2O_3$ catalyst (H/M = 0.67) is presented. Two'areas' of oxygen consumption showed up in the profile, which were attributed to corrosive chemisorption and thorough oxidation respectively. The latter is characterized by a peak around 723 K. The dispersions of the bimetallic systems are lower than the one of the 11.64 wt% $Rh/\gamma-Al_2O_3$ catalyst. Since the latter shows the same TPO profile we assign the oxygen consumption above 573 K to thorough oxidation of rhodium.

From the observed O_2/M values, we cannot calculate the exact amount of $CoAl_2O_4$ in the bimetallic catalysts formed after the first TPR. An upper and lower limit can be determined, however. On the basis of the TPR/TPO results obtained for the monometallic rhodium catalyst we assume that rhodium in the bimetallic system can be reduced to Rh^0 during TPR and completely oxidized to Rh_2O_3 during TPO. The upper limit of the amount of $CoAl_2O_4$ formed after the first TPR is obtained when assuming that the metallic cobalt during TPO was oxidized to Co_3O_4, and the lower limit when it is assumed that the cobalt was oxidized to CoO. We thus calculated that the amounts of Co in the form of $CoAl_2O_4$ for the Co_4Rh and CoRh supported catalysts were respectively, 1.43-1.87 wt% and 0.99-1.22 wt%. For the mono-metallic catalyst we calculated 1.55 wt% Co. This indicates that the presence of Rh does not prevent the formation of $CoAl_2O_4$ very much.

Reduction of the oxidized monometallic cobalt is difficult (figure 5c), it starts not until 473 K and is still incomplete at 773 K. The TPR profile is characterized by two peaks, one at about 573 K and the other at about 673 K. Comparison of the profile for bulk Co_3O_4 (figure 4a) with the one for supported cobalt oxide indicates that also in the catalyst the reduction of Co_3O_4 is a sequential process. This result is in accordance with the TPR results reported by Paryjczak et $al.$ (34). From experiments carried out at the University of Amsterdam

- we thank Peter Arnoldy for doing these measurements - it
followed that the temperature had to be raised up to 1373 K
in order to reduce the oxidized cobalt catalyst completely.
Hydrogen was consumed to a great extent between 1073 and 1373 K,
probably caused by reduction of the surface $CoAl_2O_4$ spinel.
The ratio between the hydrogen consumed during the second TPR
and the oxygen consumed during the TPO preceding the TPR
should be 2, because the oxygen consumed is converted to H_2O
in the subsequent TPR. All values observed in the TPO and
subsequent TPR runs agree with this factor of 2, within the
uncertainty of the measurements. This indicates that the
oxidized cobalt formed during TPO was reduced completely during
the subsequent TPR up to 773 K. Consequently, during TPO no new
surface spinel $CoAl_2O_4$ was formed ·that is irreducible under
773 K.

Reduction of supported Rh_2O_3 is complete above 400 K. The
TPR profile is characterized by a single consumption peak around
363 K followed by desorption of H_2. The net H_2 consumption
mounted up to 1.52 H_2/Rh indicating a reduction degree of
rhodium after reduction of 100 per cent.

The TPR profiles for the oxidized bimetallic Co-Rh/Al_2O_3
catalysts demonstrate that cobalt oxide is in intimate contact
with rhodium oxide because the reduction of the less noble
metal, cobalt, is catalyzed by the noble metal, rhodium. The
TPR profile for Co_4Rh/Al_2O_3 shows up a shoulder at 503 K which
might be ascribed to particles with either a low Rh concentration
or even without Rh present. The maxima of the TPR profiles for
the bimetallic catalysts are shifted towards higher temperatures
in comparison with the monometallic rhodium catalyst: $\Delta T = 20$ K
and 25 K for respectively, CoRh/Al_2O_3 and Co_4Rh/Al_2O_3. Although
the possibility of $CoRh_2O_4$ formation during TPO cannot be
excluded we are of the opinion that $CoRh_2O_4$ formation is not
likely because firstly, the maximum oxidation temperature of
773 K during TPO is far below the formation temperature of bulk
$CoRh_2O_4$ (T = 1073 K) and secondly, on the basis of the TPR results
of the bulk oxides we would have expected a shift of the TPR
profiles for the bimetallic catalysts of about 100 K relative

to the maximum of the TPR profile for Rh_2O_3/Al_2O_3. It is
possible that during oxidation a segregation of both metal
oxides has taken place and that after oxidation the oxides are
not far apart from each other. In that way the very first
formed rhodium may serve as a catalyst for the reduction. As
in the case of Co/Al_2O_3 no significant amount of $CoAl_2O_4$ was
formed during TPO in both bimetallic catalysts because the
ratios between hydrogen consumed during the second TPR and
oxygen consumed during TPO are 2.03 and 2.12 for respectively,
Co_4Rh/Al_2O_3 and $CoRh/Al_2O_3$ which are within the experimental
error equal to the theoretical value of 2.

The TPD profiles for the hydrogen covered catalysts
after the second TPR are presented in figure 5d. Note that
the heating rate of 15 K/min is slow so that readsorption of
hydrogen will take place and that therefore no kinetic para-
meters for hydrogen desorption can be determined. Nevertheless,
we used TPD to obtain information about the dispersion via the
total amount of hydrogen adsorbed.
The TPD profile for Rh/Al_2O_3 is characterized by a main peak
at 483 K and a shoulder at 300 K. Above 673 K hardly any
hydrogen is desorbed. From the total amount of hydrogen desorbed
one can calculate a H/M_{TPD} value of 1.26 which is significantly,
lower than the value obtained by using the hydrogen chemisorption
technique (H/M_{HC} = 1.53). We have to take into account that
the H/M_{HC} value was obtained after the first TPR, therefore,
the difference between the two values might be caused by
sintering of rhodium during the TPO and a subsequent TPR.
The TPD profiles for the three cobalt containing catalysts are
characterized by two 'areas': 1) below T = 623 K which we assign
to 'normal' hydrogen desorption, and 2) above T = 623 K, which
needs closer attention.
Although the hydrogen adsorption energy for rhodium is higher
than for cobalt, respectively 100 and 113 kJ (39) the TPD's
suggest that, compared to rhodium, hydrogen was bound stronger
on metallic cobalt. Even at 873 K adsorption of hydrogen from
cobalt was incomplete. Moreover, the total amount of hydrogen
desorbed exceeded the values calculated on the basis of the

hydrogen chemisorption results, enormously. Therefore, we think
that for the cobalt containing catalysts above 623 K the
detected hydrogen originated from another hydrogen source.
It is obvious that this phenomenon only occurs in the presence
of cobalt. We believe that the dehydroxylation of the alumina
support might play a very important role. It is known that
alumina dehydroxylates above 673 K under the formation of water
(40). Therefore, it is possible that during the TPD in the
environment of the reduced cobalt crystallites the ratio between
the partial pressures of water and hydrogen has become so high
that the equilibrium: $Co + 4/3H_2O \rightleftharpoons 1/3Co_3O_4 + 4/3H_2$ is
shifted to the right. This phenomenon has been reported
previously by Schuit et $al.$ (41) for Ni supported on SiO_2.
A TPR to 773 K subsequent to a TPD of a cobalt catalyst showed
indeed hydrogen consumption caused by reduction of cobalt oxide.
However, the amount of hydrogen consumed was a factor of 2 lower
than expected on the basis of the TPD results. We think that
during TPD between 773 and 873 K, temperatures which had never
been reached in the foregoing treatments, part of the oxidized
cobalt was converted to the cobalt surface spinel $CoAl_2O_4$ which
is not reducible below 773 K.

Up to now no direct information about the structure of
the bimetallic crystallites could be obtained from the TPR
results. As shown in figure 1 cobalt and rhodium are completely
miscible. Therefore, we assume that the regular solution model
is valid, in which case thermodynamics predict that the metal
with the lowest sublimation energy will be preferentially in
the surface region of the alloy (42). The sublimation energy
of cobalt is lower than that of rhodium and as a consequence
surface enrichment of cobalt in the reduced Co-Rh particle is
to be expected. From Extended X-ray Absorption Fine Structure
measurements we found indeed evidence for cobalt surface
enrichment in supported bimetallic Co-Rh particles (see chapter
5). When a bimetallic Co-Rh particle is exposed to oxygen at
room temperature the cobalt enrichment in the surface will even
be more pronounced because the interaction between oxygen and
cobalt is stronger than that between oxygen and rhodium. This

phenomenon is known as 'gas-induced surface enrichment' (43).
In order to demonstrate the surface enrichment of cobalt we
recorded TPR profiles for the passivated catalysts (see
Experimental Section). The profiles are presented in figure 6.
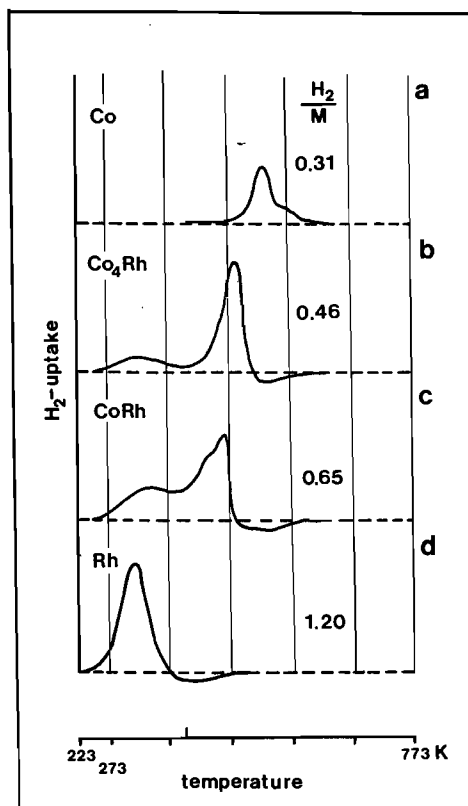
Figure 6 TPR profiles for passivated alumina-supported catalysts;
a) Co (4.44 wt%), b) Co$_4$Rh (4.57 wt%),
c) CoRh (5.40 wt%) and d) Rh (2.30 wt%) catalysts

The TPR profile for the passivated monometallic cobalt catalyst
is characterized by a single peak around 513 K. On the
assumption that during passivation oxygen is adsorbed dis-
sociatively and that only the surface was covered by oxygen
atoms with an O/M$_{surface}$ stoechiometry of 1 the dispersion
determined from the amount of hydrogen consumed during TPR is

0.31. This value is much higher than the H/M value of 0.09 measured by hydrogen chemisorption. Therefore, the hydrogen consumed during TPR of the passivated Co/Al_2O_3 catalyst indicates that corrosive chemisorption had taken place during passivation.

The TPR profile for the passivated Rh/Al_2O_3 catalyst shows a single consumption peak around 300 K, followed by desorption of H_2. Passivation of this ultra dispersed Rh catalyst has led to corrosive oxygen chemisorption, but not to full oxidation since the hydrogen consumption mounted up to 1.20 H_2/M. Reduction of the passivated bimetallic Co_4Rh/Al_2O_3 catalyst occurs mainly in the temperature range 423-523 K, whereas a small shoulder is visible around 350 K. The maximum of the TPR profile is at about 483 K, only 30 K shifted to lower temperature compared to Co/Al_2O_3. Apparently, the presence of rhodium hardly affects the reduction, which is not in accordance with the TPR results obtained for the completely oxidized systems. The seeming contradiction can be explained by the assumption of covering of rhodium by cobalt oxide. Instead of the formation of the first rhodium metal atoms being the nucleation step, now the much more difficult formation of the first cobalt metal atoms is the nucleation step. The shift of 30 K might be caused by the presence of a few rhodium atoms in the surface. An X-ray photoelectron spectroscopy measurement confirmed that rhodium in the passivated Co_4Rh/Al_2O_3 catalyst is still mainly present as metallic Rh which indicates that rhodium is hardly affected by oxygen. From the hydrogen consumed during reduction the total amount of oxidized cobalt can be calculated. On the assumption that the total amount of cobalt is oxidized to Co_3O_4 whereas rhodium is not affected, the theoretical H_2/M value is 16/15. ($4Co_3O_4 + 3Rh + 16H_2 \rightarrow 16H_2O + 3Rh + 12Co$.) However, from the 3.18 wt% cobalt 1.87 wt% has been lost caused by cobalt surface spinel formation. The theoretical H_2/M value of 0.46 indicates that cobalt was oxidized to a great extent during passivation. Thus, the passivated particles in Co_4Rh/Al_2O_3 consist of a rhodium-rich core and an outer shell consisting mainly of cobalt oxide.

The shoulder around 350 K can be assigned to either bimetallic
crystallites with a notable amount of rhodium in the outer shell
or to a rigorous passivation of small crystallites leading
to the same situation as after an oxidation.
The structure of the TPR profile for the passivated $CoRh/Al_2O_3$
catalyst is similar to the profile for Co_4Rh/Al_2O_3 (figure 6c).
However, the shoulder is more pronounced whereas the main peak
is shifted to lower temperatures. The latter indicates an in-
crease of the rhodium concentration in the outer shell.

All results obtained in the foregoing section have been
rationalized by a model which represents the formation of
bimetallic Co-Rh particles supported on alumina and the change
in structure of the particles after different treatments
(cf. figure 7).
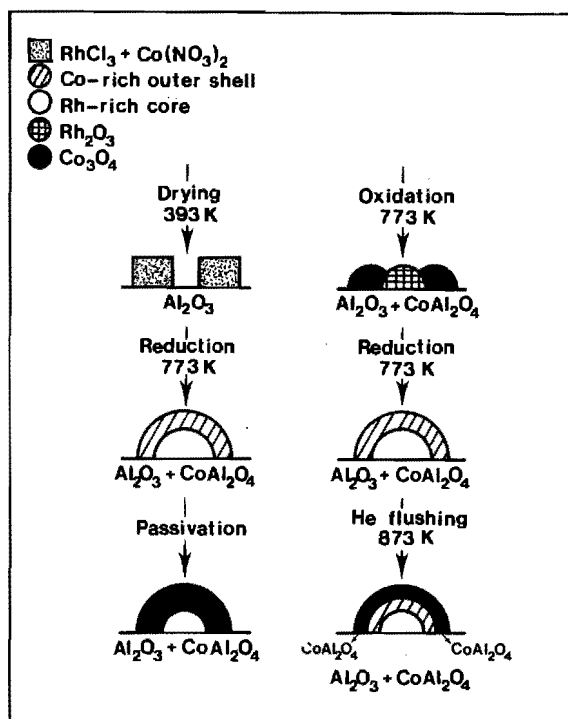
Figure 7 Formation of bimetallic Co-Rh particles during reduction
of the impregnated catalyst and the change in structure
of the particles after different treatments.

After impregnation the metal salts are in intimate contact, as proven by the first TPR (figure 5a). During TPR bimetallic Co-Rh particles are formed, the outer shell of which is enriched in cobalt. Besides formation of Co-Rh particles a part of cobalt reacts with alumina to produce $CoAl_2O_4$ which cannot be reduced below 773 K. When the reduced catalyst is exposed to oxygen cobalt is oxidized to a great extent and the resulting cobalt oxide covers a rhodium-rich core. In this situation relative high temperatures are needed to reduce the cobalt oxide because the covered rhodium cannot serve as a reduction catalyst any-more (figure 6b). A thorough oxidation of the catalyst induces a remodelling of the bimetallic particle in such a way that also Rh_2O_3 is exposed, through which a subsequent reduction is enhanced (figure 5c). During oxidation no new $CoAl_2O_4$ is formed. After reduction of the oxidized catalyst the bimetallic particles have been formed again. During the subsequent TPD the water formed by dehydroxylation of the alumina surface partly oxidizes cobalt by which a part of the formed oxide is con-verted to $CoAl_2O_4$.

4.4.3 Co, Rh and Co-Rh supported on TiO_2

4.4.3.1 Co on TiO_2

In table 1 the hydrogen chemisorption results for the passivated 2.01 wt% Co/TiO_2 catalyst, after re-reduction and evacuation at 473 K, are presented. In the literature the suppression of hydrogen chemisorption for TiO_2 supported metals after a high temperature reduction has been pointed out. This phenomenon is known as Strong Metal Support Interaction (SMSI) (31). By passivation of a catalyst in the so-called SMSI-state this state is abolished (see chapter 3), which implies that for the Co/TiO_2 catalyst re-reduced at 473 K the observed H/M value of 0.14 was not influenced by the inter-ference of SMSI. However, when the Co/TiO_2 catalyst was re-reduced at 773 K the expected decrease in the H/M value was observed (H/M = 0.06).

TPR and TPO profiles for the Co/TiO$_2$ catalyst are shown in figure 8.
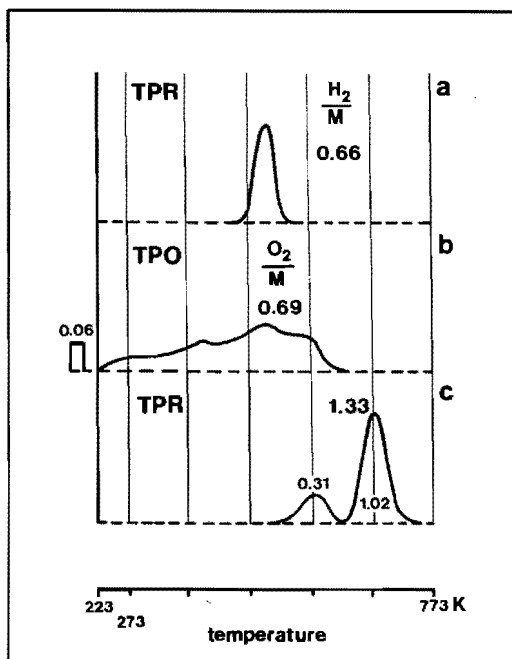
Figure 8 *TPR and TPO profiles for Co(2.01 wt%)/TiO$_2$ catalyst.*
a) TPR of passivated catalyst.
b) TPO of reduced catalyst.
c) TPR of oxidized catalyst.

The TPR profile for the passivated catalyst is characterized by a single peak at 498 K (figure 8a). Comparison of the amount of hydrogen consumed (H$_2$/M = 0.66) with the hydrogen chemisorption value of H/M = 0.14 indicates that corrosive chemisorption of oxygen has occurred during passivation.

Oxidation of the reduced catalyst already started at 223 K, as can be seen from the TPO profile (figure 8b), and was complete around 600 K. The observed O$_2$/M value of 0.69 is within the experimental error equal to the theoretical value of 0.67 on the assumption that metallic cobalt is oxidized to Co$_3$O$_4$. This demonstrates that after the first TPR the degree of

reduction was 100 per cent and that cobalt was completely oxidized to Co_3O_4 during TPO.

The resulting oxide was reduced according to the second TPR profile as presented in figure 8c. Two peaks can be distinguished, a small one around 588 K and a main peak around 686 K. Unlike the Rh/TiO_2 catalyst (see chapter 3) the second TPR profile for the Co/TiO_2 catalyst was not influenced by varying the dispersion by changing the cobalt loading from 0.5 to 8.0 wt%. In all cases the second TPR profiles hardly differ from the profile presented in figure 8c and the ratio between the areas of the peaks around 686 K and around 588 K was equal to 3 ± 0.3. The observed H_2/M value of 1.33 indicates that cobalt oxide was completely reduced to metallic cobalt. Apparently, irreducible compounds such as cobalt titanate were not formed. The occurrence of two peaks and the observed ratio of 3 suggest that the reduction of Co_3O_4 proceeds via CoO:

$$\tfrac{1}{3}Co_3O_4 + \tfrac{1}{3}H_2 \rightarrow CoO + \tfrac{1}{3}H_2O$$

$$CoO + H_2 \rightarrow Co + H_2O.$$
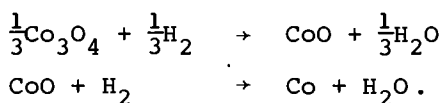
The results of the following experiment support this idea (see figure 9). The catalyst was oxidized at 773 K and subsequently reduced in a TPR until the minimum in between the two peaks was reached at 640 K (figure 9b). After Ar flushing at this temperature the partly reduced catalyst was cooled to 223 K and a second TPR profile was recorded (figure 9c). The second TPR profile is characterized by a single peak around 685 K which corresponds with the high temperature peak of the TPR profile of the completely oxidized catalyst (figure 9a). If during this latter TPR the hydrogen consumed was caused by the reduction of a part of Co_3O_4 to metallic cobalt, one would have expected a significant shift towards lower temperatures of the consumption peak in the second TPR, because the metallic cobalt formed would have acted as nucleation centres for the dissociation of hydrogen molecules. Such a shift towards lower reduction temperatures is apparent in the passivated cobalt catalyst which has its TPR peak at 498 K (figure 8a). The fact
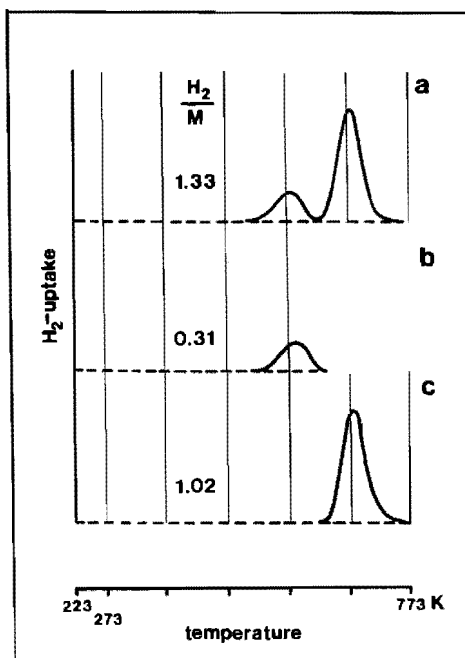
Figure 9 TPR profiles for Co(2.01 wt%)/TiO₂ catalyst.
      a) TPR of oxidized catalyst.
      b) TPR until 640 K.
      c) TPR of the catalyst which was partly reduced up
         to 640 K.

that such a lowering is not observed implies that in the first
reduction peak no metallic cobalt was formed.
Definite proof for the absence of metallic cobalt after
reduction up to 640 K was found from FMR measurements performed
on a 1.00 wt% Co/TiO$_2$ catalyst. The partly reduced catalyst
gave rise to a very small FMR signal from which a metallic
concentration of less than 4% of the present metal was
calculated, whereas from the observed H$_2$/M value of 0.33 in
TPR a cobalt concentration of 25% would have been expected if
Co$_3$O$_4$ would have been directly reduced to Co.
We thus conclude that the reduction of Co$_3$O$_4$ is a two-stage

process according to the reactions given above.

In order to obtain more information about the oxidation of reduced cobalt supported on TiO_2 we recorded TPR profiles for the 2.01 wt% Co/TiO_2 catalyst after TPO's in which the catalyst had been oxidized up to different temperatures. After reaching the final temperature the catalyst was immediately cooled to 223 K. The results are presented in figure 10.
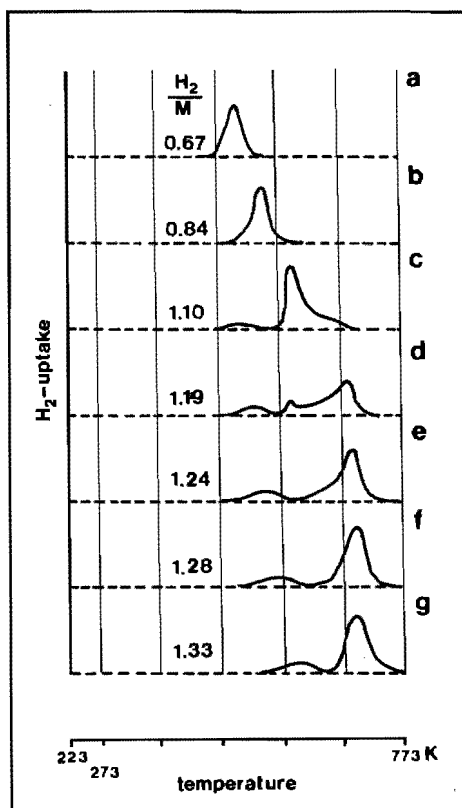
Figure 10   TPR profiles for Co(2.01 wt%)/TiO$_2$ catalyst oxidized at:
a) 423 K, b) 473 K, c) 523 K, d) 573 K,
e) 623 K, f) 673 K and g) 773 K.

The reduction profile for the catalyst oxidized at 423 K is characterized by a single peak around 503 K. The peak shifted to 555 K when the catalyst was oxidized at 473 K and also the total amount of hydrogen consumed increased. Oxidation at 523 K gave rise to a TPR profile with a main peak at 593 K, a small 'second' peak at 518 K and a shoulder around 650 K (figure 10c). With increasing oxidation temperature the main peak hardly shifted in position but decreased in intensity (figure 10d), and had disappeared when oxidation of the catalyst was complete ($T_{oxidation}$ > 600 K), whereas the 'second' peak shifted towards higher temperature and the shoulder developed into a peak which also shifted with increasing oxidation temperature. However, when the oxidation of the catalyst was complete the ratio between the intensities of the two peaks did not change significantly.

The relatively high H_2/M value observed in the TPR of the passivated catalyst implies that during passivation - oxidation at room temperature - corrosive chemisorption of oxygen takes place. To demonstrate this further we measured the FMR signal of a reduced (773 K) 1.00 wt% Co/TiO_2 catalyst which was exposed to air. From figure 11 it can be clearly seen that the intensity of the FMR signal decreased with exposure time. Note that at high g-values the signals started at absorption zero, except for the first recorded spectrum in which the ferro-magnetic particles were not yet oriented into the direction of the external magnetic field yet. The ratio between the intensity of the FMR signal for the reduced catalyst exposed to air during several weeks (figure 11f) and the one for the freshly reduced catalyst (figure 11a) is 0.20. As the intensity of an FMR signal is proportional to the square of the number of cobalt atoms in the ferro-magnetic particle, it follows that on the average 45% of the cobalt atoms in the particles had not been oxidized by passivation. The TPR profile for the passivated catalyst is characterized by a single peak (figure 8a). Because the reduction of Co_3O_4 is a two-stage process we assume that the oxide formed during passivation is CoO.
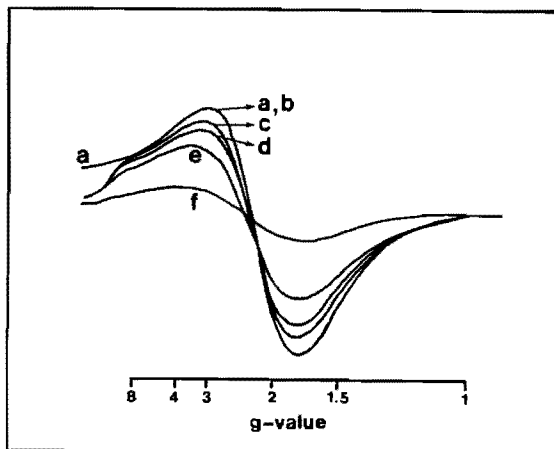
Figure 11 Decrease of FMR signal for the reduced
Co(1.00 wt%)/TiO$_2$ catalyst during passivation.
a) Reduced catalyst, b) 5 minutes after exposure to
air, c) 45 min, d) 75 min, e) 180 min and f) several
weeks.

Having explained the TPR profile of a passivated Co/TiO$_2$
catalyst (figure 8a and 10a) and that of a Co/TiO$_2$ catalyst
oxidized at 773 K (figure 8c and 10g) we are now in the position
to propose a model that can explain the TPR profiles of the
Co/TiO$_2$ catalyst oxidized at intermediate temperatures
(figure 10b-10f). In this model (cf. figure 12) three separate
stages of oxidation can clearly be distinguished if it is
assumed that small cobalt particles are much quicker oxidized
than large particles.
The first stage of oxidation is characterized by cobalt particles
which are covered by CoO (the situation after passivation).
Hydrogen can be dissociated to hydrogen atoms on the metallic
core and reduction of CoO will be accelerated. With increasing
oxidation temperature the outer shell of CoO will increase.
The reduction of CoO will still be catalyzed provided that a
metallic core is present. But this reduction will start at
increasingly higher temperatures because hydrogen must diffuse
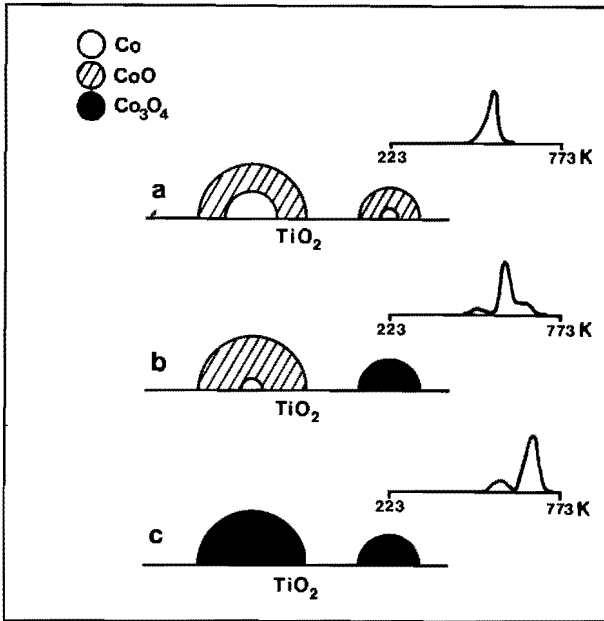
Figure 12 *Model for the three different oxidation stages of*
Co supported on TiO$_2$ during oxidation. The associated
TPR profiles are presented too.
The oxidation stages are representative for oxidation
between:
a) 223-473 K, b) 473-623 K and c) 623-773 K.

through an outer shell of CoO, which increases in thickness, in
order to start nucleation. When the oxidation temperature is
so high that the small particles are completely oxidized (and
that no metallic core is present), while the larger particles
are not completely oxidized we reach the second stage of oxida-
tion. In that case the TPR profile is characterized by three
peaks (*cf.* figure 10c and 10d). The first peak is caused by re-
duction of Co$_3$O$_4$ to CoO in the small particles, the second by the
catalyzed reduction of CoO to Co in the large particles, and the
third peak to the reduction of CoO to Co in the small particles.
After a complete oxidation of the catalyst we reach the third
stage, in which the TPR is characterized by two peaks which are

assigned to the two-stage reduction of Co_3O_4. Note that re-duction of Co_3O_4 starts at a lower temperature when the oxide is formed at a lower oxidation temperature. This phenomenon can be understood in the context of nucleation at defects. The oxide which is formed at lower temperatures is afflicted with more defects and therefore the chance of nucleation on this oxide will be enhanced.

4.4.3.2 Co-Rh on TiO$_2$

In table 1 the hydrogen chemisorption results for the passivated $Co_{1.2}Rh/TiO_2$ catalyst are presented and compared with the constituent monometallic systems. The H/M value after a re-reduction at 473 K is a direct indication of the dispersion, whereas the value after 773 K re-reduction shows evidence for SMSI behaviour.

To compare the reduction and oxidation behaviour of the bi-metallic catalyst with the constituent monometallic systems TPR and TPO profiles for the titania supported Co, Rh and Co-Rh catalysts are shown in figure 13.

The TPR profile for the impregnated Co/TiO_2 (figure 13a) is very similar to the one for dried $Co(NO_3)_2$ (not shown), and is characterized by three peaks. Taking into account that reduction of bulk CoO (figure 4b) does not start until 600 K we assign the first two peaks in the profile to reduction of residual nitrate to NO_x and the third peak around 700 K to reduction of CoO. The amount of hydrogen consumed in the latter peak ($H_2/M = 1.1$) is in agreement with this assignment. The TPR results suggest that direct reduction of supported $Co(NO_3)_2$ proceeds via CoO.

The TPR profile for the impregnated 2.3 wt% Rh/TiO_2 catalyst exhibits a fairly broad range of hydrogen uptakes. Two low temperature peaks at 323 K and 423 K are observed which are assigned to reduction of respectively, Rh_2O_3 (formed during impregnation or drying) and $RhCl_3$ (37). The total hydrogen consumption ($H_2/M = 1.7$) is, however, higher than what can be accounted for by the reduction of rhodium species solely. Again, the metal-assisted reduction of the support - hydrogen
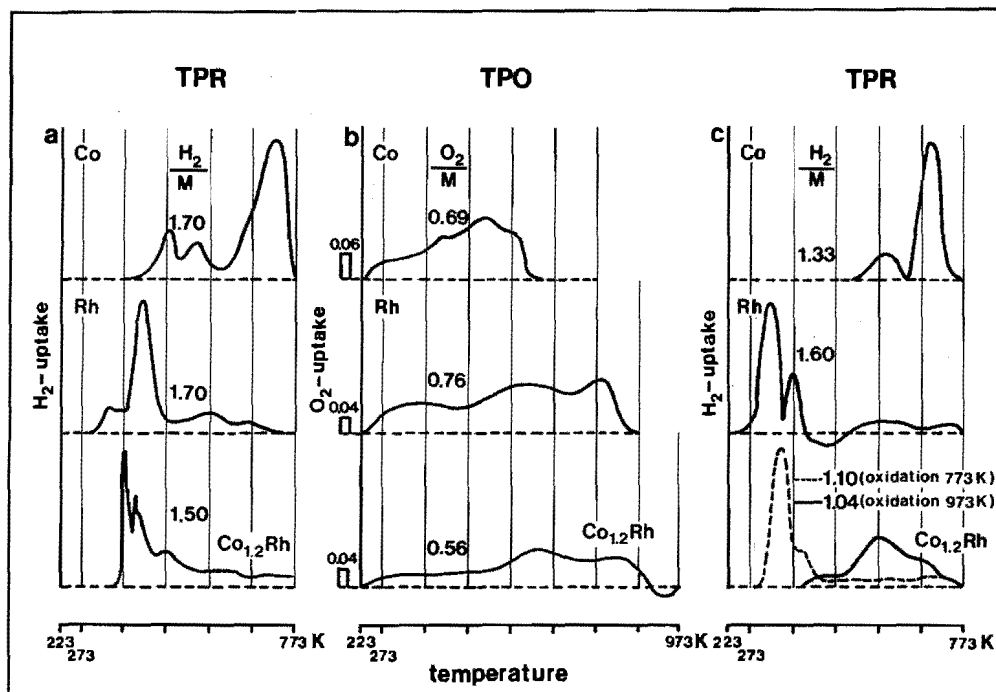
Figure 13 TPR and TPO profiles for titania-supported
Co (2.01 wt%), Co$_{1.2}$Rh (2.91 wt%) and Rh (3.20 wt%)
catalysts.
a) TPR of the impregnated and dried catalysts.
b) TPO of the reduced catalysts.
c) TPR of Co/TiO$_2$ oxidized at 773 K, Rh/TiO$_2$
oxidized at 873 K and Co$_{1.2}$Rh/TiO$_2$ oxidized
at 773 and 973 K.

consumption above 473 K - is the obvious explanation for this
high value (see chapter 3).
Reduction of the impregnated bimetallic Co$_{1.2}$Rh/TiO$_2$ catalyst
takes mainly place within the temperature range of 350-520 K,
the range in which supported RhCl$_3$ reduces too. This feature
implies that both metal salts are in intimate contact, or at
least close together, after impregnation. The during reduction
formed rhodium acts as a catalyst for the reduction of Co(NO$_3$)$_2$.

The H_2/M value of 1.5 indicates that all rhodium and cobalt
is reduced in the TPR. The over-consumption of 1.5 - 1.23 =
0.27 H_2/M is again ascribed to reduction of nitrate groups and
support. The fact that complete reduction of Rh and Co occurs
at temperatures where monometallic Rh reduces makes it very
likely that bimetallic particles are formed. To study this in
more detail TPO and subsequent TPR profiles of the bimetallic
Co-Rh and of the monometallic reference catalysts have been
measured.

The TPO profiles (figure 13b) for the reduced Co/TiO_2
and Rh/TiO_2 catalysts have been discussed before in this
chapter and in chapter 3, respectively. It can be seen that
higher temperatures are needed to oxidize Rh/TiO_2 to Rh_2O_3/TiO_2
than to oxidize Co/TiO_2 to Co_3O_4/TiO_2, even though the dis-
persion of the metallic Rh particles was better than that of
the Co particles. Oxidation of $Co_{1.2}Rh/TiO_2$ is even more
difficult than oxidation of Rh/TiO_2. A striking feature is the
oxygen consumption of $O_2/M = 0.56$ established for the bimetallic
system, which is lower than the expected value of 0.71 for the
formation of Co_3O_4 and Rh_2O_3. The observed O_2/M value of 0.56
agrees much better with the value of 0.61 calculated on the
basis of oxidation of Rh to Rh_2O_3 and of Co to CoO. This raises
the question why cobalt is oxidized to CoO in the Co-Rh system,
while monometallic Co on TiO_2 is oxidized to Co_3O_4. At the same
time, though, it proves that Co is in very close contact
with Rh in the metallic state, most likely in the form of bi-
metallic particles. The explanation for the low O_2/M value might
be that part of the oxidized cobalt forms the spinel $CoRh_2O_4$,
while the remainder (the molar Co/Rh ratio in the catalyst is
1.2, while that in $CoRh_2O_4$ is 0.5) forms epitaxial CoO. Another
explanation could be that part of the Rh_2O_3 dissolves in the
CoO formed and stabilizes this phase to further oxidation.

Subsequent TPR measurements result in profiles as presented
in figure 13c. Reduction of Co_3O_4 on TiO_2 did not start until
500 K and, as shown in the foregoing, took place via a two-
stage process. The reduction profile of Rh_2O_3 supported on
TiO_2 is characterized by a peak around 325 K which is attributed

to reduction of dispersed Rh_2O_3 (very small particles), a peak
around 385 K which is assigned to reduction of bulk-like Rh_2O_3
particles, and hydrogen consumption above 420 K which has been
attributed to metal-assisted reduction of the support (see
chapter 3).

To investigate the influence of oxidation temperature on the
reduction behaviour of the bimetallic catalyst we recorded
TPR profiles after oxidation at 773 K, at which temperature
oxidation is not yet complete (*cf*. figure 13b), and at 973 K.
It can be clearly seen that rhodium enhances the reducibility
of cobalt oxide after the catalyst had been oxidized at 773 K.
The TPR profile looks similar to the one for Rh_2O_3 on TiO_2.
This combined with the observed hydrogen consumed of 1.10 H_2/M
suggest that the partly oxidized particles consist of either
$CoO + Rh_2O_3$ or $Co_3O_4 + Rh_2O_3 + Rh$, both with rhodium ions in
the surface. The formation of cobalt rhodate is not likely be-
cause then the oxidic particles would consist of $CoRh_2O_4$ and
CoO. The partly oxidized catalyst would have to reduce around
500 K (*cf*. figure 4) which is, however, 150 K higher than
observed.

After oxidation at 973 K the TPR profile does no longer display
the low temperature peaks attributed to rhodium-assisted
reduction. The profile now much more resembles that of the
Co/TiO_2 catalyst. This indicates that the bimetallic particles
have been covered by cobalt oxide during thorough oxidation.
Apparently, a segregation of the two metal oxides did not occur.
This gives evidence for a good interaction between cobalt oxide
and rhodium oxide which might be due to formation of $CoRh_2O_4$.
The bimetallic particles after an oxidation at 973 K may con-
sist of $CoRh_2O_4$ which is covered by CoO. The observed low
H_2/M value of 1.04 is in accordance with this vision.

Generally, the results obtained with the Co-Rh system
supported on TiO_2 justify that the application of the model
presented for the formation of bimetallic Co-Rh particles
supported on alumina (*cf*. figure 7) can be extended for Co-Rh
on titania. However, two modifications of the model are

necessary. Firstly: no cobalt-titania compounds are formed, and secondly: during a thorough oxidation no segregation of the metal oxides takes place. The latter might be explained by the formation of $CoRh_2O_4$ spinel. Compared with alumina, higher temperatures are needed to oxidize the bimetallic Co-Rh particles on titania. Therefore, the formation of $CoRh_2O_4$ on titania becomes thermodynamically more favourable.

4.5 ADDITIONAL REMARKS

In this section we briefly consider the implications of our observations for other bimetallic catalysts. As we will show in chapter 5 the conceptual model of the structural changes which occur upon oxidation and reduction treatments (*cf.* figure 7) is not only valid for Co-Rh on Al_2O_3 and TiO_2 but also for Co-Rh on SiO_2. This model may even be extended to other alloys because they produce similar behaviour as long as they form solid solutions. Examples are: Fe-Rh (chapter 6), Pt-Rh (44, 45), Pt-Ir (26, 27, 46, 47), Pt-Re (25) and Ru-Cu (48).
Generally, during reduction of a co-impregnated bimetallic catalyst alloying of the two metals takes place. The noble metal serves as a catalyst for the reduction of the less noble metal. An intimate contact of the two metal salts after impregnation is not a necessary prerequisite to form bimetallic particles during reduction, as reported by Bond and Yide (48) for $RuCl_3$ and $Cu(NO_3)_2$ supported on SiO_2. Their TPR results showed that $RuCl_3$ was reduced first and the proposed mechanism of cluster formation was that the $Cu(NO_3)_2$ was reduced by hydrogen spill-over from the ruthenium, the resulting copper atoms then migrating to ruthenium particles to which surface they adhere.
The surface of the bimetallic particles are enriched in the component which exhibits the lowest sublimation energy, *e.g.*, Co in Co-Rh, Fe in Fe-Rh and Rh in Pt-Rh. A mild oxidation leads

to surface enrichment of the metal which exhibits the highest
affinity for oxygen. The bimetallic particles stay largely in-
tact after oxygen adsorption at moderate temperatures. Although
in the presence of adsorbed oxygen the clusters are thermo-
dynamically unstable, the rate of segregation of the metal
oxides is slow. This has been found for Co-Rh, Pt-Rh, Fe-Rh
and Pt-Re. Generally, a thorough oxidation induces a segragation
of the metal oxides. Thus, the intimacy of the two metals in
the metallic state is terminated by an oxidative treatment.
Segregation depends on the nature of the metals involved,
in particular the miscibility characteristics of the bulk metal
oxides, and on the strength of the interactions between metal
oxides and supports. An example of a catalyst in which no
segregation of the metal oxides takes place is Co-Rh supported
on TiO_2 (figure 13c), probably due to formation of $CoRh_2O_4$.
A low temperature reduction of an oxidized catalyst in which
segregation has taken place may lead to a catalyst in which
both metals are separated. This means that the specific ad-
vantages of alloying are lost. A high temperature reduction,
however, usually leads to co-clustering of the metals, but the
metal particles are less dispersed compared to the catalyst
before oxidation. De Jongste and Ponec (49), however, have
noted that platinum-gold alloy particles on alumina are
destroyed by oxidation but cannot be reformed by reduction
(in contrast to the same alloy on SiO_2). Therefore, as already
stated by Sinfelt (46), oxidation is to be avoided if the
original clusters are to be preserved. Furthermore, calcination
before reduction, which is frequently and effectively employed
in catalyst preparation, is probably sometimes undesirable if
highly dispersed clusters are required: direct reduction of
the precursor salts might be preferred.

4.6 CONCLUSIONS

The results described in this chapter have unambiguously shown that the TPR-TPO technique can provide useful information on the structure of Co and Rh in alumina- and titania-supported catalysts.

The addition of rhodium caused the cobalt based catalysts to be more easily reduced. In the case of cobalt containing alumina-supported catalysts, however, the presence of rhodium does not prevent the formation of cobalt aluminate, which compound proved to be irreducible below 773 K. Since the reduction of Co in impregnated as well as in oxidized bimetallic catalysts was catalyzed by the presence of rhodium we conclude that the metals in the reduced catalysts were present as bimetallic particles.

Passivation of Co_4Rh/Al_2O_3 was found to oxidize Co to a great extent, whereas rhodium was hardly affected. As the TPR profiles for the passivated Co_4Rh/Al_2O_3 and Co/Al_2O_3 catalysts look similar the structure of the bimetallic particles consists of a metallic rhodium core covered with cobalt oxide. Therefore, the reduction of cobalt oxide cannot be catalyzed by rhodium. An oxidative treatment at elevated temperatures was found to reshape the bimetallic particle in such a way that also Rh_2O_3 was exposed, and that reduction of cobalt oxide was catalyzed again.

Evidence was found for oxidation of cobalt in the reduced cobalt containing alumina-supported catalysts during He flushing at 873 K.

The TPR results obtained for the monometallic Co/TiO_2 catalyst clearly demonstrate that reduction of Co_3O_4 is a two-stage process according to the reactions:

$$Co_3O_4 + H_2 \rightarrow 3CoO + H_2O$$
$$CoO + H_2 \rightarrow Co + H_2O.$$
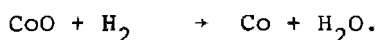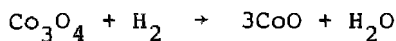
Oxidation of Co-Rh on TiO_2 at 773 K leads to particles in which
rhodium oxide was exposed. However, higher temperatures were
needed for complete oxidation of $Co_{1.2}Rh/TiO_2$. Under these
conditions formation of cobalt rhodate cannot be excluded.
The reduction behaviour of this oxidized catalyst indicated
that only cobalt oxide was exposed to the gas phase.

When the passivated titania-supported catalysts were re-
reduced at 473 K they showed normal chemisorption behaviour.
However, in case of a re-reduction at 773 K the H/M values
for all the catalysts show evidence for SMSI behaviour.

4.7 REFERENCES

1. V. Ponec, Catal. Rev.-Sci. Eng., 11, 41 (1975).
2. J.H. Sinfelt, Adv. Catal., 23, 19 (1973).
3. W.M.H. Sachtler, Catal. Rev., 14, 193 (1976).
4. M.A. Vannice and R.L. Garten, J. Mol. Catal., 1, 201
   (1975-1976).
5. R.M. Stanfield and W.N. Delgass, J. Catal., 72, 37 (1981).
6. H. Miura and R.D. Gonzalez, J. Catal., 74, 216 (1982).
7. E.R. Tucci and R.C. Streeter, Hydrocarbon Processing,
   April 1980, p. 107.
8. M. Nakamura, B.J. Wood, P.Y. Hou, and H. Wise, in
   "Proceedings of the 7th International Congress on Catalysis",
   edited by T. Seiyama and K. Tanabe, Elsevier Amsterdam
   (1981), Part A, p. 432.
9. M.M. Bhasin, W.J. Bartley, D.C. Ellgen and T.P. Wilson,
   J. Catal., 54, 120 (1978).
10. M.A. Vannice and R.L. Garten, J. Catal., 66, 242 (1980).
11. M.A. Vannice, J. Catal., 74, 199 (1982).
12. P. Villeger, J. Barrault, J. Barbier, G. LeClerq and
    R. Maurel, Bull. Soc. Chim. France (1979), p. I-413.
13. R.L. Chin and D.M. Hercules, J. Phys. Chem., 86, 360 (1982).
14. R.B. Greegor, F.W. Lytle, R.L. Chin and D.M. Hercules,
    J. Phys. Chem., 85, 1232 (1981).

15. L.W. Burggraf, D.E. Leyden, R.L. Chin and D.M. Hercules, J. Catal., 78, 360 (1982).

16. N. Topsøe and H. Topsøe, J. Catal., 75, 354 (1982).

17. R.L. Chin and D.M. Hercules, J. Catal., 74, 121 (1982).

18. P. Grange, Catal. Rev., 21, 135 (1980).

19. M.A. Vannice, J. Catal. 37, 449 (1975).

20. K.S. Chung and F.E. Massoth, J. Catal., 64, 320 (1980).

21. M. LoJacono, J.L. Verbeek and G.C.A. Schuit, J. Catal., 29, 463 (1973).

22. R. Brown, M.E. Cooper and D.A. Whan, Appl. Catal., 3, 177 (1982).

23. S.D. Robertson, B.D. McNicol, J.H. de Baas, S.C. Kloet and J.W. Jenkins, J. Catal., 37, 424 (1975).

24. J.W. Jenkins, B.D. McNicol and S.D. Robertson, CHEMTECH, 7, 316 (1977).

25. N. Wagstaff and R. Prins, J. Catal., 59, 434 (1979).

26. N. Wagstaff and R. Prins, J. Catal., 59, 446 (1979).

27. A.C. Faro Jr., M.E. Cooper, D. Garden and C. Kemball, J. Chem. Res., Paper E/183/82, 1114 (1983).

28. T. Paryjczak, J. Góralski and K.W. Jóźwiak, React. Kinet. Catal. Lett., 16, 147 (1981).

29. A.J.A. Konings, A.M. van Dooren, D.C. Koningsberger, V.H.J. de Beer, A.L. Farragher and G.C.A. Schuit, J. Catal., 54, 1 (1978).

30. H. Boer, W.J. Boersma and N. Wagstaff, Rev. Sci. Instr., 53, 349 (1982).

31. S.J. Tauster, S.C. Fung and R.L. Garten, J. Am. Chem. Soc., 100, 170 (1978).

32. W. Köster and E. Horn, Z. Metallkunde, 43, 444 (1952).

33. J. Wood, O. Lindqvist, C. Helgesson, N.G. Vannerberg, in "Reactivity of Solids", Plenum Press (1977).

34. T. Paryjczak, J. Rynkowski and S. Karski, J. Chromatogr., 188, 254 (1980).

35. N.W. Hurst, S.J. Gentry and A. Jones, Catal. Rev.-Sci. Eng., 24, 233 (1982).

36. J.M. Zowtiak, G.D. Weatherbee and C.H. Bartholomew, J. Catal., 82, 230 (1983).

37. A.E. Newkirk and D.W. Mckee, J. Catal., 11, 370 (1968).

38. M. LoJacono, M. Schiavello and C. Cimino, J. Phys. Chem., 75, 1044 (1971).

39. G.A. Somorjai, in "Chemistry in Two Dimensions: Surfaces", Cornell University Press, London (1981).

40. H. Knözinger and P. Ratnasamy, Catal. Rev.-Sci. Eng., 17, 31 (1978).

41. G.C.A. Schuit and N.H. de Boer, Recl. Trav. Chim. Pays-Bas, 70, 1067 (1951).

42. F.L. Williams and D. Nason, Surf. Sci., 45, 377 (1974).

43. R. Bouwman, G.J.M. Lippits and W.M.H. Sachtler, J. Catal., 25, 300 (1972).

44. T. Wang and L.D. Schmidt, J. Catal., 70, 187 (1981).

45. T. Wang and L.D. Schmidt, J. Catal., 71, 411 (1981).

46. J.H. Sinfelt, U.S. Patent 3,953,368 (1976).

47. J.H. Sinfelt and G.H. Via, J. Catal., 56, 1 (1979).

48. G.C. Bond and X. Yide, J. Mol. Catal., accepted for publication.

49. H.C. de Jongste and V. Ponec, J. Catal., 64, 228 (1980).

chapter 5

CHARACTERIZATION OF BIMETALLIC CoRh/SiO$_2$ CATALYSTS WITH TPR, TPO AND EXAFS SPECTROSCOPY

5.1 ABSTRACT

TPR, TPO and EXAFS experiments on CoRh/SiO$_2$ catalysts supply a clear evidence for the formation of bimetallic particles. The reduction of CoRh/SiO$_2$ occurs at lower temperatures compared to Co/SiO$_2$ indicating that rhodium serves as a catalyst for the reduction of cobalt. The Fourier transform of the Rh K-edge of the CoRh/SiO$_2$ catalyst shows that after reduction the rhodium atoms have much less cobalt neighbours than in the CoRh alloy. The intensity of the cobalt and rhodium peaks in the rhodium transform is only slightly influenced by adsorption of oxygen at room temperature, whereas the EXAFS spectrum of the Co-edge changes completely to that of cobalt oxide. From these results, it is concluded that the reduced catalyst contains bimetallic Co-Rh particles the interior of which is rich in rhodium, while the outer layer mainly contains cobalt.

5.2 INTRODUCTION

TPR results obtained on Co$_4$Rh/γ-Al$_2$O$_3$ (presented in chapter 4) proved that after oxygen adsorption at room temperature the bimetallic particles consist of an outer layer which mainly

contains cobalt oxide, whereas the core of the particle consists of metallic rhodium. The conclusion concerning cobalt enrich- ment in the surface of the passivated bimetallic particles cannot be unambiguously applied to reduced bimetallic particles since a gas-induced surface enrichment (1) of cobalt during oxygen admission may occur. In chapter 4 we predicted a cobalt enrichment in the surface of a reduced bimetallic particle on the basis of the difference in sublimation energy between cobalt and rhodium. However, experimental evidence for this en- richment has not been presented yet.

Previous studies published by Sinfelt and co-workers (2-5) have shown the usefulness of EXAFS in obtaining structural information on reduced bimetallic cluster catalysts. The bi- metallic systems investigated up to now were Ru-Cu, Os-Cu, Pt-Ir, and Ir-Rh. The first two are examples of systems com- posed of a group VIII metal and a group IB metal, while the last two consist of elements from group VIII only. The Ir-Rh system resembles the Co-Rh system best. All three elements (Co, Rh and Ir) have identical electronic structures. From EXAFS data obtained on Ir-Rh (1 wt% Ir, 0.5 wt% Rh) supported on SiO_2 and Al_2O_3 it has been concluded that the rhodium con- centration in the surface region of the iridium-rhodium particles was higher than in the interior (5).

In this chapter we present the results of a characteriza- tion study of the CoRh/SiO_2 system by using TPR, TPO and EXAFS of both the Rh and Co K-edges. SiO_2 has been chosen as a support because with respect to EXAFS measurements it does not exhibit disadvantages of Al_2O_3 and TiO_2. TiO_2 is less suitable as a support, since the absorbtion in it of the incident beam within the energy region of the Co K-edge is too high to obtain a proper EXAFS signal. When Al_2O_3 is used as a support, next to bimetallic Co-Rh particles also $CoAl_2O_4$ is formed. This means that the EXAFS of the Co K-edge is then composed of many different absorber-scatterer pairs and analysis of the signal will be difficult. Another reason for using SiO_2 as a support is that the model, developed for the formation of bimetallic Co-Rh particles on Al_2O_3 (see chapter 4), may be

tested and extended to a more general one.
Finally, we want to emphasize that the EXAFS results will be
discussed qualitatively, since a complete analysis of the
spectra has not been achieved yet. However, as will become
clear the EXAFS results as presented supply already very
useful information about the structure of the reduced bi-
metallic Co-Rh particles supported on SiO_2.

5.3 EXPERIMENTAL SECTION

Rh/SiO_2 (3.9 wt% rhodium), Co/SiO_2 (4.1 wt% cobalt), and
CoRh/SiO_2 (4.9 wt% metal, atomic ratio Co:Rh = 1:1) were
prepared by means of the incipient wetness technique. Aqueous
solutions of Co$(NO_3)_2$.$6H_2O$ (Merck P.A.), $RhCl_3$.xH_2O (39 wt%,
Drijfhout) and a mixed solution of the two metal salts for the
preparation of the bimetallic catalyst were used to impregnate
the silica support (Grace, S.D. 2-324.382, 290 m^2/g). The
impregnated catalysts were dried at room temperature overnight
and finally at 393 K for 60 hours and stored for further use.
A part of the impregnated CoRh/SiO_2 batch was directly reduced
in flowing H_2 by heating at 5 K/min to 773 K and staying at
that temperature for one hour. Before the catalysts were re-
moved, they had been passivated at room temperature by re-
placing the H_2 flow by N_2 and subsequently slowly adding O_2 up
to 20%. The Co and Rh contents of the dried catalysts were
established by using respectively atomic absorption and
colourimetry.
Hydrogen chemisorption measurements were performed in a
conventional glass system at 298 K. Before measuring the ad-
sorption isotherms the impregnated catalysts were reduced at
773 K (heating rate 5 K/min) for 1 hour under flowing hydrogen
and evacuated (10^{-2} Pa), at 773 K for Rh/SiO_2 and evacuated at
573 K for Co/SiO_2 and CoRh/SiO_2, for another hour. Lower
evacuation temperatures for the cobalt containing catalysts
were used in order to avoid formation of water by dehydroxyla-
tion of the support. As shown in chapter 4 water may oxidize
cobalt.

TPR and TPO experiments were carried out with circa 200 mg catalyst in an apparatus such as described by Boer *et al.* (6). The flow rate of gases through the reactor was 5 cm^3/min and the temperature was raised at 5 K/min within the temperature range of 223 K to 773 K. The following sequence of treatments in the TPR apparatus has been used: the sample was dried in Ar at 393 K for 1 hour and subsequently cooled to 223 K, after which a TPR profile was recorded. Next H$_2$ was removed from the reactor at 773 K for Rh/SiO$_2$ and at 573 K for Co/SiO$_2$ and CoRh/SiO$_2$ by He flushing, to avoid H$_2$ chemisorption on the catalyst during cooling. After cooling down to 223 K in He a TPO profile was measured, followed by cooling down to 223 K and flushing with Ar for 1 hour. Finally, a second TPR was recorded.

The EXAFS experiments were performed on X-ray beam line I-5 at the Stanford Synchrotron Radiation Laboratory (SSRL) with ring energies of 3 GeV and ring currents between 40 and 80 mA. The samples used for the EXAFS experiments were pressed into a thin self-supporting wafer and mounted in an EXAFS in situ cell (7). The EXAFS spectra were recorded at liquid nitrogen temperature. Spectra of the Co K-edge and Rh K-edge of CoRh/SiO$_2$ were recorded (under 100 kPa H$_2$) after the passivated catalyst had been reduced in situ at 673 K. After these measurements the sample was evacuated at room temperature and O$_2$ was added. EXAFS spectra (under 100 kPa O$_2$) were again recorded in situ. Also the Rh K-edge spectrum of bulk CoRh (atomic ratio Co/Rh = 1, see Experimental Section of chapter 4) has been measured.

5.4 RESULTS

Profiles of TPR and TPO obtained with the silica-supported Co, Rh and CoRh catalysts are shown in figure 1. The numbers at the profiles correspond to the ratio between the amount of gas consumed and the total amount of metal.
Reduction of the impregnated Co/SiO$_2$ catalyst mainly occurs
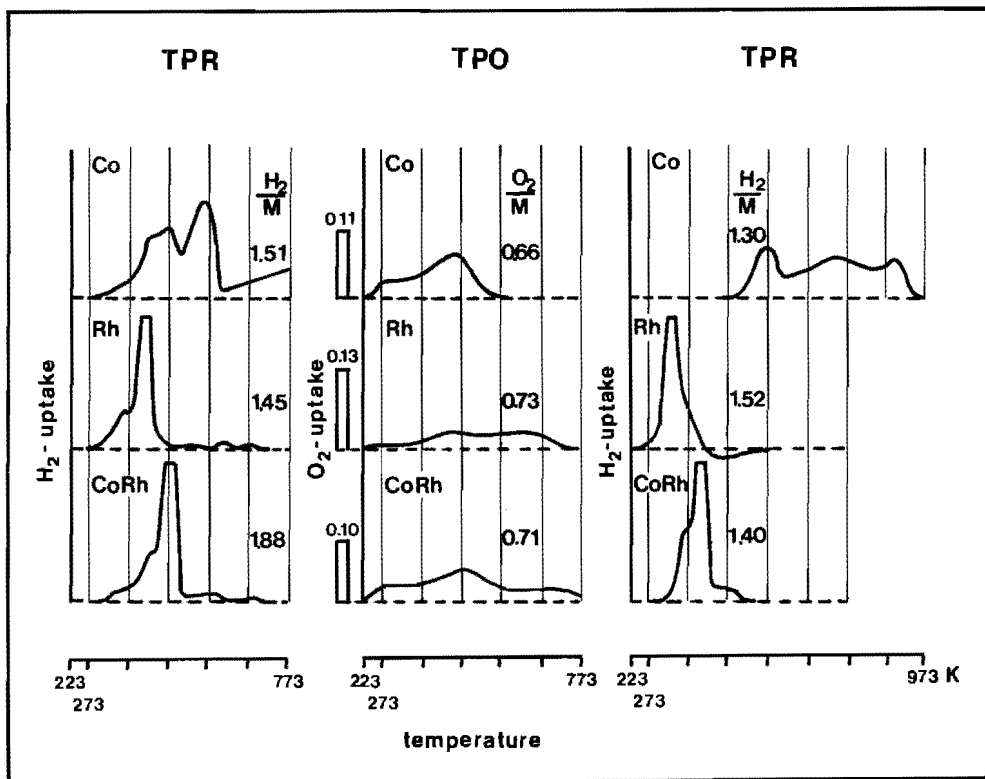
Figure 1 *TPR and TPO profiles of SiO_2-supported cobalt, rhodium and cobalt-rhodium catalysts. The numbers next to the curves refer to the total H_2 or O_2 consumption, expressed per total amount of metal atoms in the catalyst. Temperature was increased at a rate of 5 K/min. Accuracies: H_2/M: ± 5%, O_2/M: ± 10%.*

within the relative broad temperature range of 273 - 600 K. However, at 773 K reduction is not complete. The impregnated Rh/SiO_2 catalyst is already reduced at 473 K. The TPR profile is characterized by two peaks, one at 368 K, which is assigned to the reduction of Rh_2O_3 (formed during impregnation or drying) and one at 413 K, at which temperature $RhCl_3$ is reduced (8). The TPR profile of the impregnated bimetallic catalyst shows that reduction takes mainly place between 273 and 510 K. This

proves that the rate of reduction of cobalt nitrate is enhanced by the presence of rhodium. Therefore, we conclude both metal salts are likely in intimate contact with each other after impregnation. For the same reason as mentioned in chapter 4 the observed H_2/M values for the cobalt containing catalysts give no indication of the reduction degree of the metals after TPR: the simultaneous reduction of residual nitrate groups gives rise to an enhanced H_2/M value. The total amount of hydrogen consumed during TPR of Rh/SiO_2 indicates that the reduction degree of rhodium is high ($95 \pm 5\%$).

The TPO profiles of the reduced catalysts (figure 1) already show oxygen consumption at 223 K due to chemisorption. The oxidation of cobalt supported on silica is already complete at 573 K, whereas higher temperatures are needed to oxidize completely the rhodium and bimetallic catalysts. Provided that after oxidation Co_3O_4 and Rh_2O_3 are formed, the reduction degree of the metals after TPR can be determined from the observed O_2/M values. A striking feature is that without any exception the reduction degrees of all three catalysts are high, for Co/SiO_2, Rh/SiO_2 and $CoRh/SiO_2$ respectively 98, 97 and 100 $\pm$ 10%.

Subsequent TPR measurements result in profiles as presented in figure 1. In order to reduce Co_3O_4/SiO_2 completely we extended the TPR to 973 K. The TPR profile is characterized by a wide temperature range in which hydrogen is consumed. The reduction starts at 473 K and is complete at 973 K. Rh_2O_3 on SiO_2 is fully reduced below 410 K and the reduction is characterized by a single peak with a maximum at 350 K. Above 420 K the hydrogen consumption is negative which is caused by desorption of hydrogen from the catalyst surface. The TPR profile of the bimetallic catalyst is characterized by a main peak around 400 K with a shoulder at lower temperature. Note that the reduction is complete before the oxidized monometallic Co/SiO_2 catalyst starts to be reduced. This clearly indicates that after oxidation the two metal oxides are close together. The observed H_2/M values show that the reduction degrees of the three catalysts are high, for Co/SiO_2, Rh/SiO_2 and $CoRh/SiO_2$,

98, 100 and 99 ± 5%, respectively.

The hydrogen chemisorption measurements yielded H/M values of 0.13, 0.44 and 0.25 for the reduced Co, Rh and CoRh supported catalysts.

In order to obtain more information about the structure of the bimetallic particles in the reduced $CoRh/SiO_2$ catalyst EXAFS spectra were recorded.
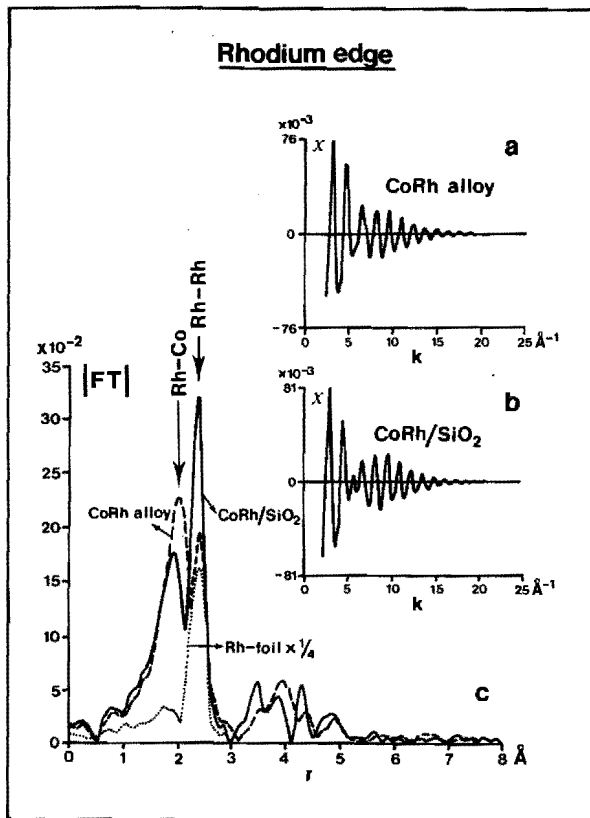
Figure 2 EXAFS of the Rh K-edge of CoRh alloy and CoRh/SiO$_2$.

   a) Normalized EXAFS data for the CoRh alloy (molar Co/Rh ratio is 1).
   b) Normalized EXAFS data for CoRh/SiO$_2$ reduced in situ at 673 K.
   c) The k^1 Fourier transforms (FT's) of the EXAFS of CoRh alloy, reduced CoRh/SiO$_2$ and also for $r < 3$Å Rh-foil. The FT's were taken over a k-range of 3 - 15 Å^{-1}.

Figure 2a and 2b show the normalized EXAFS functions $\chi(k)$ of the rhodium K-edge of, respectively, the CoRh alloy and the CoRh/SiO$_2$ catalyst reduced in situ at 673 K. The oscillations are due to rhodium as well as cobalt neighbour atoms. The associated k^1 Fourier transforms (FT's) of the functions which were taken over the range of wavevectors 3 – 15 $\mathring{A}^{-1}$ are presented in figure 2c. This figure also includes for r < 3 $\mathring{A}$ the k^1 Fourier transform (reduced 4 times) of the EXAFS of Rh-foil (see chapter 2, figure 8a) performed on a k-interval of 3 – 15 $\mathring{A}^{-1}$. Note that the peaks in the transformed function are displaced from the true interatomic distances because of the phase shifts (see chapter 2). The FT's for the bimetallic systems are characterized by two peaks, one around 2.4 $\mathring{A}$ which is assigned to rhodium nearest neighbours because the position of this peak is similar to the position of the main peak in Rh-foil, and another around 1.9 $\mathring{A}$. The latter peak cannot be assigned to the Rh sidelobe, which is caused by the non-linear k-dependences of the backscattering amplitude and the phase of rhodium (see chapter 2), because the peak intensity is much too high. As proven by X-ray diffraction (see chapter 4) the metals cobalt and rhodium in the CoRh alloy are homogeneously mixed which implies that each rhodium atom on the average is surrounded by six rhodium and six cobalt atoms and vice versa. Although a complete analysis of the EXAFS could not be achieved yet the results prove beyond any doubt a difference in bond length of the Rh-Rh bond (2.66 $\pm$ 0.02 $\mathring{A}$) and the Rh-Co bond (2.60 $\pm$ 0.02 $\mathring{A}$). The peak around 1.9 $\mathring{A}$ is then caused by interference of Rh-Rh and Rh-Co EXAFS oscillations. The peak intensity is a measure for the total amount of Rh-Co bonds and therefore we denote this peak as Rh-Co peak.

From figure 2c it can be clearly seen that for the reduced CoRh/SiO$_2$ catalyst the intensity of the Rh-Co peak is smaller, and the intensity of the Rh-Rh peak is bigger than the comparable peaks for the CoRh alloy. This indicates that the rhodium atoms in the reduced catalyst are mainly surrounded by rhodium atoms.

In order to investigate the influence of oxygen on the structure of the bimetallic particles EXAFS spectra of CoRh/SiO$_2$ were recorded after oxygen admission at room temperature to the reduced catalyst leading to a passivated catalyst. The intensity of the Rh-Co and Rh-Rh peak in the rhodium transform is slightly influenced by adsorption of oxygen (not shown). The EXAFS spectra of the Co K-edge of the reduced and the passivated CoRh/SiO$_2$ catalysts are presented in figure 3a and 3b, respectively. Since the signal-to-noise
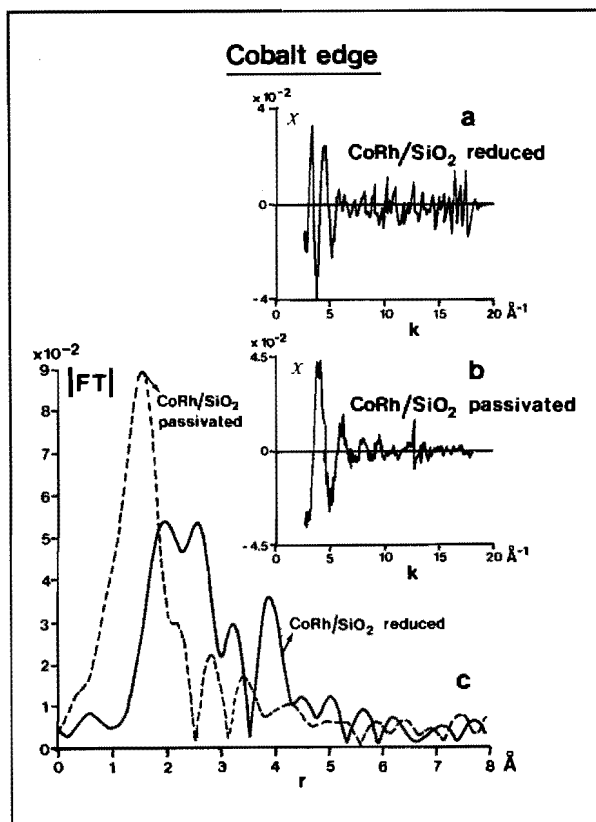
Figure 3 EXAFS of the Co K-edge of CoRh/SiO$_2$.
    a) Normalized EXAFS data for CoRh/SiO$_2$ reduced in situ at 673 K.
    b) Normalized EXAFS data for CoRh/SiO$_2$ after O$_2$ admission at room temperature to the reduced catalyst.
    c) The associated k^1 Fourier transforms taken over a k-range of 3 - 7 Å^{-1} and 3.5 - 9 Å^{-1} for respectively the reduced and passivated CoRh/SiO$_2$ catalyst.

ratio was low (caused by monochromator problems) the k^1 Fourier transforms were taken over small k-ranges, 3 - 7 $\overset{o}{A}^{-1}$ and 3.5 - 9 $\overset{o}{A}^{-1}$ for respectively the reduced and passivated CoRh/SiO$_2$ catalyst. The FT's are presented in figure 3c. This figure illustrates that oxygen adsorption at room temperature changes the coordination shell of cobalt completely. The FT of the reduced catalyst below r = 3 $\overset{o}{A}$ is characteristic for Co–Co and Co-Rh coordination, whereas the FT of the passivated catalyst is characteristic for Co-O coordination.

5.5 DISCUSSION

Regarding the formation of bimetallic Co-Rh particles on a support the results of this investigation completely fit into the picture given for Co-Rh supported on γ-Al$_2$O$_3$ in chapter 4, figure 7. However, in the case of the SiO$_2$ support no irreducible Co-SiO$_2$ compounds are formed.

The TPR profiles for the impregnated catalysts indicate that the two metal salts in CoRh/SiO$_2$ are in intimate contact because CoRh/SiO$_2$ reduces at lower temperatures than mono-metallic Co/SiO$_2$. The more noble metal of the two, rhodium, serves as a catalyst for the reduction of the less noble metal, cobalt. The Co-Rh phase diagram (see chapter 4, figure 1) shows that the two metals form a solid solution and that there is thus no driving force to separate the metals during reduction, once an alloy particle has been formed.

The EXAFS results prove that bimetallic particles are indeed formed during reduction. The Fourier transform of the oscillations of the Rh K-edge of the CoRh/SiO$_2$ catalyst shows that after reduction of the catalyst a phase, rich in rhodium, is formed – the rhodium atoms have much more rhodium neighbours than in the CoRh alloy. It is obvious that formation of a phase, rich in rhodium, is accompanied by formation of a phase, rich in cobalt. The bimetallic particles formed during reduction con-sist of an inner side which is rich in rhodium, whereas the outer layer is enriched in cobalt, since:

1) the rhodium-rich phase is hardly affected by oxygen ad-
   sorption at room temperature - the EXAFS spectrum of the
   Rh K-edge is only slightly influenced,
2) oxygen adsorption changes the coordination shell of cobalt
   completely - the EXAFS spectrum of the Co-edge after
   oxygen adsorption is characteristic for Co-O coordination.
Thus, as predicted in chapter 4 on the basis of the difference
in sublimation energy for cobalt and rhodium, EXAFS has
proven that during reduction of a Co-Rh catalyst cobalt en-
richment in the surface of the bimetallic particles takes place.

Comparison of the TPO profiles for the three catalysts
shows that the same high temperatures are needed for the com-
plete oxidation of the $CoRh/SiO_2$ as for the Rh/SiO_2 catalyst.
During TPO the cobalt-rich surface is oxidized first, as
proven by EXAFS, and therefore the oxygen consumption at
higher temperatures is caused by oxidation of the rhodium-rich
core. After oxidation cobalt and rhodium are present as Co_3O_4
and Rh_2O_3.
The TPR profile of the oxidized Co/SiO_2 catalyst shows that a
temperature of 973 K is needed to reduce the metal oxide,
whereas bulk Co_3O_4 has been reduced completely around 730 K.
This result is in accordance with Paryjczak et $al.$ (9) and has
been interpreted in terms of metal-support interaction. This
interaction may be as strong as in cobalt silicate which
serves as a 'glue' attaching the metallic particle to the
support.
Finally, we note that reduction of the oxidized bimetallic
catalyst occurs within the same temperature range as of the
oxidized Rh/SiO_2 catalyst and is complete below the temperature
above which the oxidized Co/SiO_2 catalyst starts to be reduced.
Apparently, rhodium catalyzes the reduction of cobalt oxide
which implies that both metal oxides are close to each other.

5.6 REFERENCES

1. R. Bouwman, G.J.M. Lippits and W.M.H. Sachtler, J. Catal.,
   <u>25</u>, 300 (1972).
2. J.H. Sinfelt, G.H. Via and F.W. Lytle, J. Chem. Phys., <u>72</u>,
   4832 (1980).
3. J.H. Sinfelt, G.H. Via, F.W. Lytle and R.B. Greegor, J.
   Chem. Phys., <u>75</u>, 5527 (1981).
4. J.H. Sinfelt, G.H. Via and F.W. Lytle, J. Chem. Phys.,
   <u>76</u>, 2279 (1982).
5. G. Meitzner, G.H. Via, F.W. Lytle and J.H. Sinfelt, J. Chem.
   Phys., <u>78</u>, 2533 (1983).
6. H. Boer, W.J. Boersma and N. Wagstaff, Rev. Sci. Instr.,
   <u>53</u>, 349 (1982).
7. D.C. Koningsberger and J.W. Cook, in "EXAFS and Near Edge
   Structures", edited by A. Bianconi, L. Incoccia and S.
   Stipcich, Springer-Verlag, Berlin (1983), p. 412.
8. A.E. Newkirk and D.W. McKee, J. Catal., <u>11</u>, 370 (1968).
9. T. Paryjczak, J. Rynkowski and S. Karski, J. Chromatogr.,
   <u>188</u>, 254 (1980).

chapter 6

CHARACTERIZATION OF BIMETALLIC FeRh/SiO$_2$ CATALYSTS WITH TPR, TPO AND MÖSSBAUER SPECTROSCOPY

6.1 ABSTRACT

TPR and Mössbauer spectroscopy experiments on FeRh/SiO$_2$ catalysts show a clear evidence for the formation of bimetallic particles. The degree of reduciton in FeRh/SiO$_2$ is substantially higher than in Fe/SiO$_2$ catalysts, proving that rhodium acts as a catalyst for the reduction of iron. Addition of O$_2$ to reduced FeRh/SiO$_2$ at room temperature mainly causes oxidation of iron while rhodium remains in the metallic state. This is interpreted as being due to the fact that the bimetallic Fe-Rh particles consist of an outer shell enriched in iron, while the core contains most of the rhodium.

6.2 INTRODUCTION

It is well known that alloying of two metals can markedly improve catalytic properties such as selectivity and stability, compared to the properties of the constituent monometallic catalysts (1). From the selectivity point of view the bimetallic FeRh/SiO$_2$ catalyst is a very interesting system. Bhasin et al. (2) observed a strong synergistic effect for this catalyst in CO hydrogenation at 573 K and 68 x 10^2 kPa. The selectivities to methanol (35%) and ethanol (24%) differed

strongly from that of either supported iron or supported
rhodium catalysts.

In this paper we present the results of a characterization
study of the FeRh/SiO$_2$ system using temperature programmed
reduction and oxidation (TPR and TPO). In situ Mössbauer
spectroscopy is applied to obtain information about the
chemical state of iron after completion of a TPR or TPO experi-
ment. A more detailed Mössbauer study of the FeRh/SiO$_2$ system
has been published elsewhere (3).

6.3 EXPERIMENTAL SECTION

Rh/SiO$_2$ (3.9 wt% rhodium), Fe/SiO$_2$ (3.5 wt% iron), and
FeRh/SiO$_2$ (5 wt% metal, atomic ratio Fe:Rh = 1:1) were prepared
by using the incipient wetness technique. Aqueous solutions
of Fe(NO$_3$)$_3$.9H$_2$O (Merck P.A.), RhCl$_3$.xH$_2$O (39 wt%, Drijfhout)
and a mixture of the two metal salts for the preparation of
the bimetallic catalyst were used to impregnate the silica
support (Grace, S.D. 2 - 324.382, 290 m^2/g). The impregnated
samples were dried at room temperature overnight, at 333, 353
and 373 K for 2 hours at each temperature, and finally at 393 K
for 60 hours.

TPR and TPO experiments were carried out with 5% H$_2$ in Ar
and 5% O$_2$ in He respectively, with 200 mg catalyst in an
apparatus described by Boer *et al.* (4). The gases (research-
grade, Hoekloos) were purified over a BTS column for the
removal of oxygen and over molecular sieves (Union Carbide, 5A)
for the removal of water. The flow rate of gases through the
reactor was 5 cm^3/min and the temperature was raised at
5 K/min within the temperature range of 223 to 773 K. The
following sequence of treatments in the TPR apparatus has been
used: the sample was heated in Ar at 393 K for 1 hour and sub-
sequently cooled to 223 K, after which a TPR profile was
recorded. Next H$_2$ was removed from the reactor at 773 K by
He flushing, to avoid H$_2$ chemisorption on the catalyst during
cooling. After cooling down to 223 K in He a TPO profile was
measured, followed by cooling down to 223 K and flushing with
Ar for 1 hour. Finally, a second TPR was recorded. The amount

of gas consumed during TPR and TPO is expressed per total amount of metal, H_2/M and O_2/M. As the oxidation states of rhodium and iron before reduction and after oxidation are 3+, the H_2/M value which corresponds to complete reduction of the metals is 1.5. The O_2/M value for complete oxidation of the reduced metal is 0.75.

Chemisorption measurements were performed in a conventional glass system at 298 K. Before measuring the adsorption isotherms the impregnated catalysts were reduced at 773 K (heating rate 5 K/min) for 1 hour under flowing hydrogen and evacuated (10^{-2} Pa) at 773 K for another hour. The total amount of chemisorbed H atoms per total amount of metal H/M, was determined according to the method of Benson and Boudart (5).

Mössbauer spectra were measured in situ at room temperature, with 320 mg of $FeRh/SiO_2$ pressed into a wafer with a diameter of 20 mm. The spectrometer and in situ reactor have been described previously (3, 6). The spectra were fitted by computer with calculated subspectra consisting of Lorentzian-shaped lines, by varying the Mössbauer parameters in non-linear iterative minimization routine (6).

6.4 RESULTS

TPR and TPO profiles of the silica-supported Rh, Fe and FeRh catalysts are shown in figure 1. The numbers next to the profiles correspond to the ratio between the amount of gas consumed and the total amount of metal in moles.

Reduction of the Rh/SiO_2 catalyst after impregnation and drying occurs within the temperature range of 273-473 K and is characterized by two peaks, one at 368 K, which is assigned to the reduction of Rh_2O_3 (formed during impregnation or drying) and one at 413 K, at which temperature $RhCl_3$ is reduced (7). The reduction of the Fe/SiO_2 catalyst is more difficult, it does not start until 473 K. In anticipation of the results of the second TPR, we assign the two peaks to the reduction of $Fe(NO_3)_3$ (573 K) and Fe_2O_3 (638 K), respectively. The most
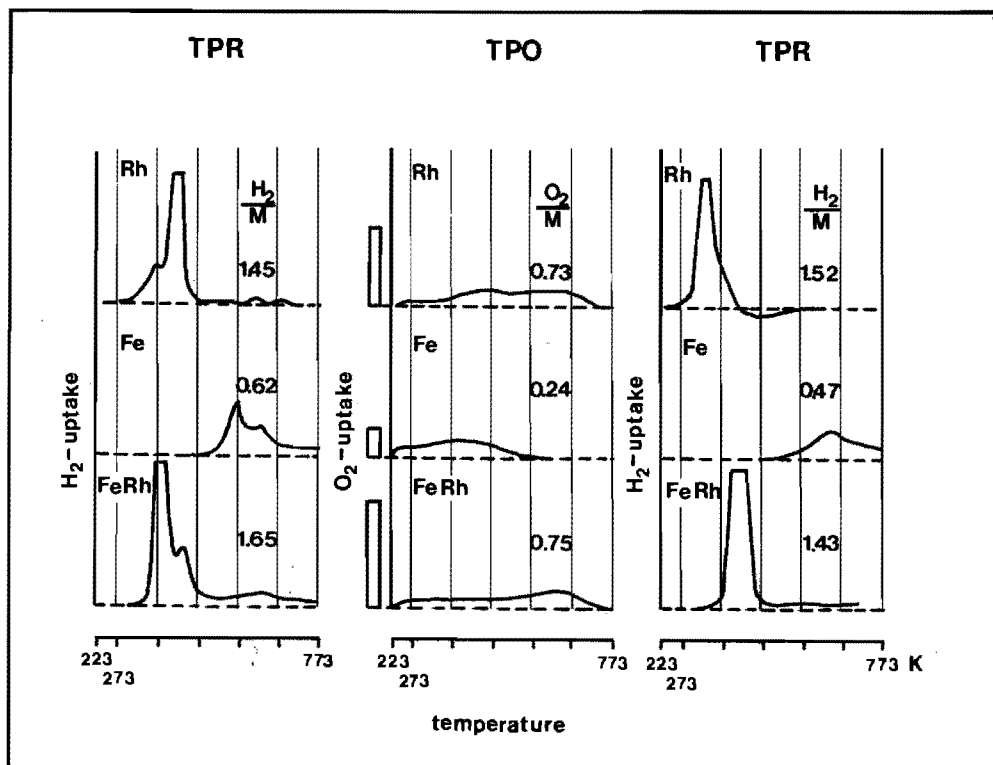
Figure 1 TPR and TPO profiles of SiO_2-supported rhodium, iron and iron-rhodium catalyst. The numbers next to the curves refer to the total H_2 or O_2 consumption, expressed per total amount of metal atoms in the catalyst. Temperature was increased at a rate of 5 K/min. Accuracies: H_2/M: ± 5%, O_2/M: ± 10%.

striking feature of the TPR profile of $FeRh/SiO_2$ is that reduction takes place mainly within the temperature range of 273-473 K. This indicates that both metal salts are in intimate contact after impregnation and that rhodium serves as a catalyst for the reduction of $Fe(NO_3)_3$ and Fe_2O_3. The shoulder at 413 K cannot be unambiguously assigned to a compound. The H_2/M values indicate that for the monometallic rhodium catalyst the re-

duction degree of rhodium is high (95 $\pm$ 5%), whereas the re-
duction degree of the iron catalyst does not exceed 42%. This
is an upper limit because part of the nitrate may be reduced
too, which would contribute to the H_2/M value. Because of this
problem the reduction degrees of the bimetallic FeRh/SiO$_2$ and
the monometallic Fe/SiO$_2$ catalyst cannot be determined exactly
from the H_2/M values.

The TPO profiles (figure 1) of the reduced catalysts in-
dicate that with all three catalysts oxygen is already con-
sumed at 223 K. The oxidation of the iron catalyst is complete
at 573 K, whereas higher temperatures are needed to oxidize
the rhodium and the bimetallic catalysts completely. From the
observed O_2/M value of 0.75 $\pm$ 10% for the bimetallic catalyst
we conclude that the degree of reduction after the thermo-
reduction was high.

Subsequent TPR measurements result in profiles as presented
in figure 1. Rh_2O_3 on SiO$_2$ is fully reduced below 413 K and the
reduction is characterized by a single peak with a maximum at
348K. Above 423 K the hydrogen consumption is negative which
is caused by desorption of hydrogen from the catalyst surface.
Reduction of iron oxide supported on silica occurs above 493 K
and at 773 K only about 30% of the oxide is reduced. The TPR
profile of the bimetallic catalyst clearly indicates that after
oxidation the two metal oxides are close together, as the
reduction is characterized by a single peak, at 418 K. The
H_2/M ratio for the bimetallic catalyst is 1.43 ($\pm$ 5%), which
corresponds to a reduction degree of 95 $\pm$ 5%.

The hydrogen chemisorption measurements yielded H/M values
of 0.44, 0.01 and 0.16 for the reduced Rh, Fe and FeRh supported
catalysts, respectively. These results clearly indicate that
the dispersion of the monometallic rhodium catalyst is high.
The low H/M value obtained for the monometallic iron catalyst
cannot be correlated with dispersion because the degree of
reduction of the catalyst is low (about 30%), as confirmed by
TPR.

The adsorption of hydrogen on reduced supported iron
catalysts is an activated process (8). Consequently, the H/M

value of the bimetallic catalyst gives the lower limit of the dispersion.

To obtain more insight into the oxidation state of the iron in the bimetallic catalyst after different stages of reduction and oxidation, Mössbauer spectra were recorded. Figure 2 shows the in situ Mössbauer spectra of the bimetallic catalyst at room temperature after different treatments as indicated in the figure.
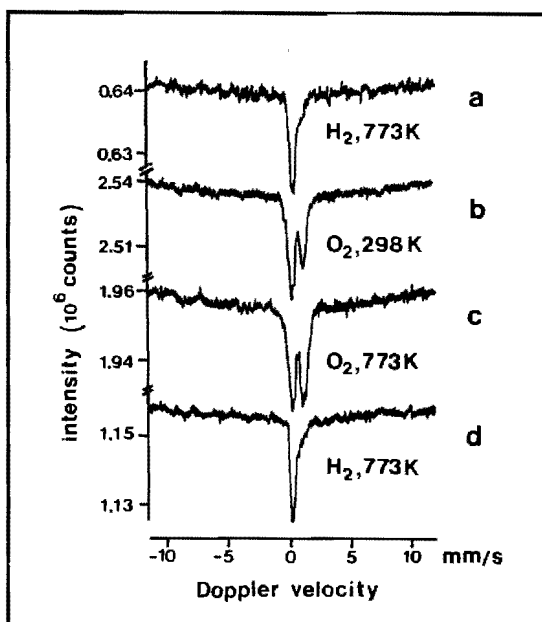
Figure 2 In situ Mössbauer at 298 K of the bimetallic FeRh/SiO$_2$ catalysts after the treatments indicated.

The spectra were analysed applying an appropriate computer program and the Mössbauer parameters are listed in table 1.

The spectrum of the FeRh/SiO$_2$ catalyst after reduction· at 773 K for 3 hours (figure 2a) consists of a large single line and a shoulder which belongs to a doublet, the left peak of which coincides with the singlet. Evidence that the inter-pretation in terms of a singlet and a doublet is correct will be presented elsewhere (9). The isomer shift of the singlet

Table 1 Mössbauer parameters of FeRh/SiO₂ at 298 K.

treatment	iron state	IS mm/s	QS mm/s	LW mm/s	spectral contribution (%)
fresh catalyst	Fe^{3+}	0.62	0.69	0.44	100
H_2, 773 K, 3h	Fe^0	0.37	-	0.44	73
	Fe^{3+}	0.61	0.88	0.33	27
O_2, 298 K	Fe^0	0.35	-	0.35	18
	Fe^{3+}	0.64	1.03	0.58	82
O_2, 773 K, 3h	Fe^{3+}	0.64	1.04	0.63	100
H_2, 773 K, 3h	Fe^0	0.35	-	0.47	75
	Fe^{3+}	0.65	0.87	0.38	25

Accuracies: IS: $\pm$ 0.03 mm/s, QS: $\pm$ 0.05 mm/s, LW: $\pm$ 0.10 mm/s, spectral
contribution: $\pm$ 5%.

IS relative to sodium nitroprusside (SNP).

(0.36 mm/s) is within the range of those for Fe-Rh bulk alloys
(10). Hence, it is assigned to Fe^0 in the bimetallic crystallite.
The Mössbauer parameters of the doublet are characteristic for
high spin Fe^{3+} ions. Therefore, we assign the doublet to
irreducible iron(III)oxide in the FeRh/SiO₂ catalyst.

The spectrum of FeRh/SiO₂ after oxidation at room tempera-
ture (figure 2b) consists for 82% of the spectral area of an
Fe^{3+} doublet and for only 18% of the singlet which is due to
Fe^0 in Fe-Rh alloy particles.

Oxidation at 773 K for 2 hours leads to a Mössbauer
spectrum (figure 2c) which consists of an Fe^{3+} doublet and
consequently only oxidic iron is present. A subsequent thermo-
reduction at 773 K for 3 hours yields a spectrum (figure 2d)
similar to the Mössbauer spectrum obtained after the first
reduction.

6.5 DISCUSSION

The results of this investigation clearly demonstrate that co-clustering of iron and rhodium in the bimetallic $FeRh/SiO_2$, catalyst occurs since:

(i) $FeRh/SiO_2$ is reduced at lower temperatures than mono-metallic Fe/SiO_2,

(ii)   the degree of reduction in the bimetallic catalyst is substantially higher than in the monometallic iron catalyst, and

(iii) the Mössbauer spectrum of reduced $FeRh/SiO_2$ indicates that most of the iron is present as Fe^0 in an Fe-Rh alloy. Apparently, rhodium, the noble metal, enhances the reducibility of the less noble metal, iron, appreciably.

Reduction of well dispersed iron on oxidic supports is difficult due to inhibition of the nucleation, $i.e.$ the reaction between molecular H_2 and the metal oxide to produce metal atoms and H_2O (11). Consequently, the degree of reduction of the Fe/SiO_2 catalysts is low, in our case only about 30%. Supported rhodium catalysts do not suffer from nucleation problems and hence a high degree of reduction up to 100% is observed. The catalytic effect of rhodium in the reduction of the bimetallic $FeRh/SiO_2$ catalyst can be explained by assuming that rhodium atoms, reduced by molecular H_2, act as nucleation centres. At these sites H_2 is dissociated to yield H atoms which are sufficiently reactive to reduce oxidic iron. This mechanism is sometimes called 'intra particle hydrogen spill-over' (12).

The Mössbauer spectrum of reduced $FeRh/SiO_2$ contains a contribution which was assigned to a doublet of iron(III)oxide. Stronger evidence for this assignment and a more detailed investigation of this oxide will be presented elsewhere (9). The presence of irreducible material in the catalyst is in accordance with the observed H_2/M value of 1.43, which is lower than the theoretical value of 1.50.

The Mössbauer spectrum of the bimetallic catalyst contains no contributions due to α-Fe or Fe^{2+}, phases which are commonly

encountered in monometallic Fe/SiO_2 catalysts (3). Hence, we
conclude that isolated iron particles have not been formed.
Although the second TPR profiles in figure 1 indicate that most
of the rhodium is present in clusters together with iron, we
cannot exclude the presence of some isolated rhodium particles
in the bimetallic catalyst, as the TPR curves in repeated runs
with oxidized Rh/SiO_2 and $FeRh/SiO_2$ overlap at temperatures
between 333 and 413 K.

Comparison of the TPO profiles for the three catalysts
suggests that iron does not promote the oxidation of rhodium in
the bimetallic catalyst. The same high temperatures are needed
for the complete oxidation of the $FeRh/SiO_2$ as for the Rh/SiO_2
catalyst. However, the Mössbauer spectrum in figure 2b shows
that oxidation at room temperature converts most of the iron
atoms into iron(III)oxide. Only about 20% of the spectrum is
due to Fe^0 atoms in the Fe-Rh alloy. The TPO curve indicates
that the degree of oxidation reached at room temperature is of
the order of 40%. Combination of these two results leads to
the conclusion that oxidation of the bimetallic $FeRh/SiO_2$
catalyst at room temperature affects mainly the iron, whereas
rhodium remains in a reduced state. An X-ray photoelectron
spectroscopy measurement confirmed that rhodium in the
passivated $FeRh/SiO_2$ catalyst is present as Rh^0 (13).

The results can be understood in the context of a 'core
and shell' model of the bimetallic particles. On the assumption
that the regular solution model is valid, the two metals are
completely miscible, the thermodynamics of this system predicts
that the metal with the lowest sublimation energy will be
enriched in the surface region of the alloy (14). As the
sublimation energy of iron is lower than that of rhodium,
surface enrichment of iron in the reduced Fe-Rh cluster is thus
to be expected. When this bimetallic cluster is exposed to O_2
at room temperature surface enrichment of iron will be even
more pronounced. After oxidation at room temperature the
particle will consist of an outer shell of mainly iron oxide
and a core of Fe-Rh alloy with a high Rh content. High tempera-
tures are necessary for a complete oxidation of the bimetallic

cluster. The TPO profile of the FeRh/SiO$_2$ catalyst above 473 K is similar to that of the monometallic rhodium catalyst and can be assigned to the oxidation of the rhodium core (15).

The TPR profile of the oxidized bimetallic catalyst (figure 1) is characterized by a single peak and suggests that the oxides are co-clustered and that no segregation of the metal oxides has occurred. The temperature at which the reduction takes place is below the temperature above which the oxidized Fe/SiO$_2$ catalyst starts to reduce and this demonstrates again that clustering of rhodium and iron enhances the reducibility of iron. However, if rhodium catalyzes the reduction of iron one would expect that reduction of mono-metallic Rh/SiO$_2$ and bimetallic FeRh/SiO$_2$ starts at the same temperature. However, the reduction of the bimetallic catalyst starts at a significantly higher temperature than that of the monometallic Rh/SiO$_2$ catalyst. This result is consistent with the proposed core and shell model. As explained before, the formation of the first rhodium metal atoms, the nucleation step, is the rate-determining step. In the case of the oxidized bimetallic catalyst the chance of nucleation on the oxide surface is diminished compared to the oxidized monometallic rhodium catalyst, because the rhodium concentration in the outer shell is low due to the surface enrichment of iron. In order to start nucleation in the core region where the rhodium content is high, hydrogen must diffuse through the outer shell of iron oxide. This process may be rate-determining for the reduction and be the cause that the reduction starts at higher temperatures than in systems where rhodium is present at the surface.

Finally, we note that reduction of the bimetallic catalyst after high temperature oxidation leads to the same Mössbauer spectrum as reduction of the impregnated catalyst. Thus, reduction and oxidation of the bimetallic FeRh/SiO$_2$ catalyst are reversible.

6.6 REFERENCES

1. V. Ponec, Catal. Rev.-Sci. Eng., 11, 41 (1975).

2. M.M. Bhasin, W.J. Bartley, D.C. Ellgen and T.P. Wilson, J. Catal., 54, 120 (1978).

3. J.W. Niemantsverdriet, A.M. van der Kraan, J.J. van Loef and W.N. Delgass, J. Phys. Chem., 87, 1292 (1983).

4. H. Boer, W.J. Boersma and N. Wagstaff, Rev. Sci. Instr. 53, 349 (1982).

5. J.E. Benson and M. Boudart, J. Catal., 4, 704 (1965).

6. J.W. Niemantsverdriet, thesis, Delft (1983).

7. A.E. Newkirk and D.W. McKee, J. Catal., 11, 370 (1968).

8. H. Topsøe, N. Topsøe and H. Bohlbro, Int. Cat. Congress Tokyo (1980).

9. J.W. Niemantsverdriet, D.P. Aschenbeck, F.A. Fortunato and W.N. Delgass, J. Mol. Catal., to be buplished.

10. C.C. Chao, P. Duwez and C.F.J. Chang, J. Appl. Phys., 42, 4282 (1971).

11. J.R. Anderson, "Structure of Metallic Catalysts", Academic Press, New York, (1975).

12. N.W. Hurst, S.J. Gentry, A. Jones and B.D. McNicol, Catal. Rev.-Sci. Eng., 24, 233 (1982).

13. C.F.J. Flipse, unpublished results.

14. F.L. Williams and D. Nason, Surf. Sci., 45, 377 (1974).

15. J.C. Vis, H.F.J. van 't Blik, T. Huizinga, J. van Grondelle and R. Prins, J. Mol. Catal., to be published.

chapter 7

A SPECTROSCOPIC AND CHEMICAL CHARACTERIZATION STUDY OF THE STRUCTURAL PROPERTIES OF RHODIUM IN AN ULTRA DISPERSED Rh/Al$_2$O$_3$ CATALYST

7.1 ABSTRACT

An investigation of the structural properties of rhodium present in an ultra dispersed 0.57 wt% Rh/γ-Al$_2$O$_3$ catalyst has been carried out with the use of a number of complementary techniques: Extended X-ray Absorption Fine Structure (EXAFS), X-ray Photoelectron Spectroscopy (XPS), Electron Spin Resonance (ESR), Temperature Programmed Reduction (TPR), CO infrared spectroscopy and hydrogen and carbon monoxide chemisorption. After reduction of the catalyst at 593 K the rhodium is quantitatively reduced and three-dimensional metallic rhodium crystallites are formed. The crystallites are attached to the support through Rh^0 to O^{2-} bonds only. CO adsorption on the reduced catalyst changes the structure of rhodium drastically. A significant disruption of rhodium-rhodium bonds takes place, ultimately leading to isolated rhodium geminal dicarbonyl species in which rhodium has an oxidation state of 1+ and in which each rhodium ion is surrounded by two carbon monoxide molecules and three oxygen ions.

7.2 INTRODUCTION

As a result of many industrial applications, *e.g.* in the hydrogenation of carbon monoxide, the reduction of NO in automobile exhaust gas and the hydroformylation of olefines, rhodium on alumina catalysts are studied extensively. The use of ultra dispersed rhodium on a support is not only of obvious importance from an economical point of view, but also from the point of view of activity and selectivity of catalytic reactions. Yao *et al.* (1) reported that going from a well dispersed phase to a particulate phase the specific activity for n-pentane hydrogenolysis decreased and for NO reduction by H_2 increased. Alterations in the reaction parameters and in the product distributions indicated strongly that the rate-determining step in the NO reduction and the reaction intermediate(s) in the n-pentane hydrogenolysis changed if the rhodium surface phase changed. The oxidation state of rhodium during reaction can be very important in view of the selectivity. There are indications that the selectivity to oxygen containing products like methanol and ethanol in the hydrogenation of carbon monoxide can be ascribed to the presence of rhodium ions (2-4).

Although many detailed characterization studies of highly dispersed rhodium catalysts have been reported, the state of the metal is not yet known exactly. There even exists a controversy about the structure and oxidation state of the rhodium after reduction by hydrogen in these ultra dispersed systems. Infrared spectroscopy has been used as a sensitive tool to study the variations in carbon-oxygen stretching frequencies of CO chemisorbed on Rh/Al_2O_3 catalysts (5-12). These variations are due to subtle changes in the character of the supported rhodium. At high rhodium loading two CO bands are observed, one around 2060 cm^{-1} and another broad band between 1800 and 1900 cm^{-1}. Both bands are assigned to CO molecules adsorbed on rhodium atom(s) on the surface of rhodium metal crystallites, the former band due to a CO molecule on top of an Rh atom, the latter band due to a CO molecule bridged between two neigh-

bouring Rh atoms. Another surface species consists of two CO molecules bound to one surface Rh (bands at 2095 and 2027 cm^{-1}, representing the symmetrical and antisymmetrical CO stretching modes, respectively). This surface species is more pronounced for catalysts with a low Rh loading. The wavenumbers correspond closely to those observed for the bridged $[Rh(CO)_2Cl]_2$ dimer and do not shift in frequency with increasing CO coverage. On the basis of these data some investigators have asserted that rhodium on alumina is monatomically dispersed and is in the Rh^{1+} state (5-9).

On the other hand there are strong indications that rhodium is present as metallic crystallites after reduction with hydrogen. Detailed studies have been performed on these dispersed systems using catalytic reactions (1, 13) (e.g. hydrogenolysis, which is catalyzed by metals only), as well as chemisorption and electron microscopy (10, 11). From the electron microscopy studies one has concluded that rhodium is present in two-dimensional metallic raft-like structures, the so-called δ-phase. Calculations have been reported which indicate that for small metallic clusters on supports indeed the raft-like two-dimensional form is more stable than the three-dimensional form (14). In the studies mentioned previously (10, 11) CO infrared measurements were also carried out and the observed $Rh(CO)_2$ species was assigned to two CO molecules adsorbed on edge atoms in two-dimensional rafts.

In general, one can envision four possibilities concerning the structure of the ultra dispersed rhodium: a) metal crystallites, either in a two- or three-dimensional form, b) isolated Rh^0 atoms, c) isolated Rh^{n+} ions and d) a combination of these three forms. Because of the results of the electron microscopy studies, which showed the existence of rhodium particles, one would be inclined to exclude model b) and c). A further unambiguous choice between model a) and d) cannot be made on the basis of existing information.

In order to obtain more insight into the structure of rhodium and the influence of CO adsorption on this structure we characterized a reduced highly dispersed rhodium catalyst

before and after CO admission, by a number of complementary
techniques. The techniques used are Extended X-ray Absorption
Fine Structure spectroscopy (EXAFS), X-ray Photoelectron
Spectroscopy (XPS), Electron Spin Resonance (ESR), Temperature
Programmed Reduction (TPR), CO infrared spectroscopy and
hydrogen and carbon monoxide chemisorption.
EXAFS is, in contrast to diffraction techniques, sensitive
to short-range order and can provide unique structural
information on highly dispersed catalysts (15-17). Preliminary
results of EXAFS measurements performed on reduced Rh/Al_2O_3
and Rh/TiO_2 catalysts have been reported before (18) and in
that study it was concluded that rhodium is not entirely
atomically dispersed.
The importance of XPS in the characterization of supported
catalysts has been demonstrated by several authors (19, 20).
Huizinga *et al.* (21) have reported an extensive XPS study of
Pt and Rh supported on γ-Al_2O_3 and TiO_2 catalysts.
In view of the above mentioned problem, dealing with the
structure of rhodium, ESR is a powerful technique to dis-
tinguish between isolated Rh^0 (d^8s^1) atoms and Rh^{2+} (d^7) ions
(an ESR signal will be present) on one side, and isolated Rh^{1+}
(d^8) ions and Rh^{3+} (d^6) ions (an ESR signal will be absent) on
the other side.
With the TPR technique one can obtain information about the
reducibility of an impregnated, a passivated, as well as an
oxidized catalyst. From the quantitative results, expressed by
H_2/Rh ratios, a distinction between a completely reduced (only
metallic rhodium is present) and a partly reduced catalyst
(the average oxidation state is positive) can be made.

In this chapter we will present the results of an in situ
study on a highly dispersed 0.57 wt% Rh/γ-Al_2O_3 catalyst before
and after CO admission, and will discuss the structure of
rhodium after reduction with hydrogen as well as the influence
of CO adsorption on the topology of rhodium. Preliminary
results of this study have been published recently (12).

7.3 EXPERIMENTAL SECTION

CATALYST PREPARATION

The 0.57 wt% Rh/γ-Al$_2$O$_3$ catalyst was prepared by incipient wetting of γ-Al$_2$O$_3$ with an aqueous solution of RhCl$_3$.xH$_2$O (Drijfhout & Zn.). The support γ-Al$_2$O$_3$ (BET area of 150 m^2/g and a pore volume of 0.65 cm^3/g) was obtained by heating boehmite (supplied by Martinswerk, GmbH) at 873 K. After impregnation the catalyst was dried in air at 393 K during 20 hours to remove the adsorbed water and stored for further use. The rhodium content was determined colourimetrically.
A 2 wt% Rh/γ-Al$_2$O$_3$ catalyst was prepared by using the dimer [Rh(CO)$_2$Cl]$_2$ as precursor. The dimer was prepared from RhCl$_3$.xH$_2$O and CO as described by McCleverty *et al.* (22). In this case the support used was a Ketjen γ-Al$_2$O$_3$ (000-1.5 E, S.A. = 200 m^2/g, P.V. = 0.60 cm^3/g). The support was dispersed in n-hexane to which a solution of [Rh(CO)$_2$Cl]$_2$ in n-hexane was added. After 2 hours this mixture had decolourized which indicated that the exchange was complete. After filtering the catalyst was vacuum dried at 298 K during 30 minutes and stored.

CHEMISORPTION

Chemisorption measurements were performed in a conventional glass system at 298 K. Researchgrade CO was used without further purification. Hydrogen was purified by passing through a Pd diffusion cell. Before measuring the CO and H$_2$ chemisorption the dried catalyst was reduced at 593 K (heating rate of 5 K/min) for one hour under flowing hydrogen and evacuated (10^{-2} Pa) at 573 K for another hour. The procedure of the measurement was as follows: after reduction and evacuation of the catalyst approximately 70 kPa H$_2$ or CO was admitted. When equilibrium was reached the pressure in the system was diminished in steps of about 10 kPa by pumping away a known amount of gas. As we measured from high to low pressure we will

use the term desorption isotherm instead of adsorption isotherm.
Following the method of Benson and Boudart (23) one obtains
the total amount of chemisorbed H atoms and CO molecules by
extrapolating the linear higher-pressure region (P > 30 kPa,
above which monolayer coverage has been reached) of the iso-
therm to zero pressure and by correcting for the extrapolated
value of the bare support.

TPR

The thermoreduction studies were performed in an apparatus
similar to the one which has extensively been described by
Boer et $al.$ (24). A mixture of 5% H_2 in Ar was used for the
reduction. This mixture was purified over molecular sieves for
the removal of water and over a BTS column for the removal of
traces of oxygen. By using a Thermal Conductivity Detector (TCD)
of the diffusion type the difference between the hydrogen con-
centration of the mixture entering and leaving the reactor can
be detected. The TCD signal monitored as a function of tempera-
ture, controlled by a LN 1300 temperature controller, yields
the TPR profile. The heating rate during all TPR measurements
was 5 K/min and the gas flow rate 5 Nml/min. Since water
is formed during reduction of the supported oxides by hydrogen,
the gas coming from the reactor is dried over magnesium
perchlorate before entering the thermal conductivity cell.
Before the reduction was performed the catalyst was dried in
argon at 393 K during one hour in the reactor of the TPR
apparatus and was subsequently cooled to 223 K (a supply of
liquid coolant is present). The amount of consumed gas during
TPR is expressed per total amount of metal, H_2/Rh. As the
oxidation state of rhodium in the impregnated and oxidized
catalyst is 3+ the theoretical H_2/Rh value is 1.5. The
accuracies of the given values are $\pm$ 5%.

ESR

To measure ESR spectra in situ we used a reactor designed by Konings *et al.* (25). X-band ESR spectra were recorded with a Varian E-15 spectrometer equipped with a TE-104 dual sample cavity. The sample temperature was kept constant between 20 and 300 K with a Cryoson CE-5348 temperature controller. Signal intensity, position of the signal and quality factor of the ESR cavity were calibrated with the aid of a Varian strong pitch sample ($g = 2.0028$, 3×10^{15} spins/cm). The ESR spectra were recorded at 20 K.

XPS

XPS measurements were carried out on a Physical Electronics 550 XPS/AES spectrometer equipped with a magnesium anode ($h\nu = 1253.6$ eV) and a double pass cylindrical mirror analyser. A PDP 11-04 computer interfaced with the XPS apparatus enabled signal averaging to be carried out. Prior to the measurements, the passivated powdered sample was pressed on a stainless steel grid, which was mounted onto a heatable transfer rod (21). The catalysts were prepared on the rod in a preparation chamber attached to the UHV work chamber. After the treatment the pre-paration chamber was evacuated to 6.6×10^{-3} Pa at 298 K after which the rod was transported via a gate valve to the work chamber and positioned in front of the analyser and X-ray source. The pressure during the measurements did not exceed 6.6×10^{-6} Pa and the temperature was approximately 313 K. The binding energies, referenced to the Fermi level, were calibrated by adjusting the C 1s energy at 284.6 eV. The Al 2p (74.4 eV) binding energy of the support was used as a check on the carbon reference.

IR SPECTROSCOPY

Infrared spectra were recorded at 298 K with a Bruker IFS 113V Fourier transform spectrometer with a resolution of 2 cm^{-1}.

The catalyst was pressed into a thin self-supporting wafer, following a pre-reduction at 593 K and passivation at room temperature, and was placed in an infrared cell suitable for in situ measurements (26). Before CO admission (50 kPa) and evacuation (10^{-1} Pa) at 298 K the catalyst was reduced and evacuated (10^{-1} Pa) at 523 K.

EXAFS

The EXAFS experiments were performed on X-ray beam line I-5 at the Stanford Synchrotron Radiation Laboratory (SSRL) with a ring energy of 3 GeV and a ring current between 40 and 80 mA. The EXAFS spectra were recorded at liquid nitrogen temperature in an in situ cell (27). The samples were pressed into a thin (0.2 mm) self-supporting wafer and mounted in the sample cell. The reduction procedure of the 0.57 wt% Rh/γ-Al$_2$O$_3$ catalyst was identical to the one preceding the chemisorption measurements. After in situ EXAFS experiments of the reduced catalyst (under 100 kPa H$_2$) the cell was evacuated at 573 K for one hour. After cooling in vacuum (10^{-2} Pa) to room temperature the sample was exposed to 100 kPa CO and the EXAFS spectrum was again recorded in situ.

The EXAFS signal $\chi(k)$ per absorbing atom was obtained from the X-ray absorption spectra by a cubic spline background subtraction. A low amplitude of the remaining EXAFS oscillations in the derivative of the background indicates a good separation of EXAFS and background. Normalization was done by a simple division by the edge jump. Because the reference compound is treated in the same way, no errors in the amplitude are introduced. The fine structure was smoothed by removing high frequency components (noise) in the spectrum via Fourier transformation. The r-region of primary interest (from 1 Å to 3.5 Å) of the Radial Structure Function (RSF) is not affected by the smoothing operation. From the smoothed data information is obtained about the type of backscattering atom, the coordination distance R, average coordination number N and the thermal and static disorder $\Delta\sigma^2$.

The EXAFS data were analysed by using reference samples with known structure (the theory-independent analysis) and the Fourier filtering approach was used. The data analysis procedure will be extensively described by Van Zon *et al*. (28). As reference compounds we used Rh-foil, powdered Rh_2O_3 and powdered $RhCl_3$. As a suitable reference compound for the rhodium geminal dicarbonyl $Rh(CO)_2$ we used the dimer $[Rh(CO)_2Cl]_2$. The powders and the dimer were mixed with respectively alumina and silica in order to obtain an optimal absorption with respect to signal-to-noise ratio.

7.4 RESULTS AND DISCUSSION

7.4.1 THE STRUCTURE OF RHODIUM AFTER REDUCTION

7.4.1.1 Results

TPR

    In figure 1 the TPR profile for the impregnated and dried $Rh/\gamma-Al_2O_3$ catalyst is given.

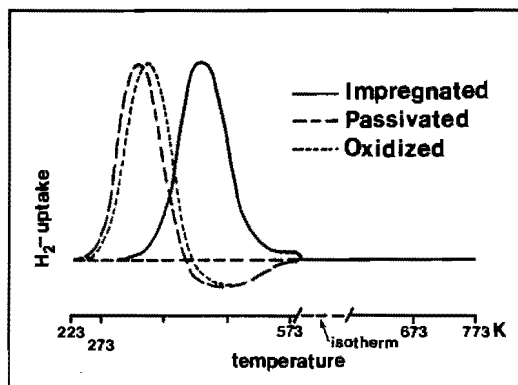*Figure 1 TPR of 0.57 wt% $Rh/\gamma-Al_2O_3$ after: impregnation, reduction at 773 K and passivation, and reduction at 773 K and oxidation at 773 K.*

The reduction was performed in two steps. First the tempera-
ture was increased up to 593 K and held at that temperature
for one hour (the normal reduction procedure of the catalyst
before each measurement), followed by a further reduction up
to 773 K. A striking feature is that after reduction at 593 K
no more hydrogen is consumed which indicates that the re-
duction has been completed. The hydrogen consumption can be
accounted for by the reaction: $RhCl_3 + 1.5 H_2 \rightarrow Rh + 3 HCl$.
The H_2/Rh value of 1.43 (table 1) shows that the majority of
Rh^{3+} has been reduced, which means that the reduction degree
is 1.43/1.50 = 0.95. These results are in accordance with those
reported by Newkirk and McKee (29). By using thermogravimetric
analysis they also found that reduction temperatures in the
range of 423-473 K are sufficient to reduce rhodium chloride
to the elemental metal.

In figure 1 also the TPR profiles are presented for a passiva-
ted (oxidation at 298 K) $Rh/\gamma-Al_2O_3$ catalyst and a catalyst
oxidized at 773 K, which had been pre-reduced at 773 K for one
hour. The corresponding H_2/Rh values are given in table 1.

*Table 1 Hydrogen consumption during Temperature Programmed
Reduction of 0.57 wt% $Rh/\gamma-Al_2O_3$ after different
treatments.*

Treatment	H_2/Rh
Impregnation	1.43
Reduction at 773 K, passivation	1.36
Reduction at 773 K, oxidation at 773 K	1.41

For the passivated catalyst an H_2/Rh value of 1.36 was observed
which shows that passivation leads to a high degree of oxida-
tion for highly dispersed rhodium supported on $\gamma-Al_2O_3$. If the

oxidation would have been complete an H_2/Rh value of 1.5 would
have been found, according to the reaction: $Rh_2O_3 + 1.5 \ H_2 \rightarrow$
$Rh + H_2O$. Notice the negative TCD signal in the temperature
region 343-623 K, which is due to the desorption of hydrogen
chemisorbed on the rhodium metal particles formed in the first
part of the TPR run. For the impregnated catalyst no negative
TCD signal was observed, however. Realizing that the reduction
of rhodium chloride is still going on above 373 K, the TCD
signal – which is the sum of hydrogen consumption by not yet
reduced Rh cations and desorption of hydrogen chemisorbed on
already formed metal – can indeed be positive above 373 K.
The TPR profile observed for the catalyst, which had been pre-
oxidized at 773 K, is characterized by a single peak at 358 K.
The total H_2/Rh value of 1.41 indicates that rhodium was mainly
present as Rh_2O_3. The peak maximum of the profile has shifted
from 343 K to 358 K when the oxidation temperature was in-
creased from 298 K to 773 K. During passivation a more open
structure of the rhodium oxide, probably with more defects,
may be formed than after oxidation of the catalyst at high
temperature. Since nucleation is a very important step in the
reduction of the oxide and since reduction starts more easily
at a defect, it can be understood that the passivated catalyst
reduces at a somewhat lower temperature.
Yao *et al.* (30, 31) found for Rh/Al_2O_3 samples which were re-
duced at 973 K and subsequently oxidized at 773 K a reduction
peak at 373 K, while in our case the peak maximum is at 358 K.
However, they used a heating rate of 8 K/min whereas we used
5 K/min. It is known that higher heating rates shift the peaks
to higher temperatures (32).
Although the degree of reduction of the impregnated catalyst may
not be 100 per cent one can exclude the possibility that after
reduction much rhodium is present as isolated Rh^{n+} ions on the
basis of the H_2/Rh value of 1.43. If the oxidation state of
rhodium would have been 1+, the maximum H_2/Rh value could only
be 1.00 which is much lower than found experimentally.

Hydrogen chemisorption

The measurement resulted in an H/Rh ratio (corrected for ad-
sorption on the bare support) of 1.7, indicating a highly dis-
persed system. H/Rh values higher than 1 on Rh/Al_2O_3 catalysts
have been observed previously (30, 33) and are explained by
multiple adsorption, although hydrogen spill-over cannot be
excluded (34).

ESR

After reduction of the catalyst at 593 K and evacuation at
298 K, to avoid condensation at low temperature, a symmetric
ESR signal was observed with g = 2.14 and ΔH = 260 G (figure 2a).

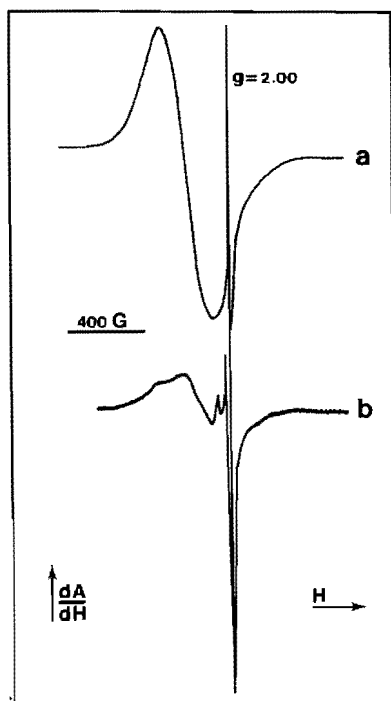*Figure 2 X-band ESR spectra of 0.57 wt% $Rh/\gamma-Al_2O_3$ recorded at*
20 K after:
a) reduction at 593 K and evacuation at 298 K,
b) reduction and evacuation at 593 K and CO admission
and evacuation at 298 K.

From the signal intensity it is calculated that 4.8% of
the rhodium atoms are paramagnetic with $S = \frac{1}{2}$. Within the
experimental error this is in accordance with the reduction
degree of 95% observed by TPR. The ESR signal is attributed
to Rh^{2+} (d^7) ions, as reported by Huizinga (35). Rh^0 ($d^8 s^1$)
atoms would also explain the signal, but the signal did not
change in intensity when the reduction was prolonged for a long
time. As the mobility of rhodium atoms is substantial, one
would expect sintering of isolated Rh^0 atoms and consequently
a decrease of the ESR signal with reduction time. Since this
did not occur we assign the ESR signal to Rh^{2+} ions and ex-
clude the possibility that isolated Rh^0 atoms are present af-
ter reduction of the catalyst.

Thus from the TPR and ESR results the following conclusion
can be drawn: in the highly dispersed 0.57 wt% $Rh/\gamma-Al_2O_3$
catalyst the majority of the rhodium is present as metal
crystallites. As suggested by Huizinga *et al.* (35) these
metallic particles might be anchored to the alumina support by
the rhodium ions observed by ESR.

XPS

We used XPS as a complementary technique in order to
support the TPR and ESR observation that the oxidation state
of rhodium after reduction of the catalyst is zero.
In table 2 the rhodium 3d $^5/2$ electron binding energies of the
impregnated and the reduced catalyst are presented. (In all
samples the 3d $^5/2$ - 3d $^3/2$ doublet separation is the same,
4.5 eV.) Although the TPR results demonstrate that after re-
duction the catalyst has been reduced completely, the rhodium
3d $^5/2$ electron binding energy of the reduced catalyst (307.5 eV)
is somewhat higher than the Rh 3d $^5/2$ value of the foil
(307.0 eV). This observation, previously reported by Huizinga
et al. (21), is explained by a so-called final state effect.
Because of screening of the created core-hole by the electrons
of neighbouring atoms the apparent binding energy is lowered.
This lowering is maximum for bulk atoms, because they have more
neighbouring atoms and thus more screening electrons. In the

Table 2 X-ray Photoelectron Spectroscopy.

	B.E. Rh 3d $5/2$ [eV]
0.57 wt% Rh/γ-Al$_2$O$_3$: Impregnation	310.7
Reduction at 593 K	307.5
Rh-foil*	307.0
0.57 wt% Rh/γ-Al$_2$O$_3$: Reduction at 593 K, evacuation at 593 K, CO admission at 298 K	308.7
Ion exchanged [Rh^{1+}(CO)$_2$Cl]$_2$/γ-Al$_2$O$_3$	308.6
[Rh^{1+}(CO)$_2$Cl]$_2$*	308.8

*Literature

reduced catalyst the metal particles are very small and con-
sequently an Rh atom will on the average have less neighbouring
atoms and as a consequence the core-hole screening will be less
effective. This leads to an apparent binding energy which is
higher than that of bulk Rh.

From the intensities of the various lines and using the
Scofield's cross sections (36) we calculated an atomic Cl/Rh
ratio of 4.8 and 4.0 for respectively the impregnated catalyst
and the catalyst reduced at 593 K for one hour. Although these
values are not very accurate, we can at least conclude that
after reduction the majority of the chloride is still present
on the surface of the support.

EXAFS

In order to obtain more insight into the structure of the metallic crystallites EXAFS measurements were performed on the catalyst reduced at 593 K for one hour. The primary EXAFS data of the rhodium K-edge of the reduced catalyst are presented in figure 3a.
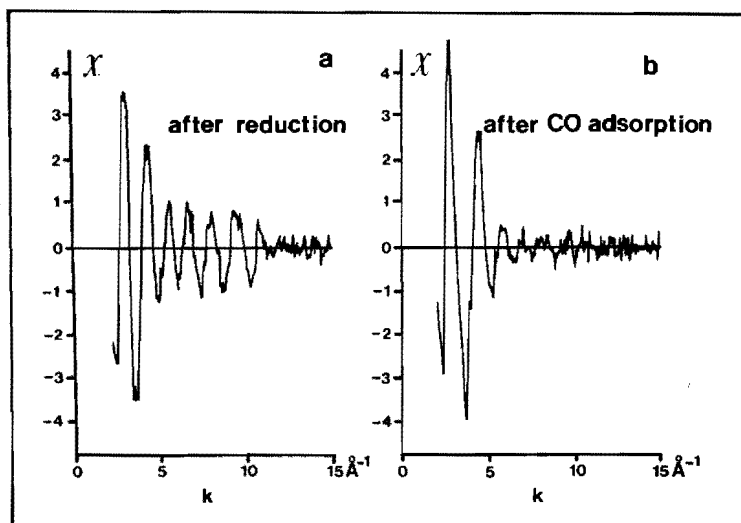
Figure 3 *The normalized primary EXAFS data of the rhodium*
K-edge at 77 K of the 0.57 wt% Rh/γ-Al$_2$O$_3$ catalyst
after:
a) reduction at 593 K (100 kPa H$_2$),
b) CO adsorption at room temperature (100 kPa CO).

As we are dealing with a reduced RhCl$_3$/γ-Al$_2$O$_3$ catalyst the only scatterer pairs which should be considered are Rh-Rh, Rh-O and Rh-Cl. A large difference exists between the back-scattering amplitude of the low-Z elements (O, Cl) and the high-Z rhodium atoms. Consequently, a distinction can be made between these two types of elements. The amplitude of the rhodium atoms above wavenumber 5 A^{-1} is much more pronounced than that of oxygen and chloride ions. Therefore, the EXAFS

oscillations presented in figure 3a are characteristic for rhodium neighbour atoms. However, as described in a previous paper a contribution from the support on the EXAFS is present (37). Since this contribution is small the EXAFS spectrum must be carefully analysed to obtain reliable structural parameters. Therefore, a modification of the usual data analysis procedure has been applied (28).

In general, the Fourier transform (FT) of an Rh-Rh EXAFS function consists of a main peak and a sidelobe on the low r-side which is typical for high-Z elements like rhodium and has its origin in the shape of the backscattering amplitude as well as the non-linear k-dependence of the phase. This implies that the sidelobe in FT of reduced Rh/Al_2O_3 may interfere in the r-region where distances due to other scatterer pairs are to be expected. By correcting FT for the rhodium phase shift and backscattering amplitude (denoted by FT'') (see chapter 2) the rhodium-rhodium contribution will appear as a single localized peak without sidelobes so that the contribution from the support can more easily be identified.

In figure 4b the imaginary part (dotted line) and the absolute value (solid line) of the k^3-weighed Fourier transform of the smoothed EXAFS data (figure 4a), performed on a k-interval from $k = 3.3 \text{ Å}^{-1}$ to $k = 8.5 \text{ Å}^{-1}$ and corrected for Rh-Rh phase shift as well as Rh-Rh amplitude, are shown. The radial structure function (RSF) is characterized by a main peak around $r = 2.7 \text{ Å}$ and a peak around $r = 1.8 \text{ Å}$. The first peak has to be assigned to an Rh-Rh nearest neighbour coordination. To determine the parameters of this rhodium coordination shell one normally uses the method of fitting in k-space. While this method may be used to obtain reliable parameters for the rhodium-rhodium contribution to the peak, it may appear un-reliable in determining the parameters for the remaining con-tributions. From the position and height of this peak a first estimate of the R, N and $\Delta\sigma^2$ values of the rhodium neighbour shell was found by matching the imaginary parts of FT'' and the transform of a calculated Rh-Rh EXAFS, using the phase shift and backscattering amplitude of Rh-foil, between $\Delta r = 2.25$ and
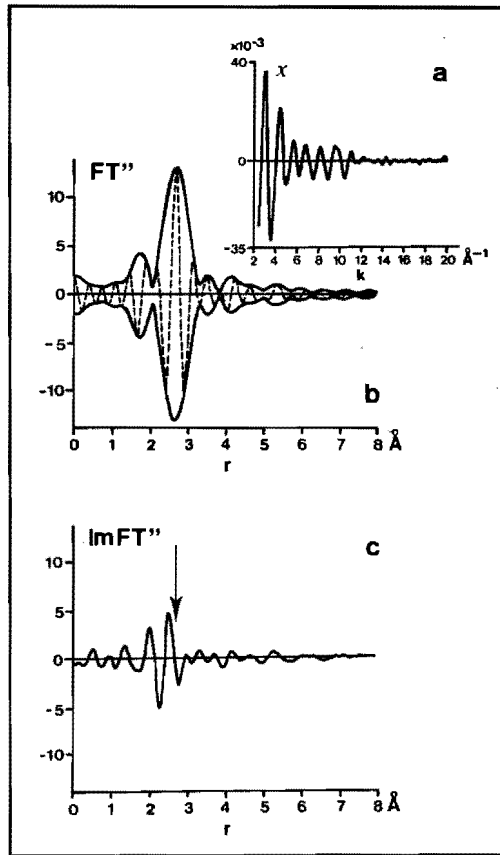
Figure 4 0.57 wt% Rh/γ-Al$_2$O$_3$ reduced at 593 K.

a) The normalized smoothed EXAFS data of the rhodium
K-edge at 77 K.

b) The associated k^3-weighed, Fourier transform (Δk =
3.3 - 8.5 Å^{-1}, Rh-Rh phase shift and backscattering
amplitude corrected).

Solid line = |FT''|, dotted line = ImFT''.

c) The imaginary part of FT.'' (Δk = 3.3 - 8.5 Å^{-1})
of the residual EXAFS function obtained by sub-
tracting the calculated Rh-Rh fine structure from
the smoothed EXAFS data.

and 3.2 Å. A criterion for a proper determination of the Rh-Rh
parameters is that the imaginary part of the Fourier transform
of the difference signal between the smoothed EXAFS function
and the calculated one shell Rh-Rh EXAFS exhibits no contribution
of Rh-Rh oscillations anymore. This is illustrated in figure 4c,
in which the imaginary part of the k^3-weighed FT'' (Δk =
3.3 - 8.5 Å^{-1}) of the difference signal between the smoothed
EXAFS data and the calculated Rh-Rh EXAFS signal is presented.
The approximate Rh-Rh parameter values used are: N(Rh-Rh) =
3.6, R = 2.68 Å (which is almost identical to the bulk value
of 2.69 Å) and $\Delta\sigma^2$ = 0.004 Å^2 (relative to Rh-foil). The
residual EXAFS function is presented in figure 5a. The
oscillation at k = 10 Å^{-1} is caused by an artifact, which is
however not caused by a defect in the monochromator, the so-
called 'glitch', because the incident X-ray intensity I_0 did
not show any anomalous behaviour at k = 10 Å^{-1}. No physical
explanation of the artifact can be suggested at the moment.
The most important feature is that there is no oscillation in
the envelope of this EXAFS. Consequently, the difference EXAFS
signal is caused by an Rh-low-Z element scatterer pair, either
an Rh-Cl or an Rh-O pair. RhCl$_3$ was used as precursor for the
preparation of the catalyst and it is possible that Rh-Cl bonds
still exist. Using the coincidence that the difference in phase
between the scatterer pairs Rh-O and Rh-Cl is nearly π, a dis-
tinction between the two pairs can be made by comparing the
imaginary parts of the Fourier transformed EXAFS signal
corrected for phase shift. It can easily be shown that the
imaginary part of the for Rh-O phase shift corrected radial
structure function of an EXAFS signal caused by Rh-Cl coordina-
tion peaks negatively at the interatomic Rh-Cl distance.
The k^1-weighed Fourier transform of the difference EXAFS signal
performed on a k-interval of 3.5 - 8.5 Å^{-1} and corrected for
Rh-O phase shift is given in figure 5b. Note that the imaginary
part is symmetric and peaks positively. Its maximum coincides
with the peak maximum of the absolute value of the RSF. Since
we used an Rh-O phase shift correction this result proves that
the signal can be accounted for by an Rh-O scatterer pair. The
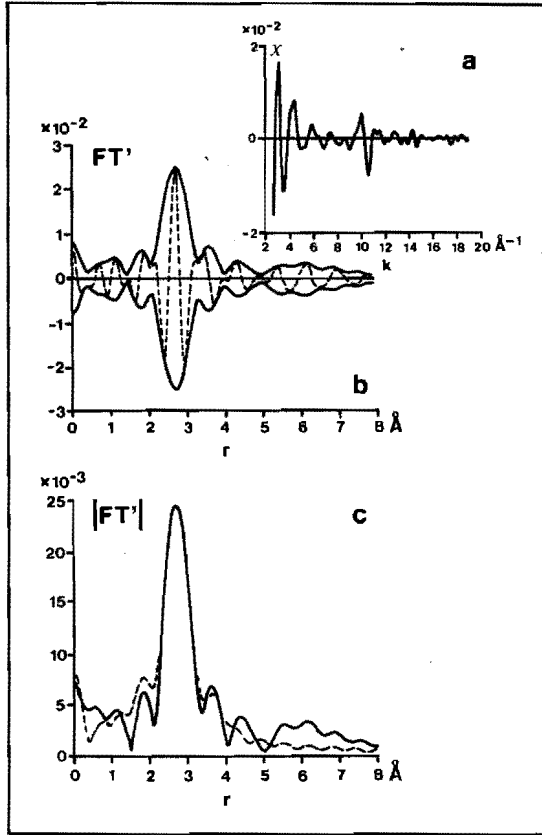
Figure 5 0.57 wt% Rh/γ-Al$_2$O$_3$ reduced at 593 K.

> a) The difference EXAFS signal of the smoothed EXAFS
> data of the rhodium K-edge and the calculated
> estimated contribution of the nearest neighbour
> rhodium atoms fine structure.
>
> b) The associated k^1-weighed Fourier transform
> (Δk = 3.5 - 8.5 Å^{-1}, Rh-O phase shift corrected).
> Solid line = |FT'|, dotted line = ImFT'.
>
> c) The k^1-weighed Fourier transforms (Δk = 3.5 -
> 8.5 Å^{-1}, Rh-O phase shift corrected) of the
> difference signal (solid line) and the calculated
> contribution of the nearest neighbour oxygen atoms
> fine structure (dotted line).

optimized parameters were determined by fitting in k-space of
the filtered EXAFS signal, obtained by inverse transformation
from r = 1.83 Å to r = 3.66 Å. The obtained parameters are:
N(Rh-O) = 1.9, R = 2.74 Å, $\Delta\sigma^2$ = 0.0 Å^2 (relative to Rh_2O_3).
The Fourier transform of the calculated Rh-O EXAFS, using the
parameters mentioned above, as well as the RSF given in figure
5b are presented in figure 5c.
The distance of the Rh-O bond is 0.69 Å longer than the bond
length in Rh_2O_3 (R = 2.05 Å). Because of the atomic and ionic
radii of rhodium (Rh^0 = 1.34 Å, Rh^{3+} = 0.68 Å) this indicates
that the Rh-O bond is a bond between an Rh^0 atom and an O^{2-}
ion which most likely originates from the support.
The coordination number N(Rh-O) has to be corrected because it
is obtained by using the backscattering amplitude of the first
shell of the reference compound Rh_2O_3. Since this amplitude
belongs to an Rh-O distance at 2.05 Å, the Rh-O amplitude at a
distance of 2.74 Å has to be corrected for the difference in photo-
electron losses, caused by inelastic scattering. This correction
equals about exp($-2\Delta R/\lambda$), where ΔR is the difference between
the two coordination distances and λ the mean free path length.
According to Stern *et al.* (38), λ will have a value of 4-5 Å
in the energy region from 100 eV to 300 eV, which is the region
where oxygen has most of its scattering power. The amplitude
correction, taking these values, is about 30%. This means that
the corrected N(Rh-O) is 1.9 x 130/100 = 2.5. The real para-
meters are given in table 3.
In order to optimize the Rh-Rh parameter values we analysed
the EXAFS function obtained by subtracting the calculated Rh-O
EXAFS from the original smoothed EXAFS data. The k^3-weighed,
Rh-Rh phase shift and amplitude corrected, forward transforma-
tion of this EXAFS function led to an RSF as presented in
figure 6a. Note that the function is symmetrical, which in-
dicates that the analysis used is very reliable because ImFT''
and |FT''| which belong to a single Rh-Rh scatterer pair should
be symmetrical.
An Rh-Rh one shell fit in k-space of the filtered EXAFS, ob-
tained by backtransformation from r = 1.58 Å to r = 3.83 Å,

156

Table 3 *EXAFS parameter values for the 0.57 wt% Rh/γ-Al₂O₃*
catalyst after reduction and CO admission.
Accuracies: N: ± 10 – 20%, R: ± 0.5 – 1%,
Δσ²: ± 10 – 20%.

TREATMENT	COORDINATION								
	Rh-Rh			Rh-O			Rh-CO		
	N	R [Å]	$\Delta\sigma^2 \times 10^2$ [Å²]	N	R [Å]	$\Delta\sigma^2 \times 10^2$ [Å²]	N	R [Å]	$\Delta\sigma^2 \times 10^2$ [Å²]
Reduction at 593 K	3.7	2.68	0.5	2.5	2.74	0.0			
Reduction at 593 K, evacuation at 593 K, CO admisssion at 298 K				3.1	2.12	0.3	1.8	*	0.7

The Rh-C and Rh-O distances are kept equal to the one in the dimer
[Rh(CO)₂Cl]₂.

yielded the following parameter values: N(Rh-Rh) = 3.7, R =
2.68 Å, $\Delta\sigma^2$ = 0.005 Å² (relative to Rh-foil) (see table 3).
The radial structure function of the calculated Rh-Rh one shell
EXAFS function is in good agreement with the transform of the
residual EXAFS presented in figure 6a (see figure 6b).
Figure 7a shows the fine structure of the catalyst and the
structure calculated with the two (Rh-O and Rh-Rh) scatterer
pairs using the optimized parameters as given in table 3. A
very good fit was obtained within the k-interval of 3.3 –
8.5 Å⁻¹. The fit in r-space of the absolute value and the
imaginary part are presented in figure 7b and 7c respectively.
    In order to demonstrate the influence of the contribution
of the Rh-O scatterer pair on the Fourier transform of the
smoothed EXAFS data the RSF's of the data, the calculated
Rh-Rh and the calculated Rh-O one shell fine structures are
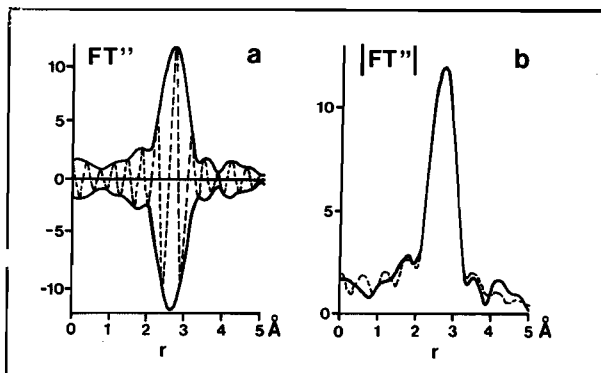
Figure 6 0.57 wt% Rh/γ-Al$_2$O$_3$ reduced at 593 K.
a) The k^3-weighed Fourier transform (Δk = 3.3 - 8.5 Å^{-1}, Rh-Rh phase shift and backscattering amplitude corrected) of the difference signal between the smoothed EXAFS data of the rhodium K-edge and the calculated contribution of nearest neighbour oxygen atoms. Solid line = |FT''|, dotted line = ImFT''.
b) The k^3-weighed Fourier transforms (Δk = 3.3 - 8.5 Å^{-1}, Rh-Rh phase shift and backscattering amplitude corrected) of the difference signal (solid line) and the calculated fine structure of the nearest neighbour rhodium atoms (dotted line).

presented in figure 8. Note that, in contradistinction to the imaginary part, the absolute value of the radial structure function of the catalyst is not simply a summation of the calculated ones. Figure 8 clearly shows the contribution of Rh-O in the main peak. The RSF of Rh-O coordination peaks at 2.33 Å while the real interatomic distance R is 2.74 Å. This is caused by the fact that an Rh-Rh phase shift correction was used. The phase factors of Rh-Rh and Rh-O coordination differs and in the case of Rh-Rh phase shift correction the r-values of Rh-O bonds shift 0.4 Å downwards relative to the real interatomic distances. The sidelobe at r = 1.8 Å is caused by interference between Rh-O and Rh-Rh oscillations.

158
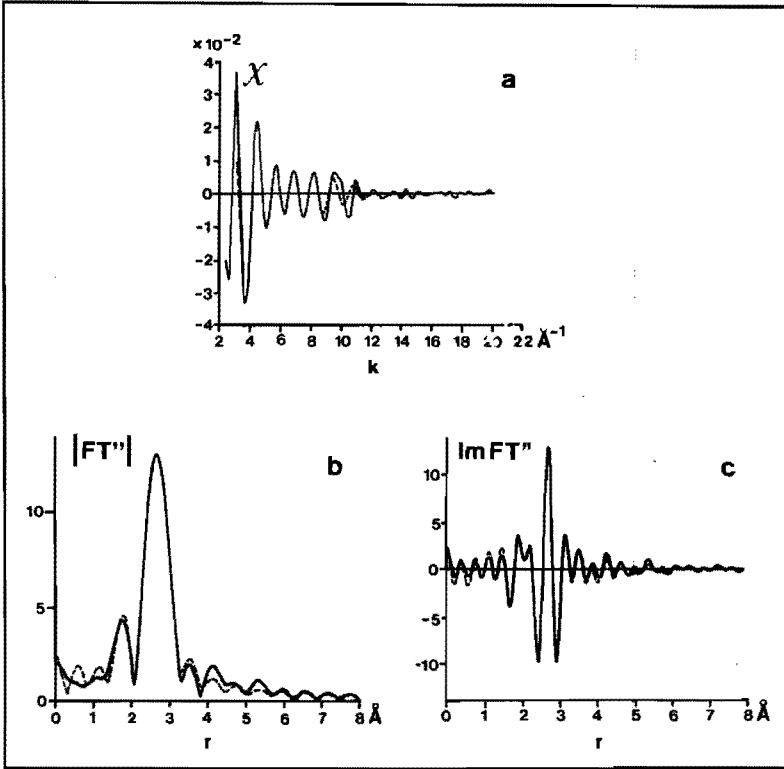
Figure 7 0.57 wt% Rh/γ-Al₂O₃ reduced at 593 K. The solid lines represent the data and the dotted lines represent the calculated two-shell fit (Rh-O, Rh-Rh) using the optimized parameter values (cf. table 3).

a) χ(k) of the rhodium K-edge as function of k.

b) The associated FT'' and

c) the associated ImFT'', (k³-weighed FT'', Δk = 3.3 - 8.5 Å⁻¹).
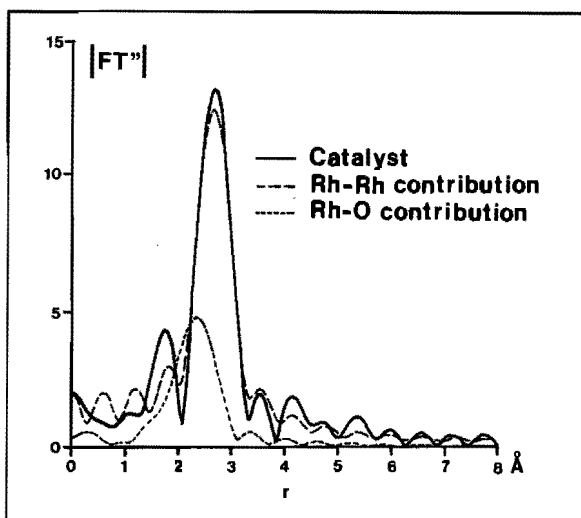
Figure 8 0.57 wt% Rh/γ-Al$_2$O$_3$ reduced at 593 K. The k^3-weighed Fourier transforms (Δk = 3.3 - 8.5 Å^{-1}, Rh-Rh phase shift and amplitude corrected) of the smoothed EXAFS data of the rhodium K-edge and the individual cal- culated contributions of the nearest neighbour rhodium and oxygen atoms.

7.4.1.2 Discussion

The TPR results show that the degree of reduction of the reduced catalyst was high (95%). We, therefore, exclude the possibility of rhodium being completely or to a great extent dispersed as isolated Rh^{1+} ions. Since an Rh^0 (d^{8}s^1) ESR signal could not be detected no isolated rhodium atoms are present either. We thus conclude that only rhodium metal crystallites exist in the highly dispersed Rh/γ-Al$_2$O$_3$ catalyst after re- duction with hydrogen, as indeed proven by the EXAFS results.

The low average coordination number of 3.7 (table 3) in- dicates that the crystallites are very small. As might have been expected a substantial contribution of rhodium-carrier

oxygen EXAFS oscillations is observed. The Rh-O interatomic distance of 2.74 Å (2.05 Å in Rh_2O_3) indicates that the interaction between the particle and the support occurs via Rh^0 atoms and oxygen ions of the alumina, and not via interdiffusion of the metal oxide and the oxidic support as proposed by Anderson (39) and well established for systems as Ni/SiO_2, Ni/Al_2O_3 and Co/Al_2O_3 (40-42). A metal-support interaction of zerovalent metal atoms and oxygen ions of the support has been proposed earlier for supported osmium carbonyl clusters (43, 44) and for rhodium catalysts (37).

On the basis of the present EXAFS results we cannot distinguish between two-dimensional and three-dimensional rhodium crystallites. However, EXAFS measurements carried out on another ultra dispersed Rh(0.47 wt%)/γ-Al_2O_3 catalyst, reduced at 773 K but with still a high H/Rh value of 1.7, resulted in an average coordination number of the Rh-Rh and Rh-O of 5.3 and 1.7, respectively, (see (45) and chapter 8). In this catalyst the rhodium metal particles are somewhat larger, compared to the crystallites of the catalyst reduced at 593 K, but are still very small as indicated by the observed relative low coordination number of the Rh-Rh and the high H/Rh value. It is obvious that the structure of the particles in both catalysts are similar then. If we are dealing with a two-dimensional structure one would expect that the average coordination number of the Rh-O distance is constant and independent of the size of the raft. However, going from a particle with N(Rh-Rh) = 3.7 to a particle with N(Rh-Rh) = 5.3 the N(Rh-O) changes from 2.5 to 1.7. Therefore, we think that the most likely structure of the metal particles is three-dimensional. This conclusion is not in accordance with the conclusion reached by Yates *et al.* on the basis of TEM measurements (10-11). However, TEM is an ex situ technique. In order to prepare a sample specimen the sample must be handled in air. Consequently, the catalyst studied in the TEM investigation will have been passivated. The TPR results show that a passivated highly dispersed rhodium catalyst will be oxidized almost completely. This then explains the TEM results, because it is

known that several transition-metal oxides, including rhodium oxide - which is stable at room temperature at an oxygen pressure above 2×10^{-19} Pa - may form a well-dispersed two-dimensional phase, the so-called δ-phase, on alumina (46).

Although the rhodium particles are very small and consequently the greater part of the rhodium atoms is exposed, the interatomic distance between the rhodium atoms is similar to the distance in Rh-foil (table 3). Many LEED studies have reported differences between the interplanar spacings of the surface layers of single crystals and bulk spacings. An example is the work on Ni(110) for which a 5% contraction has been found (47). Therefore, one would also expect a contraction of the Rh-Rh bond in the small particles. However, during the EXAFS measurements the rhodium was covered with hydrogen. Therefore, the rhodium surface atoms were coordinatively saturated, and this might result in a relaxation of the Rh-Rh bonds. For single crystal surfaces it has been observed that when a surface is covered by an adsorbed layer, the top substrate layer relaxes back (48). Moraweck *et al.* (49) have observed with EXAFS a contraction of the Pt-Pt distance in a Pt/Y-zeolite sample of 0.12 Å when the particles were measured in an He environment. A subsequent H_2 admission at room temperature relaxed the bond to a distance similar to that in Pt-foil.

At the end of this discussion we want to give a possible structure of the rhodium crystallites formed during reduction of the catalyst under investigation. According to Knözinger and Ratnasamy (50) the surface of γ-Al_2O_3 consists of different types of planes (*e.g.* (111), (110) and (100)) which are partly dehydroxylated. Since the diameter of a rhodium atom is slightly smaller than the diameter of an oxygen ion (2.69 Å *vs.* 2.80 Å) it may be possible that rhodium atoms are situated in holes of the surface of alumina which are created by dehydroxylation ($2OH^- \rightarrow$ hole + O^{2-} + H_2O). Rhodium particles may be anchored to the support by these atoms. This is illustrated in figure 9 for a rhodium crystallite, with an fcc structure and Rh-Rh and Rh-O coordination numbers which approach the experimental ones (4.2, 2.6 *vs.* 3.7, 2.5), on a partly dehydroxylated (111) plane.

162
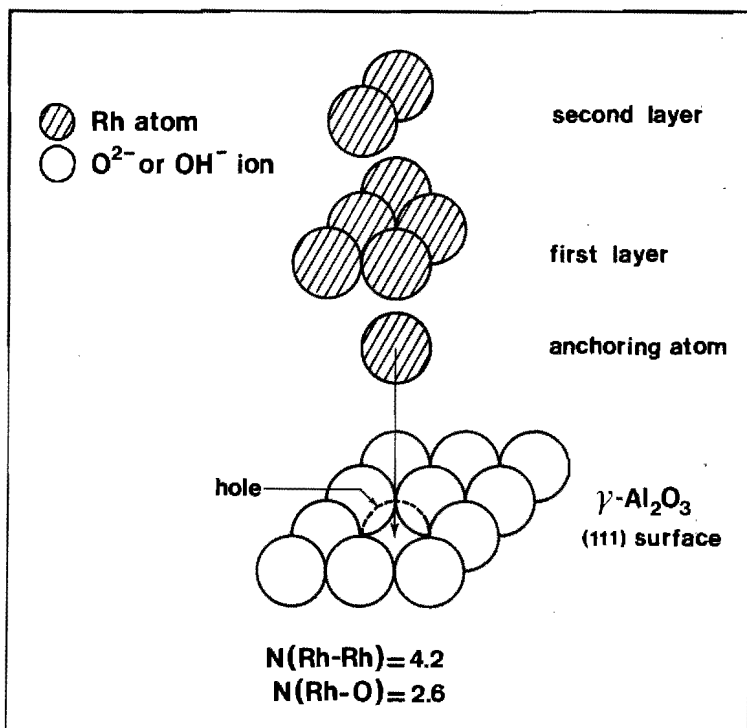
Figure 9 *Possible structure of rhodium crystallites with an fcc structure in the 0.57 wt% Rh/γ-Al$_2$O$_3$ catalyst reduced at 593 K.*

Note that a three-dimensional particle with an fcc structure and an Rh-Rh coordination number of 3.7 consists of maximum 8 atoms.

7.4.2 THE STRUCTURE OF RHODIUM AFTER CO ADMISSION

In order to elucidate the seeming contradiction between the conclusion based on CO infrared measurements that Rh is dispersed as isolated Rh^{1+} ions and the results of this study that metallic particles are present we investigated the strucutre of rhodium after CO admission.

7.4.2.1 Results

CO chemisorption

The observed CO/Rh ratio was 1.9 after correction for adsorption onto the bare support which was substantially more (43 µmol CO per gram catalyst) than for hydrogen (1 µmol H_2 per gram catalyst). The CO/Rh value of 1.9 points to the formation of rhodium geminal dicarbonyl species and furthermore indicates that the catalyst is ultra dispersed.

Infrared

Figure 10 shows the 1800-2200 cm^{-1} region of the infrared spectrum of the reduced and evacuated catalyst. After exposure to CO (50 kPa) and evacuation at 298 K only two infrared bands at 2095 and 2023 cm^{-1} are present which are assigned to the symmetrical and antisymmetrical stretching frequencies of the

Figure 10 CO infrared spectrum on a 0.57 wt% $Rh/\gamma-Al_2O_3$
(measured at 298 K).

Rh(CO)$_2$ species. This result is in accordance with the results
of Cavanagh (7) on a 0.2 wt% Rh/Al$_2$O$_3$ catalyst and of Worley
(6) and Yates (10, 11) on a 0.5 and a 1.0 wt% Rh/Al$_2$O$_3$ catalyst.

EXAFS

In figure 3b the oscillatory primary EXAFS function χ(k)
as a function of wavenumber of the rhodium K-edge of the
catalyst is shown after CO adsorption at room temperature. The
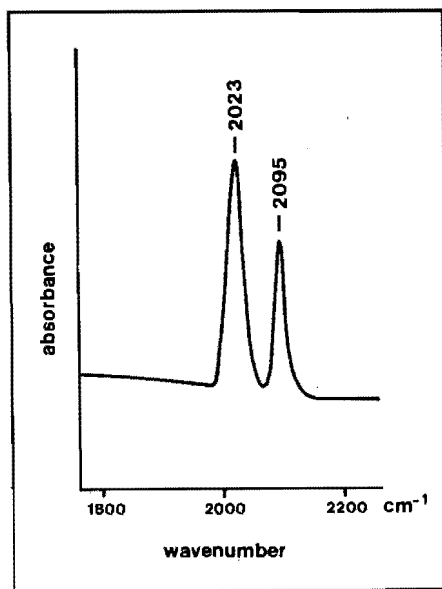most striking feature is the significant decrease of the
oscillations above k = 5 $\overset{o}{A}^{-1}$, which are typical for the Rh-Rh
metal coordination, compared to the EXAFS oscillations of the
reduced catalyst (see figure 3a). This result has been pre-
viously published by Van 't Blik *et al.* (12). It clearly shows
the dramatic influence of CO adsorption on the highly dis-
persed Rh/Al$_2$O$_3$ catalyst. A disruption of rhodium-rhodium
metallic bonds takes place as a result of the chemisorption
of CO molecules. As proven by infrared only Rh(CO)$_2$ species
exist after CO admission. An answer to the intriguing question
regarding the bindingmechanism between Rh(CO)$_2$ species and
the support might be obtained by a careful analysis of the
EXAFS data presented in figure 3b.

In order to interpret the EXAFS spectrum of the catalyst
after CO admission it is necessary to use a suitable reference
compound for the rhodium geminal dicarbonyl Rh(CO)$_2$ species
which are formed on the catalyst surface. For this purpose we
used the dimer [Rh(CO)$_2$Cl]$_2$ since it has the same CO infrared
bands as the catalyst after CO admission. The crystalline
structure of the dimer is presented in figure 11 (51). A minor
advantage for taking the dimer as a reference compound is its
good stability in an oxygen atmosphere, thus enormously
facilitating the EXAFS measurement.
The EXAFS signal of the rhodium K-edge of a physical mixture
of [Rh(CO)$_2$Cl]$_2$ and silica was recorded at liquid nitrogen
temperature in a CO atmosphere (10^2 kPa) (see figure 12a).
As can be seen from the structure of the dimer (figure 11)
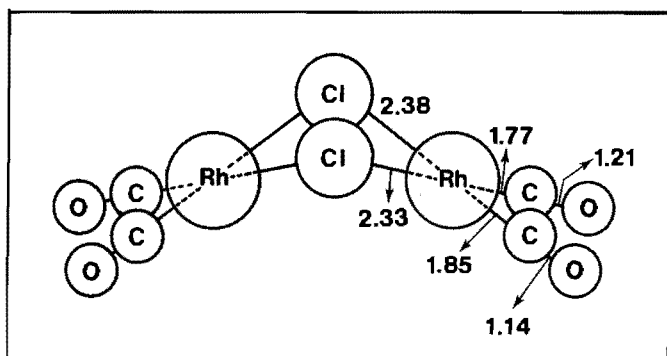
Figure 11 Bond lengths in $[Rh(CO)_2Cl]_2$.

the EXAFS is mainly caused by the three scatterer pairs: Rh-Cl,
Rh-C and Rh-O* (oxygen of the carbonyl). Figure 12 b shows
the imaginary part ImFT' (dotted line) and the absolute value
|FT'| (solid line) of the associated k^2-weighed Fourier
transform, through which the best splitting of the separate
neighbour shells in r-space was obtained. The Fourier trans-
form was performed on a k-interval from k = 2.44 $\overset{o}{A}^{-1}$ to k =
12.6 $\overset{o}{A}^{-1}$ and corrected for Rh-O phase shift.
The phase shift correction deserves some closer attention. In
general, a phase shift correction on the Fourier transform is
applied in order to obtain real interatomic distances R in
r-space as well as to obtain symmetrical functions of ImFT'
and |FT'| (52). By using an Rh-O phase shift correction the
Rh-O as well as Rh-C and Rh-Cl coordinations peak at real in-
teratomic distances in FT' because: a) the scatterer behaviour
of an Rh-C and an Rh-O scatterer pair hardly differs, and
b) it appears that the difference between the Rh-O and the
Rh-Cl phases is nearly π, which means that the imaginary part
of the Rh-O phase shift corrected radial structure function of
Rh-Cl EXAFS peaks negatively but at nearly exact real inter-
atomic Rh-Cl distance.
The contribution of each of three scatterer pairs to the FT'
is to be found then at their corresponding real interatomic
distances. Therefore, the three peaks in the radial structure
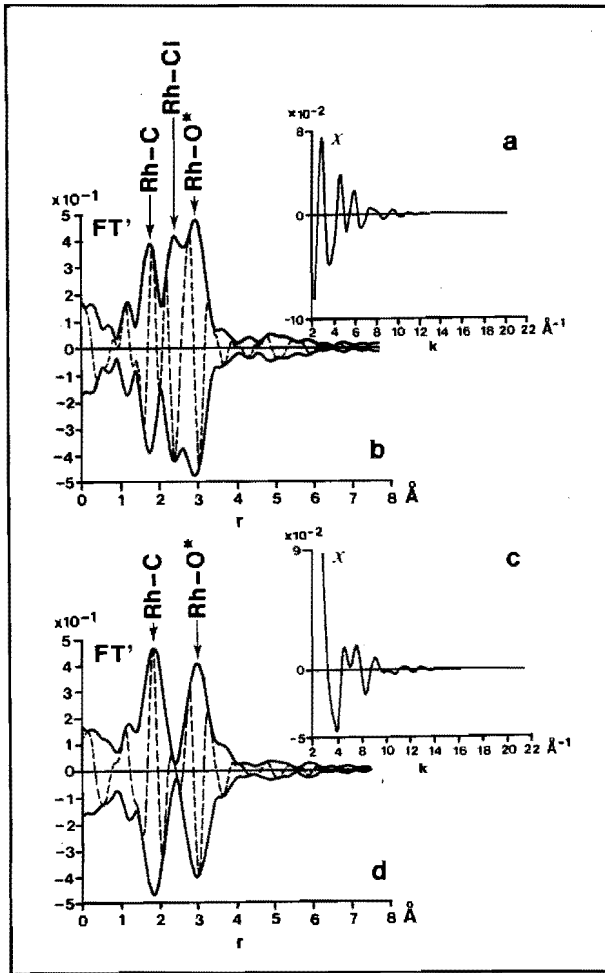
Figure 12 The dimer $[Rh(CO)_2Cl]_2$.

a) The normalized primary EXAFS data of the rhodium K-edge at 77 K.

b) The associated k^2-weighed Fourier transform ($\Delta k = 2.44 - 12.6$ $Å^{-1}$, Rh-O phase shift corrected). Solid line = $|FT'|$, dotted line = ImFT'.

c) The difference signal between the normalized EXAFS data and the calculated contribution of the nearest neighbour chlorine atoms.

d) The k^2-weighed Fourier transform of the difference signal ($\Delta k = 3.3 - 10$ $Å^{-1}$, Rh-O phase shift corrected). Solid line = $|FT'|$, dotted line = ImFT'.

function (figure 12b) are assigned to: Rh-C, Rh-Cl and Rh-O*
at R = 1.8, 2.4 and 2.9 Å, respectively. Note that the imaginary
part of Rh-Cl coordination peaks negatively around 2.4 Å.
To obtain a proper reference EXAFS signal for $Rh(CO)_2$ the
contribution of Rh-Cl has to be subtracted from the rhodium
EXAFS of the dimer. This was carried out by calculating the
Rh-Cl EXAFS with the known crystallographic parameters which
was then subtracted from the primary EXAFS data. The phase
shift and backscattering amplitude were obtained from EXAFS
measurements on $RhCl_3$. The criterion used for a proper de-
termination of the Rh-Cl parameters was a decrease of the
amplitude of the Rh-Cl peak in $|FT'|$ to the noise level. The
parameter values thus obtained were: R = 2.36 Å (from X-ray
diffraction R = 2.355 Å), N(Rh-Cl) = 2.1 and $\Delta\sigma^2 = -0.001$ $Å^2$
(relative to $RhCl_3$).
Figure 12c shows the $Rh(CO)_2$ EXAFS signal obtained by subtract-
ing the calculated Rh-Cl contribution from the primary EXAFS
function. The k^2-weighed (Rh-O phase shift corrected) Fourier
transform of the residual EXAFS signal is given in figure 12d.
The oxygens of the carbonyl ligands are clearly visible. As
the carbon atom lies between the absorber, rhodium, and the
scatterer, oxygen, one must take into account depletion of
the primary outgoing wave as well as phase changes caused by
the intervening atom. Although one might intuitively expect
atoms directly behind the first set of scatterers to have little
contribution to the EXAFS, the opposite is actually true. The
amplitude is much more pronounced than one would expect
on the basis of the simple N/r^2 dependence of the amplitude.
Apart from this amplitude anomaly the Rh-O* shows a phase shift
of π radians. (Note that the imaginary part peaks negatively
at R = 3.00 Å.) Similar deviations of the amplitude and
anomalous phase shifts have been observed previously in the
Fourier transform spectra of $Mo(CO)_6$ (53) and $Na_2Fe(CO)_4$ (54)
and they have been interpreted as the result of multiple
scattering processes.
The Rh-C and Rh-O* distance were determined by a phase analysis
of the representative Fourier-filtered signals. As no Rh-C

reference compound was available we used the theoretical phase
given by Teo and Lee (55) in order to determine the Rh-C dis-
tance. For the determination of the Rh-O* distance we used the
reference Rh-O phase which was adjusted with a factor π, for
reasons mentioned above. The obtained bond lengths of Rh-C and
Rh-O* are 1.85 Å and 3.00 Å, respectively, and are in good
agreement with the values determined by X-ray diffraction
(see figure 11).

The backscattering amplitude and phase obtained by
inverse transformation ($\Delta r = 1.25 - 3.47$ Å) of the radial
structure function as presented in figure 12d were used as
reference sample for $Rh(CO)_2$.

Let us return to the catalyst. The smoothed EXAFS func-
tions of the catalyst after CO adsorption at room temperature
(figure 13a) and the $Rh(CO)_2$ reference compound (figure 12c)
differ significantly. This indicates that the EXAFS of the
catalyst is not caused by Rh-C and Rh-O* coordination only.
The other contribution might be originated from an Rh-low-Z
element scatterer pair with which the geminal dicarbonyl is
most likely anchored to the support. The element can be an
oxygen ion and/or a chloride ion which is still present after
reduction of the catalyst as observed by XPS.
Figure 13b shows the k^3-weighed and Rh-O phase shift corrected
Fourier transform of the smoothed EXAFS data, performed on a
k-interval from $k = 3.24$ Å^{-1} to $k = 8.4$ Å^{-1}. A good splitting
of the separate neighbour shells in r-space was obtained and
within the r-interval of 1-3 Å three peaks could be dis-
tinghuished: peak A at 1.8 Å and peak C at 3.0 Å were assigned
to respectively Rh-C and Rh-O*, both originating from $Rh(CO)_2$
species, whereas peak B at 2.4 Å is a contribution of the un-
known Rh-low-Z element pair. From the imaginary part (figure
13b) it can be seen that the Rh-C signal is suppressed to a
great extent at position A', whereas the Rh-O* signal around
3.0 Å has hardly been affected by interference with peak B.
By matching the imaginary part above $r = 2.6$ Å with ImFT' of
a calculated $Rh(CO)_2$ EXAFS, using the phase and amplitude of
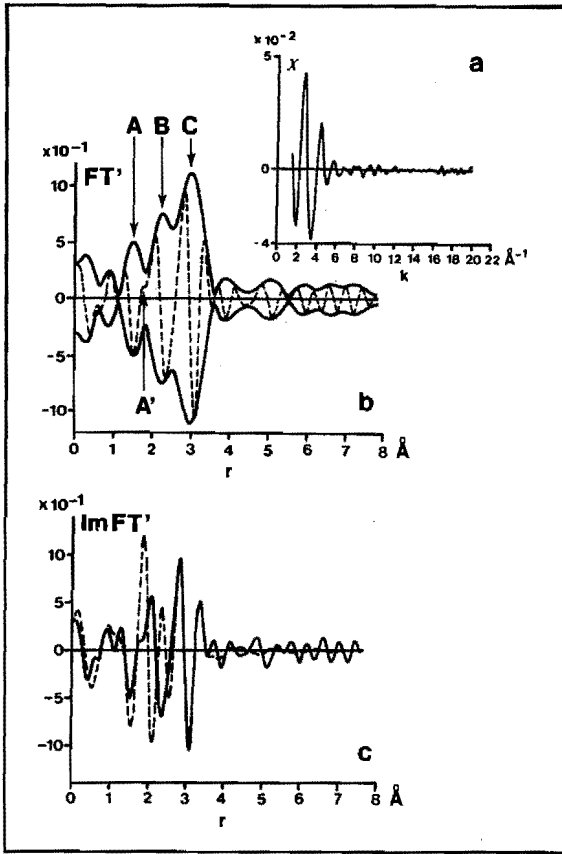
Figure 13 0.57 wt% Rh/γ-Al₂O₃ after CO admission at 298 K.

    a) The normalized smoothed EXAFS data of the rhodium K-edge
       at 77 K.

    b) The associated k^3-weighed Fourier transform ($\Delta k = 3.24 -$
       8.4 $Å^{-1}$, Rh-O phase shift corrected). Solid line = $|FT'|$,
       dotted line = ImFT'.

    c) The imaginary parts of the k^3-weighed Fourier transforms of
       the normalized smoothed EXAFS data (solid line) and the cal-
       culated contribution of Rh-Cl-O* fine structure (dotted line),
       ($\Delta k = 3.24 - 8.4$ $Å^{-1}$, Rh-O phase shift corrected).

the geminal dicarbonyl reference compound, we obtained the con-
tribution of Rh(CO)$_2$ oscillations to the EXAFS of the catalyst.
This is illustrated in figure 13c. The optimized parameter
values are: N(Rh(CO)$_2$) = 1.8, $\Delta\sigma^2$ = 0.007 $\mathring{A}^2$ relative to
[Rh(CO)$_2$Cl]$_2$. The interatomic distances were kept equal to
the Rh-C-O* distances in the dimer. The average coordination
is in good agreement with the CO chemisorption result (CO/Rh =
1.9) and again indicates that Rh(CO)$_2$ species were formed
indeed.
In order to obtain more insight into the contribution of the
unknown scatterer pair on the EXAFS signal, apart from
Rh(CO)$_2$, the difference signal between the smoothed EXAFS
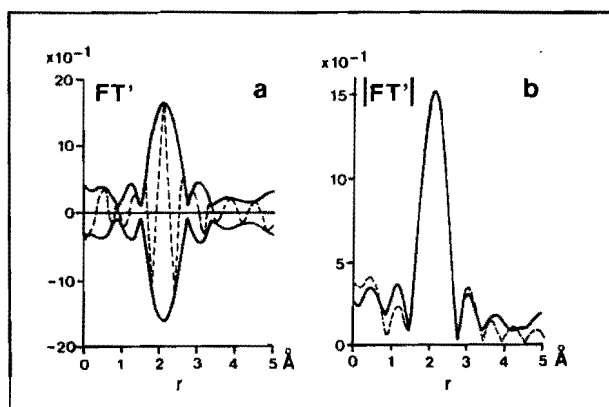
Figure 14 0.57 wt% Rh/γ-Al$_2$O$_3$ after CO admission at 298 K.
a) The k^3-weighed Fourier transform of the difference
signal between the normalized smoothed EXAFS data
and the calculated contribution of Rh-C-O* fine
structure (Δk = 3.3 - 8.4 $\mathring{A}^{-1}$, Rh-O phase shift
corrected).
b) The k^3-weighed Fourier transforms of the difference
signal (solid line) and the calculated fine
structure of nearest neighbour oxygen atoms
(dotted line) (Δk = 3.3 - 8.4 $\mathring{A}^{-1}$, Rh-O phase
shift corrected).

data and the calculated EXAFS of Rh(CO)$_2$ has been analysed.
The imaginary part and the absolute value of the k^3-weighed
Fourier transform corrected for Rh-O phase shift of the
difference signal are given in figure 14a. Note that the
imaginary part is symmetrical and peaks positively and the
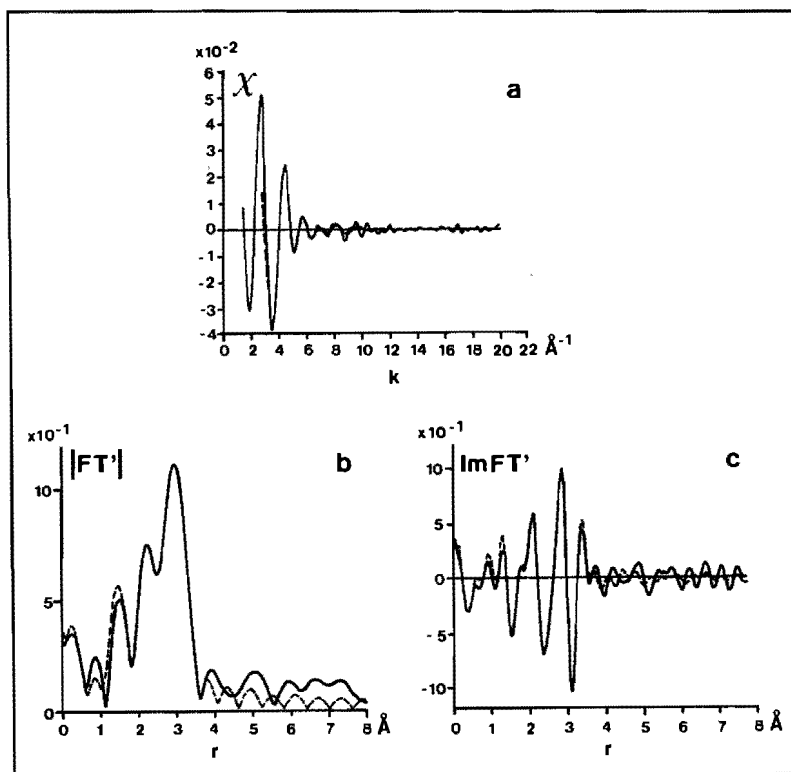
Figure 15 0.57 wt% Rh/γ-Al$_2$O$_3$ after CO admission at 298 K.
The solid lines represent the data and the dotted
lines represent the calculated two-shell fit
(Rh-C-O*, Rh-O) using the optimized parameter values
(cf. table 3).
a) χ(k) of the rhodium K-edge vs. k.
b) The associated |FT'| and
c) the associated ImFT', (k^3-weighed FT', Δk =
3.24 - 8.4 Å^{-1}, Rh-O phase shift corrected).

maximum coincides with the peak maximum of the absolute value.
Consequently, this contribution to the spectrum is caused by
Rh-O coordination. Table 3 presents the optimized parameter
values, obtained by fitting the EXAFS in k-space, by which
the difference signal is described best. The absolute values
of the radial structure functions of the calculated one shell
Rh-O EXAFS, using the optimized parameters, and the difference
signal are given in figure 14b. The average coordination num-
ber for the Rh-O distance is 3.1 which indicates that the
geminal dicarbonyl is anchored to the support by three oxygen
ions with equal interatomic distances of 2.12 Å. The bond
length of 2.12 Å indicates that rhodium is in an oxidic state.
The distance is 0.07 Å longer than the first shell distance
of Rh-O in Rh_2O_3 which implies that the average oxidation
state of rhodium is not 3+.
As a final check we calculated the EXAFS function including
Rh-support oxygen, Rh-C and Rh-O* bonds in $Rh(CO)_2$, using
the optimized parameter values (*cf.* table 3). The calculated
EXAFS shows excellent agreement with the EXAFS date (figure 15a).
The imaginary parts and the absolute values of the associated
Fourier transforms match very well, as can be seen in figure
15b and 15c, respectively.

ESR

If the oxidation state of the observed isolated $Rh(CO)_2$
species were zero, it should be possible to detect an ESR
signal of Rh^0 after CO admission, since Rh^0 (d^8s^1) is para-
magnetic. Reduction and evacuation of the catalyst at 593 K
and subsequent admission of CO and followed by an evacuation
at room temperature gave rise to the ESR spectrum presented in
figure 2b, which is completely different from the spectrum
obtained after reduction. This spectrum consists of two separate
ESR signals. Firstly, a signal with g = 2.09 (ΔH = 250 G) and
a shoulder at g = 2.26, and secondly, a signal with $g_{//}$ = 2.043
and $g_\perp$ = 2.011 ($\Delta H_\perp$ = 26 G). We assign the first ESR signal to
Rh^{2+}. The difference with the signal observed after reduction
indicates that a change in the environment of the Rh^{2+} ions has

taken place, probably due to alteration in the electronic
properties of the metal ion caused by for instance π-back
donation of electrons from Rh to CO. The line width of the
second signal is remarkably small (24 G) and we do not see any
hyperfine splitting due to the rhodium nucleus. This suggests
that this signal does not belong to a radical formed in the
neighbourhood of rhodium atoms or ions. The CO chemisorption
measurements showed that the bare support Al_2O_3 adsorbed a
considerable amount of CO molecules, a small part of which
might be paramagnetic. With thermally activated MgO and ThO_2
formation of radicals upon adsorption of CO at 298 K has in-
deed been reported (56).
Whatever the assignment of the two ESR signals is, the total
ESR intensity is very low and therefore, the ESR signals are
not very relevant for a discussion of the oxidation state of
the rhodium atoms or ions on the catalyst after CO admission.
On the other hand the fact that no substantial paramagnetic
signal caused by isolated Rh^0 (d^8s^1) atoms could be detected
is a very important feature. It proves that the oxidation
state of rhodium in the $Rh(CO)_2$ species cannot be zero and
must either be 1+ or 3+.

XPS

In order to obtain more information about the oxidation
state of the rhodium after CO admission we compared the
rhodium 3 d $^5/2$ electron binding energies of the catalyst and
the $[Rh(CO)_2Cl]_2$ exchanged alumina in which the valence of
rhodium is 1+.
The results are presented in table 2 and they clearly show that
within the experimental error both binding energies are equal
(308.6 $\pm$ 0.1 eV). This indicates that the oxidation state
of rhodium after CO admission is 1+. Thus, the oxidation state
of rhodium in the highly dispersed catalyst changes from zero,
after reduction, to 1+ when CO is admitted and consequently, CO
adsorption has to be accompanied by an oxidation process for
ultra dispersed rhodium supported on alumina.

7.4.2.2 Discussion

The EXAFS results clearly show the dramatic influence of CO chemisorption on the structure of small Rh particles in the ultra dispersed 0.57 wt% $Rh/\gamma-Al_2O_3$ catalyst. The metallic crystallites, formed during reduction, break up to rhodium geminal dicarbonyl species after CO admission, as proven by infrared and EXAFS.

In addition to the two CO molecules the geminal dicarbonyl species have also oxygen ions as ligands, as established by the analysis of the EXAFS spectrum of the CO adsorbed catalyst. The quantitative results demonstrate that rhodium is surrounded by two CO molecules and three oxygen atoms of the support. The $Rh(CO)_2$ species can be attached to the (111) surface of the $\gamma-Al_2O_3$ via 3 oxygen atoms in a way as presented in figure 16.
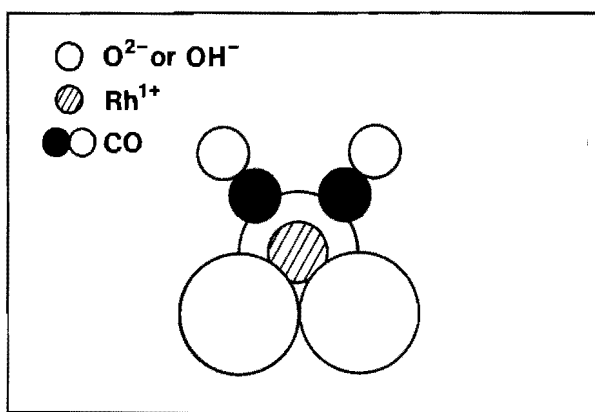
Figure 16 Possible structure of $Rh(CO)_2$ species attached to the $\gamma-Al_2O_3$ support after CO admission at 298 K.

Changes of a highly dispersed Rh/Al_2O_3 catalyst by CO adsorption have previously been reported by D.J.C. Yates and co-workers (10). They observed a sintering of the rhodium after adsorption of CO and a subsequent reduction at low temperature and assigned it to increasing mobility of rhodium atoms on which CO is adsorbed.

There are two possible ways for explaining why no Rh-Rh distances are observed in the EXAFS after CO adsorption: either the Rh-Rh distances in the resulting aggregate of $Rh(CO)_2$ species have increased somewhat and have a too large spread to see any EXAFS oscillations at higher k-value, or the $Rh(CO)_2$ species are indeed rather far apart on the support. In view of the mild conditions under which the particles have been treated we prefer the former explanation in which the small metal clusters expand under the influence of CO. This hypothesis has been proposed earlier by D.J.C. Yates *et al.* (11), who called the phenomenon a 'breathing raft'. Measurements performed on another highly dispersed rhodium catalyst, to be published elsewhere (45), showed that the aggregate of $Rh(CO)_2$ species rearranged after desorption of CO at elevated temperatures to metallic particles. Thus, the process of disruption of the metal particles by CO is reversible and these particles can indeed be called 'breathing rafts or particles'. As no paramagnetic ESR Rh^0 (d^8s^1) signal could be detected after CO admission we infer that CO adsorption has to be oxidative. The oxidation state of rhodium in the $Rh(CO)_2$ species is most likely 1+, as confirmed by XPS and IR. Two possible reactions can be envisioned to be responsible for this oxidation: either the rhodium is oxidized by hydroxyl groups of the support, by which case hydrogen formed must be released according to the reaction:

(1) $2Rh + 4CO + 2Al-OH \rightarrow H_2 + 2\ Al-O-Rh^{1+}(CO)_2$,
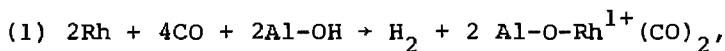
or rhodium is oxidized by a dissociatively adsorbed CO molecule;

$$CO + 3\ Rh \rightarrow RhC + 2Rh^{1+} + O^{2-}$$
$$(2)$$
$$2Rh^{1+} + 4CO \rightarrow 2Rh^{1+}(CO)_2.$$
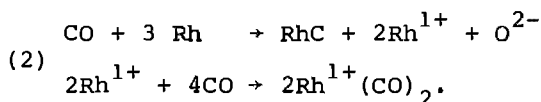
If formation of graphite occurs ($nRhC \rightarrow nRh + C_n$) a large part of the rhodium can be oxidized in this way.
Reaction (1) can be considered as a summation of three reactions

which are described in the literature (57, 58):

a) $Rh^0 + nCO \rightarrow [Rh^0(CO)_n]$

b) $6Rh^0(CO)_n + (16 - 6n)CO \rightarrow Rh_6(CO)_{16}$

c) $Rh_6(CO)_{16} + 6Al-OH \rightarrow 3H_2 + 6Al-O-Rh(CO)_2 + 4CO$.
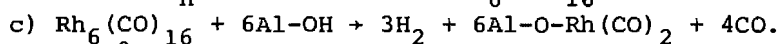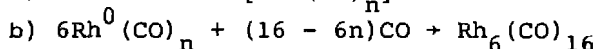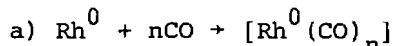
The '$Rh^0(CO)_n$' species can polymerize to small Rh_4 or Rh_6 clusters when the CO/H_2O ratio is high, whereas at low CO/H_2O ratio sizeable metallic particles will be formed (57). Reaction c) has been proposed as a possible explanation for the formation of rhodium carbonyl species from surface OH groups and $Rh_6(CO)_{16}$ by Theolier *et al.* (58).

However, a gas chromatographic analysis of the gas over the catalyst after CO chemisorption did not supply evidence for hydrogen formation and therefore, we do not think it is likely that reaction (1) has taken place.

On the other hand we have to take into account the possibility that the disruption of the rhodium-rhodium metallic bonds, going hand in hand with the oxidation of rhodium to Rh^{1+}, already occurred during evacuation of the catalyst, thus before CO was admitted. This assumption is based upon the idea that during evacuation rhodium becomes coordinatively unsaturated which can be counteracted by insertion of rhodium between the oxygen and hydrogen atom of a hydroxyl group (59). A thorough evacuation at elevated temperatures will desorb the hydrogen and leave the rhodium as Rh^{1+} ions. Reaction (1) can then be considered to consist of the following consecutive reactions:

d) $Rh + Al-OH \rightarrow Al-O-Rh^{1+} + \tfrac{1}{2}H_2$

e) $Al-O-Rh^{1+} + 2CO \rightarrow Al-O-Rh^{1+}(CO)_2$.
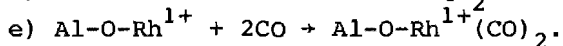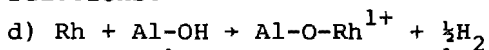
In that case the hydrogen formed cannot be detected because it is pumped away during evacuation. Note that according to the reversed reaction d) one hydrogen atom is needed to form the hydroxyl group again and consequently one should be surprised if hydrogen chemisorption measurements, carried out on ultra dispersed rhodium catalysts, lead to H/Rh values which do not exceed one.

Although this latter model is not in contradiction with our

results we prefer the second possibility, in which the dis-
sociation of CO plays an important role. The main argument
for this is based upon the observations reported by Primet
(60). He has found that reduction and evacuation at 773 K of
a dispersed Rh/Al_2O_3 catalyst, followed by adsorption of CO
at 77 K under a pressure of 0.27 kPa, only gave the CO infra-
red bands at 2075 and 1920-1870 cm^{-1} assigned to CO bonded
to Rh atom(s) in respectively the linear and multicentered
forms. Note that if Rh^{1+} ions were formed after evacuation
also absorption bands of $Rh^{1+}(CO)_2$ species had to be observed.
When the temperature of adsorption was increased, bands at
2095 and 2028 cm^{-1} assigned to $Rh^{1+}(CO)_2$ species, developed
and reached their maximum intensities after one hour of con-
tact at 300 K. The progressive formation of the doublet on in-
creasing the temperature of adsorption was correlated with
dissociation of CO on highly dispersed rhodium followed by
adsorption of CO on the oxidized surface groups ($cf.$ reaction
(2)).

Although adsorption of CO on large particles is not dissociative
at room temperature (61, 62) this is probably not the case
when the particle size decreases below 10 Å. The Boudouard
reaction ($2CO \rightarrow CO_2 + C$) can be ruled out, however, because no
CO_2 could be detected after CO admission.

For these reasons we think that the oxidation of the rhodium
atoms is coupled to the dissociation of CO. In that case,
however, the question arises how one can explain the reversi-
bility of this process, since we have observed that metal
particles are reformed when evacuating at 573 K. We propose
that this reformation of the metal crystallites, takes place
as a reductive desorption of CO according to the following
reaction:

$$(3) \quad O^{2-} + 2Rh^{1+}(CO)_2 \rightarrow 2Rh + CO_2 + 3CO.$$
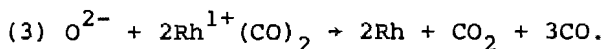
7.5 CONCLUSIONS

From the results of this study performed on a highly dis-
persed 0.57 wt% Rh/γ-Al$_2$O$_3$ catalyst two main conclusions can
be drawn.

I. After reduction at 593 K the catalyst is highly dispersed.
   Only small metal crystallites are present consisting of
   6-10 atoms and probably they have a three-dimensional
   structure. No indications for the existence of dispersed
   rhodium atoms or ions after reduction have been observed.
   The metal-support interactions involve Rh^0-(carrier)O^{2-}
   bonds.

All this demonstrates that there is no fundamental difference
between reduced Rh/Al$_2$O$_3$ catalysts with low Rh loading and
those with high Rh loading. At all loadings rhodium metal
crystallites are present on the support surface. Only the size
and morphology of these crystallites vary with Rh loading.

II. Adsorption of CO at room temperature on the 0.57 wt%
    Rh/γ-Al$_2$O$_3$ catalyst results in a significant disruption
    of the Rh crystallites, ultimately leading to isolated
    rhodium geminal dicarbonyl species in which rhodium has
    an oxidation state of 1+ and is surrounded by two carbon
    monoxide molecules and three oxygen ions. The adsorption
    of CO is oxidative and can be explained by dissociation
    of CO followed by CO adsorption on the oxidized rhodium.

The results of this study explain the apparent contradiction
between the results obtained from infrared studies and those
obtained from high resolution electron microscopy. This con-
tradiction is, indeed, apparent because as our EXAFS measure-
ments prove, CO adsorption changes the system completely. After
reduction and before CO admission small Rh metal crystallites
are present, whereas after CO admission isolated Rh(CO)$_2$
species are on the support. The presented evidence for a large

difference in structure between an Rh catalyst before and after
adsorption of CO might not be an isolated case, but might be
an example of a more general phenomenon of a drastic change in
catalyst structure upon adsorption of an adsorbate. Such cases
might especially be expected for adsorbates which are adsorbed
with large heats of adsorption on small catalyst crystallites.

7.6 REFERENCES

1. H.C. Yao, Y.F. Yu Yao and K. Otto, J. Catal., 56, 21 (1979).
2. P.R. Watson and G.A. Somorjai, J. Catal., 72, 347 (1981).
3. P.R. Watson and G.A. Somorjai, J. Catal., 74, 282 (1982).
4. T.P. Wilson, P.H. Kasai and P.C. Ellgen, J. Catal., 69,
   193 (1981).
5. A.C. Yang and C.W. Garland, J. Phys. Chem., 61, 1504 (1957).
6. C.A. Rice, S.D. Worley, C.W. Curtis, J.A. Guin and A.R.
   Tarrer, J. Chem.Phys., 74, 6487 (1981).
7. R.R. Cavanagh and J.T. Yates, J. Chem. Phys., 74, 4150
   (1981).
8. S.D. Worley, C.A. Rice, G.A. Mattson, C.W. Curtis,
   J.A. Guin and A.R. Tarrer, J. Phys. Chem., 86, 2714 (1982).
9. S.D. Worley, C.A. Rice, G.A. Mattson, C.W. Curtis, J.A.
   Guin and A.R. Tarrer, J. Chem. Phys., 76, 20 (1982).
10. D.J.C. Yates, L.L. Murrell and E.B. Prestridge, J. Catal.,
    57, 41 (1979).
11. D.J.C. Yates, L.L. Murrell and E.B. Prestridge, in "Growth
    and Properties of Metal Clusters", p. 137 (1980), edited
    by J. Bourdon, Elsevier Sci. Pub. Co., Amsterdam, The
    Netherlands.
12. H.F.J. van 't Blik, J.B.A.D. van Zon, T. Huizinga, J.C. Vis,
    D.C. Koningsberger and R. Prins, J. Phys. Chem., 87, 2264
    (1983).
13. F.W. Graydon and M.D. Langan, J. Catal., 69, 180 (1981).

14. J. Lauher, J. Catal., 66, 237 (1980).

15. D.E. Sayers, E.A. Stern and F.W. Lytle, Phys. Rev. Lett., 27, 1204 (1971).

16. J.H. Sinfelt, G.H. Via and F.W. Lytle, J. Chem. Phys., 68, 2009 (1978).

17. G.H. Via, J.H. Sinfelt and F.W. Lytle, J. Chem. Phys., 71, 690 (1979).

18. J.R. Katzer, A.W. Sleight, P. Gajarde, J.B. Michel, E.F. Gleason and S. McMillan, Disc. Faraday Soc., 72, 121 (1981).

19. E.S. Shpiro, V.I. Avaev, G.V. Antoshin, M.A. Ryashentseva and K.M. Minachev, J. Catal., 55, 402 (1978).

20. R.L. Chin and D.M. Hercules, J. Phys. Chem., 86, 360 (1982).

21. T. Huizinga, H.F.J. van 't Blik, J.C. Vis and R. Prins, Surf. Sci., to be published.

22. J.A. McCleverty and G. Wilkinson, Inorg. Synth., 8, 211 (1966).

23. J.E. Benson, and M. Boudart, J. Catal., 4, 704 (1965).

24. H. Boer, W.J. Boersma and N. Wagstaff, Rev. Sci. Instr., 53, 349 (1982).

25. A.J.A. Konings, A.M. van Dooren, D.C. Koningsberger, V.H.J. de Beer, A.L. Farragher and G.C.A. Schuit, J. Catal., 54, 1 (1978).

26. J.C. Vis, H.F.J. van 't Blik and R. Prins, to be published.

27. D.C. Koningsberger and J.W. Cook, in "EXAFS and Near Edge Structures", p. 412, 1983 edited by A. Bianconi, L. Incoccia and S. Stipcich, Springer-Verlag, Berlin, Germany.

28. J.B.A.D. van Zon, D.C. Koningsberger, H.F.J. van 't Blik and D.E. Sayers, to be published.

29. A.E. Newkirk and D.W. McKee, J. Catal., 11, 370 (1968).

30. H.C. Yao, S. Japar and M. Shelef, J. Catal., 50, 407 (1977).

31. H.C. Yao and M. Shelef, in "Proceedings of the 7th International Congress on Catalysis", edited by T. Weiyama and K. Tanabe, Elseveir, Amsterdam (1981), Part B, p. 329.

32. N.W. Hurst, S.J. Gentry and A. Jones, Catal. Rev.-Sci. Eng. 24, 233 (1982).

33. S.E. Wanke and N.A. Dougharty, J. Catal., 24, 367 (1972).

34. R.R. Cavanagh and J.T. Yates, Jr., J. Catal., 68, 22 (1981).
35. T. Huizinga, H.F.J. van 't Blik, J.C. Vis and R. Prins, J. Catal., to be published.
36. J.H. Scofield, J. Electron. Spectrosc. Relat. Phenom., 8, 129 (1976).
37. J.B.A.D. van Zon, D.C. Koningsberger, D.E. Sayers, H.F.J. van 't Blik and R. Prins, J. Chem. Phys., submitted for publication.
38. E.A. Stern, B.A. Bunker and S.M. Heald, Phys. Rev. B, 21, 5521 (1980).
39. J.R. Anderson, in "The structure of metallic catalysts", Academic Press London (1975).
40. E.G. Derouane, A.J. Simvens and J.C. Védrine, Chem. Phys. Lett., 52, 549 (1977).
41. R.B. Shalvoy, B.H. Davis and P.J. Reucroft, Surf. Int. Anal., 2, 11 (1980).
42. R.B. Greegor, F.W. Lytle, R.L. Chin and D.M. Hercules, J. Phys. Chem., 85, 1232 (1981).
43. B. Besson, B. Moraweck, A.K. Smith, J.M. Basset, R. Psaro, A. Fusi and R. Ugo, J. Chem. Soc. Chem. Comm., 569 (1980).
44. M. Deeba and B.C. Gates, J. Catal., 67, 303 (1981).
45. H.F.J. van 't Blik, J.B.A.D. van Zon, D.C. Koningsberger and R. Prins, J. Mol. Catal., to be published.
46. H.C. Yao and M. Shelef, J. Catal., 44, 392 (1976).
47. J.E. Demuth, P.M. Marcus and D.W. Jepsen, Phys. Rev. B, 11, 1460 (1975).
48. P.M. Marcus, J.E. Demuth and D.W. Jepsen, Surf. Sci., 53, 501 (1975).
49. B. Moraweck, G. Clugnet and A.J. Renouprez, Surf. Sci., 81, L631 (1979).
50. H. Knözinger and R. Ratnasamy, Catal. Rev.-Sci. Eng., 17, 31 (1978).
51. L.F. Dahl, C. Martell and D.L. Wampler, J. Am. Chem. Soc., 83, 1761 (1961).
52. P.A. Lee and G. Beni, Phys. Rev. B, 11, 1279 (1975).

53. S.P. Cramer, K.O. Hodgson, E.I. Stiefel and W.E. Newton, J. Am. Chem. Soc., 100, 2748 (1978).

54. B. Teo, J. Am. Chem. Soc., 103, 3990 (1981).

55. B. Teo and P.A. Lee, J. Am. Chem. Soc., 101, 2815 (1979).

56. D. Cordischi, V. Indovina and M. Occhiuzzi, J. Chem. Soc. Farad. Trans. I, 76, 1147 (1980).

57. A.K. Smith, F. Hugues, A. Theolier, J.M. Basset, R. Ugo, G.M. Zanderighi, J.L. Bilhou, V. Bilhou-Bougnol and W.F. Graydon, Inorg. Chem., 18, 3104 (1979).

58. A. Theolier, A.K. Smith, M. Leconte, J.M. Basset, G.M. Zanderighi, R. Psaro and R. Ugo, J. Organometallic Chem., 191, 415 (1980).

59. J.M. Basset, B. Besson, A. Choplin and A. Theolier, Phil. Trans. R. Soc. Lond., A 308, 115 (1982).

60. M. Primet, J. Chem. Soc. Farad. Trans. I, 74, 2570 (1978).

61. J.T. Yates, Jr., E.D. Williams and W.H. Weinberg, Surf. Sci., 91, 562 (1981).

62. D.G. Castner, L.H. Dubois, B.A. Sexton and G.A. Somorjai, Surf. Sci., 103, L134 (1981).

chapter 8

EXAFS DETERMINATION OF THE CHANGE IN THE STRUCTURE OF RHODIUM IN HIGHLY DISPERSED Rh/Al$_2$O$_3$ CATALYSTS AFTER CO AND/OR H$_2$ ADSORPTION AT DIFFERENT TEMPERATURES

8.1 ABSTRACT

Extended X-ray absorption spectroscopy (EXAFS) has been applied to study the Rh K-edge of two ultra dispersed Rh/Al$_2$O$_3$ catalysts containing 0.47 and 1.04 wt% rhodium, respectively. The structural properties of the Rh crystallites were determined after reduction with H$_2$, evacuation at elevated temperatures, CO admission at room temperature, CO desorption, CO admission at 523 K, at which the Boudouard reaction takes place, and after hydrogenation of CO at 523 K.

During reduction of the catalyst metallic rhodium crystallites are formed which are attached to the support via Rh^0-O^{2-} bonds, implying zerovalent rhodium. The Rh-Rh nearest neighbour distance in the particles is contracted to 2.63 Å in vacuum and relaxes to 2.68 Å (similar to the bulk value) upon hydrogen chemisorption. Adsorption of CO at room temperature upon the reduced catalysts results in a partial disruption of the small Rh crystallites, ultimately leading to rhodium geminal dicarbonyl species. A subsequent desorption of CO leads to the rearrangement of the metal clusters. The oxidation state of rhodium alters from zero to 1+ upon CO chemisorption and becomes zero again after CO desorption. After CO admission at 523 K the rhodium particles break up completely, probably because of intercalation of carbon and/or oxygen atoms. The

highly dispersed Rh/Al_2O_3 catalysts change to poorly dispersed systems after reaction between CO and H_2 at 523 K due to sintering of the metallic crystallites.

8.2 INTRODUCTION

Knowledge about the structure and oxidation state of rhodium in highly dispersed rhodium catalysts is important for an understanding of its catalytic selectivity and activity. For instance there are indications that the hydrogenation of carbon monoxide yields oxygen containing products like methanol and ethanol when rhodium ions are present (1, 2).

Many characterization studies performed on ultra dispersed rhodium supported catalysts have been reported in which a diversity of techniques has been used (3-10). The CO infrared spectrum between 1800 and 2100 cm^{-1} of an ultra dispersed rhodium catalyst is characterized by two absorption bands at 2095 and 2027 cm^{-1}. The wavenumbers correspond closely to those observed for the bridged $[Rh(CO)_2Cl]_2$ dimer and are assigned to the symmetrical and antisymmetrical stretching frequencies, respectively. On the basis of these CO infrared data some investigators have asserted that rhodium on alumina after reduction is monatomically dispersed with the rhodium in the 1+ state (3-5). On the other hand electron microscopy studies of a well reduced Rh catalyst showed the existence of metallic rhodium crystallites (6, 7). The seeming contradiction between the results obtained from infrared studies and those obtained from high resolution electron microscopy is explained by the results of an EXAFS study recently published (9, 10) and presented in chapter 7. After reduction of an ultra dispersed catalyst only metallic rhodium crystallites were observed with most likely a three-dimensional structure. After CO admission the EXAFS spectrum changed completely, however. The EXAFS oscillations above $k = 5\ Å^{-1}$, typical for Rh-Rh metal coordination, had disappeared. So the rhodium metallic particles

break up on CO adsorption, ultimately leading to isolated
rhodium dicarbonyl species. A further analysis of the EXAFS
data showed that the oscillations were caused by $O_3Rh^{1+}(CO)_2$
coordination. Each rhodium ion is surrounded by two CO molecules
(geminal dicarbonyl) and three oxygen ions of the support. The
oxidation state of rhodium changed from zero to 1+ after CO
admission and was explained in terms of an oxidative CO
chemisorption via a CO dissociation.
These results clearly demonstrate the dramatic influence of
CO adsorption at room temperature on the structure of rhodium
in highly dispersed catalysts. In general, one has te be aware
of the fact that such effects may occur when the catalysts
are studied under different gas atmospheres.

In order to obtain more information about the rhodium
structure in a highly dispersed $Rh/\gamma-Al_2O_3$ catalyst after
different treatments we have carried out an EXAFS in situ study
of a 0.47 and 1.04 wt% $Rh/\gamma-Al_2O_3$ catalyst. As we are interested
in the hydrogenation of carbon monoxide to hydrocarbons EXAFS
spectra were recorded after reduction with H_2, evacuation,
CO admission at room temperature, desorption of CO, CO admission
at 523 K at which the Boudouard reaction takes place
($2CO \rightarrow C + CO_2$) and after hydrogenation of CO at 523 K. The
EXAFS data give insight into the change of local structure of
supported rhodium under different conditions.
One of the first EXAFS studies on the effects of adsorption of
different gases on the structural and electronic properties of
supported metallic crystallites has been reported by Fukushima
et al. (11). They studied the Pt/Al_2O_3 system and observed that
O_2 adsorption caused severe structural disruption of the
crystallites, whereas CO adsorption caused only electronic
effects.

8.3 EXPERIMENTAL SECTION

Two $Rh/\gamma-Al_2O_3$ catalysts were prepared with different
rhodium loadings (0.47 and 1.04 wt%). By pore volume impregna-
tion of the support $\gamma-Al_2O_3$ (Ketjen, 000-1.5E, specific area =

$200 \, m^2/g$, pore volume $= 0.65 \, cm^3/g$) with an aqueous solution of $RhCl_3.xH_2O$ (39 wt%, Drijfhout) the metal salt was deposited on the support. After impregnation the catalysts were dried at room temperature overnight and subsequently for 16 hours at 393 K to remove the adsorbed water. The dried catalysts were directly reduced at 773 K (heating rate 5 K/min) for 1 hour in flowing hydrogen (researchgrade, Hoekloos) and passivated (oxidation at room temperature). The rhodium content of the passivated catalysts was determined colourimetrically.

Temperature Programmed Reduction (TPR) studies confirmed that after reduction at 773 K reduction of the catalysts was complete. The TPR of the passivated catalysts showed that a reduction temperature of at least 423 K was needed in order to reduce the systems and moreover that the degree of oxidation of the passivated catalysts was high, although passivation is a mild oxidation. This indicates that the dispersion of the catalysts was high (12).

Hydrogen chemisorption measurements were performed in a conventional glass system at 298 K. Before measuring the H_2 adsorption isotherms the passivated catalysts were reduced at 573 K (heating rate 5 K/min) for one hour under flowing hydrogen (purified by passing over a Pd diffusion cell) and evacuated (10^{-2} Pa) at 573 K for another hour. Following the method of Benson and Boudart (13) the hydrogen chemisorption measurements resulted in H/Rh values (the total amount of chemisorbed H atoms, corrected for adsorption on the bare support, per total amount of rhodium) of 1.7 and 1.6 for res-pectively, the 0.47 and 1.04 wt% $Rh/\gamma-Al_2O_3$ catalyst. These results indicate that both catalysts are ultra disperse. H/Rh values higher than 1 for Rh/Al_2O_3 catalysts have been observed previously (14, 15) and are explained by multiple adsorption, although hydrogen spill-over cannot be completely· excluded (16).

The samples used for the EXAFS experiments were pressed into a thin self-supporting wafer and mounted in an EXAFS in situ cell (17). The thickness of the wafer was chosen in such a way that the logarithm of the ratio between the incident and

transmitted X-ray intensity approached 1.6. The different treatments of the catalysts were carried out by using research-grade He, H_2 and CO, which were all purified over a BTS column for the removal of oxygen and over molecular sieves (Union Carbide, 5A) for the removal of water. The EXAFS experiments were carried out on X-ray beam line I-5 at the Stanford Synchrotron Radiation Laboratory (SSRL) with a ring energy of 3 GeV and ring currents of 40-80 mA. The EXAFS spectra of the rhodium K-edge were recorded at liquid nitrogen temperature. The EXAFS data were analysed by using reference samples with known crystal structure (the theory-independent analysis) and the Fourier filtering approach has been used (18). As reference compounds we have used Rh-foil, powdered Rh_2O_3 and powdered $RhCl_3$. As a suitable reference compound for the rhodium geminal dicarbonyl $Rh(CO)_2$ we have used the dimer $[Rh(CO)_2Cl]_2$ of which the Rh-Cl contribution in the EXAFS data has been subtracted. The procedure for this will be published elsewhere (10). For a detailed description of the analysis of the EXAFS function we refer to Van Zon *et al.* (19) and Van 't Blik *et al.* (10). Before analysing the EXAFS the spectra were smoothed by removing high frequency components (noise) in the spectrum via Fourier filtering. The r-region from 1 Å to 3.5 Å of the Radial Structure Function (RSF), in which we are interested, is not affected by the smoothing operation. The Fourier transforms were corrected for phase shift and/or backscattering amplitude (20). Consequently, the r-values correspond with real inter-atomic distances R if the phase used for correction originated from the same absorber-scatterer pair as the analysed one.

8.4 RESULTS

8.4.1 REDUCTION AT 673 K

Before measuring the EXAFS spectra both passivated catalysts were reduced in the cell at 673 K for 30 minutes under flowing hydrogen and cooled down to room temperature. The smoothed

EXAFS function of the rhodium K-edge of the reduced 0.47 wt%
$Rh/\gamma-Al_2O_3$ catalysts (under 100 kPa H_2, so the crystallites
were covered with hydrogen) is given in figure 1a.
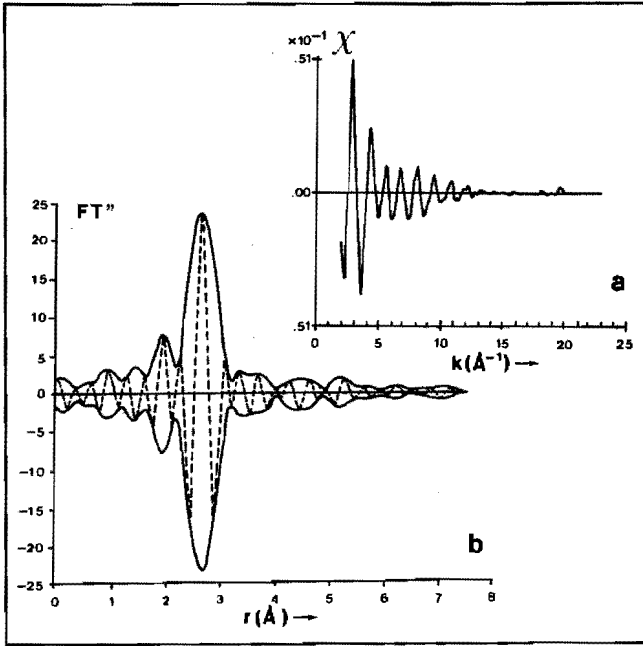
Figure 1: 0.47 wt% $Rh/\gamma-Al_2O_3$ catalyst after reduction at 673 K.
a. The normalized smoothed EXAFS data of the rhodium
K-edge at liquid nitrogen temperature.
b. The associated k^3-weighed Fourier transform
($\Delta k = 3.3 - 9.9$ $\mathring{A}^{-1}$) corrected for Rh-Rh phase
shift and backscattering amplitude. The solid line
represents the absolute value $|FT''|$ whereas the
dashed line represents the imaginary part $ImFT''$.

The oscillations are characteristic for rhodium neighbour atoms.
Figure 1b shows the imaginary part $ImFT''$ and the absolute
value $|FT''|$ of the k^3-weighed Fourier transform of the smoothed
EXAFS data, performed on a k-interval from $k = 3.3$ $\mathring{A}^{-1}$ to
$k = 9.9$ $\mathring{A}^{-1}$ and corrected for Rh-Rh phase shift and Rh-Rh back-
scattering amplitude. The EXAFS function of the reduced

1.04 wt% $Rh/\gamma-Al_2O_3$ catalyst only differs somewhat in amplitude from the one given in figure 1a.

Figure 1b clearly shows that the RSF is not symmetrical but is characterized by two peaks, a main peak around r = 2.7 Å and a peak around r = 1.8 Å. The procedure for analysing this type of radial structure function will be published else-where (19). A careful analysis of the RSF leads to the con-clusion that the EXAFS oscillations are a sum of oscillations due to metallic rhodium-rhodium and rhodium-oxygen scatterer pairs (21). The optimized parameter values, R (interatomic distance), N (average coordination number) and $\Delta\sigma^2$ (thermal and static disorder relative to reference compound), determined for the 0.47 and 1.04 wt% $Rh/\gamma-Al_2O_3$ catalyst are presented in table 1 and 2, respectively.

Table 1 EXAFS parameter values for the 0.47 wt% $Rh/\gamma-Al_2O_3$ catalyst after different treatments. Accuracies: N: $\pm$ 10-20%, R: $\pm$ 0.5-1%, $\Delta\sigma^2$: $\pm$ 10-20%.

	COORDINATION								
	Rh-Rh			Rh-O			Rh-CO		
TREATMENT	N	R [Å]	$\Delta\sigma^2$ $\times10^2$ [Å²]	N	R [Å]	$\Delta\sigma^2$ $\times10^2$ [Å²]	N	R [Å]	$\Delta\sigma^2$ $\times10^2$ [Å²]
a: reduction at 673 K	5.3	2.68	0.5	1.7	2.73	0.0			
b: a, evacuation at 673 K, CO admission at 298 K	1.2	2.68	0.4	2.6	2.10	0.6	1.7	⋇	0.5
c: reduction at 523 K, H_2/CO at 523 K	9.0	2.69	0.3						

⋇ The Rh-C and Rh-O* distances are equal to the one in the dimer $[Rh(CO)_2Cl]_2$.

Table 2 EXAFS parameter values for the 1.04 wt% $Rh/\gamma-Al_2O_3$
catalyst after different treatments. Accuracies:
N: $\pm$ 10-20%, R: $\pm$ 0.5-1%, $\Delta\sigma^2$: $\pm$ 10-20%.

TREATMENT	COORDINATION								
	Rh-Rh			Rh-O			Rh-CO		
	N	R [Å]	$\Delta\sigma^2$ x10^2 [Å^2]	N	R. [Å]	$\Delta\sigma^2$ x10^2 [Å^2]	N	R [Å]	$\Delta\sigma^2$ x10^2 [Å^2]
a: reduction at 673 K	5.9	2.68	0.5	1.5	2.73	0.0			
b: a, evacuation at 673 K	6.6	2.63	0.4						
c: b, CO admission at 298 K	1.6	2.68	0.4	2.2	2.12	0.5	1.5	x	0.5
d: c, He flushing at 573 K	7.1	2.66	0.5						
e: d, reducition at 573 K	7.8	2.68	0.4						

x The Rh-C and Rh-O* distances are equal to the one in the dimer
$[Rh(CO)_2Cl]_2$.

Figure 2a shows the smoothed EXAFS data with the calculated
Rh-Rh, Rh-O two shell EXAFS function using the optimized
parameters (*cf.* table 1). The associated k^3-weighed Fourier
transforms are presented in figure 2b.
In order to demonstrate the influence of the Rh-O as well as
the Rh-Rh contribution on the Fourier transformed smoothed
EXAFS data, the RSF's of the data, the calculated Rh-Rh one
shell and Rh-O one shell fine structures are presented in
figure 2c. Note that the RSF of Rh-O coordination peaks at
2.33 Å while the real interatomic distance R is 2.73 Å. This
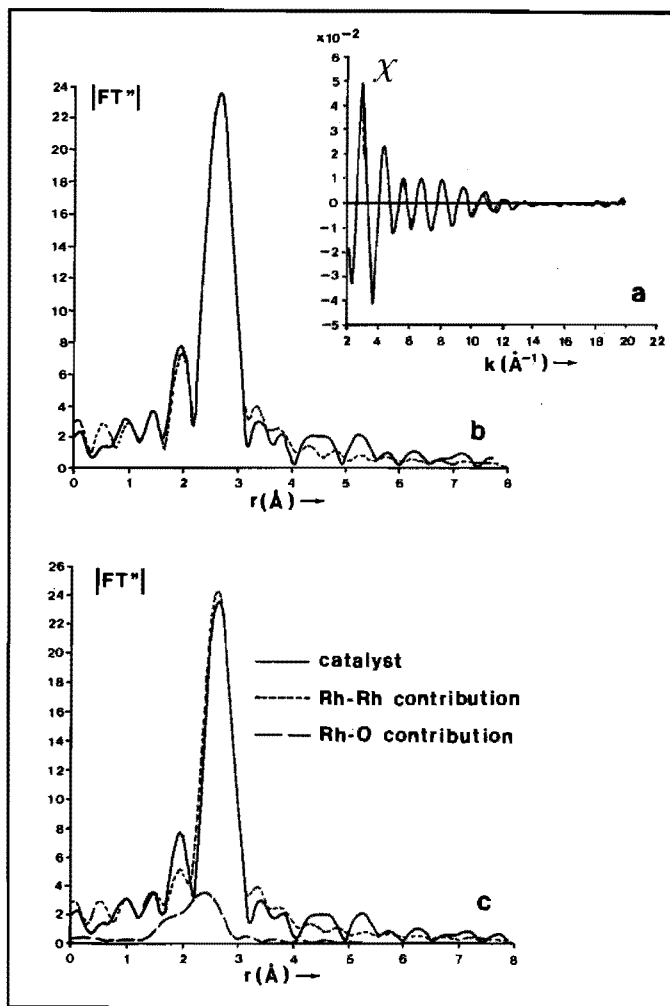
Figure 2 0.47 wt% Rh/γ-Al₂O₃ catalyst after reduction at 673 K.
   a. The solid line represents the normalized smoothed EXAFS data
      of the rhodium K-edge at liquid nitrogen temperature. The
      dashed line was obtained by calculating the two shell EXAFS
      (Rh-Rh and Rh-O) using the optimized parameters (cf. table 1).
   b. The associated absolute values of the k^3-weighed Fourier
      transforms ($\Delta k = 3.3 - 9.9$ Å^{-1}) corrected for Rh-Rh phase shift
      and amplitude. The solid line represents the Fourier transform
      of the catalyst. The dashed line represents the Fourier trans-
      form of the calculated Rh-Rh and Rh-O two shell EXAFS.
   c. The absolute values of the k^3-weighed Fourier transforms
      ($\Delta k = 3.3 - 9.9$ Å^{-1}) corrected for Rh-Rh phase shift and
      amplitude for the catalyst and the calculated Rh-Rh and Rh-O
      one shell fine structures.

is caused by the fact that an Rh-Rh phase shift correction
was used. The phase factors of Rh-Rh and Rh-O coordination
differs and in the case of Rh-Rh phase shift correction the
r-values of Rh-O bonds shift 0.4 Å downwards relative to the
real interatomic distances. The figure clearly demonstrates
that the main peak at 2.7 Å is caused by Rh-Rh coordination
and is slightly affected by Rh-O coordination while the apparent
peak at 1.8 Å is caused by interference of the two coordina-
tions.

8.4.2 EVACUATION AT 673 K

A fresh passivated 1.04 wt% Rh/γ-Al$_2$O$_3$ sample was reduced
at 673 K for one hour, evacuated (10^{-2} Pa) for another hour
and cooled to room temperature under dynamic vacuum. Helium
was admitted then up to 100 kPa. The analysis of the EXAFS
spectrum of the evacuated catalyst yielded an average Rh-Rh
coordination number of 6.6, which is significantly higher
than after reduction without evacuation (N = 5.9), and an
interatomic distance of 2.64 $\pm$ 0.01 Å indicating a contraction
of the metallic rhodium particles (see table 2). In addition,
no substantial contribution of Rh-O coordination could be
detected.

8.4.3 CO CHEMISORPTION AT 298 K

Both catalysts used in section 8.4.1 were evacuated
(10^{-2} Pa) at 673 K for one hour and subsequently cooled to
room temperature under dynamic vacuum. Once room temperature
was reached CO was admitted up to 100 kPa after which the
EXAFS spectra were recorded. As the spectra of both catalysts
hardly differ we only present in figure 3a the smoothed EXAFS
obtained from the 0.47 wt% Rh/γ-Al$_2$O$_3$ catalyst. Comparison of
the EXAFS after reduction with the EXAFS after CO admission
(see respectively, figure 1a and 3a) clearly demonstrates the
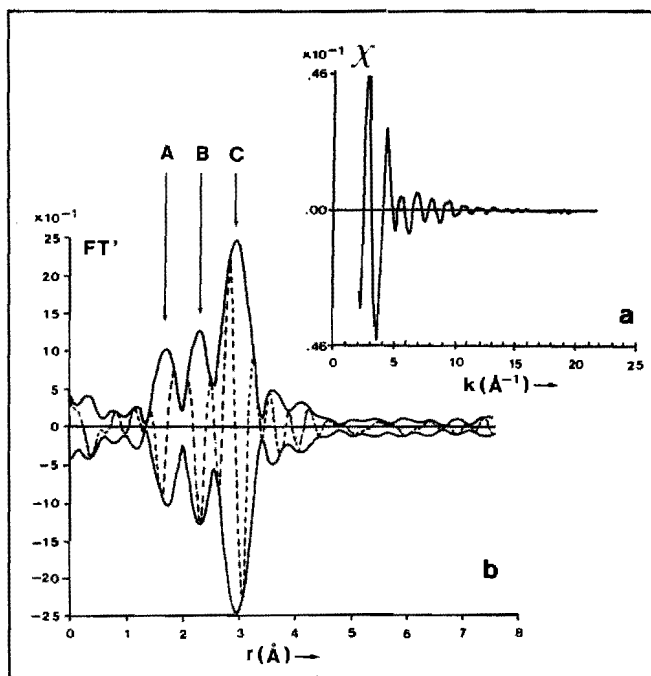
Figure 3 *0.47 wt% Rh/γ-Al*$_2$*O*$_3$ *catalyst after CO admission at*
298 *K.*
a. *The normalized smoothed EXAFS data of the rhodium*
   K-edge at liquid nitrogen temperature.
b. *The associated* k^3*-weighed Fourier transform*
   (Δk = 3.3 - 9.7 Å^{-1}*) corrected for Rh-O phase shift*
   The solid line represents | *FT'* | *and the dashed*
   line represents ImFT'.

diminution of the amplitude after CO adsorption at room tempera-
ture. Oscillations above k = 5 Å^{-1}, typical for rhodium-rhodium
coordination, are still present. This demonstrates that a
partial disruption of the small Rh crystallites has taken place
and that a small part of rhodium is present as metallic
particles, upon which CO is linearly bound, whereas the greater
part is present as isolated Rh(CO)$_2$ species. Both, the particles

and dicarbonyl species, are attached to the support via oxygen ions but with a different interatomic Rh-O distance (10). As the fraction of the total amount of rhodium in Rh-O bonds between the metallic particles and the support is low, the contribution of this scatterer pair can be neglected. Consequently, the EXAFS function is mainly caused by Rh-Rh, Rh-C-O* (actually two scatterer pairs, Rh-C and Rh-O*) and Rh-O coordination, the latter of which is the bond between the $Rh(CO)_2$ species and the support.

In figure 3b the k^3-weighed Fourier transform of the fine structure ($\Delta k = 3.3 - 9.7$ Å^{-1}) is given. Three peaks can be distinguished, peak C of which is caused partly by Rh-Rh and partly by Rh-O* coordination. Peak A is mainly caused by Rh-C, originated from the carbonyl, but may be suppressed by peak B due to interference. As the RSF is corrected for Rh-O phase shift the r-values which belong to rhodium-oxygen and rhodium-carbon coordination correspond with real interatomic distances. (The phase factors of Rh-O and Rh-C hardly differ.)

The imaginary part of the Fourier transform between $\Delta r = 1.2 - 1.8$ Å can be assigned to Rh-C coordination only. Therefore, a first estimate for the Rh-C-O* parameter values was found by calculating the EXAFS of Rh-C-O*, using the phase and backscattering amplitude of the geminal dicarbonyl reference sample, in such a way that the imaginary parts of the transformed calculated EXAFS and the transformed EXAFS data overlap between 1.2 and 1.8 Å. The optimized parameter values (see table 1) are: $N = 1.7$, $\Delta\sigma^2 = 0.005$ Å^2 (relative to $[Rh(CO)_2Cl]_2$). The interatomic distances are similar to the Rh-C-O* distances in the dimer.

As mentioned before peak C in figure 3b is caused by Rh-Rh as well as Rh-O* coordination. By subtracting the Rh-C-O* contribution from the EXAFS data the Rh-Rh contribution can be determined then. Therefore, we investigated the difference signal between the smoothed data and the calculated Rh-CO contribution, using the optimized parameter values. The Rh-Rh phase shift and backscattering amplitude corrected RSF of this signal is presented in figure 4a.
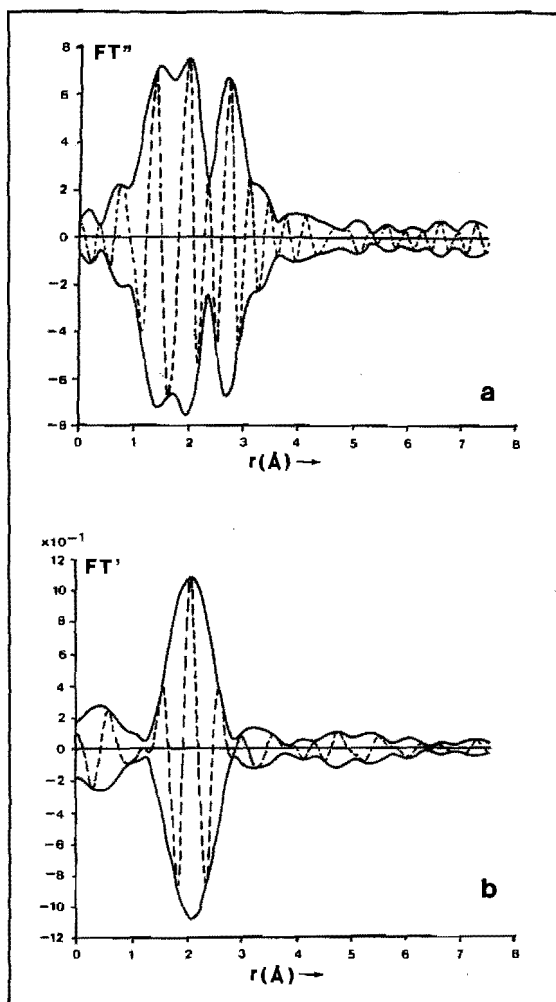
Figure 4 0.47 wt% Rh/γ-Al$_2$O$_3$ catalyst after CO admission at 298 K.

a. *The k^3-weighed Fourier transform (Δk = 3.3 - 10 Å^{-1}) corrected for Rh-Rh phase shift and amplitude of the difference signal between the smoothed data and the calculated Rh-CO contribution using the optimized parameter values (cf. table 1). The solid line represents |FT''| and the dashed line represents ImFT''.*

b. *The k^3-weighed Foureir transform (Δk = 3.3 - 8.5 Å^{-1}) corrected for Rh-O phase shift of the signal obtained by subtracting the Rh-CO and Rh-Rh contributions from the smoothed EXAFS data using the optimized parameters as given in table 1.*

In this function two regions can be distinguished:
(a) $\Delta r = 1 - 2.2$ Å, with relative broad oscillations in ImFT'',
typical for Rh-O coordination, (b) $\Delta r = 2.3 - 3.3$ Å, with a
peak around 2.7 Å, of which the maxima of ImFT'' and |FT''|
coincide. The peak belongs to the Rh-Rh nearest neighbour dis-
tance and the optimized Rh-Rh parameter values (see table 1)
were determined by fitting the filtered difference signal,
obtained by inverse transformation from $r = 2.7$ Å to $r = 3.7$ Å.
In order to obtain the Rh-O parameters the Rh-O phase corrected
RSF of the difference signal between the smoothed EXAFS data
and the sum of the calculated Rh-CO and Rh-Rh signal, using the
optimized parameters (*cf.* table 1), was analysed (see figure 4b).
A fit of the filtered difference signal ($\Delta r = 1.3 - 2.8$ Å)
yielded: $N = 2.6$, $R = 2.10$ Å and $\Delta\sigma^2 = 0.004$ Å^2. Note that
ImFT' and |FT'| are symmetric which is a necessary condition
if the EXAFS is due to a single scatterer pair.
Figure 5a shows the smoothed EXAFS data and the calculated three
shell EXAFS function using the parameters as given in table 1.
In figure 5b and 5c are respectively the ImFT' and the |FT'|
of the associated k^3-weighed Fourier transforms presented.
The optimized parameter values determined for the 1.04 wt%
Rh/γ-Al$_2$O$_3$ catalyst are presented in table 2.

8.4.4 CO DESORPTION

As shown in section 8.4.3 CO chemisorption at room tempera-
ture gave rise to disruption of rhodium-rhodium bonds. In order
to investigate if rhodium-rhodium bonds are formed again after
desorption of carbon monoxide, EXAFS spectra of the CO adsorbed
1.04 wt% Rh/γ-Al$_2$O$_3$ catalyst, described in section 8.4.3, were
recorded after each of the following consecutive treatments:
(a) evacuation (10^{-2} Pa) at room temperature for 5 minutes and
heated at 373 K under flowing He for one hour, (b) heated at
573 K under flowing He for another hour and (c) reduction with
flowing H$_2$ at 573 K.
The EXAFS spectrum after flushing with He at 373 K was identical
to the one obtained after CO admission at room temperature
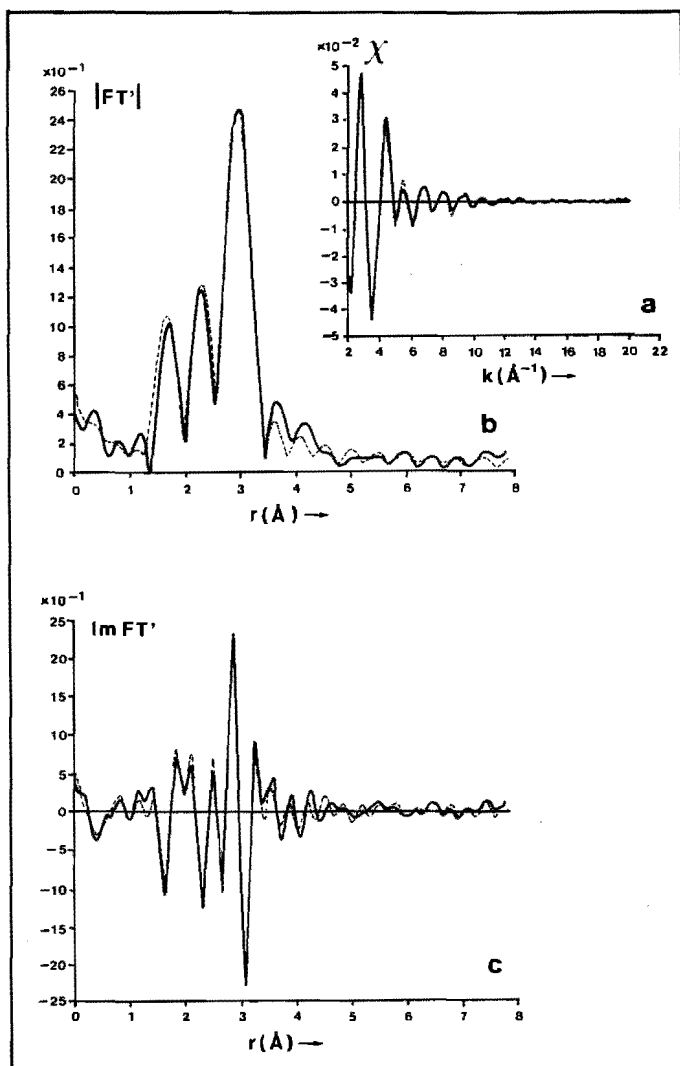
Figure 5 0.47 wt% Rh/γ-Al₂O₃ catalyst after CO admission at 298 K.

> *a. The solid line represents the normalized smoothed EXAFS data*
> *of the rhodium K-edge at liquid nitrogen temperature.*
> *The dashed line represents the calculated Rh-CO, Rh-Rh*
> *and Rh-O three shell EXAFS, using the optimized parameter*
> *values (cf. table 1).*
> *b. The absolute values of the associated Fourier transforms.*
> *c. The imaginary parts of the associated Fourier transforms.*

indicating that no desorption of CO had taken place, while after flushing with He at 573 K the spectrum had completely changed to a spectrum typical for rhodium-rhodium nearest neighbours. The optimized parameter values are: N = 7.1, R = 2.66 $\overset{\circ}{A}$ (a small contraction compared to bulk value) and $\Delta\sigma^2$ = 0.0046 $\overset{\circ}{A}^2$ (see table 2). A subsequent reduction at 573 K caused an enhancement of the average Rh-Rh coordination number from N = 7.1 to N = 7.8 while the interatomic distance increased to the bulk value (see table 2).

8.4.5 BOUDOUARD REACTION AND REACTION BETWEEN H_2 AND CO

After the EXAFS spectrum of the 0.47 wt% $Rh/\gamma-Al_2O_3$ catalyst adsorbed with CO was recorded (see section 8.4.3) the temperature was raised to 523 K under flowing CO. Under these conditions the Boudouard reaction takes place, as con- firmed by CO-pulse experiments. From the EXAFS results we can safely say that a contribution of Rh-Rh coordination is lacking. The EXAFS is very complicated and could not be analysed proper- ly because too many scatterers of different types (Rh-C from rhodium carbonyl and possible formed rhodiumcarbide, Rh-O* from rhodium carbonyl and Rh-O from the interface support/rhodium species and rhodium oxide, formed by intercalation of oxygen atoms during the Boudouard reaction) contribute.

A passivated 0.47 wt% $Rh/\gamma-Al_2O_3$ sample was reduced at 523 K for 15 minutes and subsequently a mixture of H_2 and CO (1:1) was led over the catalyst for one hour. Under these conditions hydrocarbons are formed.
The obtained EXAFS spectrum after reaction showed oscillations due to rhodium-rhodium coordination only. By fitting the fil- tered RSF in k-space the parameters of the rhodium nearest neighbour shell were determined: N = 9.0, R = 2.69 $\overset{\circ}{A}$, $\Delta\sigma^2$ = 0.003 $\overset{\circ}{A}^2$ (see table 1).

The results of the influence of different gas environments upon the Rh-Rh nearest neighbour coordination have been summarized in figure 6 and 7.
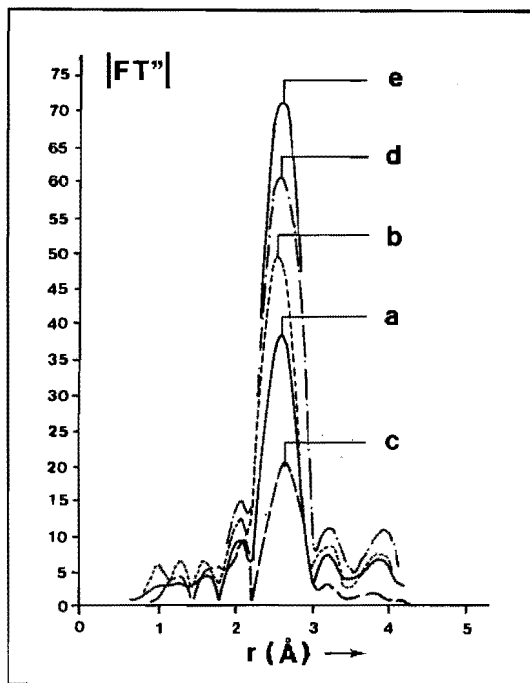
Figure 6 The radial structure functions (k^3-weighed, $\Delta k =$ 3 - 13 $\AA^{-1}$, Rh-Rh phase shift and amplitude corrected) for the 1.04 wt% Rh/γ-Al$_2$O$_3$ catalyst after the consecutive treatments:
a) reduction at 673 K, b) evacuation at 673 K,
c) CO admission at 298 K, d) He flushing at 573 K
and e) reduction at 573 K.

In figure 6 the Rh-Rh phase and amplitude corrected radial structure functions of the EXAFS spectra obtained from the 1.04 wt% Rh/γ-Al$_2$O$_3$ catalyst after different treatments are presented. In this figure the disruption of Rh-Rh bonds caused by CO chemisorption and rearrangement of the metal cluster after desorption of CO are demonstrated.
The alteration of the structure of the rhodium crystallites after the Boudouard reaction and hydrogenation of carbon monoxide is illustrated in figure 7. The different radial structure functions of the fine structures measured on the

0.47 wt% Rh/γ-Al$_2$O$_3$ catalyst are shown.
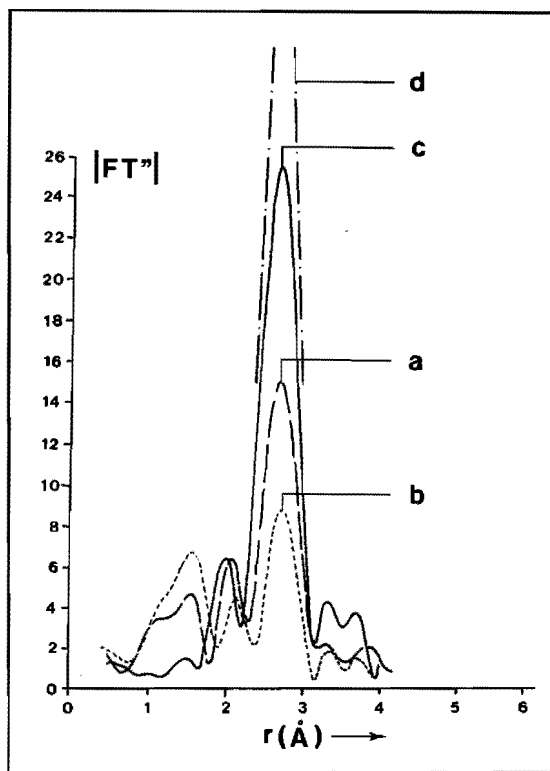
Figure 7 *The radial structure functions (k^3-weighed, Δk =*
3.3 - 10 $\AA^{-1}$, Rh-Rh phase shift and amplitude corrected)
for the 0.47 wt% Rh/γ-Al$_2$O$_3$ catalyst after the con-
secutive treatments:
a) reduction at 673 K, b) CO admission at 298 K and
c) Boudouard reaction at 523 K. d) Reduction of the
passivated catalyst at 523 K and a subsequent reaction
between H$_2$ and CO at 523 K.

8.5 DISCUSSION

The EXAFS results clearly indicate that the structure of
rhodium in a highly dispersed Rh/Al$_2$O$_3$ catalyst changes
significantly when the gas atmosphere is altered.

After reduction of the catalysts rhodium crystallites were
formed with an interatomic rhodium-rhodium distance of 2.68 Å
which approached the bulk value (2.687 Å) within the
experimental error (0.01 Å). The structure of the crystallites
after reduction can be either two-dimensional, as suggested
by Yates *et al.* (6), or three-dimensional, as suggested by
Van 't Blik *et al.* (10). On the assumption of having a square
two-dimensional particle with a (111) surface the particle
with an average coordination number of 5.3 (observed for the
reduced 0.47 wt% Rh/γ-Al$_2$O$_3$ catalyst) consists of 200 atoms,
which corresponds with a diameter of the raft of 40 Å. When the
H/Rh stoichiometry of edge and corner atoms is 2, and 1 for
the other atoms, as proposed by Yates (6), the H/Rh value would
be about 1.2. This value differs too much from the experimental
value of 1.7, so the metallic particles will most likely have
a three-dimensional structure. In that case the average
coordination number of 5.3 corresponds with a crystallite of
approximately 20 atoms of which 18 atoms have been exposed.
The observed H/Rh value of 1.7 can be understood if the H/Rh
stoichiometry is 2.
Evidence was found for Rh-O coordination. The interatomic
distance of 2.73 Å is 0.68 Å larger than the distance in
Rh$_2$O$_3$, indicating that the rhodium crystallite is attached to
the support via an interaction between zero valent rhodium
atoms and oxygen ions of the γ-Al$_2$O$_3$. This result has previously
been reported by Van Zon *et al.* (21).

After evacuation of the 1.04 wt% Rh/γ-Al$_2$O$_3$ catalyst the
rhodium-rhodium bond shortened by 0.05 Å (see table 2) which
is far beyond the experimental error. As nearly all the atoms
are situated on the surface the observed contraction is in
accordance with the prediction of Allen (22) that a contraction
of distances between atoms of a surface layer occurs with an
enhancement of the force constants. A contraction of small
metal crystallites covered with helium has been observed
previously by Moraweck *et al.* (23) who found a contraction of
0.12 Å of the Pt-Pt distance in a Pt/Y-zeolite sample.

As can be seen from table 2 evacuation causes not only a decrease of the Rh-Rh distance but also an increase of the average coordination number. In our case a change of N from 5.9 to 6.6 occurs after evacuation and He flushing. A normal sintering of the crystallites cannot be exluded but the increase can also be interpreted in terms of a 'breathing' crystallite (7). The crystallites which are covered with hydrogen are spread over the support. After desorption of hydrogen the surface atoms become (more) coordinatively unsaturated and consequently the particles curl up to crystallites with the smallest possible amount of surface atoms. Unfortunately, we have not recorded an EXAFS spectrum after a subsequent H_2 admission at room temperature in order to prove this hypothesis.

The EXAFS results clearly show that the greater part of rhodium-rhodium bonds are broken upon CO chemisorption, ultimately leading to rhodium geminal dicarbonyl species as shown previously (9, 10). Beside isolated $Rh(CO)_2$ species there are still crystallites present. During reduction of the catalyst particles of different sizes are formed and the crystallites with a large average rhodium-rhodium coordination number are not broken up after CO adsorption because the adsorption energy provided is too low to disrupt all the rhodium-rhodium bonds. Note that the measured coordination numbers as given in table 1 and 2 are expressed per absorbing Rh atom. The actual average coordination number of a species can be found by dividing the measured one with the fractional part of the total number of rhodium atoms in the species in question. An approximation of the real average rhodium-rhodium coordination number of the crystallites which were not affected during CO chemisorption can be given. The real coordination number of rhodium geminal dicarbonyl species is 2. In the case of the 1.04 wt% $Rh/\gamma-Al_2O_3$ catalyst the determined N(Rh-CO) is 1.5 (*cf*. table 2). The Rh-O* and Rh-C contribution to the EXAFS function of linearly bound carbon monoxide on the surface rhodium atoms of the crystallites still left after CO adsorption can be neglected because the relative contribution to Rh-CO

oscillations is less than 5%. The fraction f of the total number
of rhodium atoms in the $Rh(CO)_2$ species is $1.5/2 = 0.75$.
It is now also possible to estimate the real average coordina-
tion number of the crystallites which is $N(Rh-Rh)/(1-f) = 6.4$.
Evidence has been found for Rh-O coordination with an inter-
atomic distance of 2.10 Å which is 0.05 Å longer than the
distance in Rh_2O_3 and which is 0.63 Å shorter than the Rh-O
distance observed after reduction of the catalyst. As previous-
ly published (10) the Rh-O distance of 2.10 Å is attributed to
the bond between the $Rh^{1+}(CO)_2$ species and the support. The
oxidation state of rhodium changes from zero to 1+ during
CO admission and is interpreted as being due to dissociation
of carbon monoxide. The ratio $N(Rh-O)/N(Rh-CO)$ for both
catalysts is about 1.5 which indicates that on the average
each $Rh(CO)_2$ species is bound by three oxygen ions to the
support.

The stability of the $Rh^{1+}(CO)_2$ species is substantial as
illustrated by the EXAFS spectrum which did not change after
He flushing at 373 K. A striking feature is the rearrangement
of the metal clusters after desorption of carbon monoxide
at elevated temperature (573 K). This indicates that the dis-
ruption and the rearrangement of the metallic rhodium particles
is a reversible process as well as that the adsorption and
desorption of carbon monoxide is oxidative and reductive,
respectively. As proposed elsewhere (10) the reduction of the
rhodium takes place via oxidation of CO to CO_2. The size of
the formed crystallites has increased. The average coordination
number of the particles in the catalyst after CO desorption
($N(Rh-Rh) = 7.1$) is significantly higher than in the evacuated
catalyst ($N(Rh-Rh) = 6.6$). In agreement herewith, the con-
traction of the rhodium-rhodium bond ($R = 2.66$ Å) is less
pronounced than the distance in the particles in the reduced
and evacuated catalyst ($R = 2.63$ Å).
A subsequent reduction results in an increase of the average
Rh-Rh coordination number. The crystallites are covered with
hydrogen and a relaxation of the rhodium-rhodium distance
occurs ($R = 2.68$ Å). A decrease of the dispersion of a highly

dispersed Rh/Al_2O_3 catalyst after CO adsorption and a sub-
sequent reduction has also been observed by Yates *et al.* (6).

After CO flushing at 523 K at which temperature the
Boudouard reaction takes place the rhodium particles break up
completely which is probably caused by intercalation of carbon
and/or oxygen atoms. The peak around 2.8 Å in the radial
structure function (see figure 7) belongs to the Rh-O
distance originated from carbon monoxide either linearly or
bridged bound on rhodium.

During the hydrogenation of carbon monoxide a substantial
sintering of the highly dispersed 0.47 wt% $Rh/\gamma-Al_2O_3$ catalyst
occurred. The average coordination number changed from
N(Rh-Rh) = 5.3 to 9.0 which corresponds with metallic particles
consisting of about 20 and 200 atoms, respectively. This result
clearly illustrates that under reaction conditions the ad-
vantages of having a highly dispersed system can be nullified.

8.6 CONCLUSIONS

The EXAFS experiments clearly illustrate a substantial
alteration of the topology of rhodium in highly dispersed
Rh/Al_2O_3 catalysts after different treatments.

During reduction small metallic rhodium particles are
formed, and when covered with hydrogen, the Rh-Rh interatomic
distance is 2.68 Å which is similar to the Rh-foil.
The crystallites are attached to the support via rhodium-
oxygen bonds with a bond length of 2.73 Å which is 0.68 Å
longer compared to the Rh-O distance in Rh_2O_3. This indicates
that in the interface crystallite/support only zero valent
rhodium is present.

When metallic particles are covered with helium, a
contraction of the rhodium-rhodium bond occurs and the average
coordination number increases.

CO adsorption at room temperature is oxidative and in-
duces a disruption of rhodium-rhodium bonds, ultimately
leading to $O_3Rh^{1+}(CO)_2$ species. The rhodium bonds in particles

with a notible size are not affected.

The crystallites which are broken up due to CO chemisorption are rearranged again after CO is desorbed. The CO desorption occurs via a reductive reaction because the valence of rhodium changes from 1+ to zero during evacuation.

After the Boudouard reaction at 523 K ($2CO \rightarrow C + CO_2$) the rhodium-rhodium distance has disappeared, probably because of intercalation of carbon and/or oxygen atoms.

During reaction between CO and H_2 at 523 K the highly dispersed catalyst is transformed to a poorly dispersed system due to sintering of the metallic crystallites.

8.7 REFERENCES

1   a. P.R. Watson and G.A. Somorjai, J. Catal., 72 (1981) 347.
    b. P.R. Watson and G.A. Somorjai, J. Catal., 74 (1982) 282.
2. T.P. Wilson, P.H. Kasai and P.C. Ellgen, J. Catal., 69 (1981) 193.
3. C.A. Rice, S.D. Worley, C.W. Curtis, J.A. Guin and A.R. Tarrer, J. Chem. Phys., 74 (1981) 6487.
4. R.R. Cavanagh and J.T. Yates, J. Chem. Phys., 74 (1981) 4150.
5. M. Primet, J.C.S. Farad. Trans. I, 74 (1978) 2570.
6. D.J.C. Yates, L.L. Murrell and E.B. Prestridge, J. Catal., 57 (1979) 41.
7. D.J.C. Yates, L.L. Murrell and E.B. Prestridge, in "Growth and Properties of Metal Clusters", p. 137, 1980 edited by J. Bourdon, Elsevier Sci. Pub. Co., Amsterdam, The Netherlands.
8. F.W. Graydon and M.D. Langan, J. Catal., 69 (1981) 180.
9. H.F.J. van 't Blik, J.B.A.D. van Zon, T. Huizinga, J.C. Vis, D.C. Koningsberger and R. Prins, J. Phys. Chem., 87 (1983) 2264.
10. H.F.J. van 't Blik, J.B.A.D. van Zon, T. Huizinga, J.C. Vis, D.C. Koningsberger and R. Prins, J. Am. Chem. Soc., to be published.

206

11. T. Fukushima and J.R. Katzer, Int. Cat. Congress Tokyo (1980).
12. J.C. Vis, H.F.J. van 't Blik, T. Huizinga, J. van Grondelle and R. Prins, J. Mol. Cat., submitted for publication.
13. J.E. Benson and M. Boudart, J. Catal., 4 (1965) 704.
14. H.C. Yao, S. Japar and M. Shelef, J. Catal., 50 (1977) 407.
15. S.E. Wanke and N.A. Dougharty, J. Catal., 24 (1972) 367.
16. R.R. Cavanagh and J.T. Yates, Jr., J. Catal., 68 (1981) 22.
17. D.C. Koningsberger and J.W. Cook, in "EXAFS and Near Edge Structures", p. 412, 1983 editors A. Bianconi, L. Incoccia and S. Stipcich, Springer-Verlag, Berlin, Germany.
18. E.A. Stern, D.E. Sayers and F.W. Lytle, Phys. Rev. B, 11 (1975) 4836.
19. J.B.A.D. van Zon, D.C. Koningsberger, H.F.J. van 't Blik and D.E. Sayers, J. Chem. Phys., to be published.
20. P.A. Lee and G. Beni, Phys. Rev. B, 15 (1977) 2862.
21. J.B.A.D. van Zon, D.C. Koningsberger, D.E. Sayers, H.F.J. van 't Blik and R. Prins, J. Chem. Phys., submitted for publication.
22. G. Allen, Surf. Sci., 89 (1979) 142.
23. B. Moraweck, G. Clugnet and A.J. Renouprez, Surf. Sci., 81 (1979) L631.

chapter 9

THE CATALYTIC BEHAVIOUR IN H_2 + CO REACTION OF Co, Rh AND Co-Rh SUPPORTED ON Al_2O_3 AND TiO_2

9.1 INTRODUCTION

Nowadays the influence of alloying of metals on the catalytic properties and the role of the support TiO_2 in determining the catalytic behaviour of supported metal systems are two important topics in heterogeneous catalysis. The attractiveness of bimetallic catalysts lies in their superior stability and selectivity for many reactions (1-3). With respect to the Fischer-Tropsch reaction it has been shown that alloying of two metals, both of which are active catalysts, may improve the catalytic properties compared to the properties of the constituent monometallic catalysts (4-10). Using an FeRh/SiO$_2$ catalyst, Bhasin *et al.* observed an increase in selectivity to methanol and ethanol compared to either supported iron or supported rhodium catalyst (5). Wise and co-workers have reported a maximum in selectivity for C_2 plus C_3 hydrocarbons for unsupported precipitated (1:1) Fe-Co catalysts (9). Recently, Tucci and Streeter have found a very favourable synergistic effect of the Ru-Ni bimetallic system supported on alumina (7). Both conversion and selectivity to methane increase dramatically when alloying these two metals.

Although titania is a metal oxide support which has been found to strongly inhibit chemisorption of H_2 and CO on group VIII metals after reduction at ~773 K — which effect is known

as Strong Metal Support Interaction (SMSI) (11) -, some metals
have been found to have their highest activities for CO hydro-
genation when dispersed on TiO_2. An outstanding example is the
titania-supported nickel catalyst (12-15) which shows turnover
frequencies one to two orders of magnitude higher than other
Ni catalysts. The increase in activity is accompanied by an in-
crease in selectivity to higher-molecular-weight paraffins.
Titania-supported Ru did not exhibit higher activity but showed
favourable selectivity shifts towards lower methane formation
and higher olefin production (16).
Not all group VIII metals show favourable trends in catalytic
behaviour when supported on TiO_2 (17). Iron, for instance has a
very low activity probably because it becomes easily immersed
in the support (18).
    With respect to the systems under investigation in our
laboratory, Co-Rh catalysts supported on $\gamma-Al_2O_3$ and TiO_2, little
information has been published concerning the hydrogenation of
CO to hydrocarbons. Recently, however, Villeger *et al.* (6) have
shown that addition of Rh to Co results in an increase of the
selectivity to ethene and propene. About the monometallic
Co/Al_2O_3 and Rh/Al_2O_3 systems, however, much more information
is available (19, 20). It appears that Co, which was one of the
first metals to be used as a catalyst for the production of
hydrocarbon liquids and solids (21), produces more long-chain
hydrocarbons than Rh. Rh/Al_2O_3 can even be considered as a
methanation catalyst.
The Co/TiO_2 system as Fischer-Tropsch catalyst has received
very little attention in the literature. Recently, Vannice has
reported that the activities of Co/TiO_2 and Co/Al_2O_3, expressed
as turnover frequencies based on respectively adsorbed CO and
adsorbed H_2, were comparable (17). Yermakov and co-workers
used $Co_2(CO)_8$ as a precursor for the preparation of Co/TiO_2
(22). They found that fast pyrolysis of $Co_2(CO)_8$ on TiO_2 leads
to the formation of highly dispersed superparamagnetic
cobalt particles which possess an increased activity in the
hydrogenation of carbon monoxide, whereas low dispersed cobalt,
obtained by slow pyrolysis, has an activity which is one order
of magnitude lower. Over the past years rhodium supported on

titania hàs enjoyed increased interest because of its out-standing catalytic behaviour in the hydrogenation of CO (17, 23-29). Solymosi *et al.* (26) have found that the specific rate of CH_4 formation on Rh/TiO_2 was more than one order of magnitude higher than that of Rh/MgO and Rh/SiO_2 catalysts. This effect was assigned to an electronic interaction between the TiO_2 and Rh. Authors speculated that TiO_2 may influence the bonding and reactivity of species chemisorbed on metal particles.

In this chapter we will present information on the catalytic behaviour of Co, Rh and Co-Rh supported on alumina and titania in the H_2 + CO reaction. The catalysts used in this study have been characterized by methods which have been presented in chapters 3 and 4.
In the literature the anomalous catalytic behaviour of titania-supported catalysts has often been assigned exclusively to SMSI. However, in many studies reported one may doubt if the SMSI effect really was present, because in some cases the reduction temperature used was too low to create SMSI and in other cases a sintering of the metallic particles could not be excluded. Therefore, we have studied titania-supported catalysts in non-SMSI-state as well as in SMSI-state with similar dispersions.
Activity measurements performed on Rh/TiO_2 catalysts with different dispersions were carried out in order to investigate the influence of metal particle size on the catalytic behaviour in non-SMSI-state and SMSI-state.

9.2 EXPERIMENTAL SECTION

TiO_2 (anatase, Tioxide Ltd., CLDD 1367, surface area 20 m^2/g, pore volume 0.5 cm^3/g) and $\gamma-Al_2O_3$ (Ketjen, 000-1.5 E, surface area 200 m^2/g, pore volume 0.6 cm^3/g) were (co-)im-pregnated with aqueous solutions of the metal salts $Co(NO_3)_2.6H_2O$ and $RhCl_3.xH_2O$ via the incipient wetness technique to prepare monometallic Co and Rh and bimetallic Co-Rh catalysts. The catalysts were dried in air at 393 K for 24 hours, reduced

in flowing H_2 at 773 K for one hour and subsequently passivated and stored for further use. These catalysts are the same as those described in chapters 3 and 4. TPR has proven that for the Co-Rh systems alloying has taken place (see chapter 4). The monometallic catalysts will be denoted from now on by a code: CA (Co/Al_2O_3), RA (Rh/Al_2O_3), CT (Co/TiO_2) and RT (Rh/TiO_2) followed by the indication of the metal loading. The two bi-metallic catalysts Co_4Rh/Al_2O_3 (3.18 wt% Co, 1.39 wt% Rh) and $Co_{1.2}Rh/TiO_2$ (1.19 wt% Co, 1.72 wt% Rh) will be denoted as respectively, C_4RA 4.6 and $C_{1.2}RT$ 2.9.

The hydrogenation of CO was investigated in a flow micro-reactor at atmospheric pressure. The reactor and ancillary equipment are schematically presented in figure 1.

1: Oven
2: Reactor
3: Sample valve
4: Flow meter
5: 4-way valve
6: Gas supply for pre-treatment
7: Gas supply for reaction
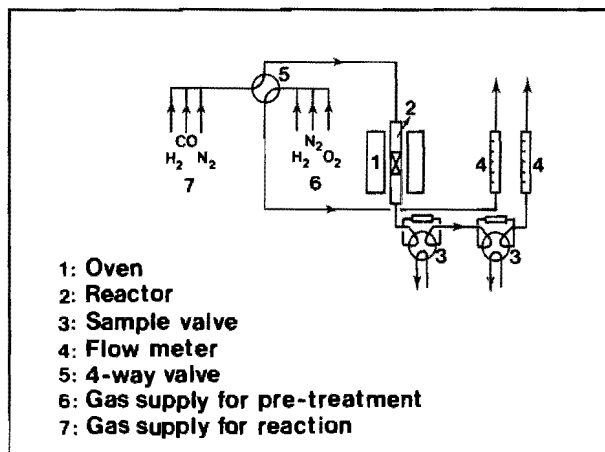
Figure 1 Schematic representation of the flow-system.

Two types of mixtures could be passed through the fixed-bed reactor, either a mixture of hydrogen, nitrogen and oxygen, with which the passivated catalysts were pretreated, or a mixture of hydrogen, carbon monoxide and nitrogen (synthesis gas). Except for oxygen the gases were purified over a BTS column and molecular sieves. The products formed during reaction were analysed on-line by gaschromatography. The GC-equipment consisted of a Packard Becker 427 gaschromatograph equipped with a 904 TCD detector, and a Pye Unicam gas-

chromatograph with a flame-ionisation detector. A column
packed with Porapack QS, using He as carrier gas allowed
complete separation of CO_2, ethene, ethane, H_2O, propene and
propane. Using a squalane column with nitrogen as carrier
gas the amount of C_1 to C_8 hydrocarbons could be determined.
The amount of catalyst used for an experiment was circa 0.2 g.
Prior to the passage of synthesis gas through the reactor, the
passivated catalyst was re-reduced in flowing hydrogen for half
an hour after which the catalyst was cooled under flowing
hydrogen to reaction temperature. The alumina-supported
catalysts were re-reduced at 773 K and the titania-supported
catalysts at 523 K or 773 K. The ratio of H_2:CO:N_2 in the
reacting gas mixture was 3:1:0 or 2:1:1. The gas hourly space
velocity used was 3000 ± 100 hr^{-1}. In order to measure under
differential conditions the conversion of CO was kept lower
than 10%. If necessary, this was achieved by diluting the
catalyst with bare support. The absence of diffusional limita-
tion was confirmed by the method suggested by Körös and
Nowak (30). Under these reaction conditions only hydrocarbons
were formed and no oxygenates.

As the difference in CO concentration between the ingoing
and outgoing gas stream could not be accurately determined the
amount of CO converted to hydrocarbons was determined in a
modified way. Under the reaction conditions used the products
formed typically show a logarithmic (Flory-Schultz or
Anderson (31)) distribution indicating that a constant ratio
of propagation and termination rates exists, especially in the
molecular range above C_2 (32):

$$\ln(\text{mole } \% \ C_n) = K + n\ln\alpha,$$

where $\ln(\text{mole } \% \ C_n)$ shows linear relation to n(carbon number
of product C_n). The probability of chain growth is α; $(1-\alpha)$ is

the probability of chain termination, *i.e.*, product formation (31, 32).

From the experimentally determined C_3 to C_8 hydrocarbons the probability of chain growth α was obtained. Assuming α to be independent of molecular size the concentrations of C_9 to C_∞ were calculated. The sum of the products nC_n ($\sum_1^\infty nC_n$) yielded the amount of CO converted to hydrocarbons.

The activity is expressed as a turnover frequency,

$$TOF_{CO} = \frac{CO\ molecules\ reacted\ to\ hydrocarbons}{surface\ metal\ atom\ \times\ sec}$$

The number of surface metal atoms was measured by hydrogen chemisorption. For the M/TiO_2 systems the H/M values were determined after a low temperature re-reduction at 473 K of the passivated catalysts. Note that the titania-supported catalysts were reduced at 773 K during preparation (and thus might have been in the SMSI-state) and passivated afterwards (which nullified the SMSI-state (see chapter 3 and 4)). This means that the determined H/M values correspond with real dispersions of the catalysts re-reduced below 773 K, without interference of possible sintering effects.

9.3 RESULTS AND DISCUSSION

9.3.1 Co, Rh and Co-Rh supported on Al_2O_3 and TiO_2

Figure 2 presents the change of activities in the H_2 + CO reaction (H_2:CO = 3:1) with time on stream over catalysts at 523 K. In the deactivation two regions can be distinguished: in the beginning of the reaction (below 4 hours) a fast decline of the reaction rate takes place, and after circa 4 hours the activity decreases in a more moderate way. Therefore, we define the 'initial activity' as the activity obtained by extrapolating the function from the first region (t < 4 hours) to reaction time zero, and the 'steady-state activity' as the activity ob-
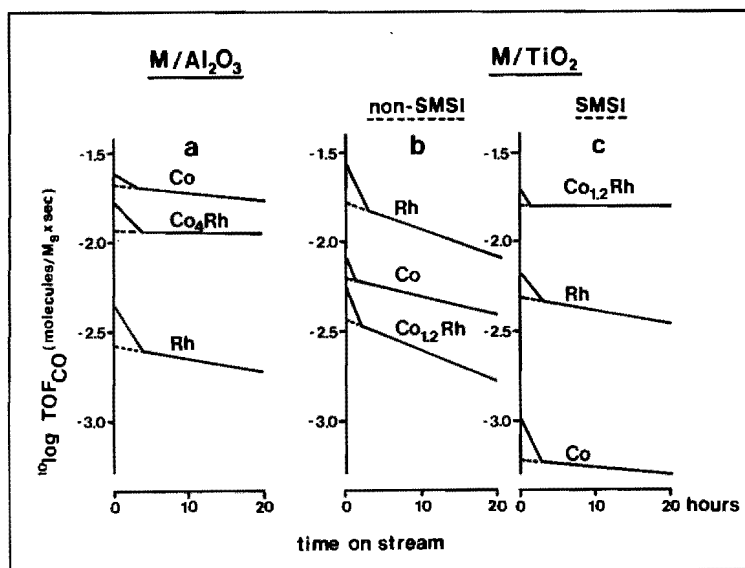
Figure 2 *Change in logarithmic turnover frequency in the H_2 +*
CO reaction with time on stream. (Pressure = 10^2 kPa,
$H_2:CO = 3:1$, reaction temperature = 523 K.)
a) Alumina-supported catalysts re-reduced at 773 K.
b) Titania-supported catalysts re-reduced at 523 K.
c) Titania-supported catalysts re-reduced at 773 K.

tained by extrapolating the second region (t > 4 hours) to
time zero.
Before passing synthesis gas through the reactor the catalyst
was re-reduced in flowing hydrogen and consequently in the
beginning of the reaction the hydrogen concentration was high.
However, the high activity in the induction period cannot be
due to this hydrogen, because a catalyst that had been flushed
with nitrogen showed the same high initial activity and the
same deactivation. We think that hydroxylation of the support
during the first hours of reaction plays a dominant role with
respect to the initial high activity. During reduction of the
catalyst in the reactor the support will be partly de-
hydroxylated. When synthesis gas is passed over the catalyst

the water formed will hydroxylate the support again. Therefore, in the beginning of the reaction the partial pressure of water will be low. This leads to an acceleration of the Fischer-Tropsch reaction:

$$nCO + (2n+1)H_2 \rightarrow C_nH_{2n+2} + nH_2O.$$
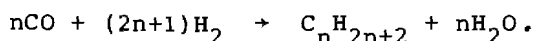
Assuming that the support was fifty percent dehydroxylated after reduction, it can be calculated indeed that under the reaction conditions used the support is completely re-hydroxylated after 2-6 hours. This idea is supported by the results reported by Nijs and Jacobs. They found for supported Ru and Co catalysts that equilibrium of the Fischer-Tropsch reaction was reached within 5 minutes when water was added to the reaction gas (33).

The product distributions obtained over each catalyst after 20 hours of reaction are shown in figure 3. The products are presented as the number of C atoms per molecule and their respective concentrations are listed as the percentage CO converted to the product in question. The C_2 and C_3 fractions are devided into respectively ethane/ethylene and propane/ propene in order to indicate the paraffin/olefin ratio.

Table 1 summarizes the activity and selectivity data for the H_2 + CO reaction at 523 K. Also the apparent activation energies, E_{CO}, for the total conversion of CO into all hydro-carbon products are presented. The energies are determined from Arrhenius plots (not shown) between a reaction temperature range of 473-573 K. The H_2 and CO partial pressures were kept constant at an H_2:CO ratio of 3 for these runs.

From the alumina-supported catalysts, Co/Al_2O_3 is the most active one (see tabel 1). The observed activity and activation energy are in good agreement with the results for a 2 wt% Co/Al_2O_3 catalyst reported by Vannice (19, 20). The mono-metallic Rh/Al_2O_3 catalyst is least active. However, the turn-over frequencies for this catalyst are underestimated, because
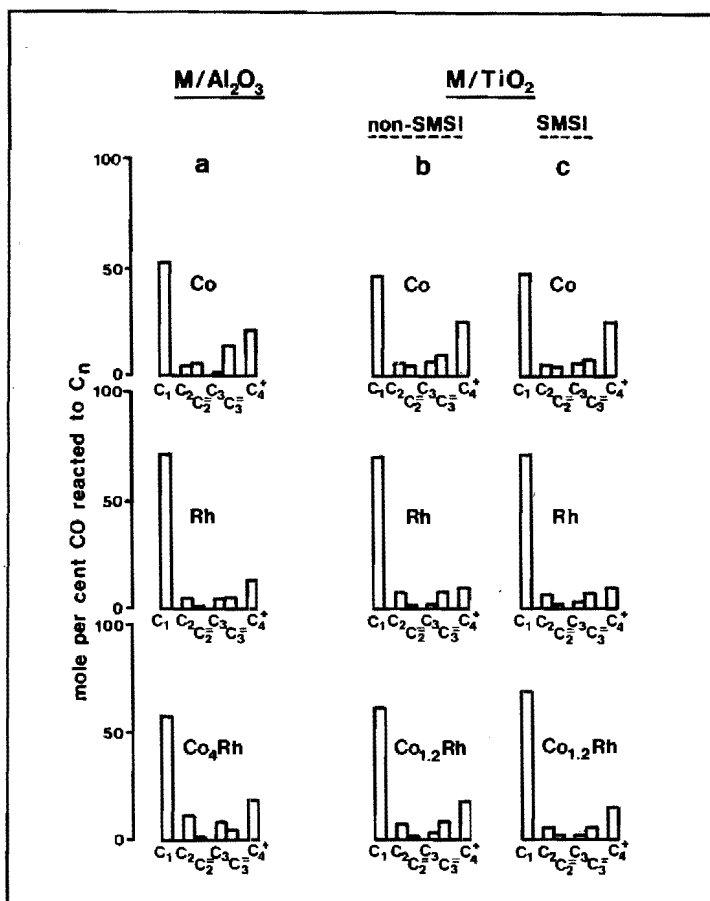
Figure 3 *Product distribution in the H_2 + CO reaction after 20 hours time on stream. (Pressure = 10^2 kPa, H_2:CO = 3:1, reaction temperature = 523 K.)*
a) Alumina-supported catalysts re-reduced at 773 K.
b) Titania-supported catalysts re-reduced at 523 K.
c) Titania-supported catalysts re-reduced at 773 K.

being consequent we used a dispersion ($\overline{D}$) of 1.53 to determine the amount of metal surface atoms. However, during Fischer-Tropsch reaction a highly dispersed rhodium catalyst is transformed to a less dispersed system ($\overline{D} \approx 0.6$), as proven by EXAFS (see chapter 8). This leads to an increase of TOF_{CO} of

Table 1 Selectivity and activity data.
        (Pressure = 10^2 kPa, H_2:CO = 3:1, reaction temperature = 523 K.)

CATALYST	H/M [4]	INITIAL TOF_{CO} × 10^2 $[\frac{molecules}{M_s \times sec}]$	STEADY-STATE		
			TOF_{CO} × 10^2 $[\frac{molecules}{M_s \times sec}]$	α [5]	E_{CO} [kJ/mol]
CA 4.4[1]	0.09	2.43	2.12	0.44	96
RA 2.3	1.53	0.47	0.27	0.40	101
C_4RA 4.6	0.13	1.70	1.21	0.48	98
CT 4.0[2]	0.07	0.80	0.63	0.47	79
RT 1.0	0.40	2.78	1.68	0.44	103
$C_{1.2}$RT 2.9	0.19	0.57	0.37	0.48	85
CT 4.0[3]	0.07	0.11	0.06	0.46	–
RT 1.0	0.40	0.69	0.50	0.42	–
$C_{1.2}$RT 2.9	0.19	2.03	1.63	0.50	–

1: The catalysts were re-reduced at 773 K.
2: The catalysts were re-reduced at 523 K.
3: The catalysts were re-reduced at 773 K.
4: Based on H_2 adsorption at room temperature after re-reduction of the M/Al_2O_3 and M/TiO_2 catalysts at respectively, 773 K and 473 K.
5: α = probability of chain growth.

about a factor of 2.5. Moreover, in anticipation of the results presented in section 9.3.2, the activity per rhodium surface atom increases a factor of 4 when the dispersion decreases from $\bar{D} > 0.5$ to $\bar{D} < 0.3$. This means that comparing the activities for a Co/Al_2O_3 and an Rh/Al_2O_3 catalyst with similar dispersions,

the activity for Rh/Al_2O_3 may even exceed the activity for Co/Al_2O_3.

The observed activation energy of 101 kJ/mol for the Rh/Al_2O_3 catalyst is in excellent agreement with the one reported by Vannice (19) for a 1 wt% Rh/Al_2O_3 catalyst (102 kJ/mol). From figure 3a it can be clearly seen that rhodium is essentially a methanation catalyst, while CO is converted to longer-chain hydrocarbons over cobalt. In agreement with the open literature describing the behaviour of cobalt and rhodium on Al_2O_3 the products formed are respectively, olefinic and paraffinic in nature.

Alloying cobalt with rhodium hardly affects the activity (table 1). A pronounced synergistic effect is thus absent. The selectivity of the alumina-supported bimetallic catalyst is similar to that of the monometallic cobalt catalyst (figure 3a). The probability of chain growth α for the bimetallic catalyst is even higher (table 1). A striking feature is that despite the cobalt-like behaviour in activity and selectivity the hydrogenation capacity is rhodium-like (figure 3a). These results can be understood in the context of cobalt enrichment in the surface layer of the bimetallic particles. Cobalt enrichment in bimetallic Co-Rh particles has been proven by EXAFS for a reduced $CoRh/SiO_2$ catalyst (see chapter 5). The surface layer of the bimetallic particles in Co_4Rh/Al_2O_3 under reaction condition might consist of cobalt atoms with a few rhodium atoms homogeneously spread over the surface. As the Fischer-Trospch (FT) reaction is a demanding reaction - an ensemble of several active metal atoms is needed for the reaction (34) - the cobalt-like behaviour of Co_4Rh/Al_2O_3 is understandable. However, the hydrogenation reaction is a facile reaction which can occur over isolated atoms (35). Therefore, the olefins formed during the FT reaction can be hydrogenated on the rhodium atoms and thus the hydrogenation behaviour of Co_4Rh/Al_2O_3 is rhodium-like.

A synergistic effect of the bimetallic catalyst is found in its stability for a FT reaction as can be clearly seen from

figure 2a. After 4 hours the turnover frequency hardly decreases
anymore. Apparently, the active sites are not deactivated by
for instance covering with graphitic carbon which may be
formed during reaction. In general, there will be a competition
between hydrogenation of carbonaceous species to hydrocarbons
and reaction between these species to graphitic carbon. On
rhodium hydrogen molecules dissociate easier than on cobalt.
Therefore, the hydrogenation of carbonaceous species on a
rhodium surface should be better. However, figure 2a shows that
the rate of deactivation for Rh/Al_2O_3 is faster than that for
Co/Al_2O_3. This indicates that reaction between carbonaceous
species on rhodium surfaces is much more pronounced. In the
case of the bimetallic Co_4Rh/Al_2O_3 catalyst, however, the
FT reaction takes place on a cobalt-rich surface, upon which
formation of graphitic carbon is relatively slow, the supply
of hydrogen atoms from the few rhodium atoms present in the
surface might be fast enough to hydrogenate the carbonaceous
species. Thus, the formation of graphitic carbon is suppressed
by an increase of hydrogen concentration on the surface. This
has been previously shown by Goodman *et al.* (36) for Ni
catalysts.
The increase in stability can also be explained by a model
proposed by Sachtler (37). This model assumes that adsorbed
carbonaceous fragments become deleterious catalyst poisons
only after atomic reorganisations resulting in graphitic
structures. The ease of such reorganisations is controlled by
the chemistry and the atomic topography of the catalyst
surface. The presence of rhodium in the cobalt-rich surface
may change the topography in such a way that epitaxy of
carbonaceous fragments is difficult through which formation
of coke is suppressed.
      The catalytic behaviour of metals supported on titania
is illustrated in table 1 for Co, Rh and Co-Rh.
First we consider catalysts which were reduced at 523 K before
FT reaction was investigated. Note that differences in
catalytic behaviour between these titania-supported catalysts

and the alumina-supported catalysts are not due to SMSI because
after reduction at 523 K the titania supported catalysts still
have the normal capacity to adsorb hydrogen. Putting the titania-
supported catalysts in order of decreasing activity gives the
following sequence: Rh > Co > Co-Rh (*cf*. table 1). The turnover
frequencies for Rh/TiO$_2$ and Co/TiO$_2$ and the activation energy
E$_{CO}$ for Co/TiO$_2$ are in good agreement with values previously
published by Vannice (17). However, the observed activation
energy for Rh/TiO$_2$ of 103 kJ/mol differs significantly from
the one given by Vannice: 134 kJ/mol. The activation energy for
the bimetallic catalyst approaches the one observed for Co/TiO$_2$.
Comparison of turnover frequencies for M/Al$_2$O$_3$ and M/TiO$_2$
catalysts shows that the TOF$_{CO}$ value for Rh is higher and the
TOF$_{CO}$ values for Co and Co-Rh are lower for the TiO$_2$-supported
catalysts. In anticipation of the results of activity measure-
ments performed on the RT- and RA-series, which will be dis-
cussed in the next section – and which show that catalysts
with low dispersions have a much higher TOF$_{CO}$ than catalysts
with high dispersions –, we attribute the enhancement in activity
for Rh/TiO$_2$ to a dispersion effect. The decrease in activity
for Co and Co-Rh is not fully understood yet.
The product distributions of the titania-supported monometallic
catalysts hardly differ from those of the corresponding metal
systems supported on alumina (compare figure 3a with 3b).
However, the α's increase (*cf*. table 1). Going from alumina to
titania the hydrogenation capacity for Co,Rh and Co-Rh did
not change significantly.
Comparison of figure 2a and 2b shows that the rates of de-
activation for the three titania-supported catalysts were
substantially higher than the corresponding rates for the Al$_2$O$_3$-
supported catalysts. As in the case of alumina the stability
of rhodium on titania is inferior to the stability of the cobalt
catalyst. The most apparent difference between Co$_4$Rh/Al$_2$O$_3$ and
Co$_{1.2}$Rh/TiO$_2$ appeared in stability. Whereas Co$_4$Rh/Al$_2$O$_3$ hardly
deactivated with reaction time the opposite is true for
Co$_{1.2}$Rh/TiO$_2$ which showed a rate of deactivation comparable
with the one observed for Rh/TiO$_2$. As the Co/Rh ratio in

$Co_{1.2}Rh/TiO_2$ is rather low it might be possible that despite
Co enrichment of the surface layer there are rhodium ensembles
on the surface. A fast formation of graphitic carbon on these
rhodium ensembles would explain why the deactivation behaviour
is comparable with that of the monometallic rhodium system.

In order to investigate the influence of reduction
temperature on the catalytic behaviour of the titania-supported
catalysts, activity measurements were performed on these
catalysts after reduction at 773 K. Differences in catalytic
behaviour of the same catalyst re-reduced at 523 K or 773 K
must be due to the SMSI. Sintering can be excluded because
during preparation of these catalysts they had already been
reduced at 773 K. Note that after this reduction the catalysts
were in SMSI-state but as discussed in chapter 3 and 4 the
subsequent passivation step nullified the SMSI-state completely.
Table 1 and figure 3 clearly indicate that the selectivities
to methane and to long-chain hydrocarbons were not significant-
ly affected by a high temperature reduction of the catalysts.
The hydrogenation capacity after the induction period of
circa 4 hours did not change either (compare figure 3b and 3c).
However, the effect of SMSI on turnover frequencies (see
table 1) and stability (see figure 2c) was striking. The
activity of Co/TiO_2 decreased almost one order of magnitude
whereas the activity of Rh/TiO_2 decreased by a factor of 4.
However, the stability for both catalysts increased after
the high temperature reduction. A remarkable feature is the
increase of TOF_{CO} and stability for $Co_{1.2}Rh/TiO_2$. The rate
of deactivation above 4 hours is nihil. Even after 4 days the
activity had not changed at all!
In chapter 6 we showed that the titania-supported catalysts
used in this study could be brought in the SMSI-state after
a reduction at 773 K: the hydrogen chemisorption capacity was
suppressed to a great extent. At the moment that the FT reaction
was started the catalysts were in the SMSI-state, but during
the reaction water was formed and it is known that SMSI is
destroyed by water (38). Thus the question arises if the
catalysts were still in the SMSI-state under the steady-state

reaction conditions. As we have no direct answer to this question an explanation of the change in catalytic behaviour for the titania-supported catalysts after a high temperature reduction can only be speculative. The differences in catalytic behaviour do not need to be caused by metal-support interaction solely. A modification of the metal surface might occur during reduction at elevated temperatures. After reduction at moderate temperatures the surfaces of the metal crystallites might be roughly structured and consequently exhibit many defects which are active sites for reaction. A high temperature reduction might smooth the surface and induce the formation of low Miller-index surfaces. Studies of well-defined Co single crystals showed that the basal plane is inactive for CO dissociation (39). CO is adsorbed associatively on rhodium single crystals at 300 K and dissociates slowly above this temperature (40). As shown by Araki and Ponec (34) and later by Biloen (41) CO dissociation precedes C-H bond formation in FT synthesis. Therefore, smoothing of the metal surface might play a role in the explanation for the decrease in activity for Co/TiO_2 and Rh/TiO_2.

The remarkable increase of the stability of $Co_{1.2}/TiO_2$ after re-reduction at 773 K suggests that the surface structure of the bimetallic crystallites had indeed changed. In the context of the models proposed for the alumina-supported bi- metallic catalyst we think that during high temperature re- duction Co enrichment is more pronounced and that therefore the amount of rhodium ensembles has markedly decreased. From the stability point of view the same situation arises as for Co_4Rh/Al_2O_3

9.3.2 RA AND RT SERIES AS CO HYDROGENATION CATALYSTS

The activity and selectivity data obtained on the H_2 + CO reaction over the catalysts at 523 K are summarized in table 2. The composition of the reactant gas used was $H_2:CO:N_2 = 2:1:1$.

First we will focus our attention to the RA series and RT series in non-SMSI-state. The table clearly demonstrates

Table 2 Selectivity and activity data.
(Pressure 10^2 kPa, $H_2:CO:N_2 = 2:1:1$, reaction temperature = 523 K.)

CATALYST	H/Rh[6]	INITIAL TOF_{CO} x 10^2 $[\frac{molecules}{Rh_s \times sec}]$	STEADY-STATE TOF_{CO} x 10^2 $[\frac{molecules}{Rh_s \times sec}]$	S_{CH_4}[7]	α[8]	$C_3^=/C_3$
RA 2.3[1]	1.53	0.31	0.17	0.59	0.44	0.80
RA 4.6	0.96	0.63	0.28	0.61	0.45	1.18
RA 8.5	0.81	0.82	0.35	0.65	0.45	1.56
RA 11.6	0.67	0.73	0.31	0.63	0.45	2.52
RT 0.3[2]	1.10	0.45	0.10	0.50	0.45	1.50
RT 0.7	0.61	0.74	0.34	0.55	0.51	2.07
RT 1.0[3]	0.40	2.10	0.47	0.49	0.48	2.52
RT 2.0	0.35	2.67	0.58	0.48	0.43	3.41
RT 3.2	0.22	4.11	1.48	0.48	0.42	2.11
RT 8.1[4]	0.12	4.06	1.43	0.50	0.42	6.50
RT 0.3[5]	1.10	0.01	0.01	0.48	0.40	1.20
RT 0.7	0.61	0.08	0.07	0.47	0.43	1.95
RT 1.0	0.40	0.40	0.20	0.43	0.42	2.31
RT 2.0	0.35	0.78	0.33	0.48	0.41	3.06
RT 3.2	0.22	1.38	0.91	0.53	0.40	2.05
RT 8.1	0.12	1.11	0.83	0.44	0.42	5.60

1: The catalysts were re-reduced at 773 K.
2: The catalysts were re-reduced at 523 K.
3: E_{CO} = 103 kJ/mol.
4: E_{CO} = 81 kJ/mol.
5: The catalysts were re-reduced at 773 K.
6: Based on H_2 adsorption at room temperature after re-reduction of the M/Al_2O_3 and M/TiO_2 catalysts at respectively, 773 K and 473 K.
7: S_{CH_4} = selectivity to methane.
8: α = probability of chain growth.

the correlation between the specific activity and dispersion
(percentage exposed). The rate of CO hydrogenation increases
by about a factor of 2.5 as the dispersion of Rh on alumina
was decreased from 1.53 to 0.67. For the RT series the activity
increases one order of magnitude going from a dispersion of
1.10 to 0.12. The increase in activity is accompanied by an
increase in the olefin-to-paraffin ratio. Neither the selectivi-
ty to methane nor the probability of chain growth is greatly
affected.

The TOF_{CO}'s in steady-state for the RA series and the RT series
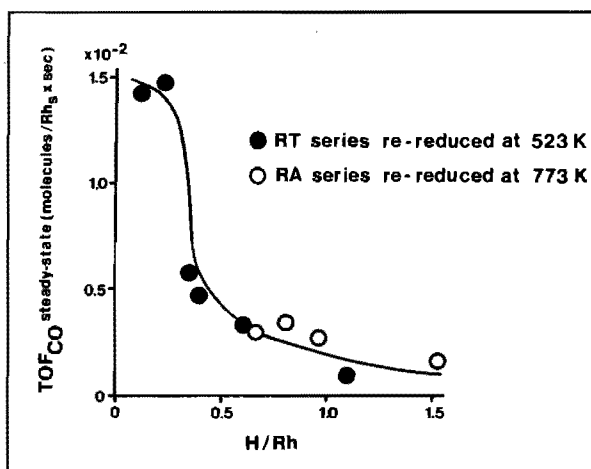are presented in figure 4 as a function of H/Rh (dispersion).

Figure 4 Steady-state turnover frequency in the H_2 + CO reaction
versus H/Rh (dispersion) for alumina- and titania-
supported Rh-catalysts. (Pressure = 10^2 kPa,
$H_2:CO:N_2$ = 2:1:1, reaction temperature = 523 K.)

The resemblance between the TOF_{CO}'s of the alumina- and
titania-supported rhodium catalysts is obvious. Both systems
reveal the same variation of activity with dispersion and the
catalysts with the same H/Rh value have, within the accuracy
of the measurements, the same turnover frequency. This leads
to the conclusion that one must pay attention to dispersion
effects when comparing activities in H_2 + CO reactions of

rhodium supported on alumina and titania. If we go back to figure 2a and compare the activities for Co/Al_2O_3 and Rh/Al_2O_3 the above mentioned result means that the activity for Rh/Al_2O_3 is much higher at a dispersion comparable with Co/Al_2O_3 ($\bar{D}$ = 0.09) and therefore may even exceed the activity of Co/Al_2O_3.

Figure 4 shows that the titania-supported catalysts with dispersions above 0.30 exhibit a very rapid decay in the turnover frequencies for the synthesis of all products. Such an influence of dispersion on the performance of supported group VIII metals for the synthesis of hydrocarbons via CO hydrogenation has been reported previously (42-45). In a detailed study Kellner and Bell (45) reported a dramatic decrease in the specific activity for Ru/Al_2O_3 catalysts with dispersions above 0.7. The decrease in activity was accompanied by a slight decrease in the probability of chain growth and a rapid decrease in the olefin-to-paraffin ratio. Vannice (42, 43) observed that the methanation activity of Ni catalysts decreased with increasing dispersion. By contrast the specific activity for methanation of Pt and Pd catalysts was found to increase with increasing dispersion.

Two explanations for the decrease in specific activity with increasing dispersion can be given. One explanation, originally proposed by King (46), is that the electronic properties of the particles may be changed. Theoretical studies (47) of the electronic properties of small metal particles show that deviations from the properties of bulk metal occur, primarily, for crystallites smaller than about 20 Å. This critical size corresponds to a dispersion of about 0.5. The observed H/Rh value of 0.3, at which a decline of the specific activity takes place, is of the right order of magnitude. A small difference in the electronic properties between large and small rhodium particles follows from XPS measurements (48). The observed Rh 3d 5/2 electron binding energies for RT 8.1 (the least dispersed catalyst) and for RT 0.3 (the most dispersed catalyst) after in situ reduction at 483 K are 307.05 and 307.25 eV, respectively. (This small variation in binding energy is most

likely caused by differences in the extra-atomic relaxation of metal particles of different sizes. In small particles there is less effective screening of the core holes created during photoemission.) This indicates a small change in the electron properties going from a rhodium loading of 8.1 to 0.3 per cent by weight.

Another explanation for the decrease in specific activity with increasing dispersion might be that the fraction of sites active for the hydrogenation of CO decreases with increasing dispersion. Such a trend would be expected if Rh atoms at the faces of crystallites were more active than those at the edges or corners (49, 50). The apparent activation energy E_{CO} for RT 8.1 is 81 kJ/mol which is significantly lower compared to the activation energy for RT 1.0 which is 103 kJ/mol. This result is in accordance with the model because it indicates a change in nature of the active sites with dispersion.

The activity and selectivity data obtained by measurements on the Rh/TiO_2 catalysts after re-reduction at 773 K are summarized in table 2. Note that the influence of dispersion on the catalytic properties of the RT-series in the SMSI-state is comparable with those in the non-SMSI-state. Significant differences between the catalysts after a low and high temperature re-reduction appear to be present in the specific activities only. Neither the selectivity in methane nor the hydrogenation capacity is affected, whereas the probability of chain growth tends to decrease.

Plots of both initial and steady-state TOF_{CO}'s as a function of dispersion for the RT series after low and high temperature re-reduction are presented in figure 5. It is obvious that by SMSI the initial specific activity is affected most. The effect of SMSI on the steady-state activity is, however, moderate. As suggested in the previous section, this result indicates that SMSI is indeed destroyed during reaction, if not completely than at least to a great extent. We consider water, formed during reaction, to be responsible for this!
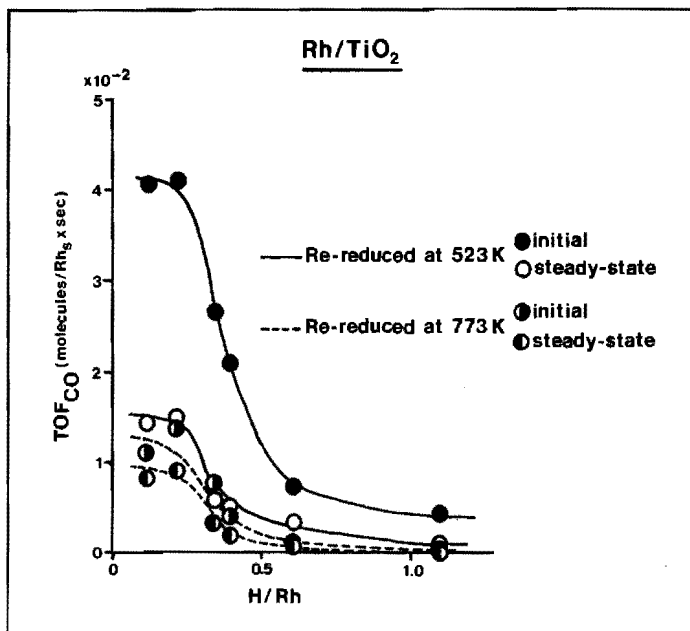
Figure 5 *Initial and steady-state turnover frequencies in the*
H_2 + *CO reaction versus H/Rh (dispersion) for titania-*
supported Rh-catalysts re-reduced at 523 k and 773 K.
(Pressure = 10^2 kPa. $H_2:CO:N_2$ = 2:1:1, reaction
temperature = 523 K.)

The difference in the initial activity between a catalyst re-
reduced at low temperature (LT) and the same catalyst re-
reduced at high temperature (HT) can only be caused by SMSI.
Therefore, the ratio TOF_{CO} initial (HT)/TOF_{CO} initial (LT) is
a measure for SMSI. Theoretically, a ratio of zero indicates
a complete suppression by SMSI, whereas a ratio of one indicates
a complete lack of SMSI. In order to investigate the in-
fluence of dispersion on SMSI we plotted TOF_{CO} initial (HT)/
TOF_{CO} initial (LT) versus H/Rh in figure 6. This figure clearly
indicates that SMSI is more pronounced for the dispersed
systems. An effect of crystallite size on the onset of SMSI
has previously been reported by Ko *et al.* (51). They have
found that with titania-supported nickel catalysts more severe
reduction conditions were necessary to induce strong metal-
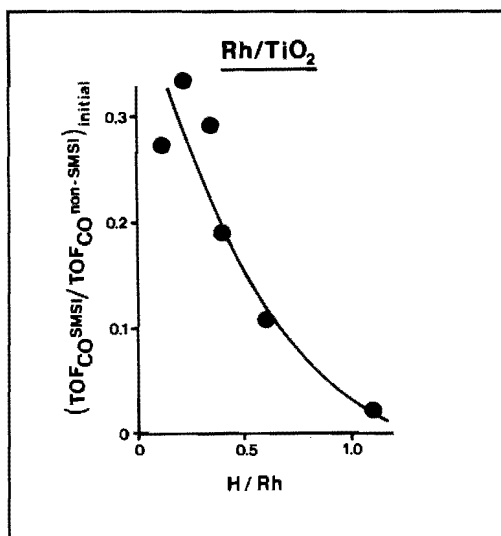support interactions when nickel crystallites were larger.

Figure 6 Ratio of initial turnover frequencies in the $H_2 + CO$
reaction of Rh/TiO_2 catalysts re-reduced at 773 K and
523 K as a function of H/Rh (dispersion). (Pressure =
10^2 kPa, $H_2:CO:N_2$ = 2:1:1, reaction temperature =
523 K.)

Many explanations for SMSI have been put forward. We refer to
a review of strong metal-support interaction by Huizinga (52).
At the moment it is too early to tell which explanation is
the best one, but two explanations may be preferred over the
others. Firstly: charge transfer from the support to the
metal, through which the electron properties of the metal
change has been described by Horsley (53). Secondly: a subtle
encapsulation of the metal, as a result of covering the metal
with suboxides of TiO_2 might also explain the reduced catalytic
activity.
We observed that in situ reduction of Rh/TiO$_2$ at 523 K or 823 K
led to essentially the same Rh 3d 5/2 binding energy (48). This
indicates that SMSI is probably not caused by a charge trans-
fer from the support to the metal or vice versa.
A plausible explanation for the decrease of the ratio TOF$_{CO}$
initial (HT)/TOF$_{CO}$ initial (LT) with dispersion might be that

SMSI is caused by encapsulation. It is obvious that small
particles are more easily encapsulated than larger ones and
that this ultimately leads to a more pronounced suppression
of the initial activity for highly dispersed systems.

9.4 CONCLUSIONS

After alloying of Co and Rh on Al_2O_3 the activity in the
H_2 + CO reaction is not much different from that of the
corresponding monometallic catalysts. The activity and
selectivity to methane and long-chain hydrocarbons for
Co_4Rh/Al_2O_3 is cobalt-like whereas the hydrogenation capacity
is rhodium-like. A positive effect of Co_4Rh/Al_2O_3 is observed
in the stability, the deactivation is clearly suppressed by
alloying.

Alloying of Co and Rh on TiO_2 in non-SMSI-state influences
the activity in H_2 + CO reaction negatively. The selectivity
to methane and long-chain hydrocarbons for $Co_{1.2}Rh/TiO_2$ is
cobalt-like and the hydrogenation capacity is rhodium-like.
The rate of deactivation for $Co_{1.2}Rh/TiO_2$ is comparable with
the one for Rh/TiO_2.

The selectivities to methane and long-chain hydrocarbons and
the hydrogenation capacity are not affected by a high tempera-
ture reduction of the titania-supported catalysts. However,
the activity of Co/TiO_2 decreases in a more moderate way,
whereas the activity of $Co_{1.2}Rh/TiO_2$ increases strongly. The
effect of a high temperature reduction of the catalysts on the
stability is positive. The rate for Co/TiO_2 and Rh/TiO_2 de-
creases and for $Co_{1.2}Rh/TiO_2$ the rate is even zero.

The activities for Rh/Al_2O_3 and Rh/TiO_2 catalysts with
similar dispersions hardly differ from each other. The specific
activity for Rh/TiO_2 increases one order of magnitude going
from a dispersion of 1.10 to 0.12. This increase is accompanied
by an increase in the olefin-to-paraffin ratio. Neither the
selectivity to methane nor the probability of chain growth is
greatly affected. The SMSI-state of Rh/TiO_2 catalysts is

destroyed to a great extent during hydrogenation of CO. The initial activities decrease after a high temperature reduction of the catalysts, whereas the steady-state activities are hardly affected. The effect of SMSI on the initial activity is a function of dispersion. The effect is more pronounced on small metallic particles.

9.5 REFERENCES

1. V. Ponec, Catal. Rev.-Sci. Eng., 11, 41 (1975).
2. J.H. Sinfelt, Adv. Catal., 23, 19 (1973).
3. W.M.H. Sachtler, Catal. Rev., 14, 193 (1976).
4. M.A. Vannice and R.L. Garten, J. Mol. Catal., 1, 201 (1975-1976).
5. M.M. Bhasin, W.J. Bartley, P.C. Ellgen and T.P. Wilson, J. Catal., 54, 120 (1978).
6. P. Villeger, J. Barrault, J. Barbier, G. LeClercq and R. Maurel, Bull. Soc. Chim. France, 1979, p. I-413.
7. E.R. Tucci and R.C. Streeter, Hydrocarbon Processing, April 1980, 107.
8. R.M. Stanfield and W.N. Delgass, J. Catal., 72, 37 (1981).
9. M. Nakamura, B.J. Wood, P.Y. Hou and H. Wise, in "Proceedings of the 7th International Congress on Catalysis", edited by T. Seiyama and K. Tanabe, Elsevier Amsterdam (1981), Part A, p. 432.
10. H. Miura and R.D. Gonzalez, J. Catal., 74, 216 (1982).
11. S.J. Tauster, S.C. Fung and R.L. Garten, J. Am. Chem. Soc., 100, 170 (1978).
12. M.A. Vannice and R.L. Garten, J. Catal., 56, 236 (1979).
13. M.A. Vannice and R.L. Garten, J. Catal., 66, 242 (1980).
14. M.A. Vannice and J. Vasco-Jara, in "Stud. Surf. Sci. and Catal.", vol. 11, edited by B. Imelik *et al.*, Elsevier Amsterdam (1982), p. 185.
15. R. Burch and A.R. Flambard, in "Stud. Surf. Sci. and Catal.", vol. 11, edited by B. Imelik *et al.*, Elsevier Amsterdam (1982), p. 193.
16. M.A. Vannice and R.L. Garten, J. Catal., 63, 225 (1980).

17. M.A. Vannice, J. Catal., 74, 199 (1982).

18. B.J. Tatarchuk and J.A. Dumesic, J. Catal., 70, 308 (1981).

19. M.A. Vannice, J. Catal., 37 449 (1975).

20. M.A. Vannice, J. Catal., 37 462 (1975).

21. H. Pichler, in "Advances in Catalysis", vol. 4, edited by
    W.G. Frankenburg *et al.*, Academic Press Inc., New York
    (1952), p. 271.

22. A.S. Lisitsyn, A.V. Golovin, V.L. Kuznetsov and Y.I.
    Yermakov, React. Kinet. Catal. Lett., 19, 187 (1982).

23. M. Ichikawa and K. Shikakura, in "Proceedings of the 7th
    International Congress on Catalysis", edited by
    T. Seiyama and K. Tanabe, Elsevier Amsterdam (1981),
    Part A, p. 925.

24. A. Takeuchi and J.R. Katzer, J. Phys. Chem., 85, 937 (1981).

25. A. Takeuchi and J.R. Katzer, J. Phys. Chem., 86, 243 (1982).

26. F. Solymosi, I. Tombácz and M. Kocsis, J. Catal., 75, 78
    (1982).

27. P. Meriaudeau, O.H. Ellestad, M. Dufaux and C. Naccache,
    J. Catal., 75, 243 (1982).

28. H. Orita, S. Naito and K. Tamaru, J. Chem. Soc., Chem.
    Commun., 1983, p. 993.

29. A. Takeuchi, J.R. Katzer and G.C.A. Schuit, J. Catal., 82,
    477 (1983).

30. R.M. Körös and E.J. Nowak, Chem. Eng. Sci., 22, 470 (1967).

31. R.B. Anderson, in "Catalysis", vol. 4, edited by P.H.
    Emmett, Reinholt, New York (1956), p. 257.

32. G. Henrici-Olivé and S. Olivé, Angew. Chem. Int. Ed. Engl.,
    15, 136 (1976).

33. H.H. Nijs and P.A. Jacobs, J. Catal., 66, 401 (1980).

34. M. Araki and V. Ponec, J. Catal., 44, 439 (1976).

35. J.H. Sinfelt, J.L. Carter and D.J.C. Yates, J. Catal.,
    24, 283 (1972).

36. D.W. Goodman, R.D. Kelley, T.E. Madey and J.T. Yates, Jr.,
    J. Catal., 63, 226 (1980).

37. W.M.H. Sachtler, J. Mol. Cat., submitted for publication.

38. D. Duprez and A. Miloudi, in "Stud. Surf. Sci. and Catal.", vol. 11, edited by Imelik *et al.*, Elsevier Amsterdam (1982), p. 179.

39. K.A. Prior, K. Schwaha and R.M. Lambert, Surf. Sci., 77, 193 (1978).

40. D.G. Castner, L.H. Dubois, B.A. Sexton and G.A. Somorjai, Surf. Sci., 103, L134 (1981).

41. P. Biloen, J.N. Helle and W.M.H. Sachtler, J. Catal., 58, 95 (1979).

42. M.A. Vannice, J. Catal., 40, 129 (1975).

43. M.A. Vannice, J. Catal., 44, 152 (1976).

44. C.H. Bartholomew, R.B. Pannell and J.L. Butler, J. Catal., 65, 335 (1980).

45. C.S. Kellner and A.T. Bell, J. Catal., 75, 251 (1982).

46. D.C. King, J. Catal., 51, 386 (1978).

47. J.R. Anderson, in "Structure of Metallic Catalysts", Academic Press, New York (1975).

48. T. Huizinga, H.F.J. van 't Blik, J.C. Vis and R. Prins, Surf. Sci. (1983).

49. R.T.K. Baker, E.B. Prestridge and R.L. Garten, J. Catal., 59, 293 (1979).

50. D.J.C. Yates, L.L. Murrell and E.B. Prestridge, J. Catal., 57, 41 (1979).

51. E.I. Ko, S. Winston and C. Woo, J. Chem. Soc., Chem. Commun., 1982, p. 740.

52. T. Huizinga, thesis, University of Technology, Eindhoven, The Netherlands.

53. J.A. Horsley, J. Am. Chem. Soc., 101, 2870 (1979).

chapter 10

SUMMARY

The investigations, reported in this thesis, deal with
three important topics in heterogeneous catalysis. The first
topic is the characterization and investigation of the catalytic
behaviour in the H_2 + CO reaction of supported group VIII
bimetallic systems. The influence of titania as support
has also been studied. The second topic is the reduction and
oxidation behaviour and the catalytic behaviour in the H_2 + CO
reaction of alumina- and titania-supported rhodium
catalysts with varying dispersions. Last but not least, attention
has been paid to the structure of the metal in ultra dispersed
alumina-supported rhodium catalysts under different conditions.
Since the results presented in chapters 3-9 have been discussed
in detail only a summary of the essential conclusions will
be given on this place.

The results described in chapter 4 and 5 have unambiguously
shown that the TPR-TPO technique can provide useful information
on the structure of bimetallic systems. By using EXAFS as a
complementary technique (chapter 5) a good insight into the
formation and structure of the cobalt-rhodium bimetallic particles
supported on alumina, silica and titania has been obtained.
The results have been explained in terms of the following model.
Generally, during reduction of the co-impregnated cobalt-
rhodium catalysts alloying of the metals takes place.

The noble metal, rhodium, serves as a catalyst for the reduction of the less noble metal, cobalt. As proven by EXAFS the surfaces of the bimetallic particles formed are enriched in cobalt. After a mild oxidation the bimetallic particles stay largely intact, although cobalt is oxidized to a great extent while rhodium is hardly affected by oxygen. A vigorous oxidation induces a segregation of the metal oxides. However, also in this case both metal oxides stay close together, because a subsequent reduction shows that the reduction of cobalt oxide is again catalyzed by rhodium. The reduction and oxidation behaviour of the cobalt-rhodium system are not exactly the same when the metals are supported on alumina, silica or titania. On alumina part of the cobalt forms a surface spinel $CoAl_2O_4$, which proved to be irreducible below 773 K. This compound may already be formed during impregnation and subsequent drying of the catalyst. Compared to the alumina- and silica-supported catalysts higher temperatures are needed to oxidize the system completely for the titania-supported catalysts. However, segregation of the metal oxides does not occur, probably due to formation of $CoRh_2O_4$.
Using TPR, TPO and Mössbauer spectroscopy, structural information on iron-rhodium particles supported on silica have been obtained (chapter 6). These results fit to a great extent the model presented for cobalt-rhodium. This fact and a comparison with other studies on supported bimetallic systems, justify a generalization of the model to other alloys, providing the constituent metals form a solid solution. Other examples where the model can be applicated are: Pt-Rh, Pt-Ir, Fe-Rh, Fe-Ni and Pt-Re.

The catalytic behaviour in the H_2 + CO reaction of the titania-supported cobalt-rhodium catalysts (measured after a low temperature reduction (non-SMSI) and high temperature reduction (SMSI)) and of the alumina-supported cobalt-rhodium catalysts have been presented in chapter 9. Alloying of cobalt and rhodium on alumina and titania in the non-SMSI state induces no improvement of the catalytic behaviour. The activities of the titania-supported catalysts are affected to a great extent after a high temperature reduciton (SMSI effect occurring). The

specific activity of cobalt decreases one order of magnitude,
that of rhodium decreases more moderately, whereas the activity
of cobalt-rhodium increases strongly. This anomalous behaviour
is not understood yet.
The selectivities to methane and long-chain hydrocarbons for
cobalt-rhodium catalysts are 'cobalt-like', and the hydrogena-
tion capacity is 'rhodium-like'. SMSI does not influence the
selectivities.
With respect to the stability of the bimetallic catalysts a
synergistic effect has been observed. The deactivation is to
a great extent suppressed by alloying. As proven by EXAFS,
the surfaces of the bimetallic particles are enriched in cobalt.
Apparently, CO hydrogenation takes then place on cobalt en-
sembles. The increase in stability has been ascribed to a sup-
pression of coke formation by the presence of rhodium atoms in
the surface of the metallic particles. The presence of rhodium
may either increase the hydrogenation of carbonaceous species
- precursors for coke formation - or change the topography of
the metal surface in such a way that epitaxy of carbonaceous
fragments is difficult.

In chapter 3 it can be clearly seen that the reduction
and oxidation behaviour of equally dispersed alumina- and
titania-supported rhodium catalysts are similar. However, this
behaviour depends on dispersion. TPR and TPO results combined
with TEM results show that two different kinds of Rh/Rh_2O_3
exist, small raft-like particles and large spherical particles.
The small Rh crystallites are easily oxidized via chemisorption
followed by formation of an oxide skin around 630 K, whereas
the larger crystallites are oxidized at higher temperatures,
around 800 K. The small Rh_2O_3 crystallites are reduced around
390 K.
The activities in H_2 + CO reaction for alumina- and
titania-supported rhodium catalysts with similar dispersions
hardly differ (chapter 9). As shown for the titania-supported
rhodium catalysts the specific activity increases one order
of magnitude going from a dispersion of 1.10 to 0.12. This

increase is accompanied by an increase in the olefin-to-paraffin ratio. Neither the selectivity to methane nor the probability of chain growth is greatly affected. Such an influence of dispersion on the performance of supported metal /catalysts for CO hydrogenation has been reported previously by Vannice, Bartholomew and Kellner for Ni and Ru and can be, for example, interpreted by a decrease with dispersion of the number of active sites, e.g., situated at faces of the crystallites.

The initial specific activities decrease after a high temperature reduction of the titania-supported rhodium catalysts (SMSI), whereas the steady-state activities are hardly affected. Thus, SMSI influences the activity negatively only in the beginning of CO hydrogenation and the effect disappears to a great extent, probably due to water formed during reaction. In spite of assertions in the literature this result proves that SMSI is not that important for Rh/TiO_2 catalysts in H_2 + CO reactions.

The effect of SMSI on the initial activity is a function of dispersion and is more pronounced for small metallic particles. This result as well as the SMSI effect itself have been interpreted in terms of encapsulation of the metallic particles by partly reduced titania during reduction at high temperature. It is obvious that small crystallites are more easily encapsulated than larger ones, which implies a more pronounced suppression of the initial activity for highly dispersed systems.

In our laboratory the procedure for analysing EXAFS spectra has been modified so as to make EXAFS suitable for studying highly dispersed metal catalysts. Unique structural information can be obtained by this method. This has been demonstrated in chapter 7 and 8, and used to elucidate the structure of rhodium in ultra dispersed rhodium catalysts after different treatments. Reduction of a highly dispersed rhodium catalyst leads to a system in which the rhodium is reduced quantitatively and present as three-dimensional metallic crystallites. As proven by EXAFS, these crystallites

are attached to the support via Rh^0-support O^{2-} bonds. It is not unlikely that essentially Van der Waals type interactions operate here. The Rh-Rh nearest neighbour distance of the hydrogen covered metallic crystallites approaches the bulk value of 2.69 Å, but is contracted to 2.63 Å in vacuum. The existence of metallic rhodium particles after reduction is in contrast with the opinion of some investigators who claim that rhodium is present as isolated Rh^{1+} ions after reduction. They came to this conclusion on basis of CO infrared results. However, this contradiction is only apparent because, as our EXAFS measurements prove, CO adsorption at room temperature changes the system completely. During admission of CO disruption of the rhodium crystallites takes place, ultimately leading to isolated $Rh^{1+}(CO)_2$ species. These fragments are anchored to the support via three O^{2-} ions. Apparently, CO adsorption is an oxidative process. A striking feature is the re-formation of metallic rhodium particles after desorption of CO at elevated temperatures, indicating a reductive desorption. During the Boudouard reaction ($2CO \rightarrow C + CO_2$) at 523 K the rhodium particles break up completely which is probably caused by intercalation of carbon and/or oxygen atoms.

Hydrogenation of CO induces a substantial sintering of a highly dispersed rhodium catalyst. The amount of metal atoms in the metallic particles of the catalyst under investigation changed from 20 to 200 during reaction. However, the presence of rhodium ions cannot be excluded. As rhodium ions have been claimed to be responsible for the selectivity to oxygenates it is very important to know if these ions are present during reaction. EXAFS may be a suitable technique to elucidate this problem, provided that an improvement of the signal-to-noise ratio can be attained. The latter can be achieved by using X-ray fluorescence detection.

SAMENVATTING

Momenteel neemt olie nog de belangrijkste plaats in als grondstof voor de produktie van benzine en de basisstoffen voor de chemische industrie, zoals bijvoorbeeld methanol. Door de steeds stijgende olieprijs en het groeiend besef dat de olie-reserves niet onuitputtelijk zijn, zijn alternatieve energie-bronnen echter sterk in de belangstelling komen te staan. Daar steenkool ongeveer 76% van de fossiele brandstoffen vertegen-woordigt (olie slechts 14%) is het een van de beste mogelijk-heden om (opnieuw) aangewend te worden als energiebron. Een van de wegen om steenkool op een milieuvriendelijke wijze om te zetten tot nuttige produkten is via de gasfase. Wanneer steenkool bij hoge temperatuur met stoom wordt vergast ont-staat een gasmengsel van koolmonoxide (CO) en waterstof (H_2), het zogenaamde synthesegas. Het gas kan met behulp van metaal-katalysatoren worden omgezet tot methaan, methanol en allerlei hogere koolwaterstoffen. IJzer (Fe), kobalt (Co) en rhodium (Rh) zijn veel gebruikte metalen om de hydrogenering van koolmonoxi-de te katalyseren. De reaktie vindt plaats aan het metaal-oppervlak. Om het metaal nu zo efficiënt mogelijk te gebruiken, wordt het op een metaaloxide (de zgn. drager) met een groot in-wendig oppervlak (100-200 m^2/g) gebracht. Meestal worden alumina (Al_2O_3) en silica (SiO_2) als dragermaterialen gebruikt. Op deze manier kunnen metaaldeeltjes met een diameter kleiner dan 50 Å (5×10^{-9} m) worden bereid, waardoor de verhouding tussen metaaloppervlak en volume (=dispersie) erg groot is (groter dan 0.5).
De laatste tijd wordt veel onderzoek verricht aan gedragen bi-metallische systemen. Het blijkt dat, wanneer twee metalen, die beiden katalytisch aktief zijn in de hydrogenering van

koolmonoxide, worden gelegeerd, het katalytisch gedrag sterk
verschilt - vaak in positieve zin - met het gemiddelde van de
afzonderlijke componenten. Dit noemt men het 'synergistisch
effect'.
Het onderzoek naar het gebruik van titania (TiO_2) als drager-
materiaal staat sterk in de belangstelling. Ondanks het feit
dat een reduktieve behandeling van metaal/TiO_2-katalysatoren
op 773 K tot sterk verminderde CO- en H_2-chemisorptie-
eigenschappen leidt (dit staat bekend als 'Strong Metal Support
Interaction' (SMSI)) blijkt volgens de literatuur dat de
aktiviteit voor de hydrogenering van CO hierdoor wordt vergroot.

Dit proefschrift handelt over de volgende drie belangrijke
facetten in de heterogene katalyse met betrekking tot de
hydrogenering van koolmonoxide:
1) karakterisering van en onderzoek naar het katalytisch ge-
   drag in de hydrogenering van CO van bimetallische kobalt-
   rhodiumkatalysatoren. Tevens is de invloed van TiO_2 als
   drager bestudeerd.
2) Reduktie- en oxidatiegedrag en het katalytisch gedrag in
   de hydrogenering van CO van Rh/Al_2O_3- en Rh/TiO_2-katalysa-
   toren met variërende dispersies (deeltjesgrootte).
3) Struktuur van het metaal in ultra-disperse (alle metaal is
   geëxposeerd), Rh/Al_2O_3-katalysatoren onder verschillende
   kondities.

De resultaten beschreven in hoofdstuk 4 en 5 laten duide-
lijk zien dat met behulp van temperatuur-geprogrammeerde
reduktie (TPR) en oxidatie (TPO) nuttige informatie omtrent
de struktuur van bimetallische systemen kan worden verkregen.
Door gebruik te maken van 'Extended X-ray Absorption Fine
Structure' (EXAFS) als een complementaire techniek (hoofd-
stuk 5) is een goed inzicht verkregen in de vorming en struk-
tuur van bimetallische Co-Rh-deeltjes op Al_2O_3, SiO_2 en TiO_2.
Aan de hand van de resultaten kan het volgende model worden
opgesteld. Gedurende reduktie van de geïmpregneerde Co-Rh-
katalysatoren (($RhCl_3$ + Co(NO_3)$_2$)/drager) worden bimetallische

deeltjes gevormd. De reduktie van het minder edele metaal
kobalt wordt gekatalyseerd door het edelere metaal rhodium.
Het is aangetoond dat het oppervlak van de gevormde bimetal-
lische Co-Rh-deeltjes verrijkt is met kobalt. Na een milde
oxidatie blijven de deeltjes intakt, ofschoon het kobalt voor
een groot gedeelte wordt geoxideerd en het rhodium nauwelijks
wordt aangetast door zuurstof. Oxidatie bij hogere tempera-
turen leidt tot segregatie van de metaaloxiden. Gedurende
reduktie van het geoxideerd systeem fungeert rhodium weer als
katalysator voor de reduktie van kobaltoxide, hetgeen betekent
dat de metaaloxiden, ondanks het feit dat ze geïsoleerd op
het drageroppervlak zitten, niet ver van elkaar verwijderd
zijn.

Het reduktie- en oxidatiegedrag van het Co-Rh-systeem op
Al_2O_3, SiO_2 en TiO_2 is echter niet identiek. Op Al_2O_3 gaat
een gedeelte van het kobalt verloren ten gevolge van de
vorming van het oppervlaktespinel $CoAl_2O_4$, dat niet gereduceerd
kan worden beneden 773 K. Het stabiele $CoAl_2O_4$ kan reeds ge-
vormd worden tijdens de impregnatie en het drogen van de
katalysator. In vergelijking met de alumina- en silica-gedragen
katalysatoren verloopt de oxidatie van het kobalt-rhodium-
systeem op titania bij hogere temperaturen. Hier vindt echter
geen segregatie van beide metaaloxiden plaats hetgeen waar-
schijnlijk toegeschreven kan worden aan de vorming van $CoRh_2O_4$.
Het $Fe-Rh/SiO_2$-systeem is gekarakteriseerd met behulp van TPR,
TPO en Mössbauerspektroskopie. De resultaten hiervan zijn be-
schreven in hoofdstuk 6 en passen in het model gepresenteerd
voor het Co-Rh-systeem. Dit en goede overeenkomsten met re-
sultaten van andere studies over bimetallische systemen recht-
vaardigen de uitbreiding van het model betreffende de vorming
en struktuur van bimetallische Co-Rh/dragersystemen, naar
andere systemen, waarin beide metalen volledig mengbaar zijn.
Voorbeelden zijn: Pt-Rh, Pt-Ir, Fe-Rh, Fe-Ni en Pt-Re.

In hoofdstuk 9 is aangetoond dat legeren van Co en Rh op
Al_2O_3 en TiO_2 ('niet-SMSI-toestand') geen merkbare verbetering
van de aktiviteit en selektiviteit in de hydrogenering van CO
induceert. De aktiviteiten van de metaalkatalysatoren op TiO_2

veranderen sterk nadat de systemen bij hoge temperatuur (773 K)
worden gereduceerd. De katalysatoren zijn dan in de 'SMSI-
toestand'. De specifieke aktiviteit van kobalt neemt een faktor
10 af, dat van rhodium een faktor 3 terwijl de aktiviteit van
kobalt-rhodium een faktor 5 toeneemt. Dit sterk afwijkend ge-
drag wordt nog niet begrepen.
De selektiviteit naar methaan en hogere koolwaterstoffen voor
Co-Rh-katalysatoren zijn 'Co-achtig' en de hydrogenerings-
kapaciteit is 'Rh-achtig'. SMSI heeft geen invloed op de
selektiviteiten.
Legeren van Co en Rh leidt tot een synergistisch effekt in de
stabiliteit van de katalysatoren. De bimetallische katalysa-
toren deaktiveren in veel mindere mate dan de overeenkomstige
monometallische systemen. Zoals aangetoond met EXAFS, zijn de
oppervlakken van de bimetallische deeltjes verrijkt met kobalt.
Kennelijk vindt de hydrogenering van koolmonoxide plaats aan
ensembles van kobaltatomen. De toename in stabiliteit wordt
toegeschreven aan de onderdrukking van coke-vorming door de
aanwezigheid van enkele rhodiumatomen in het metaaloppervlak.
De aanwezigheid van rhodiumatomen kan de hydrogenering van
koolfragmenten (precursors voor coke-vorming) vergroten, of
de topografie van het oppervlak veranderen waardoor de kool-
fragmenten niet meer epitaxisch kunnen uitgroeien tot coke.

In hoofdstuk 3 wordt aangetoond dat het reduktie- en
oxidatiegedrag van Rh/TiO_2- en Rh/Al_2O_3-katalysatoren met ge-
lijke dispersies niet verschillen. Het gedrag hangt echter wel
sterk af van de dispersie.
TPR- en TPO-resultaten gekombineerd met transmissie elektronen
mikroskopie (TEM) resultaten tonen aan dat zowel Rh als Rh_2O_3
in twee verschillende vormen voorkomen, nl. kleine platte
kristallieten en grote bolvormige kristallieten. De kleine Rh-
metaaldeeltjes oxideren gemakkelijk via chemisorptie gevolgd
door de vorming van een oxidehuid bij 630 K, terwijl de grotere
deeltjes pas bij 800 K oxideren. De kleine Rh_2O_3 kristallieten
reduceren bij 340 K en de grotere, die moeilijker te reduceren
zijn, bij 390 K.

De resultaten beschreven in hoofdstuk 9 laten duidelijk
zien dat de aktiviteiten voor de hydrogenering van CO van
Rh/TiO_2- en Rh/Al_2O_3-katalysatoren met identieke dispersies
niet significant verschillen. Voor Rh/TiO_2 geldt dat de
specifieke aktiviteit een faktor 10 toeneemt wanneer de dis-
persie varieert van 1.10 tot 0.12. De invloed van de dispersie
op de aktiviteit in CO-hydrogeneringsreakties is reeds gepu-
bliceerd voor nikkel (Ni) en ruthenium (Ru) door Vannice,
Bartholomew en Kellner. Dit verschijnsel wordt geïnterpreteerd
als een afname van het aantal aktieve plaatsen bij een toe-
name van de dispersie. De toename in aktiviteit wordt verge-
zeld door een toename in de olefine/paraffine-verhouding. De
selektiviteiten worden echter niet beïnvloed door een ver-
andering in dispersie.
Een vergelijking tussen de aktiviteit van een Rh/TiO_2-
katalysator gereduceerd bij lage temperatuur ('SMSI-toestand')
laat zien dat de initiële aktiviteit afneemt terwijl de
'steady-state' aktiviteit niet wordt beïnvloed door SMSI.
Kennelijk wordt gedurende de CO-hydrogeneringsreaktie de
'SMSI-toestand' opgeheven, mogelijk door het water dat. ge-
vormd wordt tijdens de reaktie. Uit dit resultaat blijkt
duidelijk dat SMSI niet zo belangrijk is voor het katalytisch
gedrag van Rh/TiO_2-katalysatoren als soms wordt gesuggereerd
in de literatuur.
Het effect van SMSI op de initiële aktiviteit is een funktie
van de dispersie en is geprononceerder voor katalysatoren met
hoge dispersies. Dit brengt ons dan tot het geven van een ver-
klaring voor SMSI. Niet alleen op basis van dit resultaat
maar ook op basis van resultaten uit o.a. XPS- en EXAFS-
metingen en resultaten uit de literatuur denken wij dat tijdens
de reduktie van een metaal/TiO_2-katalysator het metaal in de
drager zinkt en het metaaloppervlak bedekt wordt met Ti_4O_7.
Het zal duidelijk zijn dat kleine metaaldeeltjes sneller be-
dekt zijn met dragermateriaal dan grote deeltjes. Dit verklaart
de grotere onderdrukking van de initiële aktiviteit door SMSI
voor hoger-gedispergeerde Rh/TiO_2-katalysatoren.

In ons laboratorium is een gemodificeerde procedure ontwikkeld om EXAFS-spectra te analyseren. Hierdoor is EXAFS uitstekend geschikt voor het bestuderen van hoog-gedispergeerde metaalkatalysatoren. In hoofdstuk 7 en 8 wordt dit gedemonstreerd voor de struktuuropheldering van rhodium in ultra-disperse Rh/Al_2O_3-katalysatoren onder verschillende kondities. Reduktie van een hoog-gedispergeerde rhodiumkatalysator leidt tot een systeem waarin het rhodium aanwezig is als drie-dimensionale metaalkristallieten. Met behulp van EXAFS is bewezen dat deze deeltjes via Rh^0-O^{2-}-bindingen met het dragermateriaal zijn verbonden. Wanneer de metaaldeeltjes bedekt zijn met waterstofatomen benadert de kortste Rh-Rh-afstand in deze deeltjes die van de bulkwaarde (2.69 Å), terwijl deze afstand kontraheert naar 2.63 Å in vacuum.

De vorming van rhodiumkristallieten tijdens de reduktie van ultra-disperse katalysatoren is niet in overeenstemming met de visie van enkele onderzoekers die beweren dat rhodium na reduktie aanwezig is als geïsoleerde Rh^{1+}-ionen. Zij kwamen tot deze konklusie op basis van CO-infraroodresultaten. We hebben hier te maken met een schijnbare tegenstelling. Met EXAFS is namelijk aangetoond dat tijdens CO-adsorptie de struktuur van het systeem volledig verandert. De rhodiumkristallietjes worden opengebroken onder vorming van geïsoleerde $Rh^{1+}(CO)_2$-ionen. Het is dus juist dat tijdens CO-infraroodmetingen geïsoleerde Rh^{1+}-ionen aanwezig zijn maar dit beeld is niet juist voor het gereduceerd systeem. Uit een nauwkeurige analyse van het EXAFS-spectrum blijkt dat de $Rh^{1+}(CO)_2$-ionen via drie O^{2-}-ionen aan de drager verankerd zitten.

CO-adsorptie aan ultra-disperse Rh/Al_2O_3-katalysatoren is een oxidatief proces (Rh^{1+}-ionen worden gevormd). Een opmerkelijk resultaat is dat tijdens desorptie van CO bij 573 K de metaaldeeltjes weer teruggevormd worden. Kennelijk vindt er een reduktieve desorptie van CO plaats.

Tijdens de Boudouard reaktie ($2CO \rightarrow C + CO_2$) bij 523 K worden de rhodiumkristallieten geheel opengebroken door intercalatie van koolstof- en/of zuurstofatomen.

Tijdens de hydrogenering van CO over ultra-disperse rhodium-katalysatoren treedt een sterke sintering van de rhodium-kristallietjes op. De aanwezigheid van rhodiumionen kan echter niet worden uitgesloten. Daar rhodiumionen verantwoordelijk worden geacht voor de vorming van zuurstofhoudende produkten uit synthesegas is het van belang om de aanwezigheid van deze ionen aan te tonen onder reaktiekondities. Dit probleem zou met EXAFS opgelost kunnen worden indien de signaal/ruis-verhouding wordt verbeterd. Dit laatste kan worden bereikt door gebruik te maken van Röntgenfluorescentie-detektie.

244

DANKWOORD / ACKNOWLEDGEMENT

Op de eerste plaats wil ik Ine bedanken voor het vele
werk dat zij gehad heeft bij het doorlezen van de manus-
kripten en het verzorgen van de lay-out en het typewerk voor
dit proefschrift. Bovendien heeft zij mij steeds geholpen met
haar relativerende kijk op de vele problemen die zoal bij
het totstandkomen van een proefschrift ontstaan en met het
geduld dat zij, evenals Hester, heeft weten op te brengen.

Graag wil ik alle leden van de vakgroep Anorganische
Chemie van de Technische Hogeschool Eindhoven dank zeggen voor
de prettige wijze waarop ik met hen heb mogen werken.

Dit geldt vooral voor de mede-promovendi, niet alleen
voor de wetenschappelijke samenwerking maar ook voor de klim-
en bridgelessen, het uitzonderlijke skiplezier en de voet-
balkundige tegenwerking.

Tom Huizinga, Jan Kees Vis en Hans van Zon ben ik bovendien
zeer dankbaar voor de vele wetenschappelijke diskussies, die
voor mij - en naar ik hoop ook voor hen - zeer leerzaam en
stimulerend waren, maar evenzeer voor hun vriendschap en
kollegialiteit.

In het bijzonder wil ik Roel Prins bedanken voor het in
mij gestelde vertrouwen betreffende het verrichten van dit
promotieonderzoek en voor zijn kennis en kritische beoorde-
lingen, die mijn werk steeds ten goede zijn gekomen.

Diek Koningsberger ben ik zeer erkentelijk voor zijn hulp
en enthousiasme in Stanford, Leogang en Eindhoven.

Veel hulp heb ik gehad van Pieter van de Gender, Michel
Verhoeven, Frank Vossen, Jan Martens en Paul Vriens, die in

het kader van hun S-8-praktikum en/of afstudeeropdracht een
belangrijke bijdrage tot het in dit proefschrift beschreven
onderzoek hebben geleverd.

Joop van Grondelle dank ik voor de apparaat-technische
begeleiding, Adelheid Elemans-Mehring voor het verrichten van
analysewerkzaamheden, Wout van Herpen voor de goede technische
ondersteuning, Henk van Lieshout voor het altijd snel afhan-
delen van administratieve zaken en Frans Sanders voor zijn
behulpzaamheid die de gang van zaken vaak vergemakkelijkte.

De medewerkers van de instrumentmakerij van de CTD ben ik
dank verschuldigd voor het vervaardigen van de IR- en EXAFS-cel.

CURRICULUM VITAE

Henri, Frederik, Jozef van 't Blik, geboren op 10 juli 1954 te Geleen, begon na zijn eindexamen MULO-B, in 1970 met de studie Chemische Techniek aan de Hogere Technische School te Heerlen en behaalde zijn diploma op 17 juni 1975.
In aansluiting hierop studeerde hij Scheikundige Technologie aan de Technische Hogeschool in Eindhoven, alwaar hij op 30 januari 1980 met lof afstudeerde. Zijn afstudeerwerk bestond uit de bestudering van het gedrag van kobalt-koper-katalysatoren in de hydrogenering van koolmonoxide.

Op 21 november 1975 trad hij in het huwelijk met C.J. Quax en op 8 april 1982 werd hun dochter, Hester, geboren.

Door de Nederlandse organisatie voor Zuiver-wetenschappelijk Onderzoek werd hij in de gelegenheid gesteld op 1 maart 1980 te starten met een promotieonderzoek onder leiding van prof. dr. R. Prins in de vakgroep Anorganische Chemie van de Technische Hogeschool Eindhoven. De resultaten van dit onderzoek zijn in dit proefschrift beschreven.

Per 2 april 1984 zal hij werkzaam zijn op het Natuurkundig Laboratorium van de Nederlandse Philipsbedrijven B.V.

PUBLICATIONS

Chapters 3, 4, 5 and 9 will be submitted for publication to the Journal of Catalysis:
- J.C. Vis, H.F.J. van 't Blik, T. Huizinga, J. van Grondelle and R. Prins, J. Catal., to be published.
- H.F.J. van 't Blik, J.H.A. Martens and R. Prins, J. Catal., to be published.
- H.F.J. van 't Blik, D.C. Koningsberger and R. Prins, J. Catal., to be published.
- H.F.J. van 't Blik, T. Huizinga, J.C. Vis and R. Prins, J. Catal., to be published.

Chapters 6 and 8 have been accepted for publication:
- H.F.J. van 't Blik and J.W. Niemantsverdriet, Appl. Cat. (1984).
- H.F.J. van 't Blik, J.B.A.D. van Zon, D.C. Koningsberger and R. Prins, J. Mol. Cat. (1984).

Preliminary results of chapter 7 have been published in the Journal of Physical Chemistry. Parts of this chapter have been or will be submitted for publication:
- H.F.J. van 't Blik, J.B.A.D. van Zon, T. Huizinga, J.C. Vis, D.C. Koningsberger and R. Prins, J. Phys. Chem., 87, 2264 (1983).
- H.F.J. van 't Blik, J.B.A.D. van Zon, T. Huizinga, J.C. Vis, D.C. Koningsberger and R. Prins, J. Am. Chem. Soc., submitted for publication.
- J.B.A.D. van Zon, D.C. Koningsberger, D.E. Sayers, H.F.J. van 't Blik and R. Prins, J. Chem. Phys., submitted for publication.
- J.B.A.D. van Zon, D.C. Koningsberger, H.F.J. van 't Blik and D.E. Sayers, J. Chem. Phys., to be published.

STELLINGEN

behorende bij het proefschrift van

H.F.J. van 't Blik

24 februari 1984

1. Bij de analyse van het L_3-EXAFS-spectrum van een PtIr-
   katalysator zijn Sinfelt *et al.* ervan uitgegaan dat de inter-
   atomaire Pt-Pt, Pt-Ir en Ir-Ir afstanden aan elkaar gelijk
   zijn. Deze aanname is echter aan bedenkingen onderhevig.

   J.H. Sinfelt, G.H. Via and F.W. Lytle,
   J. Chem. Phys., 76, 2779 (1982).

2. De nodige voorzichtigheid dient in acht genomen te worden
   bij het bepalen van de afstanden tussen het absorberend atoom
   en de verschillende verstrooiende atomen uit de ligging van
   dicht bij elkaar gelegen pieken in het absolute deel van het
   complex Fourier getransformeerde EXAFS-signaal - de zogenaamde
   radiale structuurfunctie -, daar interferentie tussen afzon-
   derlijke EXAFS-bijdragen van coördinatieparen kan optreden.

   Dit proefschrift, hoofdstuk 7 en 8.

3. Om het 'inkapselingsmodel' voor de verklaring van 'Strong
   Metal Support Interaction' (SMSI) in hoog gedispergeerde
   gereduceerde M/TiO_2-katalysatoren te toetsen is EXAFS de aan-
   gewezen techniek.

4. Het verdient aanbeveling om de karakterisering van de zuurheid
   van kristallijne alumino-silikaten te standaardiseren met
   behulp van een goedkope en eenvoudige, dus voor ieder labora-
   torium toegankelijke techniek, zoals temperatuur geprogram-
   meerde desorptie van ammoniak.

   N.Y. Topsøe, K. Pedersen and E.G.
   Derouane, J. Catal., 70, 41 (1981).

5. Sinfelt *c.s.* hebben voorgesteld om het verschil tussen de totale hoeveelheid geadsorbeerd en de reversibel gebonden waterstof aan metaalkatalysatoren als maat te nemen voor de hoeveelheid gechemisorbeerd waterstof. Het feit dat dezelfde onderzoeksgroep, zonder nader commentaar, een andere methode hanteert is wellicht een goede indicatie voor de betrouwbaarheid van hun eerste methode.

> *J.H. Sinfelt, J.L. Carter and D.J.C.*
> *Yates, J. Catal.,* 24*, 283 (1972).*
> *G.H. Via, G. Meitzner, F.W. Lytle and*
> *J.H. Sinfelt, J. Chem. Phys.,* 79*, 1527*
> *(1983).*

6. De resultaten van quantum-mechanische berekeningen aan modelstoffen voor pentasil-zeolieten, zoals beschreven door J.G. Fripiat *et al.*, dienen met terughoudendheid vertaald te worden naar ZSM-5 en ZSM-11 systemen.

> *J.G. Fripiat, F. Berger-André, J.-M.*
> *André and E.G. Derouane, Zeolites,*
> 3*, 306 (1983).*

7. Met het door Retey voorgesteld radikaalmechanisme voor de door vitamine B_{12} gekatalyseerde isomerisatie van L-methyl-malonyl-coënzym A naar succinyl-coënzym A kan de gelijksoortige isomerisatie van threo-β-methyl-aspartaat naar L-glutamaat niet beschreven worden. De juistheid van het mechanisme dient dan ook ernstig in twijfel te worden getrokken.

> *J. Retey, Recent Adv. Phytochem.,*
> 13*, 1 (1979).*

8. Een nuttige taak voor de emancipatiecommissie is het ontwerpen van een wet die regelt dat alleen onzijdigen nog de dienst- plicht zullen moeten vervullen.

9. Zure regen zou met een ammoniak vrijmakend reagens benut moeten worden voor kunstbemesting.

10. Als werken een luxe wordt moet er belasting op worden geheven.